Society of Skeletal Radiology

41st Annual Meeting

March 25 – 28, 2018

2018

JW Marriott Austin
Austin, TX

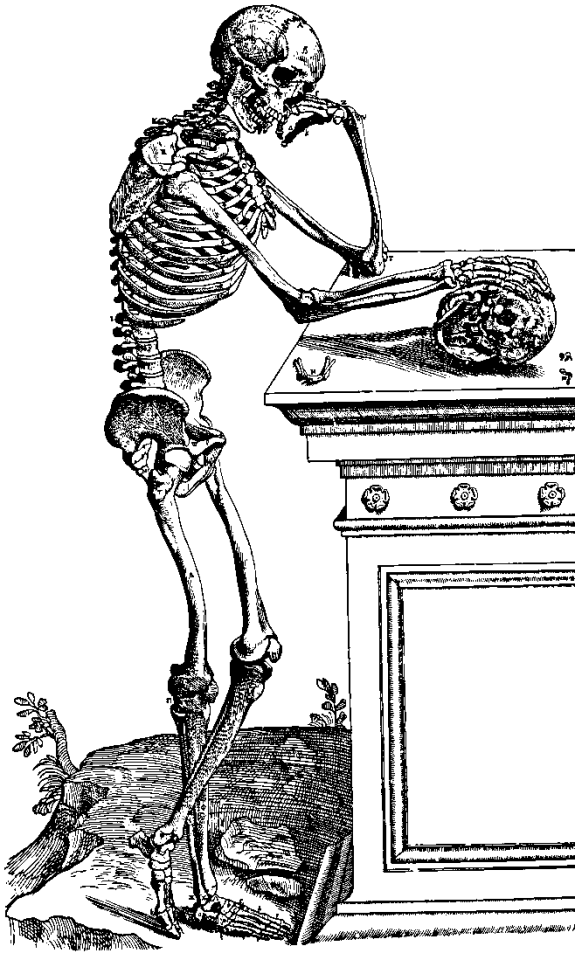

Society of Skeletal Radiology
41st Annual Meeting

March 25-28, 2018

JW Marriot Austin

Austin, TX

Table of Contents

Welcome

Society of Skeletal Radiology

41st Annual Meeting
March 25-28, 2018
JW Marriott Austin
Austin, TX

Welcome to the 41st Annual SSR Scientific Meeting at the JW Marriott Austin in Austin, Texas! We hope that you are getting excited about another fantastic scientific program in the center of music, food and friends.

This meeting is made possible only though the tireless efforts of our committee chairs, the executive committee, and our management team at Veritas Meeting Solutions. Although the meeting is the visible reward of that work, activities of the society leadership occur year-round. Thank you to all those who contribute.

A special thank you goes to Jenny Bencardino and Stephanie Bernard for coordinating this year's SAMs, with added audience participation. Thanks also to Ben Levine for coordinating the Ultrasound Hands-On Session (this year focusing on the Hip) and Daniel Wessel for coordinating the Case-of-the-Day.

Abstract and Eposter submission quality were impressive this year, with several submissions in automated intelligence related to MSK Radiology. In addition, the University of Toronto will provide an overview of their AI software, which won the RSNA Pediatric Bone-Age Challenge. As before, ePosters have been arranged into groups corresponding to the topics in the scientific sessions. SSR is proud to continue to offer the Seed Grant and Young Investigator Awards. Be sure to remind your Fellows / MIT members about this member benefit, as awards are selected by the Research Committee in January of the Meeting year.

Microphone, projected screen and Twitter interaction will be provided in order to maximize audience participation. All podium and poster authors have been asked to set up Twitter conversations regarding their presentations, so that participants can continue discussion on each topic after the allotted general discussion period for each paper. Look for the "hashtag" identifier on the presentation slides. SSR will record the SAM presentations in an effort to provide ongoing access to members through the year. More ways the Society is trying to bring value to its members!

The program committee invites you to relax and enjoy this year's offerings, both in and out of the meeting room.

Warmly,

Laura W. Bancroft, MD, FACR
2018 Program Committee Chair

2017–2018 Committees

EXECUTIVE COMMITTEE

President
Andrew Sonin, MD, FACR

President-Elect
Laura Bancroft, MD, FACR

Secretary
Lawrence White, MD

Treasurer
Donna Blankenbaker, MD

Past President
William Morrison, MD

Audit Committee
Johnny Monu, MD (Committee Chair)
Thomas Lee Pope Jr., MD, FACR
Elaine Gould, MD

Electronic Learning Committee
Jeffrey M. Brody, MD, FACR (Committee Chair)
Theodore Miller, MD
Jon Jacobson, MD
Connie Chang, MD
Travis Hillen, MD
Catherine Roberts, MD
Ken Schreibman, MD
Matthew Larrison, MD

Finance Committee
Donna Blankenbaker, MD (Committee Chair)
Doug Mintz, MD
Michael Tuite, MD

Historical Committee
Charles Resnik, MD (Committee Chair)
Barbara Weissman, MD
William Conway, MD

Membership Committee
Scott E. Preusen, MD (Committee Chair)
Jon Baker, MD
Judy Blebea, MD
Darus "Lee" Bennett, MD
Michael Fox, MD
Sarah Koles, MD

Nominating Committee
Corrie Yablon, MD (Committee Chair)
Wendy E. McCurdy, MD (Chair of Rules Committee)
Andrew Sonin, MD, FACR (President)

Practice Guidelines and Technical Standards Committee
Mary Gabriella Hochman, MD, MBA (Committee Chair)
Richard Walker, MD
Daniel Siegal, MD
Tony Wong, MD
Alex Rosioreanu, MD
Rob Wissman, MD

Program Committee
Laura W. Bancroft, MD, FACR (Committee Chair)
Lawrence M. White, MD
Catherine Roberts, MD
Mihra S. Taljanovic, MD

Research Committee
Hakan Ilaslan, MD (Committee Chair)
Andrew Cordle, MD
Meera Raghavan, MD
Jordan Scotty Gross, MD
MK Jesse, MD
Daria Motamedi, MD

Residency and Fellowship Education Committee
Bethany U. Casagranda, DO (Committee Chair)
Jennifer Demertzis, MD
Suzanne Long, MD
Rachel Hulen, MD
Ross Borzykowski, MD
Linda Probyn, MD
Soterios Gyftopoulos, MD
Hilary Umans, MD
Adam Zoga, MD

Rules Committee
Wendy E. McCurdy, MD (Committee Chair)
Jim Wu, MD
Geoffrey Riley, MD
Shaifali Kaushik, MD
Jonathan Luchs, MD
Kambiz Motamedi, MD

Socioeconomic Affairs Committee
Paul P. Harkey, MD (Committee Chair)
Erick Friedberg, MD
Lee Hoagland, MD
David W. Tsai, MD
Gregory Harkey, MD
Jonathan Flug, MD

Executive Office
Veritas Meeting Solutions
Sue O'Sullivan, Executive Director
1061 East Main Street, Suite 300
East Dundee, IL 60118
Email: admin@skeletalrad.org
Phone: 847-752-6626

Accreditation

Sponsored for Continuing Medical Education credit by Rush University Medical Center

Learning objectives

At the conclusion of this activity, the learner will be able to:

1. Apply real life situations to clinical practice;
2. Integrate knowledge and performance in the assessment and diagnosis of musculoskeletal sports injury, tumors, trauma and degenerative disease;
3. Identify the anatomy of normal MSK tissues, variants and mimicker of disease;
4. Identify morphologic, histologic and imaging characteristics of MSK disease;
5. Describe the specific pathology that accounts for the appearance of osseous and soft tissues in the setting of trauma, overuse, degeneration, inflammatory/autoimmune and neoplastic conditions on various imaging modalities;
6. Recognize the relationship of specific biomechanical activities, injuries and treatments to the appearance of joints, bone, and soft tissues on imagine, arthroscopic, and pathologic assessment;
7. Review the optimal role of imaging, surgery and histopathology in the diagnosis and management of musculoskeletal disease and health;
8. Identify the complementary role of emerging imaging techniques, modalities, and interventional/therapeutic procedures in the diagnosis and management of specific musculoskeletal conditions;
9. Illustrate competency in Ultrasound, MRI, and therapeutic approaches in the assessment and management of the musculoskeletal system.

To obtain credit you must be present for the session, complete the program evaluation, and return it to staff. Certificates of participation will be sent by e-mail 7-10 days after the closing of the Society of Skeletal Radiology Annual Meeting.

Rush University Medical Center is accredited by the Accreditation Council for Continuing Medical Education to provide continuing medical education for physicians. Rush University Medical Center designates this live activity for a maximum of 20.25 AMA PRA Category 1 Credit(s)™ Physicians should claim only credit commensurate with the extent of their participation in the activity.

It is the policy of the Rush University Medical Center Office of Interprofessional Continuing Education to ensure that its CE activities are independent, free of commercial bias and beyond the control of persons or organizations with an economic interest in influencing the content of CE. Everyone who is in a position to control the content of an educational activity must disclose all relevant financial relationships with any commercial interest (including but not limited to pharmaceutical companies, biomedical device manufacturers, or other corporations whose products or services are related to the subject matter of the presentation topic) within the preceding 12 months. If there are relationships that create a conflict of interest, these must be resolved by the CE Course Director in consultation with the Office of Interprofessional Continuing Education prior to the participation of the faculty member in the development or presentation of course content.

Specific Planner and Faculty disclosures can be found on the CME handout in your registration packet.

In accordance with requirements of the FDA, the audience is advised that information presented in this continuing medical education activity may contain references to unlabeled or unapproved uses of drugs or devices. Please refer to the FDA approved package insert for each drug/device for full prescribing/utilization information.

Self-Assessment Module (SAM)

This module (or activity) meets the ABR's criteria for a self-assessment activity in the ABR Maintenance of Certification program:

Focus Session / Self-Assessment Module I: **Axial Arthropathies: Diagnosis and Differentials** *1.5 credits*

Focus Session / Self-Assessment Module II: **Imaging of Sports Injuries** *1.5 credits*

Musculoskeletal Ultrasound Hands-On Workshop: Hip

Needs

Achieving competence in ultra sound of the hip not only depends on knowledge of anatomy and pathology, but also familiarity with various techniques of acquiring ultrasound images including positioning, placement of the probe and methods for visualization of structures and avoiding artifact. Successful ultrasound of the hip is largely dependent on the skills of the individual performing the ultrasound. One of the most effective learning formats is a hands- on workshop supervised by experienced instructors.

Objectives

At the completion of the ultrasound workshop, the participant will able to:

- Explain and perform ultrasound examination of the Hip

SSR Paper Award Winners

2017
Soterios Gyftopoulos, MD
"Cost-effectiveness of MRI Versus Ultrasound for the Detection of Full-thickness Rotator Cuff Tears"
Selected for presentation at RSNA

John Symanski, MD
"Diagnosis of Superior Glenoid Labral Tears Using MRI and MRA: A Systematic Review and Meta-Analysis"
Selected for presentation at ISS

2016
Naveem Subhas, MD
"A 5-minute shoulder MRI: Is it Good Enough?"
Selected for presentation at RSNA

MK Jesse, MD
"Radiculopathy Following Vertebral Body Compression Fracture: Is There a Role for Percutaneous Cement Augmentation?"
Selected for presentation at ISS

2015
Soterios Gyftopoulos, MD
"Rotator Cuff Tear Shape Characterization: A Comparison of 2D Imaging and 3D MR Reconstruction"
Selected for presentation at ISS

Ken Lee, MD
"Ultrasound-guided Treatment for Refractory Plantar Fasciopathy: A Randomized Controlled Pilot Study of Platelet-Rich Plasma Versus Standard of Care Corticosteroid Injections"
Selected for presentation at RSNA

2014
Mary Kristen Jesse, MD
"3D Morphologic Assessment of Normal and Abnormal Si Joints and the Potential Implications in the Development of Pain Syndrome"
Selected for presentation at ISS

Lawrence White, MD
"Femoroacetabular Impingement: Accuracy of Non-Arthrographic 3T MR Imaging in Evaluation of Intra-Articular Pathology of the Hip"
Selected for presentation at RSNA

2013
Lien Senchak, MD
"Imaging of Osteoblastoma of the Appendicular Skeleton with Pathologic Correlation:
Selected for presentation at ISS

Mary Kristin Jesse
"Morphology of Endplate Cement Estravasation Can Predict Adjacent Level Fracture in Osteoporotic Patients Undergoing Vertebroplasty and Kyphoplasty" *Selected for presentation at RSNA*

2012
Meredith Hayes, MD
"Phosphaturic Mesenchymal Tumors Imaging Features of a Rare Entity with Clinicopathologic Correlation"
Selected for presentation at ISS

Srinivasan Harish, FRCPC
"MRI of the Spine and Sacroiliac Joints for Spondyloarthropathy: Influence on Clinical Diagnostic Confidence and Patient Management"
Selected for presentation at RSNA

2011
Tal Laor, MD
"Juvenile Osteochondritis Dissecans (JOCD): Is It a Growth Disturbance of the Secondary Physis of the Epiphysis?"
Selected for presentation at ISS

Donna Blankenbaker, MD
"MR Arthrographic Appearance of the Post-Operative Acetabular Labrum"
Selected for presentation at RSNA

2010
Maxime Freire, MD
"MR Evaluation of Repair Tissue in Osteochondral Defects Following Treatment with Acellular Scaffolds: High Resolution MR-Histological Correlation in a Goat Model" *Selected for presentation at ISS*

Peter MacMahon, MD
"Injectable Corticosteroid Preparations: An Embolic RiskAssessment by Static and Dynamic Microscopic Analysis" *Selected for presentation at RSNA*

2009
Christopher J. Hanrahan, MD, PhD
"Temporal Evolution of MRI Findings after Rotator Cuff Repair" *Selected for presentation at ISS*

Kevin Johnson, MD
"Contrast-Enhanced Ultrasound Characterization of the Vascularity of the Repaired Rotator Cuff" *Selected for presentation at RSNA*

2008
Stephanie A. Bernard, MD
"Cartilage Cap Thickness Measurement on T2-Weighted MR Imaging and the Risk of Secondary Chondrosarcoma in Osteochondromas"
Selected for presentation at ISS

Kelley W. Marshall, MD
"Osteochondral Lesions of the Lateral Trochlea in the Pediatric Athlete with Elbow Pain"
Selected for presentation at RSNA

2007
Adam Zoga, MD
"The Sports Hernia: What Is It? How Do I image It? What Are Its Confounders?"
Selected for presentation at ISS

Tal Laor, MD
"The Effect of Childhood Growth on the Anterior and Posterior Cruciate Ligaments"
Selected for presentation at RSNA

2006
Eric T. Chou, MD
"Bifurcated Distal Biceps Brachii Tendon: Magnetic Resonance Imaging Appearances and Prevalence"
Selected for presentation at ISS

Lawrence M. White, MD
"Direct MR Arthrographic Assessment of Recurrent Symptoms Post Shoulder Instability Repair: Correlation with Second Look Surgical Evaluations in 40 Patients"
Selected for presentation at RSNA

2005
Steven S. Gerguis, MD
"Review of the Secondary Signs of Femoracetabular Impingement and Correlation with the Head-neck Angle Measured on the Frog-Leg Lateral View"
Selected for presentation at ISS

Suzanne E. Anderson, BMed
"Computer-assisted Software for Accurate Determination of Acetabular Coverage with Conventional Radiography"

2004
Mihra Taljanovic, MD, MS
"Bone Marrow Edema in Hip Osteoarthritis: Quantitative Assessment with MRI and Correlation with Clinical Exam, Radiographic Findings and Histopathology"

2003
Joseph R. DeMartini, MD
"Effects of MR Gradient Coil- Induced Vibration Artifacts and Inherent Pulse Sequence Imperfections on Phase"

2002
Derek R. Armfield, MD
"MRI of Posterior Medial Meniscal Root Avulsion"

2001
Patrick T. Liu, MD
"Improved Imaging of Osteoid Osteoma with Dynamic Gadolinium-Enhanced MRI"

2000
Timothy G. Sanders, MD
"MRI at Different Time Intervals Following Hamstring Harvest for ACL Reconstruction"

Patrick T. Liu Innovation in Research Award Recipient

2017
Micah Cohen, MD
"X-ray and MRI of Diabetic Foot Osteomyelitis. Review of Pathologically Proven Surgically Treated Cases: MRI Shows Better but What Does It Mean?"

2016
Robert Boutin, MD
"CT of Hip Fracture Patients: Can Muscle Size & Attenuation Predict Clinical Outcomes?"

2015
David Melville, MD
"Diffusion Tensor MR Imaging of Quadriceps Musculature in the Setting of Clinical Fragility Syndrome"

Joshua M. Polster, MD
"Enhanced Detection of CT-Occult Bone Marrow Lesions In The Lumbar Spine Using Trabecular Suppression"

2014
Gandikota Girish, MD
"Photoacoustic Imaging of Joints"

2013
Douglas P. Beall, MD
"Tissue Distribution of Clondine Following Intraforminal Implantation of Biodegradablepellets: Potential Alternative to Epidural Steroid for Radiculopathy"

2012
Joshua M. Polster, MD
"Single Energy Post – Processing Technique for Bone Marrow Imaging on CT"

2011
Kenneth Lee, MD
"Treatment of Chronic Lateral Epicondylosis Using Hyperosmolar Dextrose Solution: CanAcoustoelastography Monitor Tissue Healing?"

AIRP Award – Best Poster

2017
Xue Susan Bai, MD; Alice S. Ha, MD;
Susan Ng, MS; Katelyn Nye, BS;
John M. Sabol, PhD
"Not Your Grandma's X-ray: Utility of Advanced Reconstruction and Visualization Methods for Digital Tomosynthesis of Bone and Joint Pathology"

2016
Barrett Luce, MD; Michael Fox, MD;
David Diduch, MD
"Assessment of Femoral Trochlear Morphology on Cross SectionalImaging: Comparing the Dejour Classification and Quantitative Measurements in Patients Later Treated with Deepening Trochleoplasty"

2015
Shefali Kothary MD
"Imaging Spectrum of Pectoralis Tears"

SSR Excellence Award

2013
Luke Scalcione, MD
"Hallux Valgus: Spectrum of Imaging, Surgical Procedures, and Complications"

2011
Luis Beltran, Jason Mayo, Jenny Bencardino, Zehava Rosenberg, Luis Neto Pecci, Maria Diaz de Tuesta, Olga Ruiz
"Diagnostic Evaluation of Hip Dysplasia in the Young Adult – Emphasis on Cross-Sectional Imaging"

ACR Education Award – Best Poster

2017
Pardeep Athwal, MD; Megan K. Mills, MD; Mark Mahan, MD; Kevin R. Moore, MD; Barry G. Hansford, MD; Chrish J. Hanrahan,MD; Anna K. McGow, MD; Sarah E. Stilwill, MD
"Traumatic and Non-Traumatic Brachial Plexus Imaging: What the Practicing Radiologist Needs to Know"

2016
Usman Anwer, MD
Corrie Yoblon, MD
"A Sound Approach to Peripheral Neuropathies"

2015
Kimia K Kani, MD
"MR Imaging of Soft Tissue Injuries of the Fingers"

2014
David Melville, MD
"Osteoarthritis of the Basal Joints of the Thumb: Imaging and Management"

Young Investigator Award Winners

2017
Timothy Dickson, MD
"Clinical Findings and Imaging Appearances of Angiomyomas"

Jennifer L. Favinger, MD
"Soft Tissue Sarcoma Response to Two Cycles of Neoadjuvant Chemotherapy: a Multi-Therapy Analysis of MRI Findings and Agreement Between RECIST Criteria and SUVmax"

Corey Ho, MD
"Temporal Assessment of the Ligamentization Process of Anterior Cruciate Ligament Graft Utilizing a Nevel Ultrashort T2* Sequence (UTE)"

O. Kenechi Nwawka, MD
"Ultrasound for Brachial Plexopathy: Prospective Correlation to MRI, EMG, and Surgical and Clinical Findings"

2016
Connie Y. Chang, MD
"Quantitative CT Density Evaluation of Osseous Metastases Following Chemotherapy"

Erin FitzGerald Alaia, MD
"Imaging Features on Ibalance, New High Tibial Osteotomy: What the Radiologist Needs to Know"

Elisabeth Garwood, MD
"Clinical Utility of Shoulder Imaging in the Outpatient Setting: A Pilot Study"

Tony Wong, MD
"Utility of 3D Print Models for Pre-Operative Planning in Femoroacetabular Impingement"

2015
Shivani Ahlawat, MD
"Traumatic Neuromas: Common MRI Features"

Kimia K Kani, MD
"Concepts of Operative Treatment in Scapholunate Instability: An Imaging Perspective"

Lauren M. Ladd, MD
"Quantitative and Qualitative Comparison of 3.0t versus 1.5t Warp Imaging of Hip Prostheses"

Daniel Siegal, MD
"Sonographic Evaluation of the Distal Biceps Tendon: Accuracy and Pitfalls in the diagnosis of Partial Thickness Tears"

Andrew Wilmot, MD
"Subchondral Insufficiency Fracture of the Knee: Revising the Epidemiology and Soft Tissue Edema Pattern"

2014
Luis Beltran
"Anatomy, Diagnostic Pitfalls and Variants of the Shoulder Joint in Abduction and External Rotation MR Arthrography"

Shadpour Demehri
"Accuracy of Conventional and Functional MRI in Diagnosing Indeterminate Peripheral Nerve Sheath"

Alice Ha
"Digital Tomosynthesis to Detect Bone Healing?: Comparison to Radiography and ComputedTomography"

Kaushal Mehta
"Superolateral Hoffa's Fat Pad Edema in Collegiate Volleyball Players"

2013
Gyftopoulos, Soterios, MD
"Correlation of MIR with Arthroscopy for the Diagnosis of Subscapularis Tendon Tears"

Raghavan, Meera, MD, BS
"Radiomics of Soft tissue Sarcoma-Comuter-Aided Image Analysis and Characterization of Tumor Heterogeneity"

Rantiolu Aro, Michael, MD
"Anatomic Variations of Femoral Nerves on High Resolution 3 Tesla Magnetic Resonance Neurography and Their Relation to Abnormal Nerve and Muscle Imaging Findings"

2012
Bethany Casagranda, DO
"Coronal Oblique Imaging of The Knee: Can It Increase Radiologists' Confidence in Diagnosing Posterior Root Meniscal Tears?"

Glenn Gaviola, MD
"Assessment of Fellowship Trainee Clinical Competency and Growth with an Objective Standardized Clinical Examination Within the Musculoskeletal Fellowship Program: Initial Experience"

Jonelle Petscavage, MD, MPH
"Magnetic Resonance Imaging Findings of Adverse Reactions to Metallic Debris (ARMD) of Metal-On-Metal Total Hip Replacements"

Naveen Subhas, MD
"Metal Artifact Reduction Using a Monoenergetic Dual Energy CT Technique"

SSR Seed Grant Research Award

2017
Michael Fadell, MD
"Utilization of non-invasive MR imaging to differentiate between infectious and noninfectious fluid in septic arthritis"

2016
Kenneth S. Lee MD, Andrew B. Ross, MD
Rapid MRI protocol for the Evaluation of Potential Hip Fractures in the Elderly

Thank You to Our 2018 Exhibitors

Special thanks to the following companies for their support to the Society of Skeletal Radiology in 2018.

Platinum
AprioMed Inc.

Bronze
TBD

SSR Past Presidents

William Bonner Guilford, MD
July 1978 – June 1980

Jeremy J. Kaye, MD
July 1980 – June 1982

Cosmo L. Haun, MD
July 1982 – June 1984

William W. Daniel, MD
July 1984 – June 1986

Anne C. Brower, MD
July 1986 – June 1988

Jeno I. Sebes, MD
July 1988 – June 1990

Murali Sundaram, MD
July 1990 – June 1992

Charles S. Resnik, MD
July 1992 – June 1994

William Bonner Guilford, MD
July 1994 – June 1996

Terry M. Hudson, MD
July 1996 – June 1998

William F. Conway, MD, PhD
July 1998 – June 2000

Arthur A. De Smet, MD
July 2000 – June 2002

B.J. Manaster, MD, PhD
July 2002 – June 2004

Arthur H. Newberg, MD
July 2004 – June 2006

Cheryl A. Petersilge, MD
July 2006 – June 2008

Mark J. Kransdorf, MD
July 2008 – March 2010

Carol L. Andrews, MD
April 2010 –March 2012

Kenneth Buckwalter, MD
April 2012 – March 2014

William Morrison, MD
April 2014 – March 2016

Ultrasound Workshop Instructors

Organizer:

Benjamin Levine, MD - UCLA Medical Center
Santa Monica, CA

Lecturers:

Jon Jacobson, MD – University of Michigan
Ann Arbor, M

Theodore Miller, MD – Hospital for Special Surgery
Mamaroneck, NY

Instructors:

Oganes Ashikyan, MD – Univ. of Texas Southwestern
Dallas, TX

Meg Chiavaras, MD, PhD – McMaster University
Hamilton, ON, CAN

Mark Cresswell, MD – University of British Columbia
Vancouver, BC, CAN

Mark Diamond, MD – Henry Ford Hospital
Detroit, MI

Gina A. DiPrimio, MD – The Ottawa Hospital
Ottawa, ON, CAN

Jordan Gross, MD – Keck School of Medicine of USC
Los Angeles, CA

Tudor Hughes, MD – Univ. of California, San Diego
San Diego, CA

Nick Kolanko, MD –Stoney Brook Medical Center
Stoney Brook, NY

Robert Lopez, MD – Charlotte Radiology, PA
Charlotte, NC

Kevin McGill, MD – Henry Ford Hospital
Detroit, MI

Kambiz Motamedi, MD – UCLA
Los Angeles, CA

Akira Murakami, MD – Boston University
Boston, MA

Matthew O'Brien, MD –Brigham & Women's Hosp.
Boston, MA

Linda Probyn, MD –University of Toronto
Toronto, ON, CAN

Mitchell Scheer, MD –Henry Ford Hospital
Detroit, MI

Mihra Talijanovic, MD – University of Arizona
Tucson, AZ

Thank You to the Following Companies for the In Kind Support of Ultrasound Equipment Loaned for this Workshop

TBD

SSR RED FUND Donors

2017-2018 Contributors

Paul Morgan Aitchison, MD
Behrang Amini, MD, PhD
Carol L. Andrews, MD
Laura W. Bancroft, MD, FACR
Royce James Biddle, MD
Cary Bizzell, MD
Brandon Black, MD
Judy Sanna Blebea, MD
George Thomas Bolton, MD, DVM
Jeffrey M. Brody, MD, FACR
Nathalie Josee Bureau, MD
Lisabeth Ann Bush, MD
Patrick Cherry, MD
Robert Hanley Choplin, MD
Ivan Christopher Davis, MD
William Rhey Dunfee, MD
Timothy R. Enright, MD
Peter Thomas Evangelista, MD
Donald Joel Flemming, MD
Siddi Ganie, MD
Michael S. Gibson, MD
Angel Alberto Gomez, MD, MPH
Elaine Susan Gould, MD
W. Bonner Guilford, MD
Mary Gabriella Hochman, MD, MBA
Brian A. Howard, MD
John C. Hunter, MD
James S. Jelinek, MD
Mark J. Kransdorf, MD
Laura Haeryun Lee, MD
Kenneth S. Lee, MD
Laurie M. Lomasney, MD
Jonathan S. Luchs, MD
Kelley Woodruff Marshall, MD
David Alan May, MD
Wendy E. McCurdy, MD
Joshua M. McDonald, MD
Timothy Eisdell Moore, MD
Yoav Morag, MD
William Brian Morrison, MD
Darra Thomas Murphy, MD, FFR(RSCI), FRCPC
Erik N. Nelson, MD
Alan Patrick Northington, MD
Cheryl A. Petersilge, MD
Brian David Petersen, MD
Scott E. Preusen, MD, JD
Andres Rahal, MD, PhD
Michael L. Richardson, MD
Trenton D. Roth, MD
Hamid Salamipour, MD
David C. Salonen, MD, FRCPC
Marcos Loreto Sampaio, MD
John Michael Smith, MD
Andrew Sonin, MD, FACR
Troy F. Storey, MD
James Anthony Thesing, DO
D. Dean Thornton, MD
Joseph Triolo, MD
Josue Vazquez, MD
Lawrence M. White, MD
James Neal Wise, MD
Corrie M. Yablon, MD

Program Schedule Overview

General Session will be located in the Lone Star Ballroom E-H unless otherwise noted.

Sunday, March 25, 2018

7:00 a.m.– 7:55 a.m.	CONTINENTAL BREAKFAST
7:00 a.m. – 5:00 p.m.	REGISTRATION/INFORMATION DESK OPEN
7:00 a.m. – 1:30 p.m.	EXHIBIT HALL OPEN
7:00 a.m. – 4:30 p.m.	*POSTER SESSION*
7:45 a.m. – 8:50 a.m.	**SSR ANNUAL BUSINESS MEETING**
9:00 a.m. – 9:15 a.m.	2017 SEED GRANT RESEARCH AWARD RECIPIENT PRESENTATION
9:15 a.m. – 10:15 a.m.	OPENING SESSION
10:15 a.m. – 10:20 a.m.	**CASE OF THE DAY**
10:20 a.m. – 10:45 a.m.	BREAK – VISIT EXHIBIT HALL
10:45 a.m. – 12:00 p.m.	EMERGING TECHNOLOGIES
12:00 p.m. – 12:05 p.m.	**CASE OF THE DAY**
12:05 p.m. – 1:30 p.m.	LUNCH (in Exhibit Hall or Industry Sponsored Lunch Symposium)
1:30 p.m. – 3:00 p.m.	**FOCUS SESSION/SELF ASSESSMENT MODULE (SAM I)** ***"Axial Arthropathies: Diagnosis and Differentials"***
3:00 p.m. – 3:10 p.m.	BREAK – VISIT EXHIBIT HALL
3:10 p.m. – 4:40 p.m.	**FOCUS SESSION/SELF ASSESSMENT MODULE (SAM II) "*Imaging of Sports Injuries*"**
4:40 p.m. – 5:00 p.m.	SAM EXAM

Monday, March 26, 2018

7:00 a.m. – 7:55 a.m.	CONTINENTAL BREAKFAST
7:00 a.m. – 12:35 p.m.	REGISTRATION/INFORMATION DESK OPEN
7:00 a.m. – 12:30 p.m.	EXHIBIT HALL OPEN
7:00 a.m. – 12:30 p.m.	*EPOSTER SESSION*
7:45 a.m. – 8:00 a.m.	SSR INVITED KEYNOTE PRESENTATION
8:00 a.m. – 10:00 a.m.	UPPER EXTREMITY
10:00 a.m. – 10:05 a.m.	**CASE OF THE DAY**
10:05 a.m. – 10:30 a.m.	BREAK – VISIT EXHIBIT HALL
10:30 a.m. – 12:30 p.m.	INTERVENTION / POSTOPERATIVE
12:30 p.m. – 12:35 p.m.	**CASE OF THE DAY**
1:00 p.m. – 3:00 p.m.	**MSK ULTRASOUND HANDS-ON WORKSHOP/ HIP** (*separate registration and fee required)*
6:00 p.m. – 9:30 p.m.	SSR ANNUAL BANQUET – BRAZOS HALL (2 BLOCKS FROM HOTEL)

Tuesday, March 27, 2018

7:00 a.m. – 7:55 a.m.	CONTINENTAL BREAKFAST
7:00 a.m. – 12:35 p.m.	REGISTRATION/INFORMATION DESK OPEN
7:00 a.m. – 12:30 p.m.	EXHIBIT HALL OPEN
7:00 a.m. – 12:30 p.m.	*EPOSTER SESSION*
8:00 a.m. – 10:00 a.m.	HIP / PELVIS
10:00 a.m. – 10:05 a.m.	**CASE OF THE DAY**
10:05 a.m. – 10:30 a.m.	BREAK – VISIT EXHIBIT HALL
10:30 a.m. – 12:30 p.m.	TRAUMA / MISCELLANEOUS
12:30 p.m. – 12:35 p.m.	**CASE OF THE DAY**
1:00 p.m.	SSR Annual Golf Outing (*separate registration and fee required) – Shuttle leaves at 12:00 p.m.*
5:00 p.m.	OPTIONAL - Bat Bridge and Pub Crawl

Wednesday, March 28, 2018

7:00 a.m. – 7:55 a.m.	CONTINENTAL BREAKFAST
7:00 a.m. – 12:30 p.m.	REGISTRATION/INFORMATION DESK OPEN
7:00 a.m. – 10:30 a.m.	EXHIBIT HALL OPEN
7:00 a.m. – 10:30 a.m.	*EPOSTER SESSION*
8:00 a.m. – 10:00 a.m.	TUMOR
10:00 a.m. – 10:05 a.m.	**CASE OF THE DAY**
10:05 a.m. – 10:30 a.m.	BREAK – VISIT EXHIBIT HALL
10:30 a.m. – 12:30 p.m.	LOWER EXTREMITY

SSR Hotel Floor Plan - Level 3

SUNDAY

Society of Skeletal Radiology

41st Annual Meeting

March 25-28, 2018

Saturday, March 24, 2018

4:00 p.m.–6:00 p.m. **Registration/Information Desk Open**
Location: Lone Star Foyer

Sunday, March 25, 2018

7:00 a.m.–7:55 a.m. **Continental Breakfast**

7:00 a.m.–5:00 p.m. **Registration/Information Desk Open**

7:00 a.m.–1:30 p.m. **Exhibit Hall Open**

7:00 a.m.–4:30 p.m. **ePoster Session**

7:45 a.m.–8:50 a.m. **SSR Annual Business Meeting**

9:00 a.m.–10:15 a.m. **OPENING**
Moderators: Christine Chung, MD, Lynne Steinbach, MD

9:00 a.m. SG 2017 **2017 SEED GRANT RESEARCH AWARD RECIPIENT PRESENTATION**

9:15 a.m. #1 **MEDICARE CLAIMS CHARACTERIZATION OF SSR MEMBERSHIP CLINICAL PRACTICE PATTERNS**
Daniel Wessell, MD, PhD[1]; Richard Duszak, II, MD[2]; Wang Wenyi, MA[3]; Danny Hughes, PhD[3,4]; Andrew Rosenkrantz, MD[5]
[1]Mayo Clinic Florida, Jacksonville, FL, USA; [2]Emory University School of Medicine, Atlanta, GA, USA; [3]Harvey L. Neiman Health Policy Institute, Reston, VA, USA; [4]Georgia Institute of Technology, Atlanta, GA., Reston, VA, USA; [5]NYU Langone Health, New York, NY, USA
(Presented by: Daniel Wessell, MD, PhD, Mayo Clinic Florida)

9:30 a.m. #2 **TEXTURAL 3T MRI MEASURES OF PROXIMAL FEMUR BONE QUALITY AS BIOMARKERS OF FRACTURE RISK**
Kate Harrington, MD; Harrison Besser, MS; Gregory Chang, MD
NYU Medical Center/ Hospital for Joint Diseases Langone Medical Center, New York, NY, USA
(Presented by: Kate Harrington, MD, NYU Medical Center/ Hospital for Joint Diseases Langone Medical Center)

9:45 a.m. #3 **COST-EFFECTIVENESS OF MR ARTHROGRAPHY VERSUS MRI FOR SLAP TEARS**
Naveen Subhas, MPH, MD[1]; Jordan Conroy[2]; James Koo[3]; Morgan Jones, MD, MPH[1]; Anthony Miniaci, MD[1]; Soterios Gyftopoulos, MD, MS[3]
[1]Cleveland Clinic, Cleveland, OH, USA; [2]University Hosp of Cleveland / Case Western Reserve Univ Sch of Med, Cleveland, OH, USA; [3]NYU Medical Center/ Hospital for Joint Diseases Langone Medical Center, New York, NY, USA
(Presented by: Naveen Subhas, MPH, MD, Cleveland Clinic)

10:00 a.m. #4 **WOMEN IN ACADEMIC MUSCULOSKELETAL RADIOLOGY**
Kate Harrington, MD; Gregory Chang, MD
NYU Medical Center/ Hospital for Joint Diseases Langone Medical Center, New York, NY, USA
(Presented by: Kate Harrington, MD, NYU Medical Center/ Hospital for Joint Diseases Langone Medical Center)

10:15 a.m.–10:20 a.m. **CASE OF THE DAY**
Presenting Author: Andrew Chow, MD

10:20 a.m.–10:45 a.m. Break - Visit the Exhibit Hall

Sunday, March 25, 2018

10:45 a.m.–12:00 p.m. **EMERGING TECHNOLOGY**
Moderators: Christopher Beaulieu, MD, PhD, Corrie Yablon, MD

10:45 a.m. #5 **CT PIPELINE FOR SARCOPENIA SCREENING USING THE AUTOMATED MUSCLE ANALYSIS TOOL**
Leon Lenchik, MD[1]; Ryan Barnard, MS[1]; Josh Tan, MS[1]; Stephen Kritchevsky, PhD[1]; Ashley Weaver, PhD[1]; Joel Stitzel, PhD[1]; Robert Boutin, MD[2]
[1]Wake Forest University School of Medicine, Winston-Salem, NC, USA; [2]University of California, Davis, Sacramento, CA, USA
(Presented by: Leon Lenchik, MD, Wake Forest University School of Medicine)

11:00 a.m. #6 **3D-MRI VERSUS 3D-CT IN THE EVALUATION OF OSSEOUS ANATOMY IN FEMOROACETABULAR IMPINGEMENT**
Mohammad Samim, MD; Nima Eftekhary, MD; Thomas Youm, MD; Roy Davidovitch, MD; Jonathan Vigdorchik, MD; Soterios Gyftopoulos, MD
NYU Medical Center/ Hospital for Joint Diseases Langone Medical Center, New York, NY, USA
(Presented by: Mohammad Samim, MD, NYU Medical Center/ Hospital for Joint Diseases Langone Medical Center)

11:15 a.m. #7 **HUMAN VS. MACHINE: DISTINGUISHING ENCHONDROMA FROM CHONDROSARCOMA WITH A BAYESIAN NETWORK**
Christopher Beaulieu, MD, PhD; Bao Do, MD
Stanford University School of Medicine, Stanford, CA, USA
(Presented by: Christopher Beaulieu, MD, PhD, Stanford University School of Medicine)

11:30 a.m. #8 **OPPORTUNISTIC CT BONE DENSITY MEASUREMENTS CORRELATE WITH LONG-TERM OUTCOME IN PATIENTS WITH PROXIMAL FEMUR FRACTURES**
Jennifer Ni Mhuircheartaigh, MD; Daon Ha, MD; Ching-Di Chang, MD; Colm McMahon, MBBS; Jim Wu, MD
Beth Israel Deaconess Medical Center Harvard Med School, Boston, MA, USA
(Presented by: Jennifer Ni Mhuircheartaigh, MD, Beth Israel Deaconess Medical Center Harvard Med School)

11:45 a.m. #9 **PREDICTIVE UTILITY OF QUANTITATIVE SUPRASPINATUS TENDON AND MUSCLE SHEAR WAVE ULTRASOUND ELASTOGRAPHY: IS THERE A CORRELATION?**
Dana Lin, MD; Christopher Burke, MD; James Babb, PhD; Ronald Adler, MD, PhD
NYU Medical Center/ Hospital for Joint Diseases Langone Medical Center, New York, NY, USA
(Presented by: Dana Lin, MD, NYU Medical Center/ Hospital for Joint Diseases Langone Medical Center)

12:00 p.m.–12:05 p.m. **CASE OF THE DAY**
Presenting Author: Michael Brown, MD

12:05 p.m.–1:30 p.m. **LUNCH** (In Exhibit Hall or Industry Sponsored Lunch Symposium)

1:30 p.m.–3:00 p.m. **Focus Session/Self Assessment Module I** ***"Axial Arthropathies: Diagnosis and Differentials"***

3:00 p.m.–3:10 p.m. **Break** - Visit the Exhibit Hall

3:10 p.m.–4:40 p.m. **Focus Session/Self Assessment Module II "*Imaging of Sports Injuries*"**

4:40 p.m.–5:00 p.m. **SAM Exam**

Related ePosters

EMERGING TECHNOLOGIES

Poster #1 **WHOLE BODY (WB)-MRI WITH 3D VOLUMETRIC SEQUENCES AND ISOTROPIC RESOLUTION: A METHOD FOR FAST AND HIGH RESOLUTION WHOLE BODY IMAGING**

Shivani Ahlawat, MD; Jaishri Blakeley; Mike Jacobs, PhD; Laura Fayad, MD, MS
Johns Hopkins University, Baltimore, MD, USA

Poster #2 **Some New Angles on the Magic Angle: What MSK Radiologists Know and Don't Know**

Michael Richardson, MD[1]; Behrang Amini, MD, PhD[2]; Todd Richards, PhD[1]
[1]University of Washington / Harborview Medical Center, Seattle, WA, USA; [2]The University of Texas M.D. Anderson Cancer Center, Houston, TX, USA

Poster #3 **QUANTITATIVE ASSESSMENT OF CHANGE IN UPPER EXTREMITY MUSCLE STIFFNESS FOLLOWING FLUID INJECTION USING SHEAR WAVE ELASTOGRAPHY**

O. Nwawka, MD; Shivi Duggal, MD; Bin Lin, MS; Nicholas Gutierrez, MD; Theodore Miller, MD
Hospital for Special Surgery, New York, NY, USA

Poster #4 **3D PRINTING MAKES AN IMPOSSIBLE CASE POSSIBLE**

Carissa White, MD; Marc-Anthony Lecky; David Nelson; Mauricio Silva, MD; Anthony Scaduto, MD
David Geffen School of Medicine at UCLA, Los Angeles, CA, USA

Poster #5 **CLINICALLY RELEVANT RADIOLOGICAL INSIGHTS PROVIDED BY EN FACE MICROSCOPIC VISUALIZATION OF EROSIONS COMPLICATING ARTHRITIS, GRANULOMATOUS DISEASE, NEOPLASIA AND VASCULAR DISEASE**

Bruce Rothschild, MD
West Virginia University School of Medicine, Morgantown, WV, USA

2017 Seed Grant Research Award

Utilization of non-invasive MR imaging to differentiate between infectious and noninfectious fluid in septic arthritis

Michael F. Fadell II, MD[1]; Sarah Parker M.D.[1]; Seonghwan Yee, PhD[2]; John Hughes, PhD[2]
[1]Children's Hospital Colorado / University of Colorado Aurora, CO USA; [2]University of Colorado Aurora, CO USA
(Presented by: Michael F. Fadell II, MD)

Summary statement of the clinical impact/need for this research: Septic arthritis is a serious but treatable condition. Accurate diagnosis is critical to providing timely treatment and avoiding serious complications. The current standard of care requires invasive joint aspiration to sample joint fluid. A substantial proportion of patients who undergo joint aspiration do not have infected joint fluid in our clinical experience– an estimated 20% at our hospital and an estimated 32% reported in the literature. Accurate non-invasive methods are needed to avoid the associated risks and potential complications. A non-invasive imaging alternative allowing for the differentiation between normal and infected joint fluid would be a significant improvement in the evaluation of pediatric septic arthritis, with the added potential for future use in the adult population.

This will be the first study to modify existing MRI sequences to identifying sterile joint fluid in patients with suspected septic arthritis, thereby preventing the need for an invasive joint aspiration in a large percent of patients. All prior studies utilizing MRI in the evaluation of infected joint fluid have been retrospective reviews of medical records – our proposed research will be the first prospective study in this area.

Specific Aims:

Aim 1: Optimize currently utilized IR and DWI, to identify noninfectious joint fluid in pediatric patients with suspected musculoskeletal infections, specifically septic arthritis.

Aim 2: Validate the methods in a sample of children undergoing standard diagnostic workup for suspected septic arthritis, using laboratory, microbiology, and cytology results as the gold standard for presence of infection.

We specifically hypothesize that Inversion Recovery (IR) and Diffusion Weighted Imaging (DWI) can, with optimized and tailored acquisition parameters, identify the unique characteristics of noninfectious joint fluid in the workup of pediatric patients with concern for septic arthritis and/or periarticular musculoskeletal infections. Such identification would represent a significant improvement over the current diagnostic MRI used in the evaluation of these patients that are currently unable to differentiate sterile from infectious joint effusions. Knowledge gained from an augmented MRI protocol including all or some of the above-mentioned sequences could prevent invasive joint aspiration in a large percentage of these patients.

Research plan: We propose to tailor currently utilized MRI sequences, specifically inversion recovery (IR) and diffusion weighted imaging (DWI) to help identify non-infectious joint fluid. Using a range of inversion times, we will examine how the IR signal can be 'tuned' to null signal from normal joint fluid whilst still providing signal from infectious fluid. Similarly, using a range of diffusion weightings (b values), we will examine how DWI can be used to identify signal associated with the restricted and highly viscous infectious fluid. The goal of this pilot study is to provide preliminary evidence for a definitive prospective study that will provide the highest level of evidence for physicians treating suspected septic arthritis in children.

Podium #1

Medicare Claims Characterization of SSR Membership Clinical Practice Patterns

Daniel Wessell, MD, PhD[1]; Richard Duszak, II, MD[2]; Wang Wenyi, MA[3]; Danny Hughes, PhD[3,4]; Andrew Rosenkrantz, MD[5]
[1]Mayo Clinic Florida, Jacksonville, FL, USA; [2]Emory University School of Medicine, Atlanta, GA, USA; [3]Harvey L. Neiman Health Policy Institute, Reston, VA, USA; [4]Georgia Institute of Technology, Atlanta, GA., Reston, VA, USA; [5]NYU Langone Health, New York, NY, USA
(Presented by: Daniel Wessell, MD, PhD, Mayo Clinic Florida)

Purpose: To characterize Medicare services billed by current SSR members.

Materials and Methods: With SSR Executive Committee permission, national provider identifiers (NPIs) were manually identified for all SSR members (who had all attested to >50% of one's practice in musculoskeletal [MSK] radiology). NPIs permitted member cross-linking to the 2015 CMS Physician and Other Supplier Public Use File to then identify all services each billed Medicare. Service codes were mapped to seven mapping-validated subspecialties (MSK, abdominal, breast, cardiothoracic, neuroradiology, nuclear medicine, and vascular-interventional radiology [VIR]) using the Neiman Imaging Types of Service classification system. Radiologists' percentages of work RVUs (wRVU) in each subspecialty were computed. Various subgroup analyses were performed.

Results: Of 1,014 SSR members, 49.5% performed ≥50% of their wRVUs in MSK (Table 1). In terms of billed wRVUs, 53.4% of these radiologists mapped to a secondary subspecialty of neuroradiology in terms of billed wRVUs, 16.3% to abdominal, 11.8% to cardiothoracic, and 5.2% to VIR. Of all SSR members, 45.6% were generalists (i.e., no subspecialty crossed the majority wRVU threshold), but 37.4% of them performed a plurality of work in MSK. No other subspecialty accounted for greater than 2% of SSR members. A higher percentage of MSK wRVUs was significantly associated ($p<0.001$) with an academic affiliation (66.8% vs. 44.5%) as well as two different markers of greater SSR engagement: 1) attending the 2014 SSR meeting (63.5% vs. 49.9%) and 2) serving as an SSR committee member (75.7% vs. 51.6%) (Table 2). Of all other 27,618 Medicare-participating radiologists nationally meeting inclusion criteria, 3.2% (879) had ≥50% of their wRVUs in MSK but are not SSR members.

Conclusion: Medicare claims-based practice classification provides unique insight into SSR membership. This information may help better understand current membership needs, plan future meeting content, and guide further society growth.

Modality % - Radiography / Fluoroscopy:	50
Modality % - CT:	10
Modality % - MRI:	30
Modality % - US:	9
Modality % - Nuclear Medicine:	9

Table 1-Primary subspecialty based on billed Medicare claims among 1,014 SSR members. Radiologists are only assigned a subspecialty if their highest % wRVUs in any subspecialty exceeds 50%, and are deemed generalists if not achieving a 50% threshold.

Subspecialty	n	%
Musculoskeletal	502	49.5%
Generalist	462	45.6%
Neuroradiology	17	1.7%
Abdominal	13	1.3%
Vascular and interventional	7	0.7%
Cardiothoracic	7	0.7%
Breast	5	0.5%
Nuclear medicine	1	0.1%

Table 1: Primary Subspecialty Categorization

Table 2-Comparison of claims-based MSK subspecialization among characteristics of SSR members

Cohort	n	Mean±SD % wRVUs in MSK*	% (n) exceeding 50% threshold of wRVUs in MSK**
Did not attend 2014 SSR meeting	786	49.9%±28.8%	44.8% (352)
Attended 2014 SSR meeting	228	63.5%±27.4%	65.8% (150)
Not SSR committee member	958	51.6%±28.8%	47.4% (454)
SSR committee member	56	75.7%±23.0%	85.7% (48)
Private practice	313	44.5%±26.3%	34.8% (109)
Academic	266	66.8%±27.7%	72.6% (193)

-Academic vs. private only listed when available for given radiologist in SSR member database.
-*All three comparisons based on radiologist characteristics significant at p<0.001 using Mann-Whitney test
-**All three comparisons based on radiologist characteristics significant at p<0.001 using Fisher's exact test

Table 2: Subgroup Analyses

Podium #2

TEXTURAL 3T MRI MEASURES OF PROXIMAL FEMUR BONE QUALITY AS BIOMARKERS OF FRACTURE RISK

Kate Harrington, MD; Harrison Besser, MS; Gregory Chang, MD
NYU Medical Center/ Hospital for Joint Diseases Langone Medical Center, New York, NY, USA
(Presented by: Kate Harrington, MD, NYU Medical Center/ Hospital for Joint Diseases Langone Medical Center)

Purpose: To determine the relationships between textural 3T MRI derived measures of proximal femur bone quality and age, body mass index (BMI), and fracture risk.

Materials and Methods: The study had institutional review board approval. The proximal femurs of 23 female subjects were imaged on a 3T MRI scanner. Scanning parameters were TR/TE=37ms/4.92ms, flip angle=25^0, bandwidth=130Hz/pixel, field of view=120 mm, in-plane voxel dimension=0.775mmx0.775mm, parallel imaging (GRAPPA) factor=2, slice thickness=2 mm. 40 coronal slices were segmented using an in-house software program (FireVoxel). We computed mean bone volume, mean signal intensity (SI), and mean signal intensity inhomogeneity (standard deviation/mean) within volumes of interest for total, cortical, and trabecular compartments of the proximal femur. We used standard statistical methods to correlate these parameters with age, BMI, and FRAX hip fracture score.

Results: Subjects' mean age was 60.9 years (SD +/- 9.9) and mean BMI was 22.9 kg/m^2 (SD +/-4.3). The mean total hip T-score was -1.9 (SD +/-1.2). Higher BMI correlated with lower cortical SI inhomogeneity (r=0.66, p=0.0005). Higher age correlated with lower SI inhomogeneity of total, trabecular, and cortical bone compartments (r=0.51, p=0.01; r=0.43, p= 0.03; and r=0.45, 0.03 respectively). Higher FRAX score also correlated with lower cortical and total bone SI inhomogeneity. (r=0.50, p=0.03; r=0.53, p=0.02) A higher total hip T-score correlated with lower total bone SI inhomogeneity (r=0.46, p=0.02). There was no significant correlation with cortical or trabecular bone SI inhomogeneity (p=0.4, p=0.097 respectively).

Conclusion: Lower MRI-computed proximal femur SI inhomogeneity correlates with higher age, BMI, FRAX score and total hip BMD T-score. This may reflect the ability of textural metrics computed from 3T MRI to detect changes in bone quality with changes in age, BMI, and fracture risk. Larger cohort studies are needed to confirm these results.

Modality % - Radiography / Fluoroscopy:	0
Modality % - CT:	0
Modality % - MRI:	100
Modality % - US:	0
Modality % - Nuclear Medicine:	0

Podium #3

COST-EFFECTIVENESS OF MR ARTHROGRAPHY VERSUS MRI FOR SLAP TEARS

Naveen Subhas, MPH, MD[1]; Jordan Conroy[2]; James Koo[3]; Morgan Jones, MD, MPH[1]; Anthony Miniaci, MD[1]; Soterios Gyftopoulos, MD, MS[3]
[1]Cleveland Clinic, Cleveland, OH, USA; [2]University Hosp of Cleveland / Case Western Reserve Univ Sch of Med, Cleveland, OH, USA; [3]NYU Medical Center/ Hospital for Joint Diseases Langone Medical Center, New York, NY, USA
(Presented by: Naveen Subhas, MPH, MD, Cleveland Clinic)

Purpose: To determine if direct magnetic resonance arthrography (MRA) is more cost-effective than a non-contrast magnetic resonance imaging (MRI) in the management of superior labral anterior to posterior (SLAP) tears.

Materials and Methods: Our base case was a 25-year-old with clinical findings of a SLAP tear in whom an imaging test is being ordered for further management. Decision analysis software (TreeAge Pro) was used to create a model from the healthcare perspective to evaluate the cost-effectiveness of 4 imaging strategies: 3-Tesla (T) MRA, 3T MRI, 1.5T MRA and 1.5T MRI. Probability and utility estimates were obtained from published literature. Commercial insurance and Medicaid reimbursements were estimated using 2017 Medicare rates. Effectiveness was measured in quality-adjusted life years (QALY) over a 2-year period and costs were calculated in 2017 U.S. dollars.

Results: 3T MRI was the least expensive ($5975) and most effective (1.62278 QALY) strategy for our base case and was dominant to 3T MRA ($6569, 1.61732 QALY), 1.5T MRA ($6790, 1.60517 QALY) and 1.5T MRI ($6823, 1.58544 QALY). The results remained robust and did not change over a reasonable range of costs, utilities and probabilities in 1-way sensitivity analyses. 3T MRA only becomes a cost-effective option if the specificity of 3T MRI drops below 91% with a willingness-to-pay (WTP) threshold of $100,000 or below 88.5% with WTP threshold of $50,000. If 3T is excluded from the analysis, 1.5T MRA is dominant for our base case but 1.5T MRI also becomes a cost effective option if its specificity is higher than 68%.

Conclusion: 3T MRI is the most cost-effective option for management of SLAP tears. If a 3T magnet is not available, 1.5T MRA is the most cost effective option. In both circumstances, the most cost effective option is the test with highest specificity.

Modality % - Radiography / Fluoroscopy:	0
Modality % - CT:	0
Modality % - MRI:	100
Modality % - US:	0
Modality % - Nuclear Medicine:	0

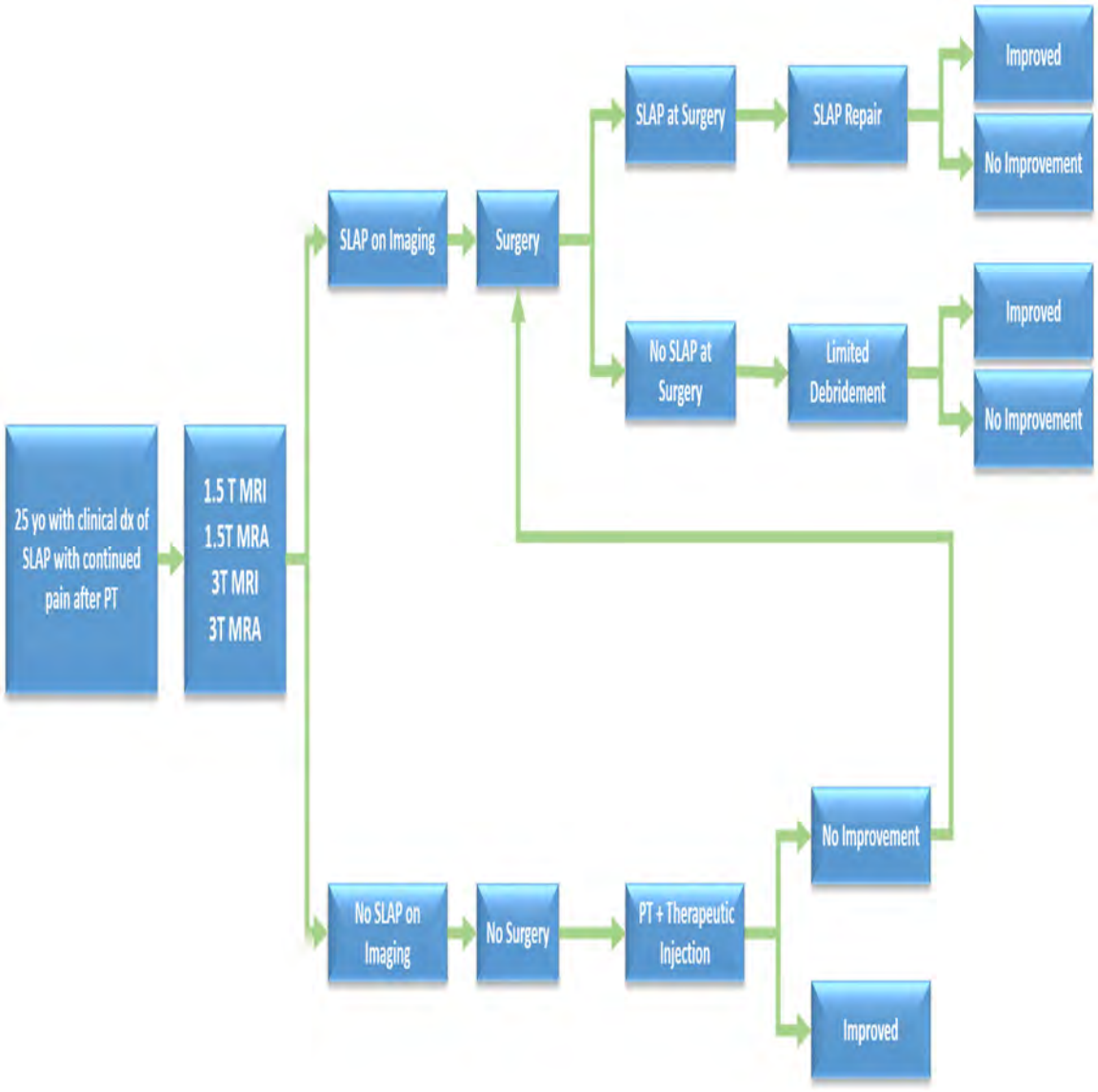

Flow Diagram for Management of SLAP

Podium #4

Women in Academic Musculoskeletal Radiology

Kate Harrington, MD; Gregory Chang, MD
NYU Medical Center/ Hospital for Joint Diseases Langone Medical Center, New York, NY, USA
(Presented by: Kate Harrington, MD, NYU Medical Center/ Hospital for Joint Diseases Langone Medical Center)

Purpose: To determine the proportion of women working in academic musculoskeletal (MSK) radiology divisions and how this compares to national benchmarks for women in academic medicine.

Materials and Methods: A list of academic radiology departments across the United States was compiled using the U.S. News and World Report listing of Best Hospitals for Orthopedics and Rheumatology. Faculty information for each MSK radiology division was obtained using websites pertinent to each department. National figures were obtained from the Association of American Medical Colleges and used as a benchmark for comparison.

Results: 24 MSK radiology divisions were identified with a total of 207 MSK trained radiologists. Female radiologists made up 33% of the MSK trained faculty (n=69). This compares to 38% of fulltime female faculty in academic medicine. 76 Assistant Professor roles were identified, of which 35% were occupied by female faculty (n=27). At the Associate Professor level, 35% of faculty were females (n=11). At the Professor level, only 23% were female (n=10); this compares with a national benchmark of 21% for women in academic medicine. Six MSK radiologists held either Chair or Vice-Chair roles and 3 of these, or 50%, were female; this compares to a national benchmark of 15%. Of the 24 Chief or Director roles identified, 30% of these were held by women; this compares to a national benchmark of 24% for women in academic medicine. Finally, only 25% of the roles specific to education, such as fellowship or residency program director, were filled by women (n=4).

Conclusion: The proportions of women within various roles in academic MSK radiology are similar to and in some instances higher than corresponding national benchmarks. However, there remains a large discrepancy between the sexes with an overall male majority. Awareness of this fact is the first step required to help correct this imbalance.

Modality % - Radiography / Fluoroscopy:	20
Modality % - CT:	20
Modality % - MRI:	20
Modality % - US:	20
Modality % - Nuclear Medicine:	20

Podium #5

CT Pipeline for Sarcopenia Screening using the Automated Muscle Analysis Tool

Leon Lenchik, MD[1]; Ryan Barnard, MS[1]; Josh Tan, MS[1]; Stephen Kritchevsky, PhD[1]; Ashley Weaver, PhD[1]; Joel Stitzel, PhD[1]; Robert Boutin, MD[2]

[1]Wake Forest University School of Medicine, Winston-Salem, NC, USA; [2]University of California, Davis, Sacramento, CA, USA

(Presented by: Leon Lenchik, MD, Wake Forest University School of Medicine)

Purpose: Although sarcopenia can be evaluated opportunistically with routine CT, this requires time-consuming manual segmentation of muscles, unrealistic for large datasets. The purpose was to validate a pipeline for sarcopenia screening on CT images using an Automated Muscle Analysis Tool (AMAT).

Materials and Methods: AMAT pipeline was validated using 480 non-contrast chest CT exams in the National Lung Screening Trial. For validation, left paraspinous muscle was manually segmented at T12 level, using Mimics (Materialise, Leuven, Belgium) with muscle thresholds set at -29 to150 Hounsfield units (HU).

AMAT was developed using open-source medical image analysis tools: Advanced Normalization Tools and the Oxford Centre for Functional Magnetic Resonance Imaging of the Brain Software Library. AMAT employs a three-dimensional stage to identify the appropriate level (T12) and a two-dimensional stage to segment the muscle. The pipeline for automated processing of CT exams was developed using Snakemake (Python-based system) and produces a set of masked images for quality assurance.

Spearman's test was used to assess correlation between manually and automatically segmented attenuation. Using +30HU as a threshold for sarcopenia, the sensitivity and specificity of the pipeline were determined.

Results: AMAT pipeline failed to produce numerical results in 1.25%(6/480) of cases. In the remaining 98.75%(474/480), mean attenuation of muscle was 42.9HU(SD=7.3) using manual segmentation and 46.3HU(SD=8.9) using the pipeline. Mean accuracy error for muscle attenuation was 5.0HU(range:0-32.0). For muscle attenuation, the pipeline had moderate correlation with manual segmentation (r=0.71). For diagnosis of sarcopenia (+30HU threshold), the pipeline had 60.0% sensitivity and 98.5% specificity. Quality assurance of masked images excluded 11.1% (56 of 474) of cases. In the remaining 418, AMAT pipeline had 78.6% sensitivity and 99.5% specificity.

Conclusion: Initial validation results of the AMAT pipeline are promising. This automated large-scale screening for sarcopenia could be adapted to other body regions.

Modality % - Radiography / Fluoroscopy:	0
Modality % - CT:	100
Modality % - MRI:	0
Modality % - US:	0
Modality % - Nuclear Medicine:	0

AMAT pipeline quality assurance

Podium #6

3D-MRI versus 3D-CT in the Evaluation of Osseous Anatomy in Femoroacetabular Impingement

Mohammad Samim, MD; Nima Eftekhary, MD; Thomas Youm, MD; Roy Davidovitch, MD; Jonathan Vigdorchik, MD; Soterios Gyftopoulos, MD
NYU Medical Center/ Hospital for Joint Diseases Langone Medical Center, New York, NY, USA
(Presented by: Mohammad Samim, MD, NYU Medical Center/ Hospital for Joint Diseases Langone Medical Center)

Purpose: CT imaging with 3D reconstruction has become increasingly popular for its accurate depiction and quantification of abnormal bone morphology in femoroacetabular impingement (FAI), allowing for improved preoperative planning. While effective, CT predisposes typical young FAI patients to increased radiation and additional cost. The purpose of this study was to determine if 3D-MR of the hip can be used to accurately demonstrate hip morphology in the setting of FAI compared with 3D CT.

Materials and Methods: We performed a retrospective review of patients who underwent both CT and MRI of the same hip and met these inclusion criteria: (1) suspected to have FAI based on physical examination, (2) had no prior hip surgery, (3) had CT and MR with 3D of the same hip within a six-month time period. The 3D images were evaluated for the presence of cam lesion, cam location, femoral neck shaft angle (NSA), anterior inferior iliac spine (AIIS) morphology, and lateral center edge angle (LCEA).

Results: Seventeen patients met our inclusion criteria. There was 100% agreement in the presence and location of the cam lesion (19/19) comparing the 3D MRI to CT. The simple kappa coefficients for cam presence and locations were both 1. There were 3 Type I and 16 Type II AIIS variants on 3D CT with 89.5% (17/19) agreement for the AIIS morphology between 3D MRI and CT. There was 64.7% agreement between the NSA (11/17) and LCEA (11/17) measurements on the 3D MRI and CT.

Conclusion: 3D-MRI was as accurate or near as accurate as CT in determining clinically relevant osseous hip parameters. We argue that in the evaluation of FAI, 3D-MR is sufficient to evaluate both soft tissue and osseous anatomy, sparing the need for a CT scan and its associated radiation and cost.

Modality % - Radiography / Fluoroscopy:	0
Modality % - CT:	50
Modality % - MRI:	50
Modality % - US:	0
Modality % - Nuclear Medicine:	0

Figure 1. Cam deformity and its location. 3D volume rendered CT (A and B) and MR (C and D) images of the let femur demonstrate large anterior cam deformity (arrows).

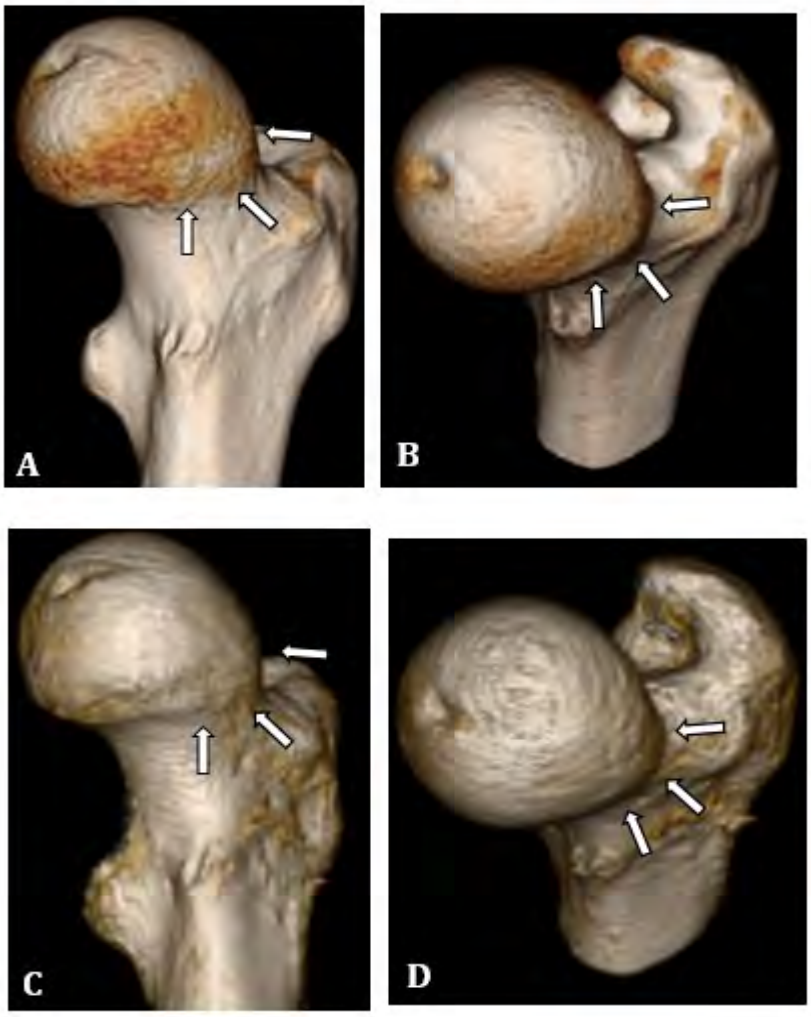

Figure 1. Cam deformity and its location (arrows). 3D volume rendered CT (A and B) and MR (C and D) images.

Figure 2. Anterior inferior iliac spine morphology. 3D volume rendered CT (A and B) and MR (C and D) images of the left hip demonstrate type II anterior inferior iliac spine as images rotate in two different views (arrows).

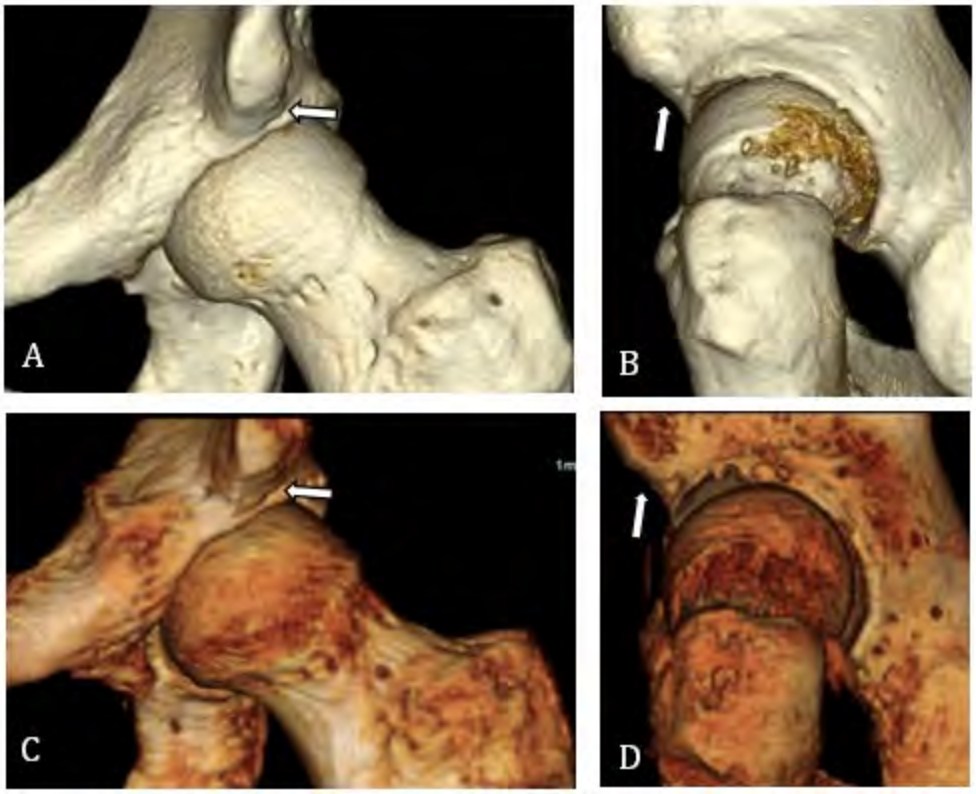

Figure 2. AIIS morphology (type II: arrows). 3D volume rendered CT (A and B) and MR (C and D) images of the left hip.

Podium #7

HUMAN VS. MACHINE: DISTINGUISHING ENCHONDROMA FROM CHONDROSARCOMA WITH A BAYESIAN NETWORK

Christopher Beaulieu, MD, PhD; Bao Do, MD
Stanford University School of Medicine, Stanford, CA, USA
(Presented by: Christopher Beaulieu, MD, PhD, Stanford University School of Medicine)

Purpose: Chondroid tumors are common, and radiographic features are key in distinguishing enchondromas from chondrosarcomas. We previously created a naïve Bayesian network ("the Machine") from a collection of 811 bone tumor cases across 66 diagnoses. In the current study, the Machine was tested on classification of 106 chondroid lesions and compared with that of 28 radiologists.

Materials and Methods: Within the 811 tumor colllection, 106 chondroid tumors (65 enchondroma, 41 chondrosarcoma) were encoded with 18 features including skeletal location, age, sex, margin, matrix, endosteal scalloping, border (1A, 1B, 1C), etc. A naïve Bayesian network utilized these features to compute class probabilities using leave-one out, 106-fold cross validation. For comparison against radiologists, a random subset of 21 tumors was selected consisting of 17 enchondromas and 4 chondrosarcomas. Twenty-eight trainee or in-practice radiologists were recruited locally and from the One-Case-A-Day collaborative. Each radiologist completed an online quiz recording a binary classification of each lesion.

Results: For the complete set of 106 tumors, the Machine correctly classified 71/106 lesions (66.9%). For the subset of 21 cases pitting radiologists against the Machine, the Machine correctly classified 15/21 lesions (71.4%). Only 4 radiologists performed as well or better than the Machine (71.4-81.0%), with 24 performing less well (47.6-66.7%; mean 58.7; SD 5.8; mode 61.9). The Machine performed equal to or exceeded the performance of 24/28 radiologists (85.7%). For each tumor, the correct number of classifications across the 28 radiologists ranged between 5 and 27 (mean 17; SD 7.1; mode 13). Example lesions are shown in the figures.

Conclusion: Initial performance of the Machine is comparable or better than radiologists, but varying lesion appearances make for a challenging task. With further development, we hope to establish a clinically-useful support system to aid radiologists in classifying bone lesions.

Modality % - Radiography / Fluoroscopy:	100
Modality % - CT:	0
Modality % - MRI:	0
Modality % - US:	0
Modality % - Nuclear Medicine:	0

Fig 1. Enchondroma in the 4th proximal phalanx, correctly classified by the Machine and by 26/28 radiologists (93%).

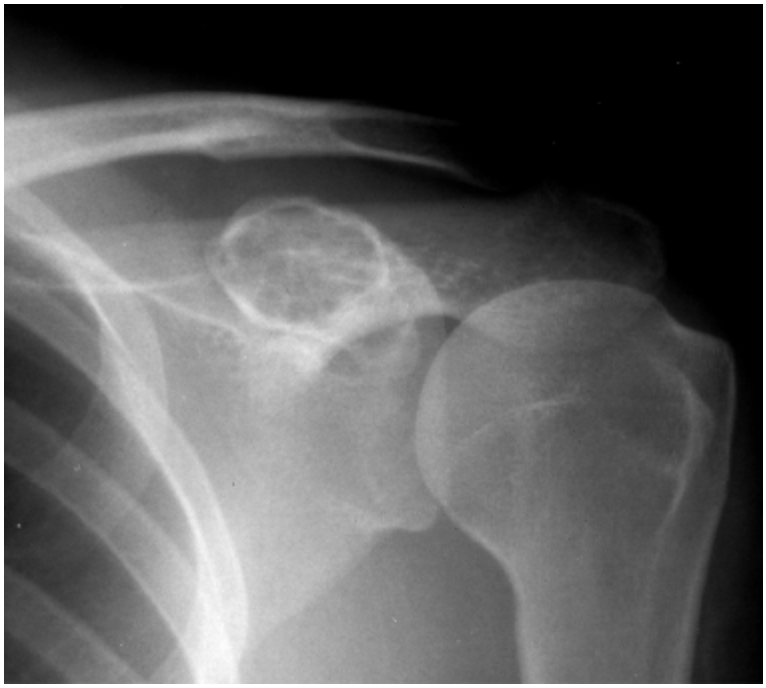

Fig 2. Enchondroma in the coracoid, correctly classified by 22/28 radiologists (79%), but incorrectly classified as chondrosarcoma by the Machine.

Podium #8

OPPORTUNISTIC CT BONE DENSITY MEASUREMENTS CORRELATE WITH LONG-TERM OUTCOME IN PATIENTS WITH PROXIMAL FEMUR FRACTURES

Jennifer Ni Mhuircheartaigh, MD; Daon Ha, MD; Ching-Di Chang, MD; Colm McMahon, MBBS; Jim Wu, MD
Beth Israel Deaconess Medical Center Harvard Med School, Boston, MA, USA
(Presented by: Jennifer Ni Mhuircheartaigh, MD, Beth Israel Deaconess Medical Center Harvard Med School)

Purpose: Low bone mineral density is a known risk factor for hip fracture and has been shown to correlate with a worse outcome. Recent publications have shown that it is possible to obtain opportunistic bone density measurements on a standard CT. The purpose of this study was to assess whether opportunistic bone density measurements obtained from CT studies performed to evaluate proximal femur fractures correlate with long-term survival.

Materials and Methods: A database of patients undergoing a CT pelvis from the emergency room for acute trauma between 1/2000 and 8/2016 was screened to identify patients with proximal femur fractures. Patients were excluded if <50 years old, had no surgical treatment, had other major traumatic injuries, or pathologic femur fractures. Measurements of mean Hounsfield Units (HU) were obtained at L5. As described by previous authors, mean HU <110 was considered low CT bone density. Data were also collected on short (up to 30 days) and long-term mortality, length of hospital stay and readmission rates. Survival analysis was performed using Kaplan-Meier curves and the cox proportional hazards model.

Results: 91 studies were identified in the database, of those 87 CTs included L5 and formed the study group. 49 patients (56.3%) had CT bone density measurements <110 HU. Short term mortality (<30 days) was 4.4%, total mortality was 31.9% (29 deaths). There was no association between short term mortality and CT bone density measurements (p=0.265). There was a significantly worse long-term outcome in patients with low CT bone density measurements (p=0.043).

Conclusion: Patients with low CT bone density have a significantly worse survival following a hip fracture than those without low CT bone density. Reporting this finding in the setting of a hip fracture can increase the diagnostic utility of the study.

Modality % - Radiography / Fluoroscopy:	0
Modality % - CT:	100
Modality % - MRI:	0
Modality % - US:	0
Modality % - Nuclear Medicine:	0

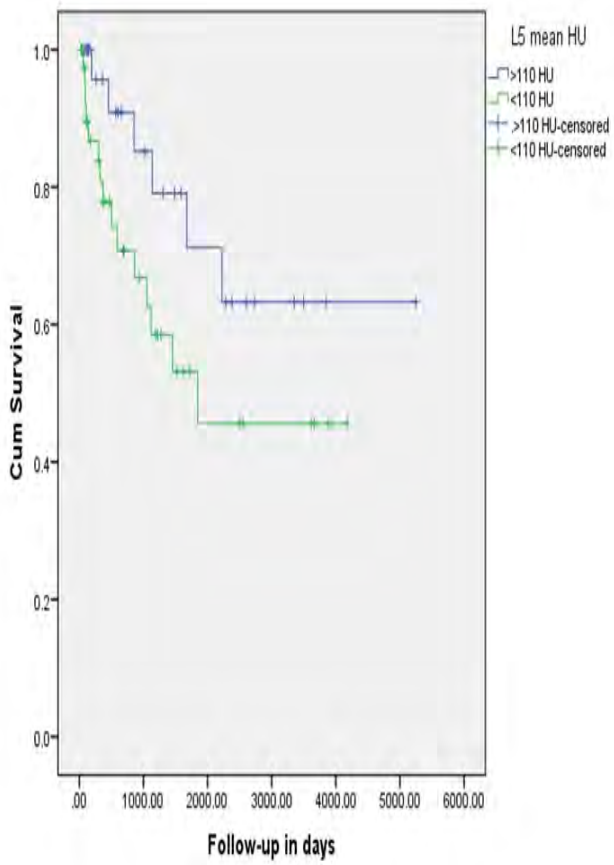

Kaplan-Meier curve comparing long-term survival in patients with low and normal CT bone density measurements.

Podium #9

PREDICTIVE UTILITY OF QUANTITATIVE SUPRASPINATUS TENDON AND MUSCLE SHEAR WAVE ULTRASOUND ELASTOGRAPHY: IS THERE A CORRELATION?

Dana Lin, MD; Christopher Burke, MD; James Babb, PhD; Ronald Adler, MD, PhD
NYU Medical Center/ Hospital for Joint Diseases Langone Medical Center, New York, NY, USA
(Presented by: Dana Lin, MD, NYU Medical Center/ Hospital for Joint Diseases Langone Medical Center)

Purpose: To correlate quantitative shear wave velocities (SWV) in the supraspinatus muscle (SSM) with that of the tendon (SST), and to evaluate whether SSM SWV changes precede morphologic fatty atrophy.

Materials and Methods: An IRB-approved, HIPAA-compliant study of 45 patients (22 men, 23 women) with mean age of 59 (range 39-84) was conducted. Grayscale ultrasound and shear wave elastography images of the SST and SSM were performed with a 9MHz linear transducer on a Siemens S3000 scanner with VTIQ software (Siemens). Sample volume SWV values were obtained of the proximal (PSST) and distal tendon (DSST). Mean SSM SWV was reported from the software region of interest or calculated from sample volumes. Exclusion criteria included history of rotator cuff repair and non-target measurements on bone or peribursal fat. Qualitative tendon pathology grading was as follows: 1=normal or mild tendinosis without tear, 2=moderate or severe tendinosis without tear or mild tendinosis with low-grade partial tear, 3=partial tear with at least moderate tendinosis, and 4=full-thickness tear. All patients demonstrated normal grayscale appearance of the SSM, without evidence of fatty atrophy. Pearson and Spearman rank correlations were used for statistical analysis.

Results: No statistically significant correlation was found between mean SSM SWV and mean PSST, DSST, or overall tendon SWV (R=0.14, p=0.396; R=0.04, p=0.832; R=0.06, p=0.731, respectively). There was no statistically significant correlation between SSM SWV and tendon grade (R=0.13, p=0.435) (Figure 1). Mean PSST, DSST, and overall tendon SWV demonstrated weak negative correlation with qualitative tendon grade (R=-0.22, p=0.183; R=-0.32, p=0.054; R=-0.30, p=0.045, respectively) (Figure 2).

Conclusion: Supraspinatus muscle SWV does not appear to vary with quantitative tendon SWV or qualitative tendon grading. A weak negative correlation between supraspinatus tendon SWV and qualitative tendon grade is compatible with tendon softening with progressive tendinopathy.

Modality % - Radiography / Fluoroscopy:	0
Modality % - CT:	0
Modality % - MRI:	0
Modality % - US:	100
Modality % - Nuclear Medicine:	0

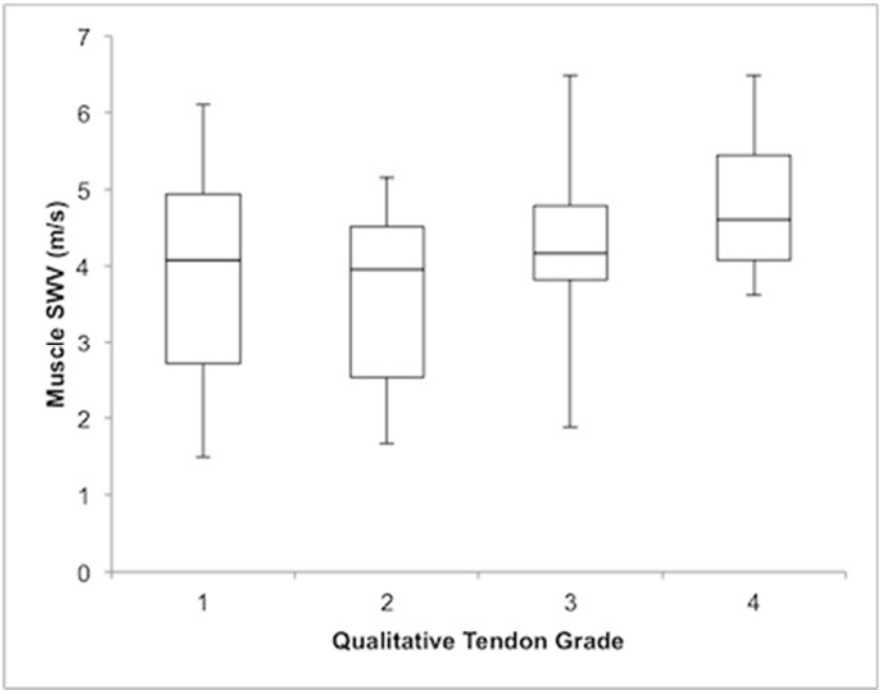

Box plot of supraspinatus SWV versus qualitative tendon grade demonstrating no statistically significant correlation, although there was a tendency toward a weak positive correlation.

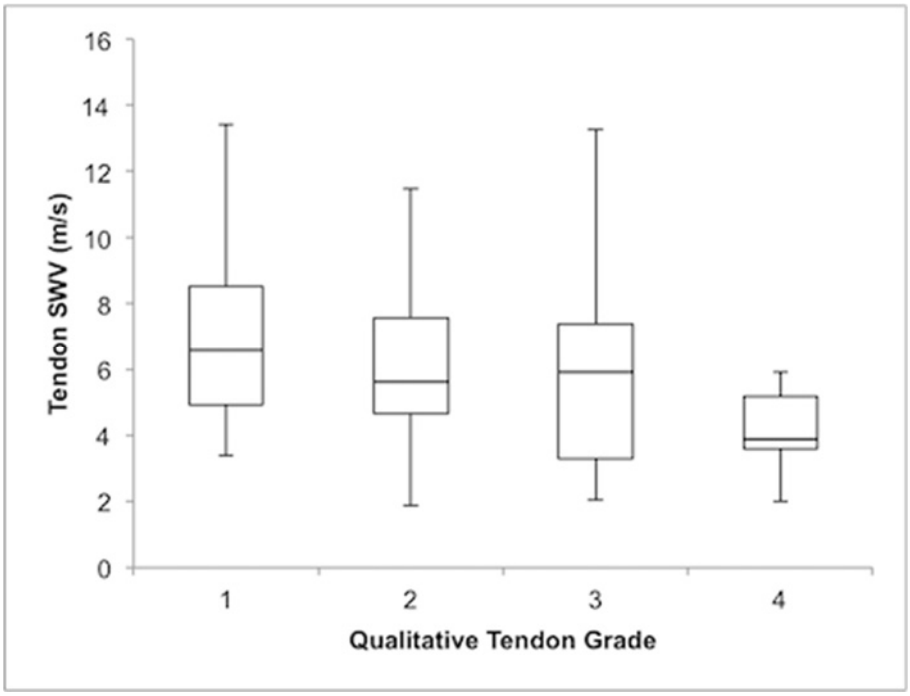

Box plot of overall supraspinatus tendon SWV versus qualitative tendon grade. Mean overall tendon SWV demonstrated weak negative correlation with qualitative tendon grade (R=-0.30, p=0.045).

MONDAY

Society of Skeletal Radiology

41st Annual Meeting

March 25-28, 2018

Monday, March 26, 2018

7:00 a.m.–7:55 a.m. **Continental Breakfast**

7:00 a.m.–12:35 p.m. **Registration/Information Desk Open**

7:00 a.m.–12:30 p.m. **Exhibit Hall Open**

7:00 a.m.–12:30 p.m. **ePoster Session**

7:45 a.m.–8:00 a.m. **SSR INVITED KEYNOTE PRESENTATION**
Moderators: Laura Bancroft, MD, FACR

8:00 a.m.–10:00 a.m. **UPPER EXTREMITY**
Moderators: Jarrod Dale, MD, Jennifer Demertzis, MD

8:00 a.m. #10 **SUPERIOR CAPSULAR RECONSTRUCTION OF THE SHOULDER – ALL YOU WANTED TO KNOW!**
Manickam Kumaravel, MD
Memorial Hermann Hospital - Texas Medical Center/ University of Texas HSC at Houston, houston, USA
(Presented by: Manickam Kumaravel, MD, Memorial Hermann Hospital - Texas Medical Center/ University of Texas HSC at Houston)

8:15 a.m. #11 **MULTILEVEL GLENOID MORPHOLOGY AND RETROVERSION ASSESSMENT IN WALCH B2 AND B3 TYPES**
Mohammad Samim, MD; Mandeep Virk, MD; Joseph Zuckerman, MD; Soterios Gyftopoulos, MD
NYU Medical Center/ Hospital for Joint Diseases Langone Medical Center, New York, NY, USA
(Presented by: Mohammad Samim, MD, NYU Medical Center/ Hospital for Joint Diseases Langone Medical Center)

8:30 a.m. #12 **OPTIMIZING METHODS TO QUANTIFY INTRAMUSCULAR FAT IN ROTATOR CUFF TEARS WITH NORMALIZATION**
Ankur Garg, MD[1]; Paul Micevych[1]; Rajan Khanna[2]; Lucas Buchler, MD[1]; Guido Marra, MD[1]; Matthew Saltzman, MD[1]; Todd Parrish, PhD[1]; Amee Seitz, PhD[1]
[1]Northwestern Memorial Hospital ;Northwestern University Feinberg School of Medicine, Chicago, IL, USA; [2]Loyola University Chicago Stritch School of Medicine, Chicago, IL, USA
(Presented by: Ankur Garg, MD, Northwestern Memorial Hospital ;Northwestern University Feinberg School of Medicine)

8:45 a.m. #13 **PACINIAN CORPUSCLES: BRIGHT PALMAR BLIND-SPOTS ON MRI**
Nicholas Rhodes, MD[1]; David Rubin, MD[2]; Lehman Julia, MD[1]
[1]Mayo Clinic, Rochester, MN, USA; [2]Mallinckrodt Institute of Radiology, Saint Louis, MN, USA
(Presented by: Nicholas Rhodes, MD, Mayo Clinic)

9:00 a.m. #14 **HYPERINTENSE T2 SIGNAL IN THE ULNAR NERVE AT THE CUBITAL TUNNEL: NORMAL OR ABNORMAL?**
Carissa White, MD; Behrad Golshani, MD; Benjamin Plotkin, MD; Kambiz Motamedi, MD; Leanne Seeger, MD; Benjamin Levine, MD
David Geffen School of Medicine at UCLA, Los Angeles, CA, USA
(Presented by: Carissa White, MD, David Geffen School of Medicine at UCLA)

9:15 a.m. #15 **CHARACTERIZATION OF GLENOID BONE REMODELING IN PROFESSIONAL BASEBALL PLAYERS**
Jonathan Rassi, MD; Naveen Subhas, MD; Jennifer Bullen, MS; Joshua Polster, MD
Cleveland Clinic, Cleveland, OH, USA
(Presented by: Jonathan Rassi, MD, Cleveland Clinic)

9:30 a.m. #16 **DIFFUSION TENSOR IMAGING OF THE MEDIAN NERVE WITH ULTRASOUND CORRELATION IN PATIENTS WITH CARPAL TUNNEL SYNDROME BEFORE AND AFTER FLEXOR RETINACULAR RELEASE**

Lana Gimber, MD, MPH[1]; Elizabeth Krupinski, PhD[2]; Tolga Turker, MD[1]; Giles Becker, MD[1]; Lea MacKinnon, MD[1]; Tyson Chadaz, MD[1]; Mihra Taljanovic, MD, PhD[1]
[1]University of Arizona HCS - Tucson, Tucson, AZ, USA; [2]Emory University, Atlanta, GA, USA
(Presented by: Lana Gimber, MD, MPH, University of Arizona HCS - Tucson)

9:45 a.m. #17 **ACCURACY OF MRI AND MRA IN DETECTING ROTATOR CUFF TEARS IN PATIENTS WITH CALCIFIC TENDINOSIS**

Michael Fox, MD[1]; Jonathan Flug, MD[2]; Joseph Brinkman[3]; David Hartigan, MD[2]; Mark Kransdorf, MD[2]; Spencer Chivers, MD[2]; Taryar Zaw, MD[2]
[1]Mayo Clinic, Phoenix, AZ, USA; [2]Mayo Clinic Hospital, Phoenix, AZ, USA; [3]Creighton, Omaha, NE, USA
(Presented by: Michael Fox, MD, Mayo Clinic)

10:00 a.m.–10:05 a.m. **CASE OF THE DAY**
Presenting Author: Kurt Scherer, MD

10:05 a.m.–10:30 a.m. **Break** - Visit the Exhibit Hall

10:30 a.m.–12:30 p.m. **INTERVENTION/POSTOPERATIVE**
Moderators: MK Jesse, MD, Kambiz Motamedi, MD

10:30 a.m. #18 **LATISSIMUS DORSI TENDON TRANSFER PROCEDURES: PRE- AND POST-OPERATIVE MR IMAGING FEATURES**

Lawrence White, MD; Linda Probyn, MD; Patrick Henry, MD; Timothy Dwyer, MBBS, PhD; Michael McKee, MD
University of Toronto, Toronto, ON, Canada
(Presented by: Lawrence White, MD, University of Toronto)

10:45 a.m. #19 **FOUR YEAR RETROSPECTIVE REVIEW OF PERINEURAL INJECTIONS ABOUT THE UPPER EXTREMITY**

Pamela Walsh, MD; William Walter, MD; Christopher Burke, MD; Ronald Adler, MD, PhD
NYU Medical Center/ Hospital for Joint Diseases Langone Medical Center, New York, NY, USA
(Presented by: Pamela Walsh, MD, NYU Medical Center/ Hospital for Joint Diseases Langone Medical Center)

11:00 a.m. #20 **MAGNETIC RESONANCE ARTHROGRAPHY OF THE WRIST: DOES DISTAL RADIOULNAR JOINT INJECTION ALTER MANAGEMENT?**

Nathaniel Meyer, MD; Corrie Yablon, MD; Yoav Morag, MD; Jon Jacobson, MD
University of Michigan Medical Center, Ann Arbor, MI, USA
(Presented by: Nathaniel Meyer, MD, University of Michigan Medical Center)

11:15 a.m. #21 **DIAGNOSTIC UTILITY OF LAVAGE FOR PERIPROSTHETIC JOINT INFECTION: ARE THE CULTURE RESULTS RELIABLE?**

Dana Lin, MD; Christopher Burke, MD; Nathan Jia, BS; Joseph Zuckerman, MD; Gina Ciavarra, MD
NYU Medical Center/ Hospital for Joint Diseases Langone Medical Center, New York, NY, USA
(Presented by: Dana Lin, MD, NYU Medical Center/ Hospital for Joint Diseases Langone Medical Center)

11:30 a.m. #22 **POTENTIAL IMPORTANCE OF BIOPSY OF SOFT TISSUE NEOPLASM NECROSIS**
Mark Murphey, MD[1]; Michael Shvarts, MD[1]; Steven Kong, MD[2]; Anthony Zaklama, MD[3]; Dhruv Kumar, MD[4]; James Jelinek, MD[4]
[1]American Institute for Radiologic Pathology, Silver Spring, MD, USA; [2]SimonMed, Riverside, CA, USA; [3]Geisinger Health, Danville, PA, USA; [4]Medstar Washington Hospital Center, Washington, DC, USA
(Presented by: Mark Murphey, MD, American Institute for Radiologic Pathology)

11:45 a.m. #23 **CT-GUIDED DISCITIS-OSTEOMYELITIS BIOPSIES: NEEDLE GAUGE AND MICROBIOLOGY RESULTS**
Connie Chang, MD; F. Simeone, MD; Joao Vicentini, MD; Sandra Nelson, MD
Mass General Hospital, Boston, MA, USA
(Presented by: Connie Chang, MD, Mass General Hospital)

12:00 p.m. #24 **INTRAMUSCULAR BOTULISM TOXIN TYPE A (BTA) INJECTION FACILITATES ABDOMINAL WALL RECONSTRUCTION (AWR) OF RECURRENT LARGE-DEFECT HERNIAS**
Robert Lopez, MD[1]; Robert Raible, MD[1]; James Coumas, MD[1]; Taylor Stone, MD[1]; Paul Colavita, MD[2]; Vedra Augenstein, MD[2]; Kent Kercher, MD[2]; Todd Heniford, MD[2]
[1]Charlotte Radiology, Charlotte, NC, USA; [2]Carolinas Health Care System, Charlotte, NC, USA
(Presented by: Robert Lopez, MD, Charlotte Radiology)

12:15 p.m. #25 **IMAGING APPEARANCE OF THE ULNAR NERVE FOLLOWING SURGICAL INTERVENTION**
Nicholson Chadwick, MD; Yoav Morag, MD; Brandon Smith, MD, MS; Corrie Yablon, MD; Sung Moon Kim, MD; Kate Chang, MS; Lynda Yang, MD, PhD
University of Michigan Medical Center, Ann Arbor, MI, USA
(Presented by: Nicholson Chadwick, MD, University of Michigan Medical Center)

12:30 p.m.–12:35 p.m. **CASE OF THE DAY**
Presenting Author: Tom Chen, MD

1:00 p.m.–3:00 p.m. ***Musculoskeletal Ultrasound Hands-On Workshop/Hip**

6:00 p.m.–9:30 p.m. **Annual Banquet** - Brazos Hall (2 blocks from hotel)

Related ePosters

UPPER EXTREMITY

Poster #7 **Superior Capsular Reconstruction for Irreparable Rotator Cuff Tears: Imaging Features and Complications**
Pamela Walsh, MD; Mohammad Samim, MD; Luis Beltran, MD
NYU Medical Center/ Hospital for Joint Diseases Langone Medical Center, New York, NY, USA

Poster #8 **GENDER DIFFERENCES IN GLENOID REMODELING IN GLENOHUMERAL DEGENERATIVE JOINT DISEASE**
Christopher Peters, MD; Anna Zajicek, MD; Christopher Peters, MD; Kent Rinehart, MD; Matthew Teusink, MD
University of Nebraska Medical Center, Omaha, NE, USA

Poster #9 **Os Subscapulare: imaging findings and clinical relevance**
Alex Bergman, MD[1]; Hilary Umans, MD[2]; Jonathan Ticker, MD[3]
[1]Jacobi Medical Center, Bronx, NY, USA; [2]Lenox Hill Radiology and Imaging Associates, New York, NY, USA; [3]Orlin and Cohen Orthopedic Associates, Merrick, NY, USA

Poster #10 **"Reducing" Radiologists' Anxiety about Carpal Instability**
Jonelle Petscavage-Thomas, MD, MPH; Eric Walker, MD; Weaver Kesler, MD
Penn State Milton S. Hershey Medical Center, Hershey, PA, USA

Poster #11 **FOOSH Injuries of the Elbow with an Emphasis on Posterolateral Elbow Instability: A Multimodality Pictorial Review.**
Christopher Nall, MD; Robert Colvin, DO; Shashin Doshi, MD
Beaumont Health System, Royal Oak, MI, USA

Poster #12 **RADIOLOGIC EVALUATION OF ABNORMALITIES OF THE STERNUM AND STERNOCLAVICULAR JOINTS**
Sailaja Yadavalli, MD, PhD; Jason Esterle, MD; Christopher Nall, MD
Beaumont Health System, Royal Oak, MI, USA

INTERVENTION/POSTOPERATIVE

Poster #13 **CT GUIDED CORE NEEDLE BONE BIOPSY IN THE WORKUP OF OSTEOMYELITIS: DIAGNOSTIC YIELD AND EFFECT ON PATIENT CARE.**
Donald von Borstel, DO; Cameron Smith, DO; Gregory Bradley, DO; Sindhura Alapati, MD
Oklahoma State University Medical Center, Tulsa, OK, USA

Poster #14 **THE POSTOPERATIVE MRI: IS IT TUMOR RECURRENCE OR NODULAR SCAR?**
Lana Gimber, MD, MPH[1]; Samuel Oats, MD[1]; Lea MacKinnon, MD[1]; Mihra Taljanovic, MD, PhD[1]; James Warneke, MD[1]; Matthew Seidel, MD, MS[1]; Laura Fayad, MD[2]
[1]University of Arizona HCS - Tucson, Tucson, AZ, USA; [2]Johns Hopkins University, Baltimore, MD, USA

Poster #15 **CURRENT TRENDS IN MODALITY SELCETION FOR IMAGE-GUIDED MUSCULOSKELETAL PROCEDURES:FACTORS THAT INFLUENCE ULTRASOUND VERUS NON-ULTRASOUND UTILIZATION**
Judah Goldschmiedt, MD; Danielle Williams, MD; Chaitanya Shilagani, DO
Westchester Medical Center, Valhalla, NY, USA

Related ePosters

Poster #16 **UTILITY OF CORE NEEDLE BIOPSY TO DIFFERENTIATE ANEURYSMAL BONE CYST FROM TELANGIECTATIC OSTEOSARCOMA**

Benjamin Levine, MD; Vishal Hedge, MD; Kambiz Motamedi, MD; Leanne Seeger, MD; Scott Nelson, MD; Nicholas Bernthal, MD
University of California, Los Angeles, Los Angeles, CA, USA

Poster #17 **DIAGNOSTIC YIELD OF ULTRASOUND GUIDED AND CT GUIDED SOFT TISSUE LESION BIOPSIES**

Kambiz Motamedi, MD; Kim Lee, MD; Benjamin Levine, MD; Leanne Seeger, MD
David Geffen School of Medicine at UCLA, Los Angeles, CA, USA

Poster #18 **ULTRASOUND-GUIDED ASPIRATION OF INTRAMUSCULAR HEMATOMAS: EFFICACY AND RELATIONSHIP TO SONOGRAPHIC APPEARANCE**

Edward Yoon, MD; Theodore Miller, MD; Susan Lee, MD
Hospital for Special Surgery, New York, NY, USA

Poster #19 **COMPARISON BETWEEN IMAGE-GUIDED AND LANDMARK-BASED GLENOHUMERAL JOINT INJECTIONS FOR THE TREATMENT OF ADHESIVE CAPSULITIS: A COST-EFFECTIVENESS STUDY**

Soterios Gyftopoulos, MD, MS[1]; Valentino Abballe, MD[1]; Mandeep Virk, MD[1]; James Koo, PhD[1]; Heather Gold, PhD[1]; Naveen Subhas, MPH, MD[2]
[1]NYU Medical Center/ Hospital for Joint Diseases Langone Medical Center, New York, NY, USA; [2]Cleveland Clinic, Cleveland, OH, USA

Poster #20 **CLINICAL AND PATIENT-REPORTED OUTCOMES AFTER IMAGE-GUIDED INTRA-ARTICULAR THERAPEUTIC HIP INJECTIONS: A RETROSPECTIVE STUDY**

William Walter, MD[1]; Craig Bearison, BS[2]; James Slover, MD, MS[1]; Heather Gold, PhD[1]; Soterios Gyftopoulos, MD, MSc[1]
[1]NYU Medical Center/ Hospital for Joint Diseases Langone Medical Center, New York, NY, USA; [2]New York University School of Medicine, New York, NY, USA

Poster #21 **EFFICACY OF INTRA-ARTICULAR HIP STEROID INJECTION AND SUBSEQUENT SURGERY**

Benjamin Levine, MD; Wilson Lai; Kambiz Motamedi, MD; Leanne Seeger, MD; Sharon Hame, MD
University of California, Los Angeles, Los Angeles, CA, USA

Poster #22 **VALUE OF PRE-OPERATIVE FLUOROSCOPIC-GUIDED SUBTALAR ARTHROGRAPHY**

Richard Walker, MD, FRCPC; Rachael Da Cunha, MD, FRCSC; Jason Boubalos, MD; Tara Heric, RN; Jeremy Lamothe, MD, PhD, FRCSC; Ian Le, MD, FRCSC
University of Calgary, Calgary, AB, Canada

Keynote Abstract

PREDICTING SKELETAL AGE - INSIGHTS FROM THE 2017 RSNA MACHINE LEARNING COMPETITION

Alexander Bilbily MD[1]; Mark Cicero MD; Lawrence White MD
[1]Toronto Joint Department of Medical Imaging, University of Toronto, Toronto, Ontario, Canada

Purpose: Develop a computer algorithm to predict skeletal age from pediatric hand x-rays.

Material & Methods: The competition was split into three phases (dataset sizes provided in each phase from 2 U.S. hospitals are in parentheses): Training (n=12,612), Leaderboard (n=1,425) and Test (n=200). Images, gender, and bone age in months were provided for the training set. We used a 85:15 training:validation split to train our deep convolutional neural network which consisted of an Inception V3 module which took the images at 500 x 500 pixels as input and concatenated it with the gender input (0-female, 1-male). This was followed by two additional 1000-neuron fully-connected layers before the single node linear output (in months).

Training was done on a single NVIDIA P40 GPU for 500 epochs using the ADAM optimizer to minimize the mean absolute deviation (MAD). Real-time image augmentation was used with up to 20% horizontal/vertical translation, 30 degrees rotation, and random horizontal flip. At inference, we created 10 random augmentations of the candidate image and fed those to an ensemble of the top 5 trained models. The 50 outputs were averaged and rounded to the nearest integer - representing the final bone-age prediction in months.

Results: Our top 3 models achieved a MAD of 5.99 months on the validation set and our fourth and fifth model achieved a MAD of 6.00 months. Our approach resulted in a MAD of 4.265 months on the test set achieving first place in the 2017 RSNA pediatric bone-age machine learning competition.

Conclusion: Specifically designed multi-input deep neural networks are effective at predicting pediatric bone-age. The algorithm presented here represents the current state-of-the-art for bone-age prediction.

Podium #10

SUPERIOR CAPSULAR RECONSTRUCTION OF THE SHOULDER – ALL YOU WANTED TO KNOW!

Manickam Kumaravel, MD
Memorial Hermann Hospital - Texas Medical Center/ University of Texas HSC at Houston, houston, USA
(Presented by: Manickam Kumaravel, MD, Memorial Hermann Hospital - Texas Medical Center/ University of Texas HSC at Houston)

Purpose: Superior capsular reconstruction of the shoulder, is a new technique used in treating patients with chronic massive rotator cuff tears, multiple rotator cuff surgeries, and in "irreparable rotator cuff tear "scenarios. Radiologists benefit from being familiar with the concept, so as to be able to provide appropriate assessment with both pre-and post-operative imaging.

Materials and Methods: Exhibit aims to:

1. Elucidate the pathophysiology of the superior aspect of capsule of the shoulder and the role of chronically torn supra and infraspinatus, in shoulder movement.
2. Discuss indications for superior capsular reconstruction.
3. Discuss in detail the various surgical techniques in superior capsular reconstruction
4. Role of imaging in planning superior capsular reconstruction – radiographs, and MRI
5. Review imaging of superior capsular reconstruction with examples of postoperative imaging and complications.
6. Recognize pitfalls associated with imaging of superior capsular reconstruction.

Results: Content organization:

1. Illustration of techniques of superior capsular reconstruction with cartoons and intraoperative pictures and video.

2. Detailed imaging including radiographs, and MRI images of preplanning scenarios, including examples of normal postoperative appearances and complications.

3. Comprehensive discussion of imaging algorithm of superior capsular reconstruction.

Conclusion: Educational objectives:

On studying the exhibit, the reviewer will be able to

1. Understand the need for the newer technique of superior capsular reconstruction.

2. Understand the techniques of superior capsular reconstruction.

3. Have a detailed knowledge of the surgical techniques, imaging appearance of superior capsular reconstruction – including normal and abnormal MRI appearances and treatment algorithms.

Modality % - Radiography / Fluoroscopy:	10
Modality % - CT:	10
Modality % - MRI:	80
Modality % - US:	0
Modality % - Nuclear Medicine:	0

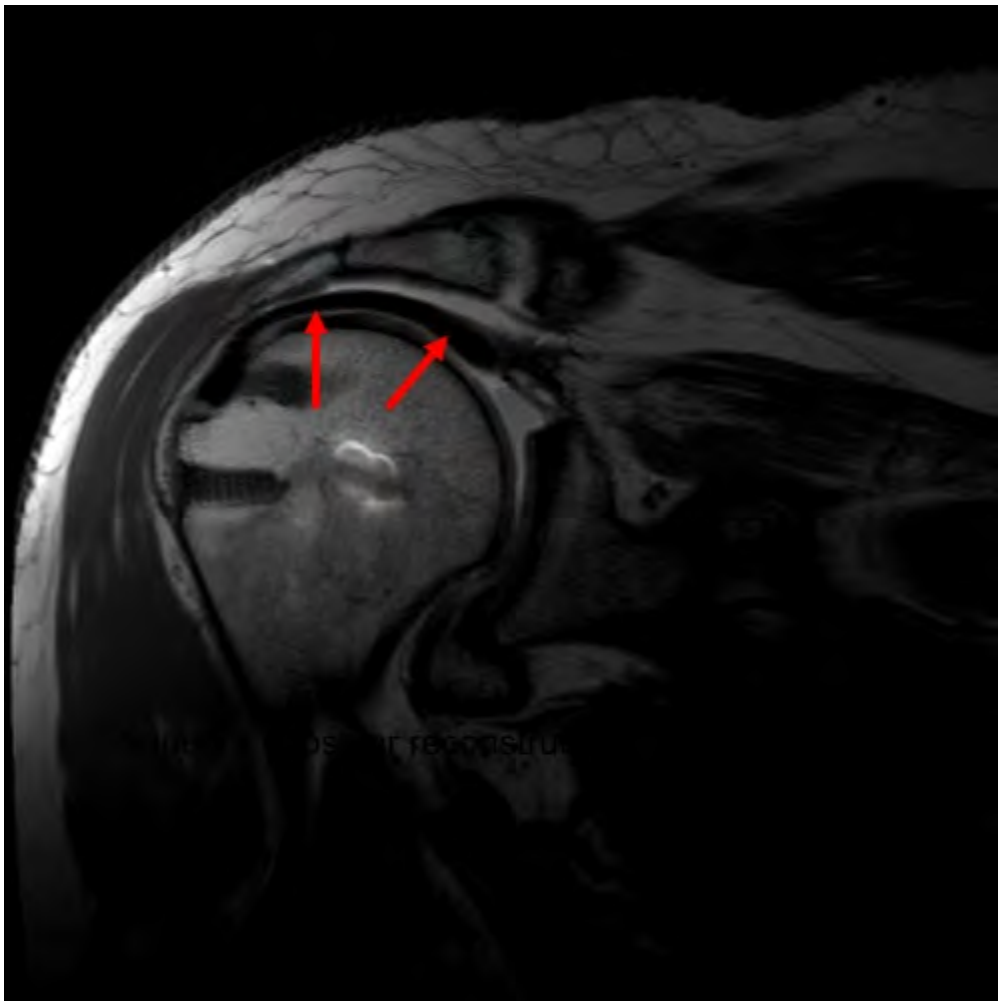

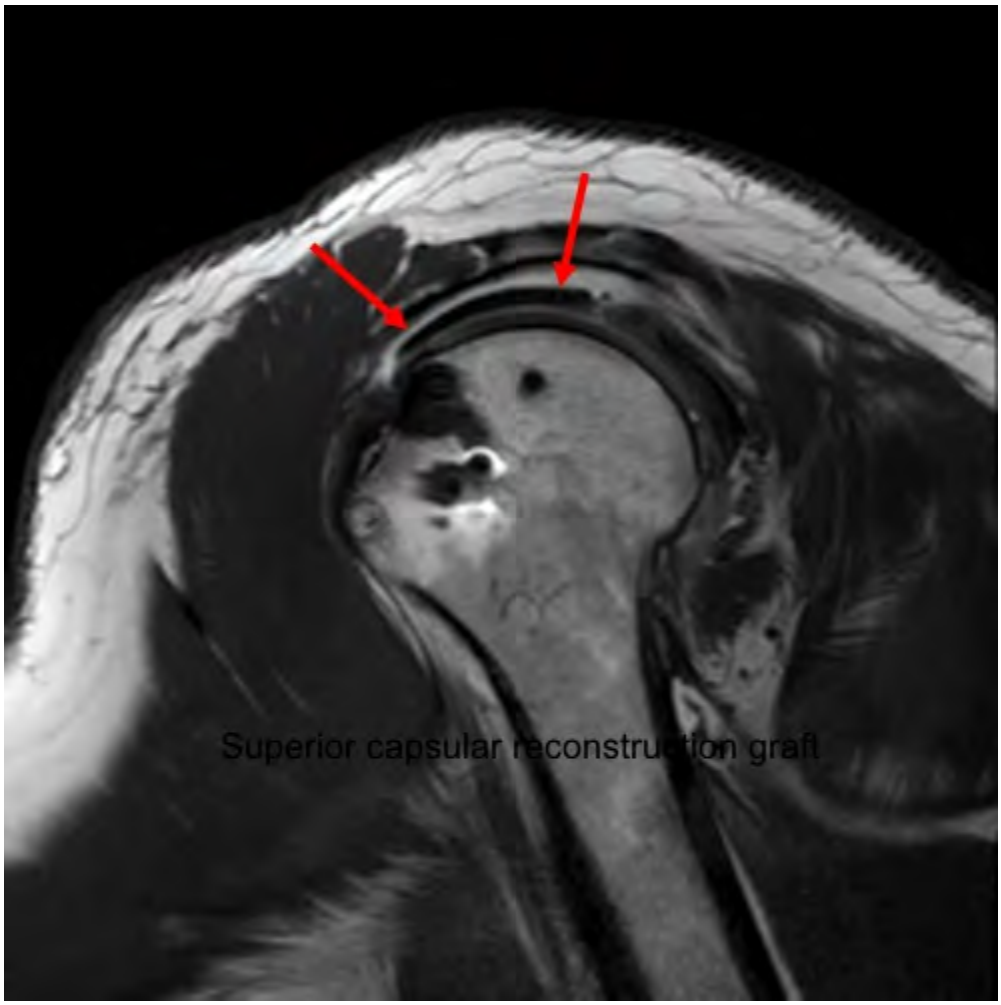

1. Coronal demonstrates the point of anchor of the graft , reconstructing the superior capsule
2. Sagittal demonstrating graft location and subacromial space.

Podium #11

Multilevel Glenoid Morphology and Retroversion Assessment in Walch B2 and B3 Types

Mohammad Samim, MD; Mandeep Virk, MD; Joseph Zuckerman, MD; Soterios Gyftopoulos, MD
NYU Medical Center/ Hospital for Joint Diseases Langone Medical Center, New York, NY, USA
(Presented by: Mohammad Samim, MD, NYU Medical Center/ Hospital for Joint Diseases Langone Medical Center)

Purpose: As glenohumeral osteoarthritis progresses, there is increased risk for posterior glenoid bone loss which impacts an increasingly common treatment for these patients, total shoulder arthroplasty. Defining the level of maximum posterior bone loss and accurate assessment of its severity, using glenoid version measurements, are crucial to correctly align the glenoid prosthesis with glenoid to prevent prosthetic failure. While the importance of this information is clear, how these measurements should be performed remains in question with several techniques described in the literature. The purpose of this study was to define the most accurate level to measure glenoid version on CT for the most clinically relevant variants of posterior glenoid bone loss, Walch B2 and B3 types.

Materials and Methods: 386 consecutive CT shoulder studies performed for shoulder arthroplasty preoperative planning between 2013-2016 were retrospectively reviewed. Patients with B2 and B3 glenoid types were included. Two radiologists measured glenoid retroversion independently according to Friedman method on true axial CT images using the "intermediate glenoid line", at three glenoid heights: 25% (upper) 50% (equator) and 75% (lower).

Results: 29 B2 and 8 B3 glenoid types were included. There was no statistically significant difference found in the retroversion measurements performed by each reader at the three glenoid levels on the B2 or B3 glenoid types (Mean angles (%) in upper, equator and lower in B2: 16.5, 17,0 and 17.5 and B3: 20.6, 20.7 and 23.2, respectively). There was substantial inter-reader correlation ($r \geq 0.7$) in angle measurements.

Conclusion: Our study suggests that glenoid version can be accurately measured at any level between 25% -75% of the glenoid height for Walch B2 and B3 types. We recommend that the glenoid equator be used as the reference in order to assure consistent and reliable version measurements in this group of patients.

Modality % - Radiography / Fluoroscopy:	0
Modality % - CT:	100
Modality % - MRI:	2
Modality % - US:	0
Modality % - Nuclear Medicine:	0

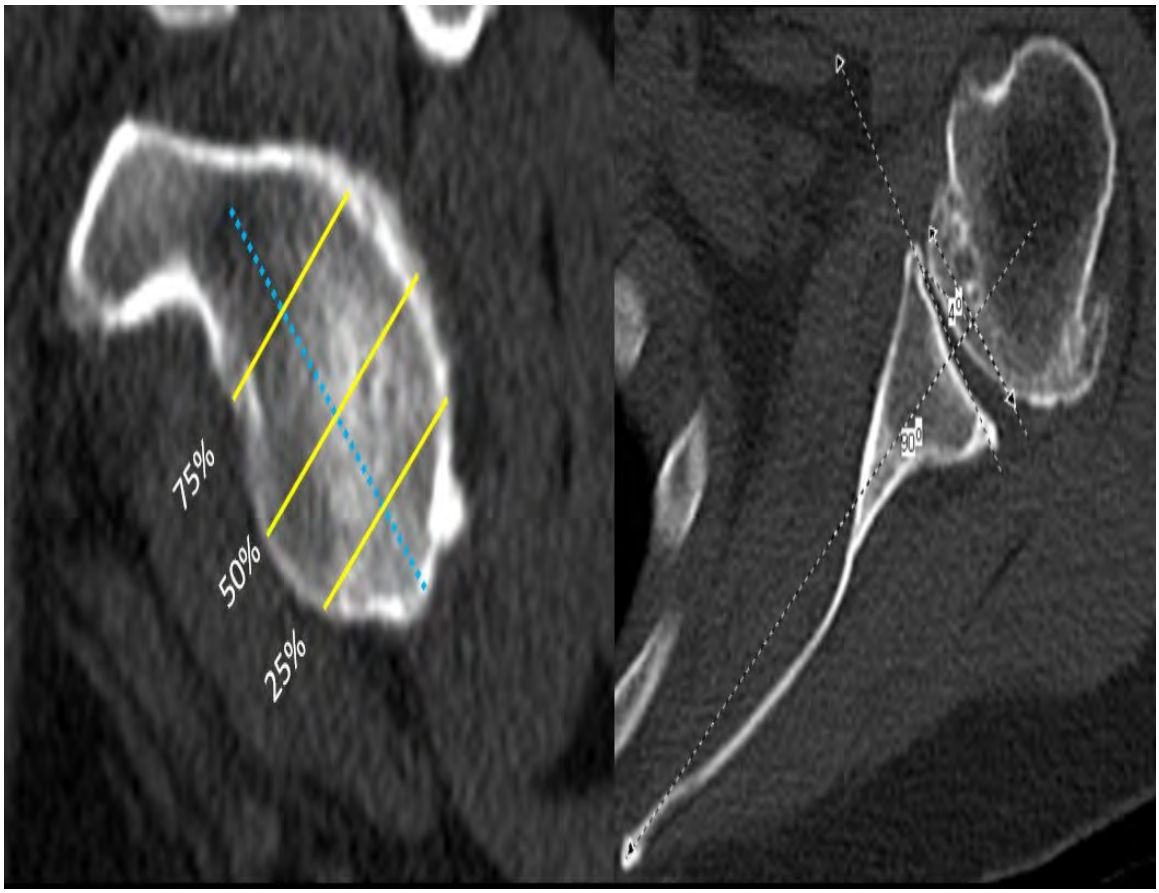

Sagittal CT image shows the three glenoid heights: 25% (upper) 50% (equator) and 75% (lower). Axial CT image shows example of the retroversion measurement.

Podium #12

OPTIMIZING METHODS TO QUANTIFY INTRAMUSCULAR FAT IN ROTATOR CUFF TEARS WITH NORMALIZATION

Ankur Garg, MD[1]; Paul Micevych[1]; Rajan Khanna[2]; Lucas Buchler, MD[1]; Guido Marra, MD[1]; Matthew Saltzman, MD[1]; Todd Parrish, PhD[1]; Amee Seitz, PhD[1]

[1]Northwestern Memorial Hospital ;Northwestern University Feinberg School of Medicine, Chicago, IL, USA; [2]Loyola University Chicago Stritch School of Medicine, Chicago, IL, USA

(Presented by: Ankur Garg, MD, Northwestern Memorial Hospital ;Northwestern University Feinberg School of Medicine)

Purpose: Normalizing intramuscular fat fraction (%fat) in rotator cuff muscles to %fat in an unaffected muscle may provide a method to control for individual differences. Our study purpose is to determine which normalization method best accounts for individual confounders, such as BMI and age, when quantifying fat infiltration in cuff tears.

Materials and Methods: Consecutive symptomatic patients (n=41; 26 males; age=57.95±12.88 years; BMI=29.73±5.84) underwent shoulder MRI including 3D multi-echo two-point Dixon fat/water sequences. Tear size was evaluated by a musculoskeletal radiologist blinded to surgeon diagnosis. %Fat in Dixon images was quantified in the rotator cuff (SS, IS, SC, TM), combined infraspinatus/teres minor (IS/TM), teres major, and triceps muscles using a customized MATLAB program (Figure 1). Fat fractions were normalized by dividing %fat in rotator cuff muscle by that in teres major, triceps, and teres minor. Relationships between %fat and BMI, age, and tear size were evaluated pre/post normalization in each rotator cuff muscle and compared for significant differences post-Fisher transformation (p<0.05).

Results: Pre-normalization, there were significant relationships (p<0.05) between %fat and BMI/age in all rotator cuff muscles (r_{BMI}=0.34–0.43; r_{AGE}=0.45–0.60). Significance was lost in all muscles after teres major-normalization (p>0.05). In contrast, triceps-normalization maintained significance between %fat and age in two muscles (SS; p=0.0302; IS/TM; p=0.0280) and teres minor-normalization maintained significance between %fat and BMI in one (SC; p=0.0391). Pre-normalization, there were also significant relationships (Figure 2) between %fat and tear size (p<0.05; r =0.40–0.60) in all muscles. All %fat-tear size relationships weakened post-normalization, but teres major-normalized relationships showed the strongest remaining correlations (r=0.21–0.36).

Conclusion: Normalization with teres major eliminated confounding relationships between %fat and age/BMI and best preserved relationships between tear size and %fat. Normalization to teres major serves as a quick, effective technique to ameliorate individual differences when quantifying %fat in cuff tears.

Modality % - Radiography / Fluoroscopy:	0
Modality % - CT:	0
Modality % - MRI:	100
Modality % - US:	0
Modality % - Nuclear Medicine:	0

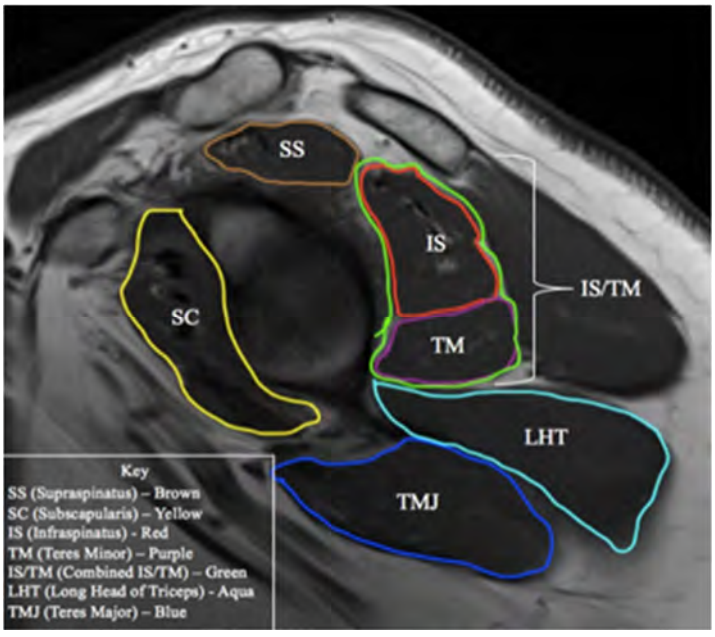

Figure 1. Sagittal oblique MR image with the outline of segmented regions shown at the level of the glenohumeral joint.

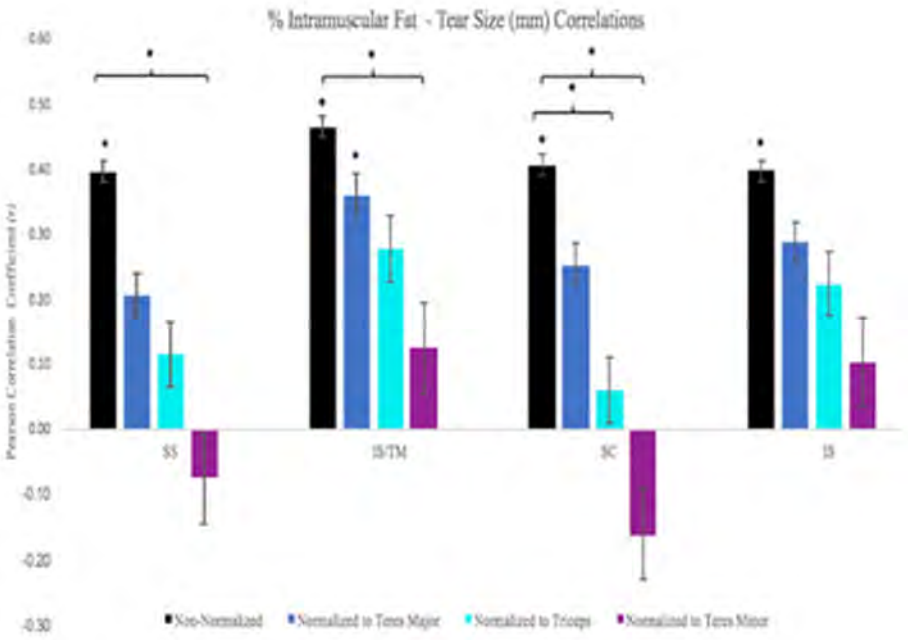

Figure 2. %Fat-tear size correlation coefficients across non-normalized and three normalized conditions for supraspinatus (SS), combined infraspinatus/teres minor (IS/TM), subscapularis (SC), and infraspinatus (IS); *p<0.05.

Podium #13

PACINIAN CORPUSCLES: BRIGHT PALMAR BLIND-SPOTS ON MRI

Nicholas Rhodes, MD[1]; David Rubin, MD[2]; Lehman Julia, MD[1]
[1]Mayo Clinic, Rochester, MN, USA; [2]Mallinckrodt Institute of Radiology, Saint Louis, MN, USA
(Presented by: Nicholas Rhodes, MD, Mayo Clinic)

Purpose: Pacinian corpuscles, the main touch receptors to pressure and vibration, are ubiquitous in the deep dermis and hypodermis of the fingers and palms. Sporadic reports of painful hyperplastic or hypertrophied Pacinian corpuscles have appeared in the pathology and dermatology literature. Nevertheless, their existence is largely unknown to most radiologists. We frequently noted hyperintense nodules in the palms of patients on water-sensitive MRI sequences, but were unable to explain their etiology. We hypothesize that the MRI finding of palmar hyperintense nodules (i.e., "palmar dots") represents Pacinian corpuscles.

Materials and Methods: We review the anatomy and distribution of Pacinian corpuscles and review the medical literature concerning them. We review our MR imaging of the hands and wrists and present a “typical” patient demonstrating T2/STIR hyperintense, nonenhancing palmar nodules. We present MRI correlation of two recently encountered patients who had Pacinian corpuscles identified at surgical exploration and pathologic analysis.

1. **Results:** “Palmar dots” vary in size, number, and density, but are present in all patients.
2. The appearance of a “palmar dot” on MRI (i.e., T2/STIR hyperintense focus without enhancement) is in keeping with the anatomy of the Pacinian corpuscle.
3. The distribution of “palmar dots” on MRI correlates with the known distribution of Pacinian corpuscles on anatomic dissection.
4. On pathologic evaluation of two cases of dissected Pacinian corpuscles, the pre-surgical MRIs demonstrated correlating “palmar dots”.

Conclusion: Our observations support the hypothesis that “palmar dots”, ie T2/STIR hyperintense nodules within the palms, are Pacinian corpuscles.

Modality % - Radiography / Fluoroscopy:	0
Modality % - CT:	0
Modality % - MRI:	100
Modality % - US:	0
Modality % - Nuclear Medicine:	0

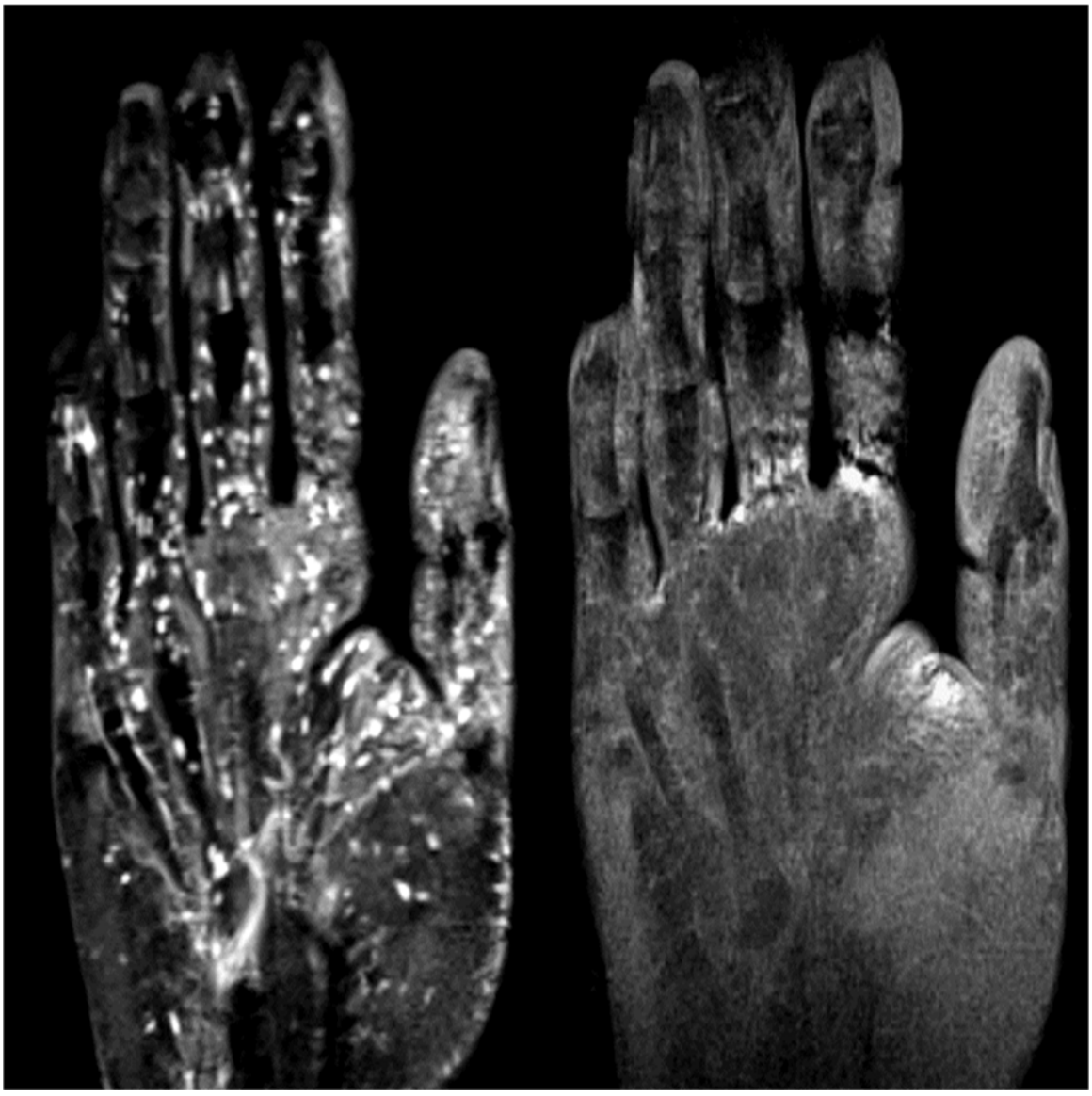

Fig.1: Typical "palmar dots". Coronal STIR (left) and post-gadolinium T1fs (right) images demonstrate the nonenhancing, STIR hyperintense foci in the palmar soft tissues.

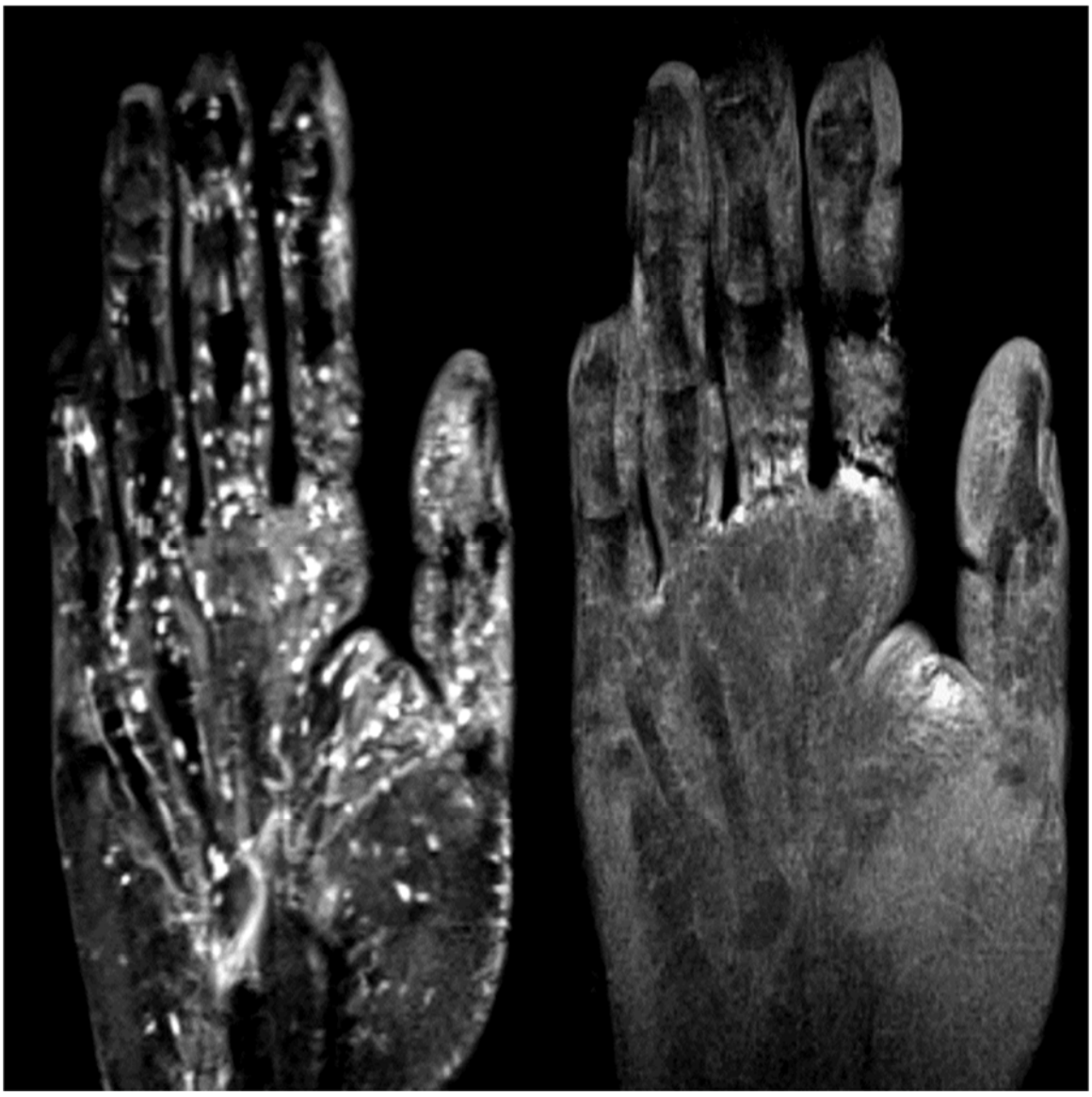

Fig.2: T2fs (left) and post-gadolinium SPGRfs (right) images. Large arrowhead marks partially included neuroma. Numerous adjacent T2 hyperintense and nonenhancing Pacinian corpuscles (long white arrow).

Podium #14

HYPERINTENSE T2 SIGNAL IN THE ULNAR NERVE AT THE CUBITAL TUNNEL: NORMAL OR ABNORMAL?

Carissa White, MD; Behrad Golshani, MD; Benjamin Plotkin, MD; Kambiz Motamedi, MD; Leanne Seeger, MD; Benjamin Levine, MD
David Geffen School of Medicine at UCLA, Los Angeles, CA, USA
(Presented by: Carissa White, MD, David Geffen School of Medicine at UCLA)

Purpose: Increased T2 signal within the ulnar nerve in the cubital tunnel is often observed on MRIs performed for unrelated clinical indications. The clinical significance of this finding is unknown. We hypothesized that hyperintense T2 signal in the ulnar nerve at the cubital is commonly asymptomatic.

Materials and Methods: Following IRB approval, all adult elbow MRIs performed at our institution between January 1 and August 31, 2017 were queried. A total of 87 patients were identified. 12 patients were excluded because the study indication or clinical notes documented ulnar nerve or medial elbow symptoms. 23 patients were excluded due to confounding issues such as a history of ipsilateral arm radiation therapy, mass effect on the ulnar nerve or motion artifact. The 54 remaining MRIs were independently reviewed by a musculoskeletal fellowship trained attending radiologist and a musculoskeletal radiology fellow. Using the axial T2 fat saturated sequence, signal of the ulnar nerve in the cubital tunnel and just distal to the cubital tunnel was evaluated. Signal was recorded as increased if it was significantly higher than the radial nerve on the same image slice.

Results: For reader #1, 63% of patients demonstrated increased T2 signal in the ulnar nerve at the cubital tunnel, and 33% just distal to the cubital tunnel. For reader # 2, 67% of patients had increased T2 signal in the ulnar nerve at the cubital tunnel, and 35% just distal to the cubital tunnel. Inter-observer reliability was high, with Cohen's kappa equaling 0.91 for signal in the cubital tunnel and 0.96 for signal just distal to the cubital tunnel.

Conclusion: Hyperintense T2 signal in the ulnar nerve at the cubital tunnel is a common, asymptomatic finding on MRIs performed for unrelated indications, and is likely not of clinical significance.

Modality % - Radiography / Fluoroscopy:	0
Modality % - CT:	0
Modality % - MRI:	100
Modality % - US:	0
Modality % - Nuclear Medicine:	0

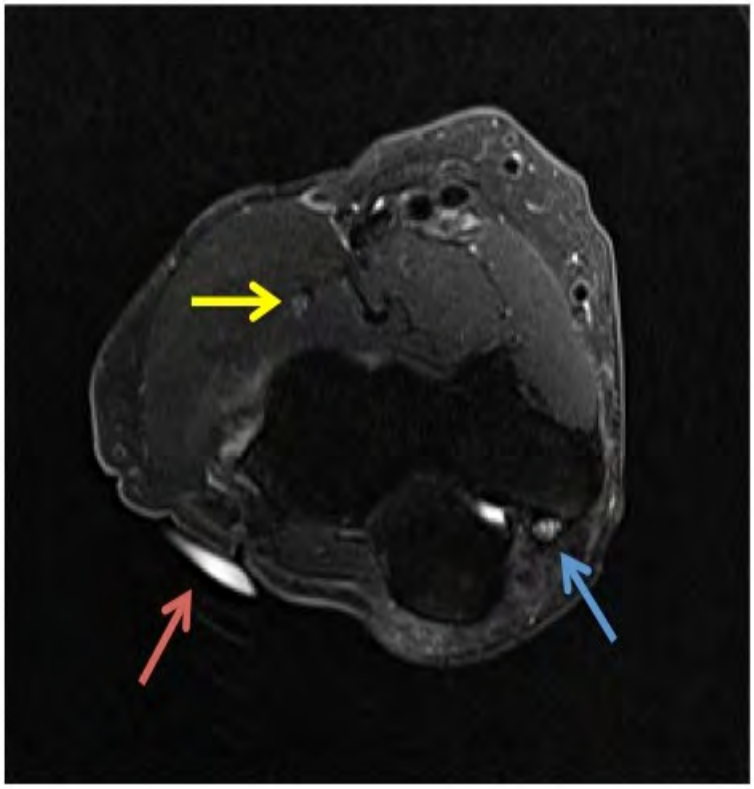

Axial T2W fat-sat image, demonstrating hyperintensity of the ulnar nerve (blue) compared to the radial nerve (yellow). Pain marker (red) is on the lateral side.

Podium #15

CHARACTERIZATION OF GLENOID BONE REMODELING IN PROFESSIONAL BASEBALL PLAYERS

Jonathan Rassi, MD; Naveen Subhas, MD; Jennifer Bullen, MS; Joshua Polster, MD
Cleveland Clinic, Cleveland, OH, USA
(Presented by: Jonathan Rassi, MD, Cleveland Clinic)

Purpose: Adaptive bony changes in overhead throwing athletes have been demonstrated in the humerus and glenoid resulting in increased humeral torsion and global glenoid retroversion compared to non-throwers. There has been limited characterization of glenoid remodeling in professional throwing athletes in the literature, which has been described as planar retroversion of the glenoid surface. Our experience suggests localized convex remodeling of the posterior/posterior-superior glenoid margin suggesting a relationship to posterior-superior impingement. This study was designed to characterize the morphology, location, and frequency of adaptive glenoid changes in professional baseball players.

Materials and Methods: Two musculoskeletal radiologists independently reviewed a blinded, randomized list of 80 shoulder MRIs consisting of 40 professional baseball players and 40 age-matched controls. Glenoid morphology was scored for the presence of localized posterior glenoid bone remodeling and the clockface position of remodeling. Interreader agreement, prevalence of remodeling in athletes versus controls, and association of glenoid remodeling with additional posterior glenoid pathology were determined.

Results: There was moderate agreement on the presence of glenoid bone remodeling in 75% (60/80) of subjects (Kappa 0.49, 95% CI: 0.31, 0.68). There was greater prevalence of glenoid remodeling in throwing athletes than controls (reader 1 p-value 0.001; reader 2 p-value 0.254). The most apparent location of glenoid remodeling was posterior to posterior-superior (reader 1 median clockface 9.5, IQR: 9-9.5; reader 2 median clockface 10, IQR: 9.5-10.5). The association between the presence of other posterior glenoid abnormalities (e.g., posterior labral tears, Bennett lesions, or chondral abnormalities) was marginally significant between subjects with and without glenoid remodeling (24/38=63% vs 18/42=43%, p=0.078).

Conclusion: Glenoid remodeling in professional baseball players is identified on MRI and manifests as localized, convex morphology most commonly in the posterior or posterior-superior glenoid. There is an increased incidence of associated soft tissue injuries in subjects with glenoid remodeling.

Modality % - Radiography / Fluoroscopy:	0
Modality % - CT:	0
Modality % - MRI:	100
Modality % - US:	0
Modality % - Nuclear Medicine:	0

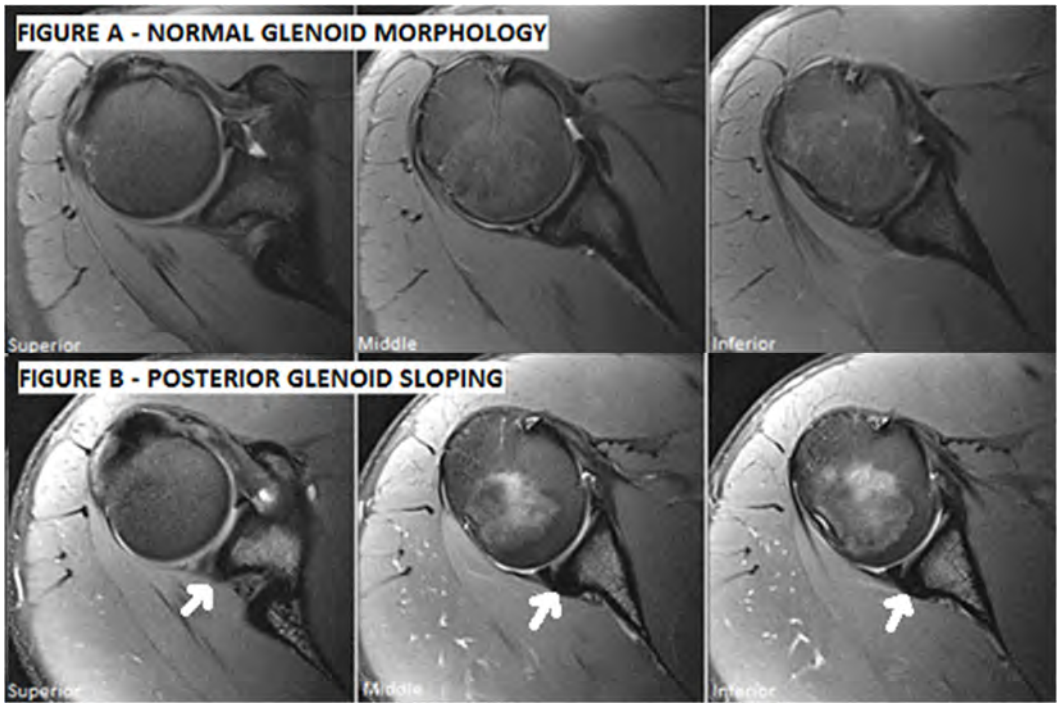

Figure A demonstrates normal glenoid morphology in axial plane at superior, middle, and inferior aspects. Figure B demonstrates posterior glenoid sloping (arrow).

Podium #16

DIFFUSION TENSOR IMAGING OF THE MEDIAN NERVE WITH ULTRASOUND CORRELATION IN PATIENTS WITH CARPAL TUNNEL SYNDROME BEFORE AND AFTER FLEXOR RETINACULAR RELEASE

Lana Gimber, MD, MPH[1]; Elizabeth Krupinski, PhD[2]; Tolga Turker, MD[1]; Giles Becker, MD[1]; Lea MacKinnon, MD[1]; Tyson Chadaz, MD[1]; Mihra Taljanovic, MD, PhD[1]
[1]University of Arizona HCS - Tucson, Tucson, AZ, USA; [2]Emory University, Atlanta, GA, USA
(Presented by: Lana Gimber, MD, MPH, University of Arizona HCS - Tucson)

1. **Purpose:** Investigate the relationship of diffusion tensor imaging (DTI) and ultrasound (US) in evaluating carpal tunnel syndrome (CTS) before and 3 and 6 months after carpal tunnel release in correlation with preoperative nerve conduction studies (NCS).
2. Compare DTI and US examination results in CTS subjects versus asymptomatic volunteers.

Materials and Methods: Six CTS subjects diagnosed by NCS were evaluated with DTI and US examination before, and 3 and 6 months following carpal tunnel release. Five healthy volunteers underwent single DTI and US examinations. DTI parameters included fractional anisotropy (FA) and apparent diffusion coefficient (ADC). US parameters included cross-sectional area and hyperemia. Measurements were taken at the levels of pronator quadratus, pisiform, and hook of hamate by 2 musculoskeletal radiologists. Relationships between DTI parameters, US, and NCS as well as inter-reader agreement were analyzed.

Results: Subject mean age was 50.7 years (sd=12.7). DTI inter-reader agreement ranged from good to excellent (K=0.64-0.99). Strong negative NCS correlations were seen between motor latency and FA (range -0.63 to -0.87) in addition to motor velocity and nerve area (range -0.59 to -0.86). Nerve hyperemia was seen in all pre-operative cases versus no controls. There was significant difference in nerve area in preoperative versus control wrists at the hamate (p=0.002), with other levels trending to significance. In preoperative versus 6 month postoperative wrists, there were significant differences in FA at pisiform (p=0.02), nerve area at pronator quadratus (p=0.01), and nerve area at hamate (p=0.03).

Conclusion: This study showed multiple strong correlations between NCS values with DTI and US in CTS subjects. Nerve area and hyperemia were the most significant findings in pre-operative CTS patients versus controls, with additional significant changes on US and DTI seen in pre-operative versus post-operative studies.

Modality % - Radiography / Fluoroscopy:	0
Modality % - CT:	0
Modality % - MRI:	50
Modality % - US:	50
Modality % - Nuclear Medicine:	0

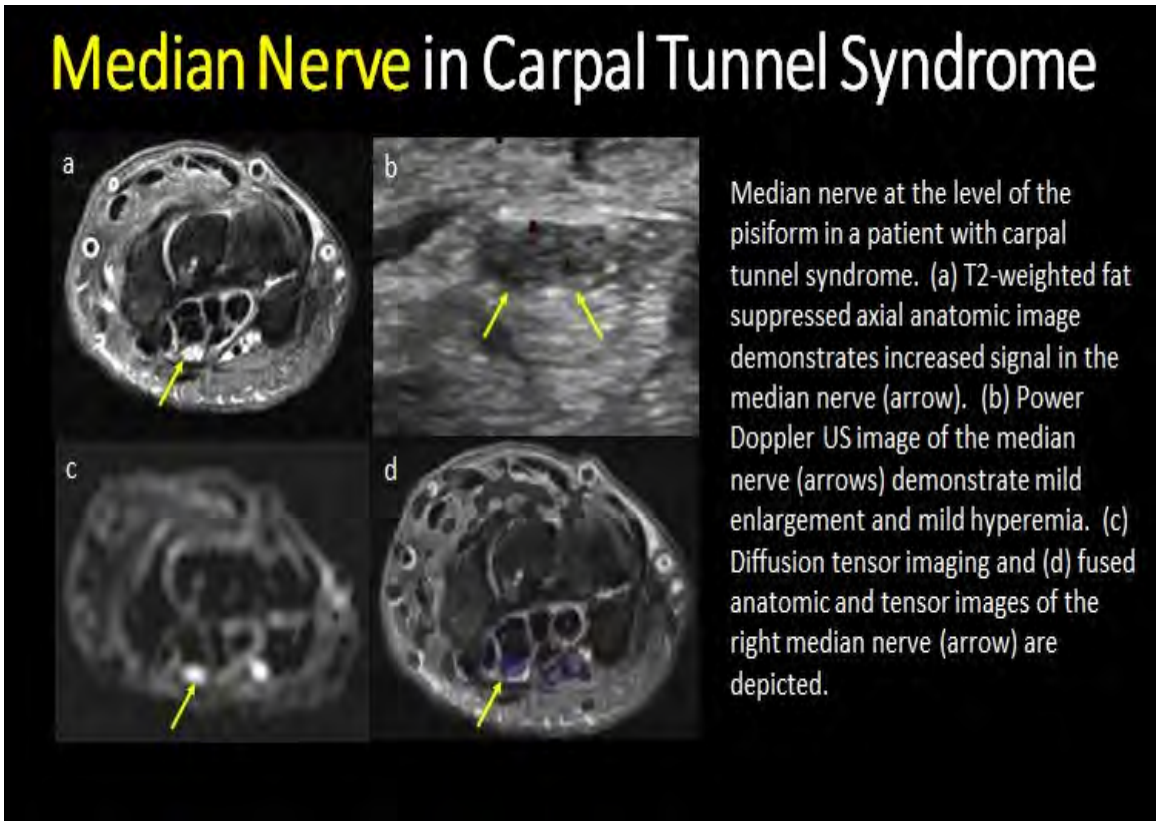

MRI, ultrasound, and diffusion tensor imaging of the median nerve at the level of the pisiform in a patient with carpal tunnel syndrome.

Podium #17

ACCURACY OF MRI AND MRA IN DETECTING ROTATOR CUFF TEARS IN PATIENTS WITH CALCIFIC TENDINOSIS

Michael Fox, MD[1]; Jonathan Flug, MD[2]; Joseph Brinkman[3]; David Hartigan, MD[2]; Mark Kransdorf, MD[2]; Spencer Chivers, MD[2]; Taryar Zaw, MD[2]

[1]Mayo Clinic, Phoenix, AZ, USA; [2]Mayo Clinic Hospital, Phoenix, AZ, USA; [3]Creighton, Omaha, NE, USA

(Presented by: Michael Fox, MD, Mayo Clinic)

Purpose: Given the inflammation sometimes associated with calcific tendinosis, diagnosing a rotator cuff tear with MRI can be challenging. We conducted a retrospective review of patients with calcific tendinitis, MRI or magnetic resonance arthrography (MRA) and subsequent surgery/procedure to determine the sensitivity, specificity and accuracy of MRI/MRA in this patient population.

Materials and Methods: Patients with calcific tendinitis, radiographs, MRI/MRA and shoulder surgery were independently reviewed by an MSK radiologist and MSK fellow for the presence of calcification and presence/degree of cuff tear (LG (low-grade), HG (high-grade) and FT (full thickness)).

100 MRI/MRAs were reviewed with 23 exams excluded for the following reasons: TSA with no mention of cuff (n=6); Surgery beyond 1 year (n=4); Percutaneous tenotomy/aspiration (n=5); No op-report available (n=3); Duplicate exam (n=5).

No tear/LG groups and HG/FT groups were combined for analysis.

Results: 77 exams (MRI=69;MRA=8) in 74 patients (mean age 60;range 25-83; 45F:29M) formed the study group. Exact agreement on group assignment was present in 81% of exams (62/77). The sensitivity, specificity and accuracy for rotator cuff tears on MRI was 69%, 83%, 74% and 73%, 83% and 77% for Readers 1 and 2 respectively. The sensitivity, specificity and accuracy of MRA for rotator cuff tears was 100%, 100%, 100% and 67%, 100% and 88% for Readers 1 and 2 respectively.

Conclusion: The overall sensitivity and accuracy of MRI for diagnosing rotator cuff tears in the setting of calcific tendinitis is decreased compared to reports for detecting cuff tears in the general population, with similar specificity. This is likely related to the inflammatory effect of the calcific tendinosis and the high number of false negatives. MRA performed better which suggests that in patients with calcific tendinitis, the use of MRA should be considered.

Modality % - Radiography / Fluoroscopy:	15
Modality % - CT:	0
Modality % - MRI:	85
Modality % - US:	0
Modality % - Nuclear Medicine:	0

Podium #18

LATISSIMUS DORSI TENDON TRANSFER PROCEDURES: PRE- AND POST-OPERATIVE MR IMAGING FEATURES

Lawrence White, MD; Linda Probyn, MD; Patrick Henry, MD; Timothy Dwyer, MBBS, PhD; Michael McKee, MD
University of Toronto, Toronto, ON, Canada
(Presented by: Lawrence White, MD, University of Toronto)

Purpose: To evaluate the pre- and post-operative MRI appearance of the shoulder following latissimus dorsi tendon-transfer (LDTT) surgery.

Materials and Methods: A retrospective review of pre- and 1-year post-operative shoulder MR imaging in 12 consecutive LDTT cases was performed.

All MR imaging studies were evaluated for rotator-cuff tendon tears, tendon retraction, muscular fatty atrophy (Goutallier grade$\geq$3), acromio-humeral distance, and full-thickness (focal-or-diffuse) glenohumeral cartilage loss. Evaluation of post-operative exams additionally included; anatomic course, integrity and signal characteristics of the transferred latissimus dorsi (LD) tendon, and its surgical fixation.

Results: 20 MRI exams (8 pre-operative, 12 post-LDTT) were evaluated in 12 patients (mean-age; 58, range 45-67).

MR imaging 1-year post LDTT, showed supraspinatus tears in all cases (12/12). Additional tears were seen of infraspinatus (10/12), and subscapularis (3/12). Mean tendon retraction was 4.2cm (range 2.4-4.9cm). Fatty atrophy of rotator-cuff musculature was observed in 10 patients. Mean acromio-humeral distance was 3.3mm (range 1-5mm). Full-thickness glenohumeral cartilage loss was observed in 1 case.

No statistically significant differences in rotator-cuff tearing/retraction (p-values all > 0.05), muscle atrophy (p=0.480), acromio-humeral distance (p=0.170), or glenohumeral cartilage loss (p=1), were observed between pre-operative and 1-year post-operative LDTT MR imaging studies.

Postoperative exams showed supero-lateral oblique course of the LD tendon posteriorly, superficial to teres minor, and deep to deltoid. LD tendon continuity/integrity could be followed in 11 cases, with heterogeneous signal, throughout its fixation along middle-superior facets of the greater tuberosity

Conclusion: LDTT can be assessed and followed postoperatively at MRI. Rotator cuff tearing, tendon retraction, muscle fatty atrophy, acromio-humeral distance, and glenohumeral cartilage loss may be unchanged compared to preoperative findings, following LDTT surgery and are not reflective of surgical complication/failure. Familiarity with the spectrum of “expected” postoperative findings is critical in accurate interpretation of shoulder MRI exams in this patient group.

Modality % - Radiography / Fluoroscopy:	0
Modality % - CT:	0
Modality % - MRI:	100
Modality % - US:	0
Modality % - Nuclear Medicine:	0

Podium #19

FOUR YEAR RETROSPECTIVE REVIEW OF PERINEURAL INJECTIONS ABOUT THE UPPER EXTREMITY

Pamela Walsh, MD; William Walter, MD; Christopher Burke, MD; Ronald Adler, MD, PhD
NYU Medical Center/ Hospital for Joint Diseases Langone Medical Center, New York, NY, USA
(Presented by: Pamela Walsh, MD, NYU Medical Center/ Hospital for Joint Diseases Langone Medical Center)

Purpose: To present a 4 year clinical experience with ultrasound-guided therapeutic perineural injections of upper extremity peripheral nerves and evaluate utility of ultrasound guidance for diagnosis of intrinsic or perineural pathologies.

Materials and Methods: A retrospective keyword PACS search was conducted for upper extremity therapeutic perineural injections (May 2012-January 2017), yielding 342 cases. 175 were excluded because no perineural injection was performed. 5 patients underwent injection of more than one nerve during one visit, yielding 174 perineural injections among 130 patients. Retrospective chart review was undertaken to determine patient demographics, clinical indications, presence of structural pathology, as well as presence of pain relief at interval clinical follow-up.

Results: 174 injections among 130 patients were reviewed (mean age=57.75 years [15-97], 68 female (52%), 62 male (48%)). The most commonly injected nerves included the ulnar (n=81, 46%) and median (n=61, 35%) nerves. The least common was the suprascapular nerve (n=1, 0.6%). Ultrasound at the time of injection revealed $\geq$1 structural abnormality in 110 (63%) cases. The most common was nerve enlargement (n= 101, 92%), although a variety of structural abnormalities were detected, including prior ulnar nerve transposition (n=7, 4%), epicondylitis (n=4, 2%), thickening at the arcade of Frohse (n=3, 2%), low triceps insertion (n=2), ganglion cyst (n=1, 0.5%), anconeus epithrochlearis (n=1, 0.5%), and post-traumatic neuromas (n=1, 0.5%). Interval clinical follow-up was available for 68 patients, of which 51 (75%) reported symptomatic relief. Complications are relatively rare, occurring in only 1 (0.4%) case.

Conclusion: Ultrasound-guided perineural injections about the upper extremity can be safely performed and provide lasting symptomatic relief for a variety of clinical indications. Sonographic evaluation at the time of injection allows identification of structural abnormalities that may contribute to neuropathic symptoms and allow more specific targeting, specific therapy, or surgical guidance.

Modality % - Radiography / Fluoroscopy:	0
Modality % - CT:	0
Modality % - MRI:	0
Modality % - US:	100
Modality % - Nuclear Medicine:	0

Two cases of ulnar neuropathy with ultrasound-mediated diagnosis of specific pathology at the time of perineural injection.

Podium #20

Magnetic Resonance Arthrography of the Wrist: Does Distal Radioulnar Joint Injection Alter Management?

Nathaniel Meyer, MD; Corrie Yablon, MD; Yoav Morag, MD; Jon Jacobson, MD
University of Michigan Medical Center, Ann Arbor, MI, USA
(Presented by: Nathaniel Meyer, MD, University of Michigan Medical Center)

Purpose: Background:

Wrist magnetic resonance arthrography (MRA) is commonly performed with one radiocarpal joint (RCJ) injection. At our institution, if no contrast extends from the RCJ into the distal radioulnar joint (DRUJ) through the triangular fibrocartilage complex (TFCC), then an additional injection of the DRUJ using iodinated contrast is performed to assess for a partial non-communicating, or one-way valve full thickness tear of the TFCC. Although the literature has shown DRUJ injections improve the detection of such tears, it is unknown whether this alters surgical management.

Purpose:

The aim of this retrospective study was to see if a clinical benefit is derived from the inclusion of a DRUJ injection in wrist MRA.

Materials and Methods: The radiology database was searched for all wrist MRA's performed from January 2011 - May 2016 . Fluoroscopic arthrogram reports were reviewed for findings of contrast extension through the TFCC. MRA images and reports were reviewed on patients who subsequently underwent wrist arthroscopy or open surgical exploration. The presence of all types of TFCC tears was noted, including non-communicating peripheral tears extending from the DRUJ. Findings were correlated with surgical reports and interventions were noted.

Results: 282 patients underwent wrist MRA. 34 of 282 patients underwent wrist arthroscopy or open exploration. 21 of 34 surgical patients had DRUJ injections in addition to a RCJ injection. Of these, 8 patients had suspected non-communicating TFCC tears with possible extension to the DRUJ. One patient went directly to open repair of a peripheral TFC/capsular injury. All other lesions intervened on were identified on arthroscopy using a radiocarpal portal. In no cases was the DRUJ inspected arthroscopically.

Conclusion: DRUJ injection during wrist MRA does not alter surgical management. Thus, DRUJ injections should not be included in the wrist MRA protocol.

Modality % - Radiography / Fluoroscopy:	20
Modality % - CT:	0
Modality % - MRI:	80
Modality % - US:	0
Modality % - Nuclear Medicine:	0

Fluoroscopic spot image shows a needle injecting radiopaque contrast into the distal radioulnar joint. The radiocarpal joint was injected prior to the DRUJ injection.

MR arthrogram shows a subtle partial undersurface tear at the ulnar foveal attachment of the TFC. There is also a large peripheral TFCC tear.

Podium #21

DIAGNOSTIC UTILITY OF LAVAGE FOR PERIPROSTHETIC JOINT INFECTION: ARE THE CULTURE RESULTS RELIABLE?

Dana Lin, MD; Christopher Burke, MD; Nathan Jia, BS; Joseph Zuckerman, MD; Gina Ciavarra, MD
NYU Medical Center/ Hospital for Joint Diseases Langone Medical Center, New York, NY, USA
(Presented by: Dana Lin, MD, NYU Medical Center/ Hospital for Joint Diseases Langone Medical Center)

Purpose: Image-guided joint aspiration is often requested for clinically suspected periprosthetic joint infection (PJI). For "dry taps" when no native joint fluid can be aspirated, a lavage with non-bacteriostatic saline can be performed. The purpose of this study is to determine the diagnostic utility of lavage versus native joint fluid aspiration in the setting of clinically suspected PJI.

Materials and Methods: IRB approval was obtained and informed consent was waived for this retrospective study. A PACS search from 2011-2017 for image-guided aspirations yielded 918 procedures, of which 630 were excluded for non-articular and non-arthroplasty aspirations, antibiotic cement spacers, and lack of clinical information in the electronic medical record. The study cohort included 288 procedures from 173 patients who underwent operative or non-operative management. The reference standard was the intraoperative culture for operative patients and clinical follow-up for conservatively managed patients. A Fisher exact test was used for statistical analysis.

Results: The study cohort consisted of 98 females, 75 males, mean age 64 (range 34-90) with the following arthroplasty types: 176 hips, 65 knees, and 47 shoulders (Figure 1). Of 288 procedures, 105 were performed with lavage and 183 were native joint fluid aspirations; 112 were subsequently operatively managed. The mean follow-up for non-operative patients was 5 months (range 0-42). For native joint fluid aspiration versus lavage, accuracy was 81% vs. 73% (p=0.14), sensitivity was 58% vs. 28% (p=0.03), specificity was 88% vs. 91% (p=0.66), negative predictive value was 89% vs. 77% (p=0.02), and positive predictive value was 55% vs. 53% (p=1.00), respectively (Table 1).

Conclusion: Lavage is less sensitive with a lower negative predictive value for the diagnosis of PJI compared to native joint fluid aspirations, possibly due to a lower pretest probability of infection and the inherent dilutional effects of the procedure.

Modality % - Radiography / Fluoroscopy:	5
Modality % - CT:	5
Modality % - MRI:	0
Modality % - US:	90
Modality % - Nuclear Medicine:	0

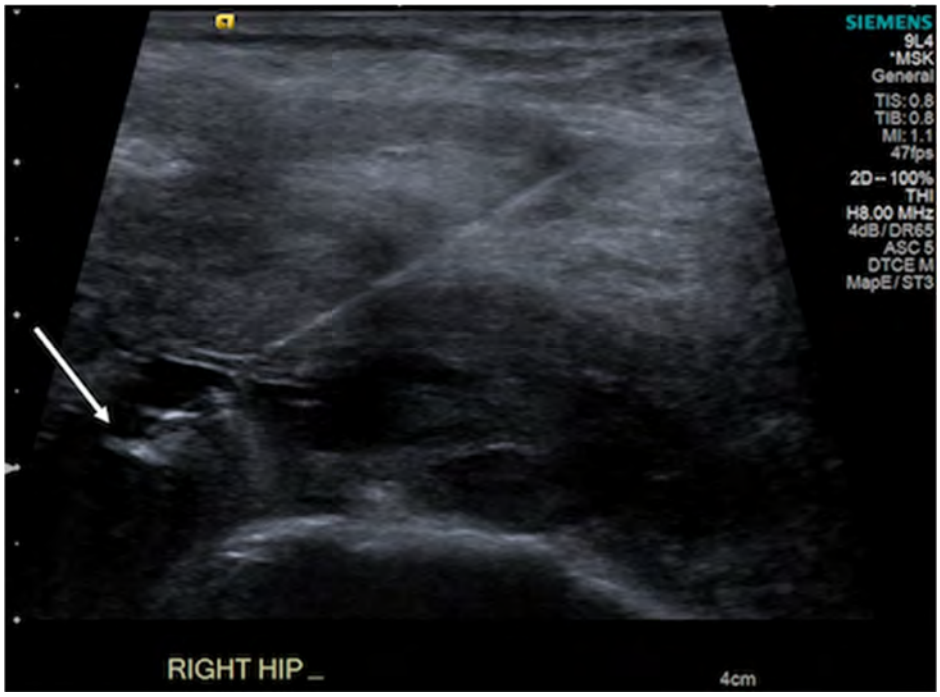

Grayscale ultrasound image, long axis to the hip joint from an anterior approach demonstrates the needle (arrow) within a complex effusion in a post-arthroplasty patient.

	Native Fluid		Lavage		
	Estimate	95% CI*	Estimate	95% CI*	p-value
Accuracy	81% (149/183)	75-87%	73% (77/105)	64-82%	0.136
Sensitivity	58% (22/38)	42-73%	28% (8/29)	14-46%	0.025
Specificity	88% (127/145)	81-93%	91% (69/76)	82-96%	0.655
NPV	89% (127/143)	83-93%	77% (69/90)	67-85%	0.017
PPV	55% (22/40)	39-71%	53% (8/15)	29-79%	1.00

*CI = confidence interval

Native joint fluid aspiration versus lavage for PJI.

Podium #22

POTENTIAL IMPORTANCE OF BIOPSY OF SOFT TISSUE NEOPLASM NECROSIS

Mark Murphey, MD[1]; Michael Shvarts, MD[1]; Steven Kong, MD[2]; Anthony Zaklama, MD[3]; Dhruv Kumar, MD[4]; James Jelinek, MD[4]
[1]American Institute for Radiologic Pathology, Silver Spring, MD, USA; [2]SimonMed, Riverside, CA, USA; [3]Geisinger Health, Danville, PA, USA; [4]Medstar Washington Hospital Center, Washington, DC, USA
(Presented by: Mark Murphey, MD, American Institute for Radiologic Pathology)

Purpose: Historically, musculoskeletal biopsy technique has emphasized excluding necrosis in material submitted for histologic evaluation. In our experience, there are certain situations in which not including the necrosis can lead to inaccurate pathologic downgrading of the neoplasm. Our purpose is to describe a small set of soft tissue neoplasms in which biopsy excluding necrosis initially led to pathologic downgrading of the lesion.

Materials and Methods: We retrospectively reviewed 19 cases of soft tissue neoplasms from our archives in which initial biopsy suggested a low-grade sarcoma. These included cases of undifferentiated soft tissue sarcoma(n=7), leiomyosarcoma(n=3), malignant peripheral nerve sheath tumor(n=4), myxofibrosarcoma(n=2) and dermatofibrosarcoma protuberans with fibrosarcomatous transformation(n=3). Subsequent to radiologic-pathologic correlation and resection, lesions were higher grade neoplasms leading to an increase in overall tumor staging.

Results: These cases depict the importance in certain situations of biopsy of not only the solid portions of a neoplasm but also areas suspicious for necrosis. Necrosis is one of the factors in the French Federation (FNCLCC) Grading System, and its identification can lead to increased lesion grade and stage. Selectively not biopsying these areas for pathologic evaluation can lead to downgrading and downstaging and suboptimal initial treatment. It can be difficult on MR to distinguish hemorrhage or cyst formation from necrosis. It is important in these situations for discussion between pathologist and radiologist concerning this possibility and potential need for biopsy of areas concerning for necrosis. Rebiopsy may be necessary in some cases.

Conclusion: It may be important in certain cases of soft tissue neoplasm to biopsy both solid areas and regions of potential necrosis so as not to inaccurately lead to histologic downgrading and downstaging of the lesion. This concept is contrary to a basic tenet many of us were taught but is important to understand to optimize patient treatment.

Modality % - Radiography / Fluoroscopy:	5
Modality % - CT:	0
Modality % - MRI:	95
Modality % - US:	0

Modality % - Nuclear Medicine:

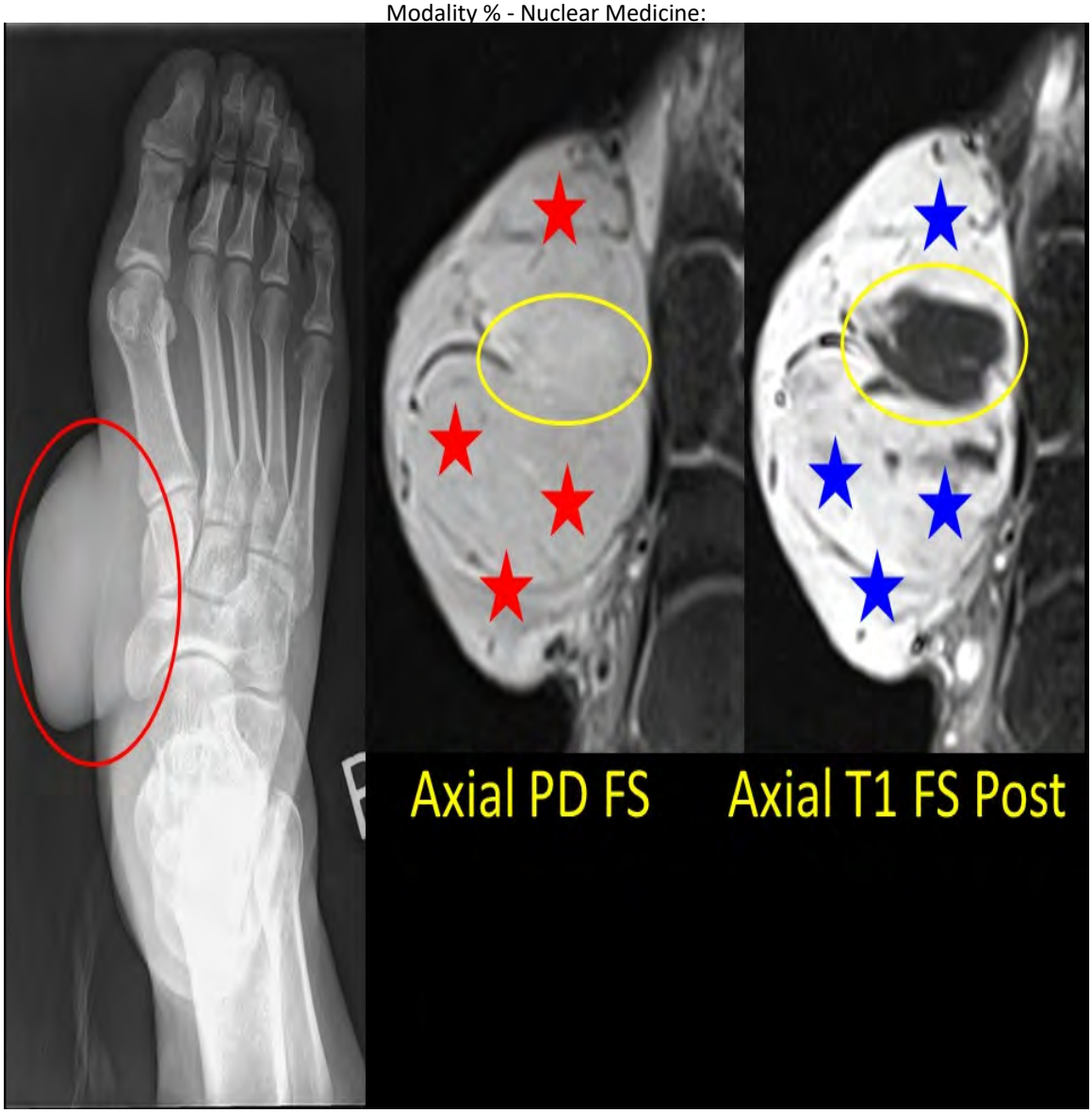

Red Circle: Protuberant subcutaneous foot mass
Red Star: Prominently T2 hyperintense
Blue Stars: Diffusely enhancing.
Yellow Circles: Focal, nonenhancing cystic area concerning for necrosis.

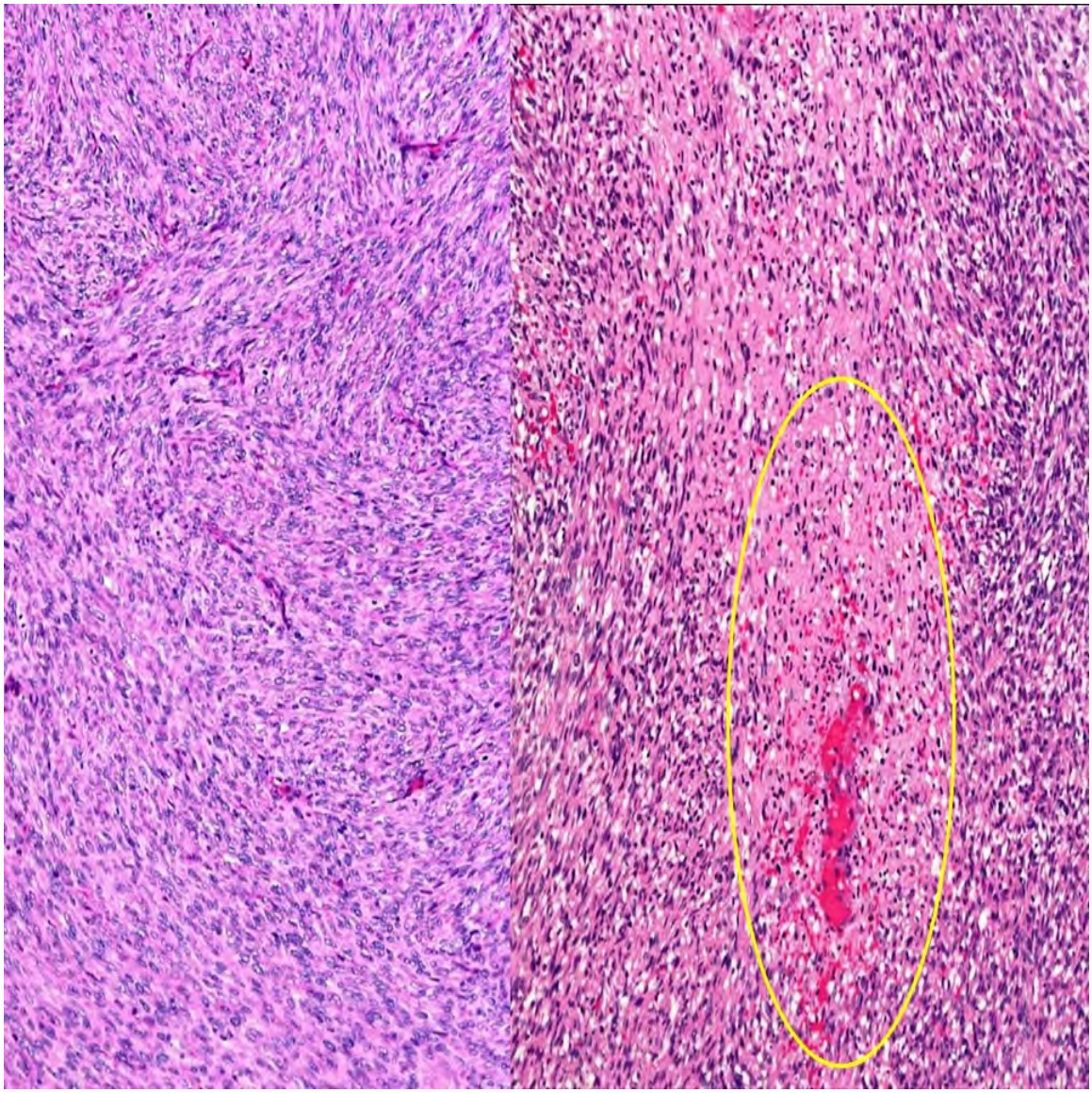

Original biopsy(left) with classic, storiform pattern of DFSP.
Yellow Circle: Area of necrosis at resection showing fibrosarcomatous transformation of DFSP, leading to higher pathologic grade

Podium #23

CT-GUIDED DISCITIS-OSTEOMYELITIS BIOPSIES: NEEDLE GAUGE AND MICROBIOLOGY RESULTS

Connie Chang, MD; F. Simeone, MD; Joao Vicentini, MD; Sandra Nelson, MD
Mass General Hospital, Boston, MA, USA
(Presented by: Connie Chang, MD, Mass General Hospital)

Purpose: To compare the microbiology results and needle gauge for CT-guided biopsies of suspected acute discitis-osteomyelitis.

Materials and Methods: All CT-guided biopsies performed for suspected cases of acute discitis-osteomyelitis at our institution between May 2014 and September 2017 were reviewed. Location of the biopsy, needle type and gauge, microbiology, pathology, and clinical and imaging follow-up were obtained through chart review.

Results: A total of 72 (age 54 ± 19 (4 -89) years; 24 F, 48 M) biopsies were performed. The distribution of biopsies were: 1/72 (1%) cervical, 17/72 (24%) thoracic, 54/72 (75%) lumbar. There were 34/72 (47%) bone/disc biopsies, 28/72 (39%) disc only biopsies, 7/72 (10%) bone only biopsies, and 3/71 (4%) paravertebral soft tissue biopsies. The gold standard was pathology for 57/72 (79%), clinical and imaging follow up for 15/72 (21%).

The overall sensitivity and specificity including all samples were 52 and 90%.

The sensitivity and specificity for samples using 12 gauge and larger needles were 82% and 67%, compared with 45% and 100% for samples using 13 gauge and smaller needles.

The sensitivity and specificity for samples using 13 gauge and larger needles were 76% and 75%, compared with 42% and 100% for samples using 14 gauge and smaller needles.

The sensitivity and specificity for samples using 14 gauge and larger needles were 60% and 75%, compared with 40% and 100% for samples using 15 gauge and smaller needles.

Conclusion: The use of a larger gauge biopsy needle may increase the likelihood of culturing the causative microorganism for CT-guided biopsies of acute discitis-osteomyelitis.

Modality % - Radiography / Fluoroscopy:	0
Modality % - CT:	100
Modality % - MRI:	0
Modality % - US:	0
Modality % - Nuclear Medicine:	0

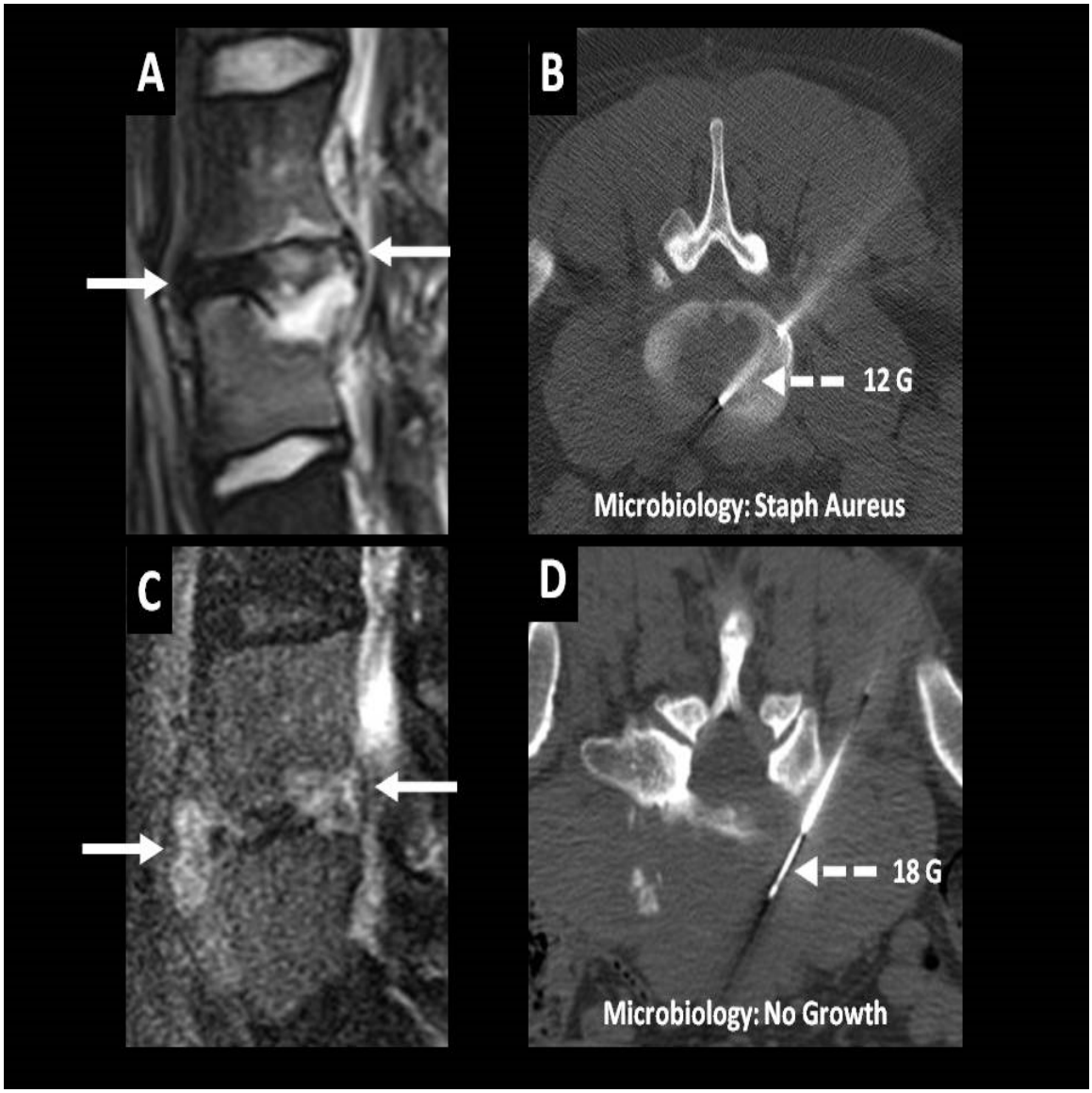

A) and C) show destruction of the disc and endplates, consistent with discitis osteomyelitis. B) and D) show biopsy images, needle gauges, and microbiology results.

Visual comparison of 16 gauge and 13 gauge cores.

Podium #24

INTRAMUSCULAR BOTULISM TOXIN TYPE A (BTA) INJECTION FACILITATES ABDOMINAL WALL RECONSTRUCTION (AWR) OF RECURRENT LARGE-DEFECT HERNIAS

Robert Lopez, MD[1]; Robert Raible, MD[1]; James Coumas, MD[1]; Taylor Stone, MD[1]; Paul Colavita, MD[2]; Vedra Augenstein, MD[2]; Kent Kercher, MD[2]; Todd Heniford, MD[2]

[1]Charlotte Radiology, Charlotte, NC, USA; [2]Carolinas Health Care System, Charlotte, NC, USA

(Presented by: Robert Lopez, MD, Charlotte Radiology)

Purpose: Incisional ventral hernias occur in about 20% of patients after laparotomy. Hernia recurrence occurs in up to 73% of patients with large, ventral hernias with "loss of domain" (more viscera residing outside the abdominal cavity than inside). Hernia recurrence and complication rate can be significantly reduced if the midline is closed over mesh without having to bridge a fascial gap. Preoperative BTA injection into the abdominal wall muscles can facilitate AWR by allowing stretching of the abdominal wall to facilitate fascial reapproximation. We report a single center experience in the technique and efficacy of percutaneous BTA injection to facilitate AWR of recurrent, large-defect ventral hernias.

Materials and Methods: Retrospective review of BTA injection cases was performed. Under U/S or CT guidance, the external and internal oblique muscles at up to six sites were injected with 16 units BTA. The transversalis muscles were injected with 8 units of BTA. Peri-operative findings and post-operative outcomes were recorded.

Results: 20 patients underwent percutaneous BTA injection and had ≥ 3 months follow-up. A range of 42 to 300 units BTA were used (average dose: 182.8 units). Average ventral hernia defect size was very large: 22.9 x 17.5cm. 18 patients were injected bilaterally and 2 unilaterally. There were no immediate or delayed injection–related complications. Average time to surgical AWR after injection was 34.6 days (range: 7-72 days). Average follow-up was 13.1 months (range: 3-52 months). Successful fascial closure of the defect was possible in 19 out of 20 patients with partial/near complete closure in 1. There was no recurrence of hernias in any patients.

Conclusion: Pre-operative intramuscular BTA injection facilitates AWR with higher clinical success then compared to historical controls. Intramuscular BTA injection may prove a significantly beneficial pre-operative adjunct for selected patients.

Modality % - Radiography / Fluoroscopy:	0
Modality % - CT:	60
Modality % - MRI:	0
Modality % - US:	40
Modality % - Nuclear Medicine:	0

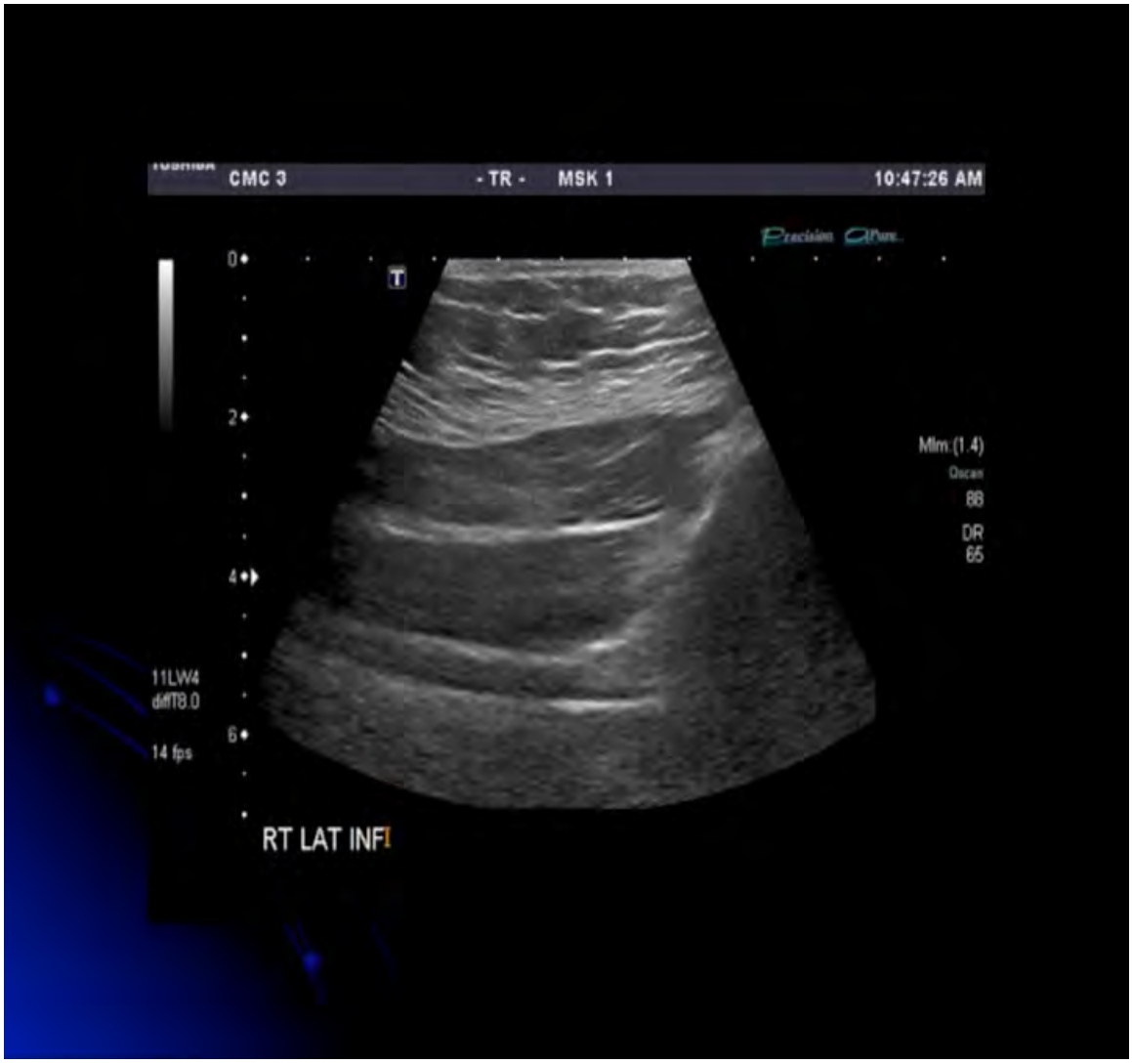
CMC 3
- TR -
MSK 1
10:47:26 AM
0
2
4
6
T
Mlm.(1.4)
Dscan
88
DR
65
11LW4
dMTB.0
14 fps
RT LAT INFI

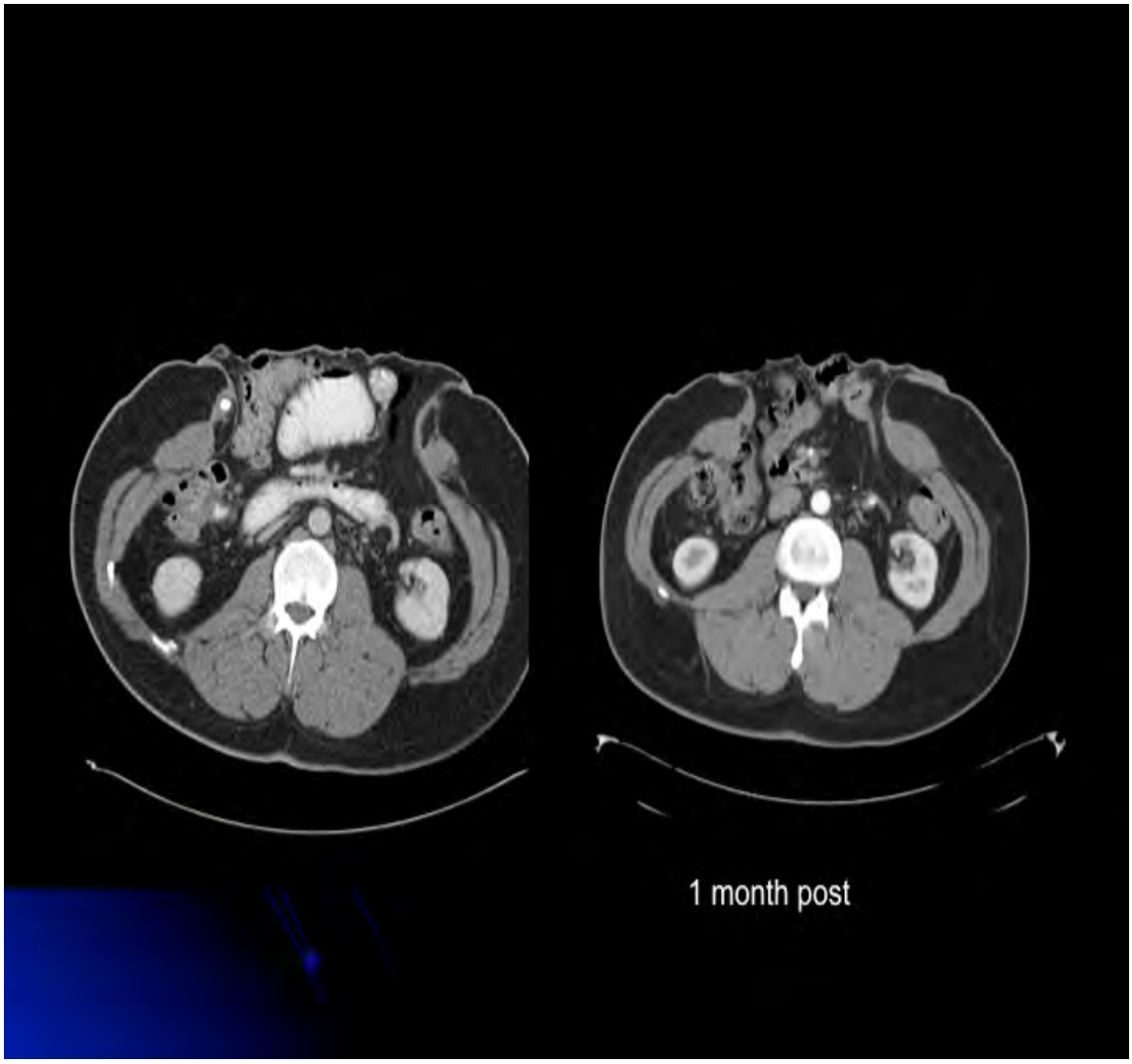

Longitudinal US of abdominal wall muscles prior to BTA injection.
Axial CT before and one month after BTA with decrease in hernia diameter.

Podium #25

IMAGING APPEARANCE OF THE ULNAR NERVE FOLLOWING SURGICAL INTERVENTION

Nicholson Chadwick, MD; Yoav Morag, MD; Brandon Smith, MD, MS; Corrie Yablon, MD; Sung Moon Kim, MD; Kate Chang, MS; Lynda Yang, MD, PhD
University of Michigan Medical Center, Ann Arbor, MI, USA
(Presented by: Nicholson Chadwick, MD, University of Michigan Medical Center)

Purpose: To describe various ulnar nerve decompression techniques and corresponding appearance on imaging.

Materials and Methods: Following IRB approval, a retrospective search of the radiology data base for patients following ulnar nerve transposition/decompression and of the hospital data base for patients referred to the peripheral nerve clinic between the 1/1/2007 – 8/30/2017 was performed. Patient demographics (sex, age) and clinical information (initial presentation, surgical procedure) was obtained from the patient records. Diagnostic imaging studies obtained after surgical decompression of the ulnar nerve were reviewed in consensus and imaging findings were documented. Correlation between the surgical technique and imaging appearance was performed.

Results: A case series of patients with ulnar nerve transposition/decompression will be presented. Different ulnar nerve decompression techniques and their imaging findings will be discussed including a discussion of potential complications following specific procedures.

Conclusion: It is important for the radiologist who performs MRI or US of the elbow to be aware of the various ulnar nerve transposition/decompression procedures that are performed. This knowledge will facilitate rapid and accurate diagnosis of normal and abnormal appearance of the ulnar nerve in the context of surgical decompression.

Modality % - Radiography / Fluoroscopy:	10
Modality % - CT:	0
Modality % - MRI:	60
Modality % - US:	30
Modality % - Nuclear Medicine:	0

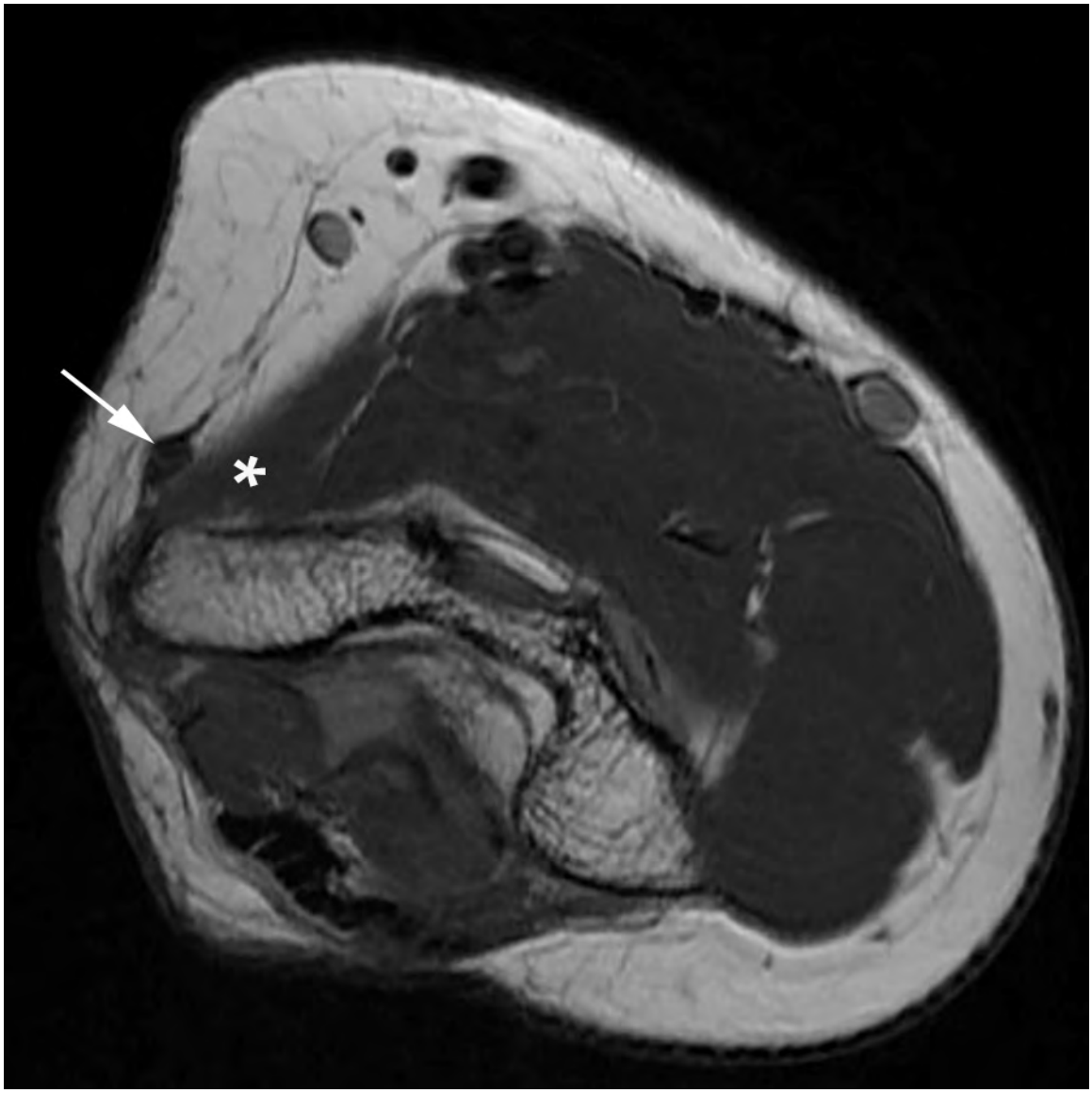

Axial T1 image depicts subcutaneous ulnar nerve transposition with the ulnar nerve (arrow) within the subcutaneous tissues superficial to the flexor pronator muscle mass (asterisk)

Axial T2 image with fat saturation depicts submuscular ulnar nerve transposition with the ulnar nerve (arrow) deep to the flexor pronator muscle mass (asterisk)

TUESDAY

Society of Skeletal Radiology

41st Annual Meeting

March 25-28, 2018

Tuesday, March 27, 2018

7:00 a.m.–7:55 a.m. **Continental Breakfast**

7:00 a.m.–12:35 p.m. **Registration/Information Desk Open**

7:00 a.m.–12:30 p.m. **Exhibit Hall Open**

7:00 a.m.–12:30 p.m. **ePoster Session**

8:00 a.m.–10:00 a.m. **HIP/PELVIS**

Moderators: Cheryl Petersilge, MD, Troy Storey , MD

8:00 a.m. #26 **CAM TYPE FEMOROACETABULAR IMPINGEMENT: ALPHA ANGLES VERSUS VOLUMETRIC BUMP SEGMENTATION AND CORRELATION WITH SURGICAL FINDINGS**

Avneesh Chhabra, MD
University of Texas Southwestern Medical Center at Dallas, Dallas, TX, USA
(Presented by: Avneesh Chhabra, MD, University of Texas Southwestern Medical Center at Dallas)

8:15 a.m. #27 **FLUOROSCOPICALLY GUIDED ILIOPSOAS BURSA INJECTIONS: INSTITUTIONAL EXPERIENCE WITH FOCUS ON POST PROCEDURE COMPLICATIONS**

Manisha Raythatha, MD; Damon Spitz, MD; Samuel Madoff, MD; Joseph Tang, MD; Joel Newman, MD
New England Baptist Hosp. Tufts University School of Med, Boston, MA, USA
(Presented by: Manisha Raythatha, MD, New England Baptist Hosp. Tufts University School of Med)

8:30 a.m. #28 **ASSOCIATION BETWEEN SEVERITY OF HETEROTOPIC OSSIFICATION AROUND THE HIP JOINT AND THE INTERVAL BETWEEN THE TIME OF INJURY AND SURGERY**

Daichi Hayashi, MD, PhD[1]; Corey Ho, MD[2]; Dennis Caruana[3]; David Komatsu, PhD[1]; James Nicholson, MD[1]; Musa Mufti, MD[1]; Jie Yang, PhD, MS[1]; Chencan Zhu[1]; Elaine Gould, MD[1]
[1]Stony Brook University Medical Center HSC, Stony Brook, NY, USA; [2]University of Colorado Denver, Aurora, CO, USA; [3]NY Cancer & Blood Specialists, East Setauket, NY, USA
(Presented by: Daichi Hayashi, MD, PhD, Stony Brook University Medical Center HSC)

8:45 a.m. #29 **RADIOGRAPHS IN SCREENING FOR FEMORAL CAM MORPHOLOGY: HOW MANY ARE SUFFICIENT?**

Tony Wong, MD; Joanna Weeks; Mark Francescone, MD; Michael Rasiej, MD; Jonathan Kazam, MD
Columbia-Presbyterian Medical Center, New York, NY, USA
(Presented by: Tony Wong, MD, Columbia-Presbyterian Medical Center)

9:00 a.m. #30 **QUANTIFYING FEMORAL HEAD AND NECK ASPHERICITY IN FAI AND INSTABILITY VERSUS CONTROLS USING RADIAL 3DCT AND VOLUMETRIC BUMP SEGMENTATION**

Avneesh Chhabra, MD
University of Texas Southwestern Medical Center at Dallas, Dallas, TX, USA
(Presented by: Avneesh Chhabra, MD, University of Texas Southwestern Medical Center at Dallas)

9:15 a.m. #31 **PELVIS MRI AND MR LUMBOSACRAL NEUROGRAPHY: IMPACT ON ULTRASOUND-GUIDED PELVIC PERINEURAL INJECTIONS.**
Sonali Lala, MD; William Walter, MD; Ronald Adler, MD, PhD; Christopher Burke, MD
NYU Medical Center/ Hospital for Joint Diseases Langone Medical Center, New York, NY, USA
(Presented by: Sonali Lala, MD, NYU Medical Center/ Hospital for Joint Diseases Langone Medical Center)

9:30 a.m. #32 **SCIATIC NERVE VARIANTS IN PATIENTS DIAGNOSED WITH SCIATICA: IS THERE A CORRELATION?**
Hayat Khan, MD; Tamara Fierst, MD; Sayed Ali, MD; Padmaja Jonnalagadda, MD; Stephen Ling, MD; Mark Weiner, MD; Omer Awan, MD
Temple University Hospital, Philadelphia, PA, USA
(Presented by: Hayat Khan, MD, Temple University Hospital)

9:45 a.m. #33 **DIAGNOSIS OF ISCHIOFEMORAL IMPINGEMENT BY A NOVEL ULTRASOUND TECHNIQUE**
Yaron Berkowitz, MB BChir, MRCS, FRCR[1]; Simon Greenwood, MBChB, MSc, MRCP, FRCR[1]; Hatim Alabsi, MBBS[2]; Charis McNabney, MB BCh, BAO[1]; Darra Murphy, MB BCh, BAO, FRCPC[1]; Mark Cresswell, MB BCh, FRCR, FRCPC[1]
[1]St Paul's Hospital, Vancouver, BC, Canada; [2]King Abdulaziz University, Jeddah, Saudi Arabia
(Presented by: Yaron Berkowitz, MB BChir, MRCS, FRCR, St Paul's Hospital)

10:00 a.m.–10:05 a.m. **CASE OF THE DAY**
Presenting Author: Hailey Allen, MD

10:05 a.m.–10:30 a.m. **Break** - Visit the Exhibit Hall

10:30 a.m.–12:30 p.m. **TRAUMA/MISCELLANEOUS**
Moderators: Mark Cresswell, MBBCh, BSc, Hilary Umans, MD

10:30 a.m. #34 **BREAK FROM PLAY: INCIDENCE AND IMPLICATIONS OF FRACTURE IN CORE MUSCLE INJURY**
Joseph Delic, MD; Andrew Ross, MD, MPH; Donna Blankenbaker, MD
University of Wisconsin Hospital & Clinics, Madison, WI, USA
(Presented by: Joseph Delic, MD, University of Wisconsin Hospital & Clinics)

10:45 a.m. #35 **EFFECT OF ANALYTICS DRIVEN CUSTOM WORKLISTS ON MUSCULOSKELETAL MRI INTERPRETATION TIMES IN AN ACADEMIC SETTING**
Tony Wong, MD; Jonathan Kazam, MD; Michael Rasiej, MD
Columbia-Presbyterian Medical Center, New York, NY, USA
(Presented by: Tony Wong, MD, Columbia-Presbyterian Medical Center)

11:00 a.m. #36 **LOW DOSE METAL ARTIFACT REDUCTION CT IN ARTHROPLASTY IMAGING: A CADAVERIC AND CLINICAL STUDY**
Naveen Subhas, MD, MPH[1]; Bong Jae Jun, PhD[1]; Eric Ricchetti, MD[1]; Nancy Obuchowski, PhD[1]; Andrew Primak, PhD[2]; Joseph Iannotti, MD, PhD[1]
[1]Cleveland Clinic, Cleveland, OH, USA; [2]Siemens Healthcare, Cleveland, OH, USA
(Presented by: Naveen Subhas, MD, MPH, Cleveland Clinic)

11:15 a.m. #37 **SUBCHONDRAL INSUFFICIENCY FRACTURE OF THE KNEE (THE OLD SONK): NOVEL MRI-BASED GRADING SYSTEM AND ITS CLINICAL IMPLICATION**
Felix Gonzalez, MD[1]; Yara Younan, MD[1]; Johanness Roedl, MD[2]; Monica Umpierrez, MD[1]; Adam Singer, MD[1]; Gulshan Sharma, PhD, MPH[3]; Adam Zoga, MD[2]; William Morrison, MD[2]
[1]Emory University Dept. of Radiology, MSK Division, Atlanta, GA, USA; [2]Thomas Jefferson University Hospital, Philadelphia, PA, USA; [3]Cumming School of Medicine, Calgary, AB, Canada
(Presented by: Felix Gonzalez, MD, Emory University Dept. of Radiology, MSK Division)

11:30 a.m. #38 **ULTRASOUND EVALUATION OF RADIAL NERVE PALSY ASSOCIATED WITH HUMERAL SHAFT FRACTURE TO GUIDE OPERATIVE VERSUS CONSERVATIVE TREATMENT**
Mihra Taljanovic, MD, PhD; Melissa Esparza, MD; Lana Gimber, MD, MPH; Lisa Truchan, MD; Tyson Chadaz, MD; Christina Boulton, MD; Jason Wild, MD
University of Arizona HCS - Tucson, Tucson, AZ, USA
(Presented by: Mihra Taljanovic, MD, PhD, University of Arizona HCS - Tucson)

11:45 a.m. #39 **"OSTEITIS": HITHER, THITHER OR WITHER? PREDICTION OF OSTEOMYELITIS IN PATIENTS WITH EQUIVOCAL MRI FINDINGS**
William Morrison, MD; Alessandra Sax, MD; Adam Zoga, MD; Johannes Roedl, MD; Jeffrey Belair, MD
Thomas Jefferson University Hospital, Philadelphia, PA, USA
(Presented by: William Morrison, MD, Thomas Jefferson University Hospital)

12:00 p.m. #40 **BONE BRUISE VS. NON-DISPLACED FRACTURE AT MRI: A GRADING SYSTEM TO PREDICT RETURN TO PLAY**
Jeffrey Belair, MD[1]; Adam Zoga, MD[1]; William Morrison, MD[1]; Roedl Johannes, MD[1]; Blake Bowden, MD[2]
[1]Thomas Jefferson University Hospital, Philadelphia, PA, USA; [2]Augusta University, Augusta, GA, USA
(Presented by: Jeffrey Belair, MD, Thomas Jefferson University Hospital)

12:15 p.m. #41 **EVALUATION OF ATRAUMATIC MUSCULOSKELETAL PAIN IN THE EMERGENCY DEPARTMENT BY DUAL ENERGY CT (DECT) WITH VIRTUAL NONCALCIUM APPLICATION FOR BONE MARROW EDEMA AND COLOR OVERLAY: BEYOND FRACTURES**
E Garwood, MD; Soterios Gyftopoulos, MD; Emilio Vega, BS; Michael Mechlin, MD
NYU Medical Center/ Hospital for Joint Diseases Langone Medical Center, New York, NY, USA
(Presented by: E Garwood, MD, NYU Medical Center/ Hospital for Joint Diseases Langone Medical Center)

12:30 p.m.–12:35 p.m. **CASE OF THE DAY**
Presenting Authors Brian Y. Chan, MD

Related ePosters

HIP/PELVIS

Poster #23 **MRI OF THE LUMBOSACRAL PLEXUS: WHAT THE PRACTICING RADIOLOGIST NEEDS TO KNOW**
Hailey Allen, MD; Megan Mills, MD; Miriam Peckham, MD; Lubdha Shah, MD; Kent Sanders, MD; Sarah Stilwill, MD
University of Utah Medical Center / SOM, Salt Lake City, UT, USA

Poster #25 **MUSCLE BULK DIFFERENCES IN FAI AND HIP INSTABILITY VERSUS CONTROLS**
Avneesh Chhabra, MD
University of Texas Southwestern Medical Center at Dallas, Flowermound, TX, USA

Poster #26 **A COMPREHENSIVE REVIEW OF PROXIMAL FEMORAL FRACTURES AND THEIR COMPLICATIONS**
Kimia Kani, MD[1]; Hyojeong Mulcahy, MD[2]; Jack Porrino, MD[2]; Felix Chew, MD[2]
[1]University of Maryland School of Medicine, Baltimore, MD, USA; [2]University of Washington / Harborview Medical Center, Seattle, WA, USA

TRAUMA/MISCELLANEOUS

Poster #27 **ULTRASOUND FOR THE EVALUATION OF RADIAL NERVE PATHOLOGY: CORRELATION TO MRI FINDINGS**
Edward Yoon, MD; O. Nwawka, MD
Hospital for Special Surgery, New York, NY, USA

Poster #28 **UTILITY OF MRI IN EVALUATING FOR OSTEOMYELITIS IN PATIENTS WITH CELLULITIS**
Devon Klein, MD[1]; Brian Lee, MD[2]; Hariklia Bezhani, DPM[1]; Guillaume Stoffels, MS, MA[1]
[1]Lenox Hill Hospital, Northwell Health, New York, NY, USA; [2]Beth Israel Deaconess Medical Center Harvard Med School, Boston, MA, USA

Poster #29 **MUSCLE EDEMA - RECOGNIZING PATTERNS AND ASSOCIATED CAUSES**
Sailaja Yadavalli, MD, PhD; Michael Hierl, MD; David Marcantonio, MD
Beaumont Health System, Royal Oak, MI, USA

Poster #30 **CALCIUM HYDROXYAPATITE DEPOSITION DISEASE: A MULTI-MODALITY REVIEW FOR THE PRACTICING RADIOLOGIST AND RADIOLOGIST IN TRAINING, WITH EMPHASIS ON CLINICAL PRESENTATION, PATHOGENESIS AND IMAGING APPEARANCE.**
Jason Esterle, MD; David Marcantonio, MD; Christopher Nall, MD
Beaumont Health System, Royal Oak, MI, USA

Poster #31 **REVIEW AND UPDATE ON IMAGING OF CHEST WALL INJURIES**
Kimia Kani, MD[1]; Hyojeong Mulcahy, MD[2]; Jack Porrino, MD[2]; Felix Chew, MD[2]
[1]University of Maryland School of Medicine, Baltimore, MD, USA; [2]University of Washington / Harborview Medical Center, Seattle, WA, USA

Poster #32 **EVALUATION OF GADOLINIUM DEPOSITION IN THE BRAIN FOLLOWING MAGNETIC RESONANCE ARTHROGRAM**
Lauren Ladd, MD; Krish Singhal, MD; Mark Frank, MD, MBA; Stephen Kralik, MD
Indiana University, Indianapolis, IN, USA

Poster #33 **MRI INTERPRETATION RATHER THAN TISSUE DIAGNOSIS DETERMINES ACUTE OSTEOMYELITIS MANAGEMENT: ONE INSTITUTION'S EXPERIENCE**
Josephina Vossen, MD, PhD; Peter Haar, MD, MS; Curtis Hayes, MD; Michael Perone, MD; Kevin Hoover, MD, PhD
Virginia Commonwealth University Medical Center, Richmond, VA, USA

Related ePosters

Poster #34 **PERIOSTEAL THICKENING AS THE ONLY VISUALIZED SIGN OF OSTEONECROSIS ON RADIOGRAPHS.**

Josephina Vossen, MD, PhD; Candice Kim, BS; Peter Haar, MD, PhD; Curtis Hayes, MD; Kevin Hoover, MD, PhD
Virginia Commonwealth University Medical Center, Richmond, VA, USA

Poster #35 **THE INCIDENCE, ONSET AND DISTRIBUTUION OF CRYSTAL DEPOSITION WITHIN THE CERVICAL SPINE**

Eric Walker, MD[1]; Dylan Simmons, DO[2]; Joshua Tice, MD[3]; Jonelle Petscavage-Thomas, MPH, MD[1]
[1]Penn State Milton S. Hershey Medical Center, Hershey, PA, USA; [2]Emory University Dept. of Radiology, MSK Division, Atlanta, GA, USA; [3]West Reading Radiology Associates, West Reading, PA, USA

Poster #36 **DAY OF WEEK, SITE OF SERVICE, AND PATIENT COMPLEXITY DISPARITIES IN MUSCULOSKELETAL MRI INTERPRETATIONS BY RADIOLOGISTS VS. NON-RADIOLOGISTS**

Paige Sharp, MD[1]; Richard Duszak, Jr., MD[1]; Wenyi Wang, MA[2]; Danny Hughes, PhD[2]; Neil Lall, MD[3]; Paul Harkey, MD[1]
[1]Emory University Dept. of Radiology, Atlanta, GA, USA; [2]Harvey L. Neiman Health Policy Institute, Reston, VA, USA; [3]Ochsner Health System, New Orleans, LA, USA

Poster #37 **Imaging Features of Calciphylaxis**

Ryan Franke, MD; Mark Kransdorf, MD; Michael Fox, MD; F. Chivers, MD; Jonathan Flug, MD
Mayo Clinic, Phoenix, AZ, USA

Podium #26

CAM TYPE FEMOROACETABULAR IMPINGEMENT: ALPHA ANGLES VERSUS VOLUMETRIC BUMP SEGMENTATION AND CORRELATION WITH SURGICAL FINDINGS

Avneesh Chhabra, MD
University of Texas Southwestern Medical Center at Dallas, Dallas, TX, USA
(Presented by: Avneesh Chhabra, MD, University of Texas Southwestern Medical Center at Dallas)

Purpose: To determine the correlation of 3DCT measurements of CAM type femoro-acetabular impingement [FAI] with surgical findings of labral tear & cartilage loss.

Materials and Methods: Digital search of symptomatic FAI patients who underwent hip surgery for a CAM-type FAI from July 2013 to August 2016 yielded 43 patients. Demographic data, clinical and surgical findings were recorded. Two readers indepedently evaluated 3DCT images to calculate volumes of the femoral head and bump as well as alpha angles on radial images. Correlations between CT and surgical findings were obtained. Inter-reader reliability was determined using intraclass correlation [ICC].

Results: Thirteen men & fourteen women were included with a mean age of 37.3 ± 10.4 years. The most common clinical finding was positive FADIR [19/27, 70.4%]. Twenty-seven labral tears and twenty cartilage defects were found on surgery. Significant correlations between the femoral bump & head volumes with the extent of the labral tear [p- values = 0.008 and 0.003 respectively] existed. No significant correlations were found between alpha angles at 1 and 2 O'clock & extent of the labral tear [p-values >0.05] or any measurement with cartilage loss [p>0.05]. Inter-reader reliability was excellent to moderate [ICC= 0.85 & 0.52] for femoral head and bump volumes, and fair to poor [ICC = 0.40 & 0.05] for alpha angles at 1 and 2 o'clock, respectively

Conclusion: 3D Volumetric measurements of CAM type FAI significantly correlate with the extent of the labral tears with superior inter-reader reliability than the commonly used alpha angle, rendering it a more clinically relevant method to quantify CAM morphology.

Modality % - Radiography / Fluoroscopy:	5
Modality % - CT:	95
Modality % - MRI:	0
Modality % - US:	0
Modality % - Nuclear Medicine:	0

Podium #27

FLUOROSCOPICALLY GUIDED ILIOPSOAS BURSA INJECTIONS: INSTITUTIONAL EXPERIENCE WITH FOCUS ON POST PROCEDURE COMPLICATIONS

Manisha Raythatha, MD; Damon Spitz, MD; Samuel Madoff, MD; Joseph Tang, MD; Joel Newman, MD
New England Baptist Hosp. Tufts University School of Med, Boston, MA, USA
(Presented by: Manisha Raythatha, MD, New England Baptist Hosp. Tufts University School of Med)

Purpose: Impingement of the iliopsoas tendon is a recognized cause of hip pain and can occur following total hip arthroplasty (THA) or as a result of snapping hip syndrome. One treatment option is iliopsoas bursa anesthetic and steroid injection. We report our experience with fluoroscopically guided iliopsoas bursa injections with a focus on post procedural complications.

Materials and Methods: Retrospective review of 397 iliopsoas bursa injections performed over 5 year period (2012 to 2017). Patient age range 21 to 84 years (average 60.2 years). Presence/absence of THA, pre-procedural anticoagulation status, anesthetic type/volume, fluoroscopy time, and post procedure complications are reviewed.

Results: 344 patients had prior THA while 53 cases were native hips. Average procedural fluoroscopy time was 11.6 seconds with no documented cases of post procedural infection or hematoma. In 82 cases (21%), Bupivacaine 0.5% anesthetic was administered. In the remaining 315 cases (79%), Lidocaine 1% anesthetic was utilized. Anesthetic volume ranged from 2 to 5 cc. In 4 of 397 patients (1%) transient post procedural numbness/weakness occurred. In 3 of these 4 cases Bupivacaine was used. Two patients had resolution of symptoms without further sequela. Two patients, both of whom received Bupivacaine 0.5%, had more serious complications. One experienced ipsilateral lower extremity numbness/weakness shortly following discharge resulting in a fall and bilateral distal fibular fractures. The other experienced prolonged numbness and weakness requiring overnight hospital observation.

Conclusion: Fluoroscopically guided iliopsoas bursa injection is a safe, expedient, non-operative treatment for iliopsoas impingement and can be performed conveniently in an outpatient setting regardless of coagulation status. Though post procedure complications remain rare, the possibility of paresthesia/weakness may result in significant morbidity. Therefore, patients should be provided with instructions prior to the procedure to arrange transportation and should be monitored for numbness/weakness prior to discharge.

Modality % - Radiography / Fluoroscopy:	100
Modality % - CT:	0
Modality % - MRI:	0
Modality % - US:	0
Modality % - Nuclear Medicine:	0

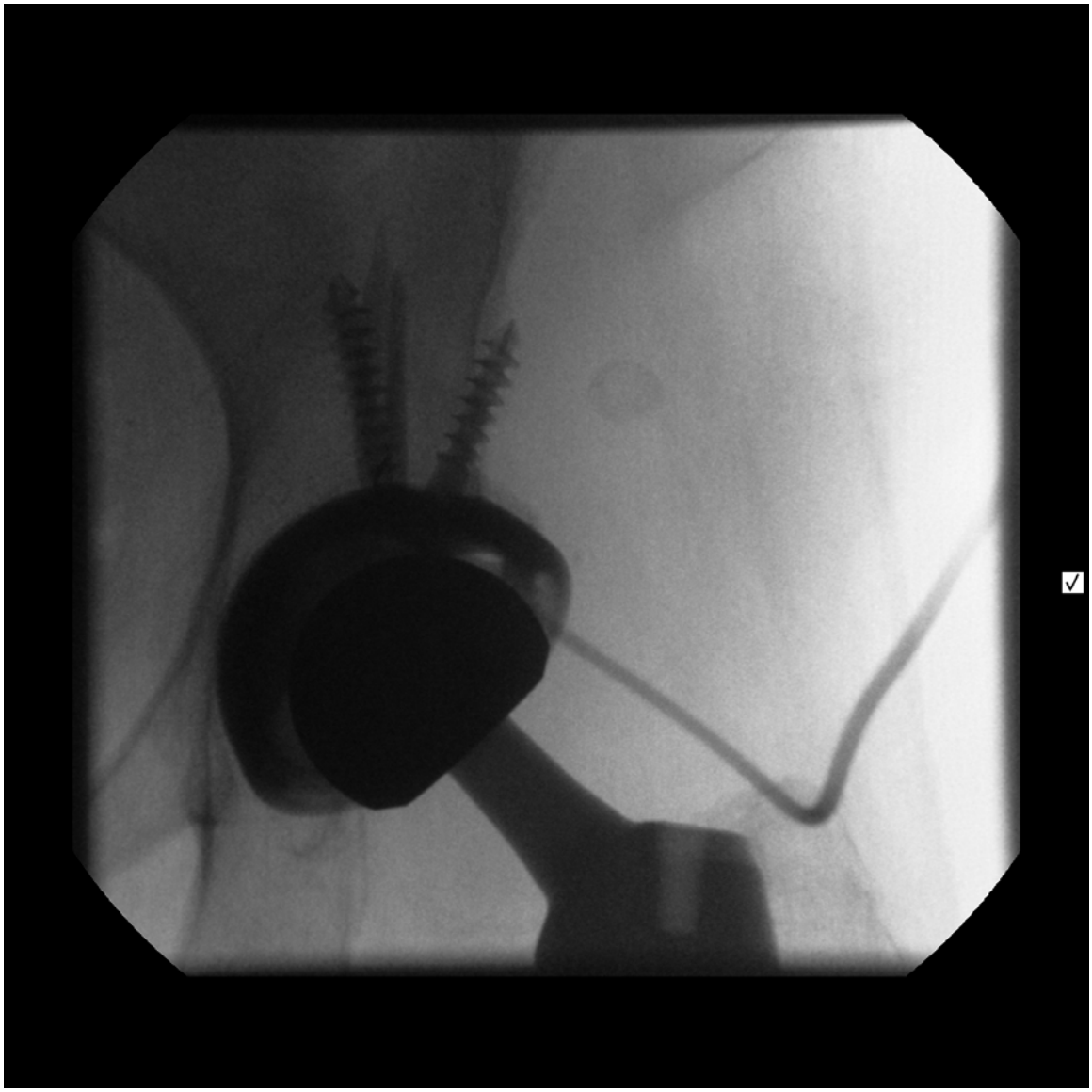

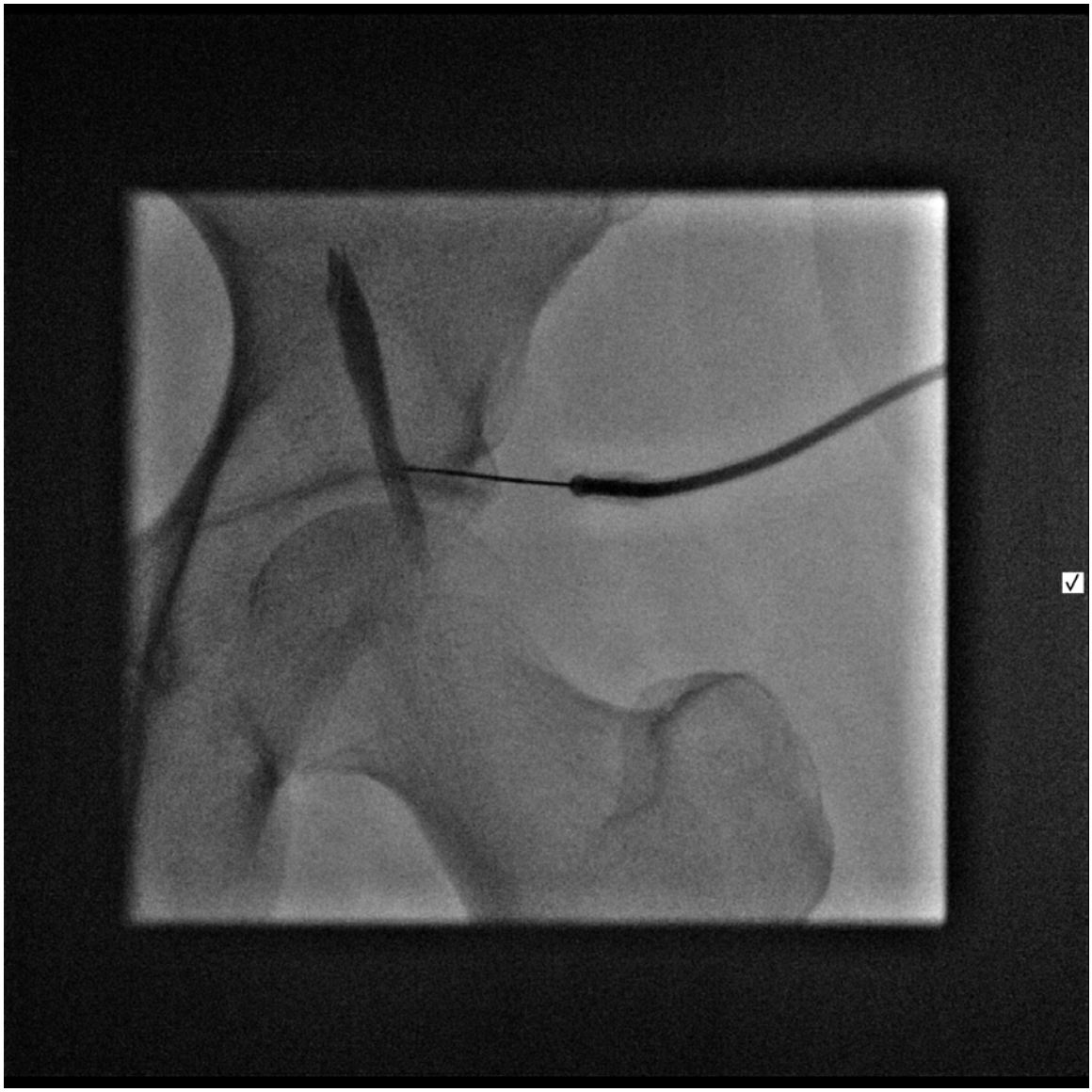

Fluoroscopically guided iliopsoas bursa injection

Podium #28

ASSOCIATION BETWEEN SEVERITY OF HETEROTOPIC OSSIFICATION AROUND THE HIP JOINT AND THE INTERVAL BETWEEN THE TIME OF INJURY AND SURGERY

Daichi Hayashi, MD, PhD[1]; Corey Ho, MD[2]; Dennis Caruana[3]; David Komatsu, PhD[1]; James Nicholson, MD[1]; Musa Mufti, MD[1]; Jie Yang, PhD, MS[1]; Chencan Zhu[1]; Elaine Gould, MD[1]

[1]Stony Brook University Medical Center HSC, Stony Brook, NY, USA; [2]University of Colorado Denver, Aurora, CO, USA; [3]NY Cancer & Blood Specialists, East Setauket, NY, USA

(Presented by: Daichi Hayashi, MD, PhD, Stony Brook University Medical Center HSC)

Purpose: Heterotopic ossification (HO) is a relatively common complication following hip surgeries such as total hip arthroplasty or internal fixation. Development of HO is an important clinical issue as this can reduce the patient's functional status. Studies have demonstrated mixed results regarding its association with time interval to surgery. Our study aimed to further investigate this association.

Materials and Methods: With IRB approval, our retrospective study included 151 patients (113 women, 38 men, age range 33-95 years) who were treated for hip fractures by open reduction and internal fixation or total hip arthroplasty. Charts were reviewed for time interval to surgery, laterality, surgical approach, and patient age. Patients who had any post-operative complications were excluded.

One attending musculoskeletal radiologist and one musculoskeletal radiology fellow, blinded to clinical information, read the pelvis/hip radiographs independently and graded the degree of HO based on the Brooker Classification (5-point grading scale from 0 to 4).

Statistical analysis was performed utilizing Chi-square, Kruskal-Wallis, and Score tests in addition to a proportional odds model. Analysis was performed using SAS 9.4 and significance level set at 0.05.

Results: Thirty eight patients had no HO, 43 had grade 1, 55 had grade 2, and 15 had grade 3 or greater HO. A majority of patients (59.6%) had a surgical intervention within 2 days of acute injury. Time interval to surgery was significantly associated with severity of HO (p=0.0015). No significant association was found between age, gender, surgical approach, or laterality (p=0.0705-0.7383).

Conclusion: There is a strong association regarding the severity of postoperative heterotopic ossification and time interval between injury and surgery. We suggest that patients presenting with femoral neck fractures should undergo surgical fixation with urgency to reduce the degree of postoperative heterotopic ossification.

Modality % - Radiography / Fluoroscopy: 100
Modality % - CT: 0
Modality % - MRI: 0
Modality % - US: 0
Modality % - Nuclear Medicine: 0

Table 1: Descriptive table for patients' characteristics and surgery information by HO class

Variable		Total (N=151)	0 (N=38)	1 (N=43)	2 (N=55)	3+ (N=15)	P-value*
Days to surgery		2±3	2±1	2±3	2±3	6±6	0.0015
Age		81±11	82.5±16	83±11	80±11	77±10	0.2812
Gender	Female	113 (74.83%)	34 (30.09%)	32 (28.32%)	38 (33.63%)	9 (7.96%)	0.0705
	Male	38 (25.17%)	4 (10.53%)	11 (28.95%)	17 (44.74%)	6 (15.79%)	
Approach	Anterolateral	4 (2.65%)	0 (0.00%)	3 (75.00%)	1 (25.00%)	0 (0.00%)	0.1882
	Lateral	33 (21.85%)	5 (15.15%)	8 (24.24%)	15 (45.45%)	5 (15.15%)	
	Posterior	114 (75.50%)	33 (28.95%)	32 (28.07%)	39 (34.21%)	10 (8.77%)	
Side	Left	82 (54.30%)	20 (24.39%)	24 (29.27%)	28 (34.15%)	10 (12.20%)	0.7383
	Right	69 (45.70%)	18 (26.09%)	19 (27.54%)	27 (39.13%)	5 (7.25%)	

*: For categorical variables, p-value was based on Chi-squared test with exact p-value from Monte Carlo simulation; For continuous variables, median±IQR were reported and p-value was based on Kruskal-Wallis test.

Figure 1. Table showing descriptive data for patients' gender, age, days to surgery, surgery approach and side by HO class.

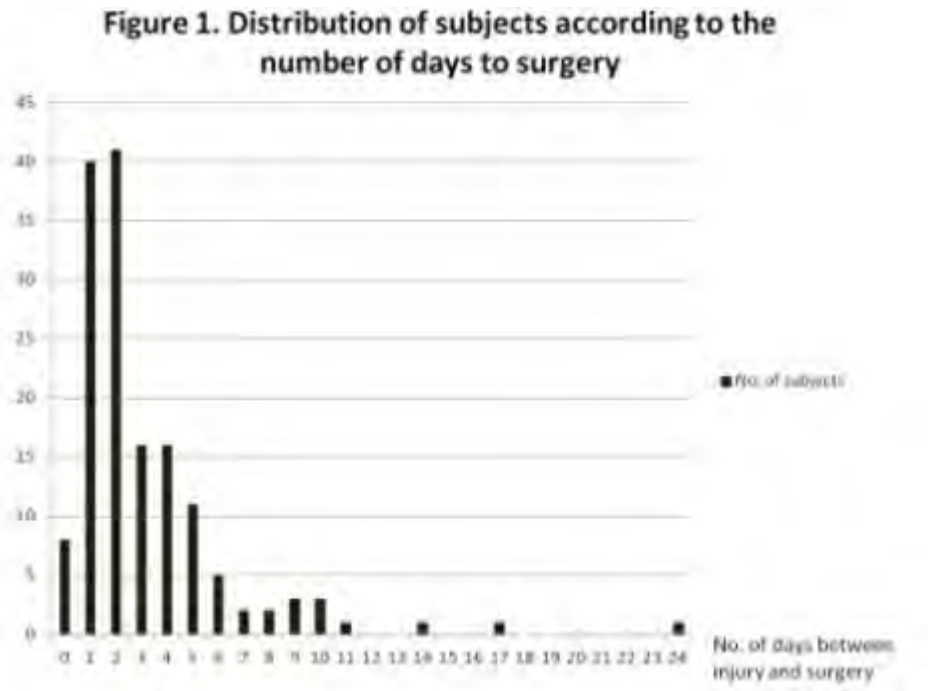

Figure 2. Bar graph showing distribution of subjects according to the number of days to surgery.

Podium #29

Radiographs in screening for femoral cam morphology: How many are sufficient?

Tony Wong, MD; Joanna Weeks; Mark Francescone, MD; Michael Rasiej, MD; Jonathan Kazam, MD
Columbia-Presbyterian Medical Center, New York, NY, USA
(Presented by: Tony Wong, MD, Columbia-Presbyterian Medical Center)

Purpose: To compare a 2-view to 5-view radiograph series for femoral cam screening

Materials and Methods: A search was performed for patients with a 5-view radiograph series (AP pelvis and AP, Dunn, frog lateral, and false profile of the hip) ordered by a single surgeon during past year. This yielded 181 hips for 149 patients (63 F and 87 M, avg. age 33 ± 11 yrs.). Three radiologists (R1 and R2 MSK trained, R3 Body trained) blindly and independently reviewed all hips. First, the AP pelvis and Dunn hip views were assessed for visual presence of a femoral cam, Tonnis grade, and acetabular rim calcification. Two weeks later, all 5 views were evaluated similarly.

MRI/CT scan available for 82 hips defined a cam ($\alpha \geq 60°$) . Intra-reader and inter-reader variability were calculated using Cohen's and Fleiss' kappa.

Results: Diagnosis of cam on 2-view vs. 5-view:

Sensitivity: R1 (84% vs. 85%), R2 (95% vs. 95%), R3 (100% vs. 98%)

Specificity: R1 (56% vs. 56%), R2 (41% vs. 37%), R3 (7% vs. 11%)

PPV: R1 (79% vs. 80%), R2 (41% vs. 37%), R3 (69% vs. 69%)

NPV: R1 (63% vs. 65%), R2 (79% vs. 77%), R3 (100% vs. 75%)

%hips cam seen only on 5-view: MSK trained (3%) Non-MSK trained (2%) (Figures 1&2)

Intra-observer variability for AP pelvis and Dunn (k): R1 (0.81, 0.75), R2 (0.92, 0.93), R3 (0.46, 0.38)

Inter-observer variability for cam identification on 2-view vs. 5-view (k): 0.33 vs. 0.37

Increase of Tonnis grade from 0/1 to 2/3 with additional views: 0-1% of cases (all readers)

Acetabular mineralization only on 5-view: 0-8% of cases (all readers)

Conclusion: A 2-view radiograph series (AP pelvis and Dunn hip) can screen patients for femoral cam morphology with similar sensitivity compared to a 5-view radiograph series.

Modality % - Radiography / Fluoroscopy:	100
Modality % - CT:	7
Modality % - MRI:	0
Modality % - US:	0
Modality % - Nuclear Medicine:	0

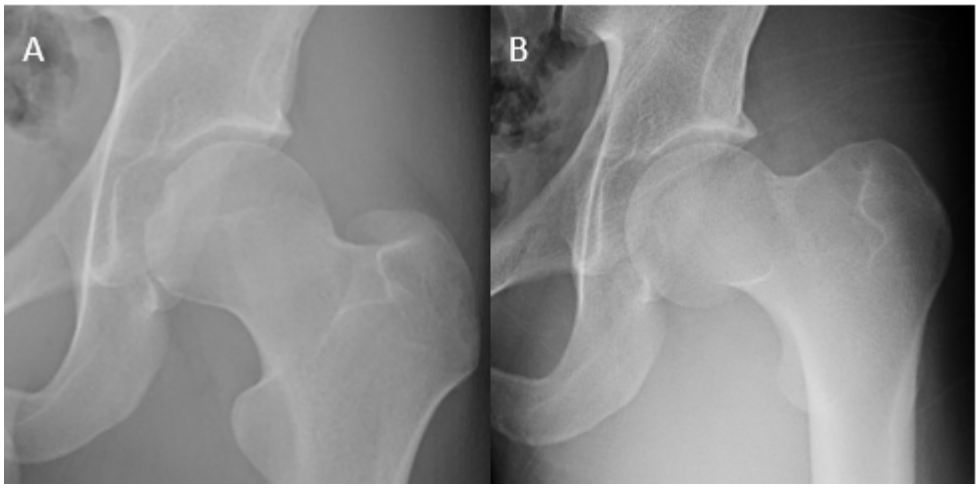

Fig 1: Coned AP pelvis (A) and Dunn left hip (B) views interpreted as having no cam by all 3 readers

Fig 2: Additional Frog lateral left hip view interpreted as having cam by all 3 readers.

Podium #30

QUANTIFYING FEMORAL HEAD AND NECK ASPHERICITY IN FAI AND INSTABILITY VERSUS CONTROLS USING RADIAL 3DCT AND VOLUMETRIC BUMP SEGMENTATION

Avneesh Chhabra, MD
University of Texas Southwestern Medical Center at Dallas, Dallas, TX, USA
(Presented by: Avneesh Chhabra, MD, University of Texas Southwestern Medical Center at Dallas)

Purpose: Evaluate 3DCT analysis of head and bump anatomy in quantifying pathology in FAI and hip dysplasia versus controls.

Materials and Methods: 3DCT cases with final diagnosis of hip dysplasia or FAI were compared with controls. Alpha angles using radial imaging and 3D volumetric bump segmentations were obtained bilaterally. ROC analysis and Linear mixed models were used. Normal hips of control subjects were compared to hips of Dysplasia or FAI cases in an inter-patient comparison. Intra-patient comparisons were also obtained.

Results: 25 FAI (age= 31+/-7.4), 16 dysplasia (age= 29.9 +/-9.0), and 38 controls (age= 41.7 +/- 7.8) were analyzed. FAI and dysplasia consistently presented with higher alpha angles at 2 o'clock (p= 0.002) and 3 o'clock (p=0.023) and higher bump-head volume ratios than controls (p<0.001). FAI had larger bumps than patients with dysplasia. Contralateral normal hips in patients with both dysplasia and FAI showed significantly less head-neck junction abnormalities. Segmented bump/head ratio was significantly higher in asymptomatic contralateral hips of patients with FAI than control hips (p = <.0001) while alpha angles could not show this relationship (alpha 12, p = 1, alpha 1, p = 0.752, alpha 2, p = 0.319, alpha 3, p = 0.314). Alpha angle at 2 O'clock (AUC = 0.82) and segmented bump to head ratios (AUC = 0.81) best illustrates developmental variation in FAI and dysplasia.

Conclusion: Patients with both FAI and dysplasia exhibited different anatomy of the femoral head on using alpha angle measures and 3D analysis than asymptomatic controls. 3D segmentation bump analysis was able to describe the pathology in both FAI and dysplasia, proving to be an accurate, simpler way, to measure femoral head abnormalities.

Modality % - Radiography / Fluoroscopy:	5
Modality % - CT:	95
Modality % - MRI:	0
Modality % - US:	0
Modality % - Nuclear Medicine:	0

Podium #31

PELVIS MRI AND MR LUMBOSACRAL NEUROGRAPHY: IMPACT ON ULTRASOUND-GUIDED PELVIC PERINEURAL INJECTIONS.

Sonali Lala, MD; William Walter, MD; Ronald Adler, MD, PhD; Christopher Burke, MD
NYU Medical Center/ Hospital for Joint Diseases Langone Medical Center, New York, NY, USA
(Presented by: Sonali Lala, MD, NYU Medical Center/ Hospital for Joint Diseases Langone Medical Center)

Purpose: Assess the impact of MR pelvic and lumbosacral neuorgraphy on ultrasound-guided pelvic perineural injections.

Materials and Methods: A retrospective review of all ultrasound-guided pelvic perineural injections with prior MR pelvic and/or lumbosacral neurographic imaging over a 5-year period was performed. Demographics, presence of structural pathology on imaging, and immediate and interval pain relief was recorded.

Results: 30 total injections were performed among 20 patients accounting for multiple injections in a single visit or multiple visits [mean age at injection: 52.03 (range 23-77), female (n= 24, 80%) male (n=6; 20%)]. In 24 cases a combination of steroid and anesthetic solution was administered. In the remaining 6 cases, only anesthetic solution was administered. Most commonly, injections involved the sciatic nerve (n = 21; 70%). Other injections in our series include pudendal (n=5, 16.7%), genitofemoral (n=2; 6.7%), lateral femoral cutaneous (n=1, 3.3%) and ilioinguinal (n= 1, 3.3%) nerves. Concurrent therapeutic procedures were performed in 10 cases (33%). Pre-procedure MR imaging revealed structural abnormality of the nerve or adjacent soft tissues in 11 of 22 MRIs performed amongst the 20 patients (50%). Pre-procedure ultrasound revealed structural abnormalities associated with the nerve in 9 cases of 19 cases that had complete documentation (47%). Of 26 injections with complete documentation, immediate improvement of symptoms was reported in 22 cases (85%). The remaining 4 cases either began with no pain (n=3), or reported no change in symptoms (n=1). Variable degrees of long-term symptom relief was achieved in 4 injections out of 11 steroid injections for which follow-up was available (37%).

Conclusion: Ultrasound-guided perineural injections can be performed for treatment of a variety of pelvic neuropathies. MR imaging prior to sonographic intervention demonstrated an abnormality in nearly half of cases, and is a useful tool to appropriately target perineural injections.

Modality % - Radiography / Fluoroscopy:	0
Modality % - CT:	0
Modality % - MRI:	50
Modality % - US:	50
Modality % - Nuclear Medicine:	0

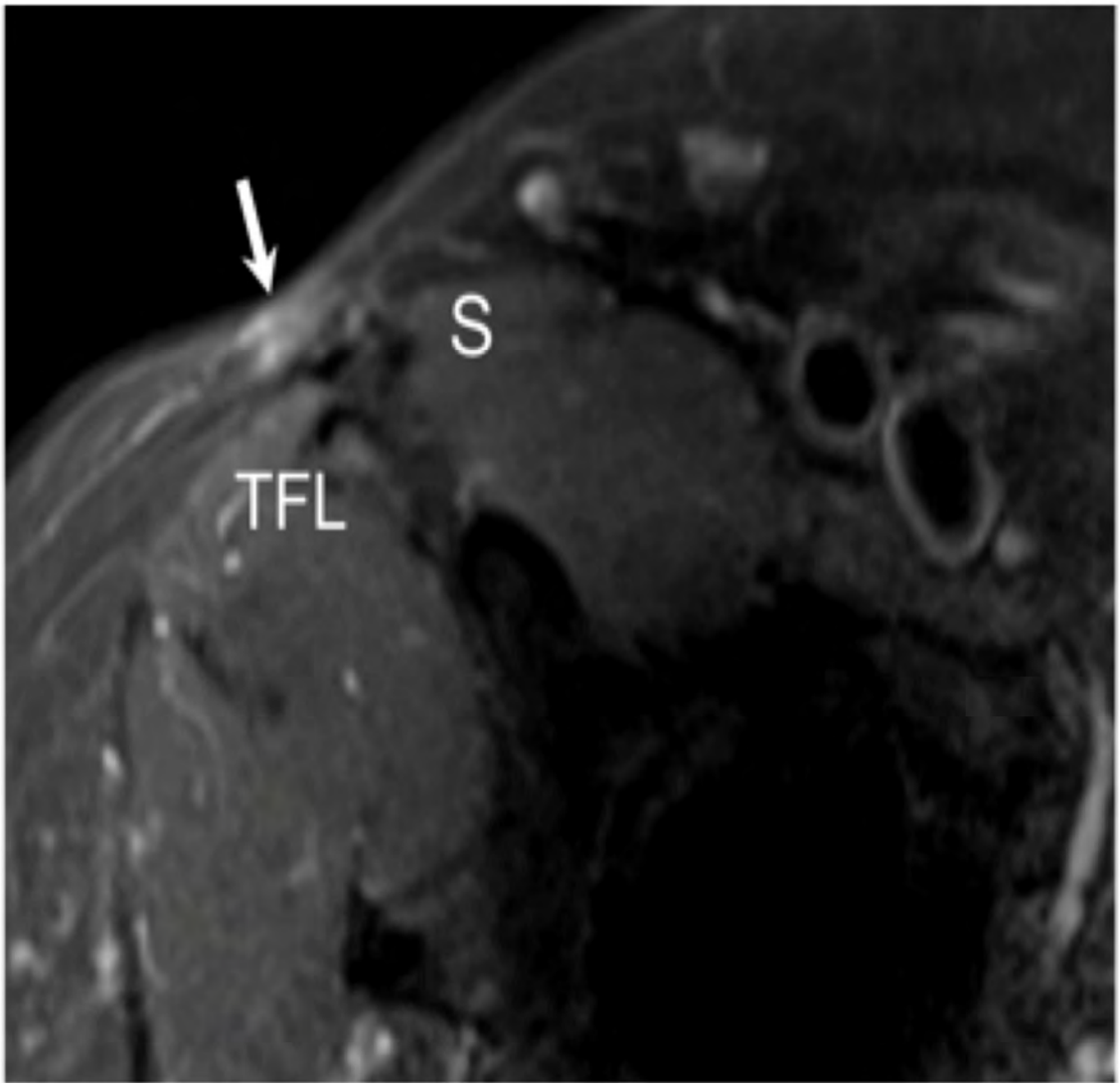

Meralgia parasthetica after hip arthroplasty. Subcutaneous scar (arrow) is overlying the sartorius and tensor fascia lata along the course of the lateral femoral cutaneous nerve.

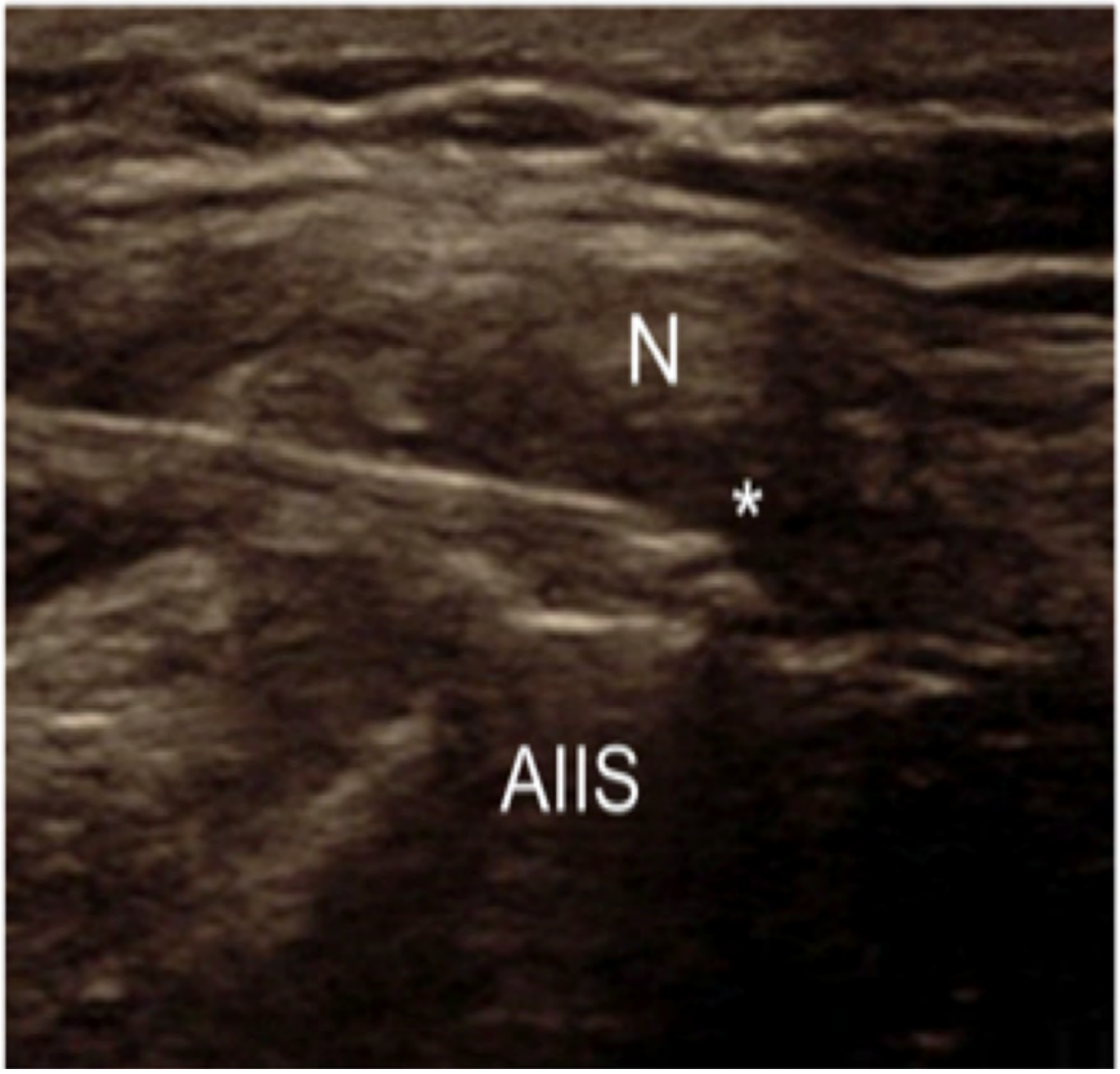

Ultrasound-guided lateral femoral cutaneous nerve block with perineural injection of bupivicaine (asterisk) at the level of the anterior inferior iliac spine prior to cryoablation.

Podium #32

SCIATIC NERVE VARIANTS IN PATIENTS DIAGNOSED WITH SCIATICA: IS THERE A CORRELATION?

Hayat Khan, MD; Tamara Fierst, MD; Sayed Ali, MD; Padmaja Jonnalagadda, MD; Stephen Ling, MD; Mark Weiner, MD; Omer Awan, MD
Temple University Hospital, Philadelphia, PA, USA
(Presented by: Hayat Khan, MD, Temple University Hospital)

Purpose: Compression of the sciatic nerve in its path along the piriformis muscle can produce sciatica-like symptoms. Prior studies have identified 6 predominant types of sciatic nerve variations with type 1 being the most common (83.1%) followed by type 2 (13.6%). However, the prevalence of sciatic nerve variation in those diagnosed with sciatica has not been studied.

Materials and Methods: With IRB approval, the charts of 70 patients clinically diagnosed with sciatica who had an MRI of the pelvis/hip were retrospectively studied. All cases contained T1 axial and T1 sagittal images. MRIs were interpreted by a board certified fellowship trained musculoskeletal radiologist to identify the type of sciatic nerve variant.

Results: Four cases were excluded due to poor imaging. Of the remaining 66 patients, 4 had bilateral sciatica resulting in a sample size of 70 limbs. Of these, 41 (58.6%) had type 1 sciatic nerve anatomy, 26 (37.1%) had type 2 and 3 had type 3 (4.3%). There were no cases of type 4, 5 and 6. A test of proportions determined the difference between normal sciatic nerve variants and the sciatica subgroup. The proportions of type 1 and 2 variations were significantly different from the normal distribution ($p<0.001$). Type 3 proportions were also different from the normal distribution ($p=0.029$) while types 4, 5 and 6 variants were not ($p>0.5$).

Conclusion: There is a difference in the proportions of sciatic nerve variants in sciatica patients. Clinicians may request routine MRIs of the hip/pelvis in those presenting with sciatica-like symptoms to look for irritation of the nerve at the piriformis muscle and thus provide targeted conservative treatment. In cases where this is inadequate and surgery is warranted, pre-operative MRIs may help to prevent iatrogenic injury to the nerve.

Modality % - Radiography / Fluoroscopy:	0
Modality % - CT:	0
Modality % - MRI:	100
Modality % - US:	0
Modality % - Nuclear Medicine:	0

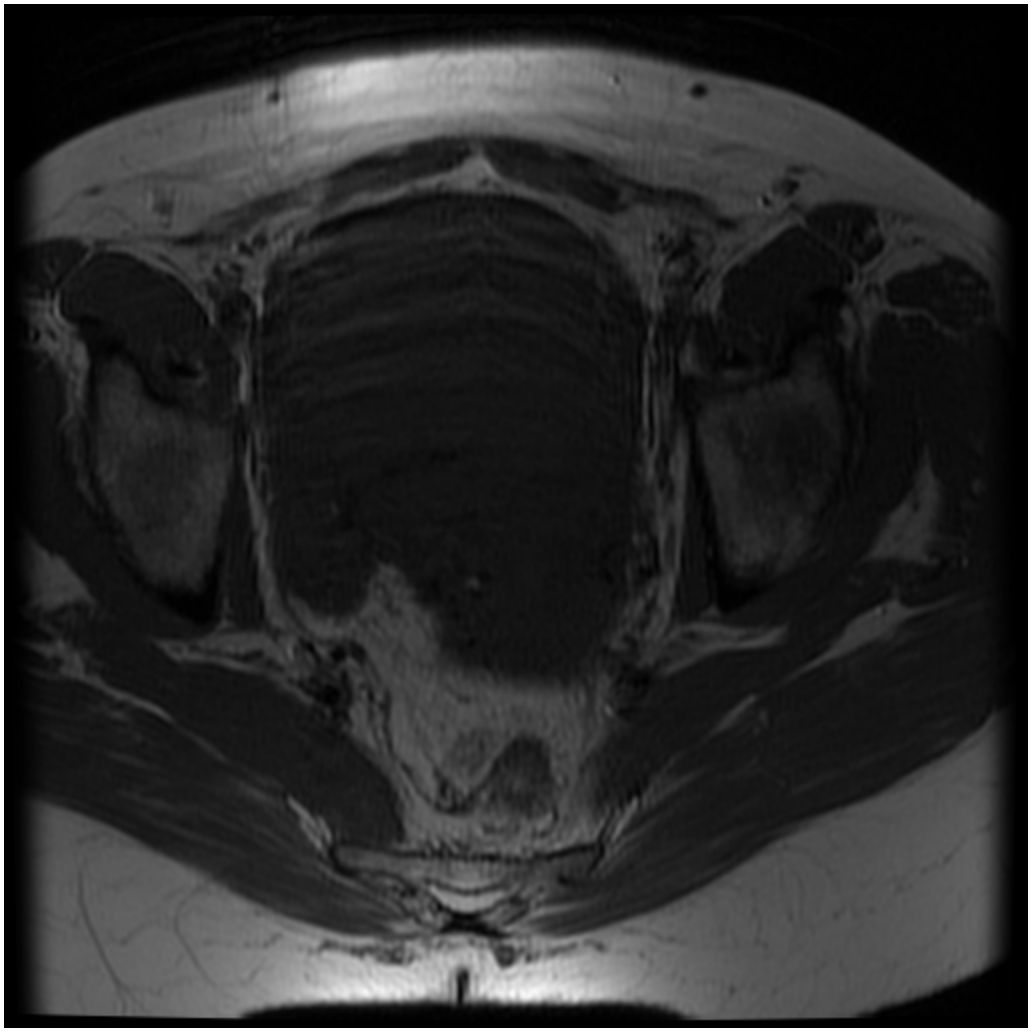

Axial T1 weighted image demonstrates a type I sciatic nerve on the right with the nerve coursing anterior to the piriformis muscle.

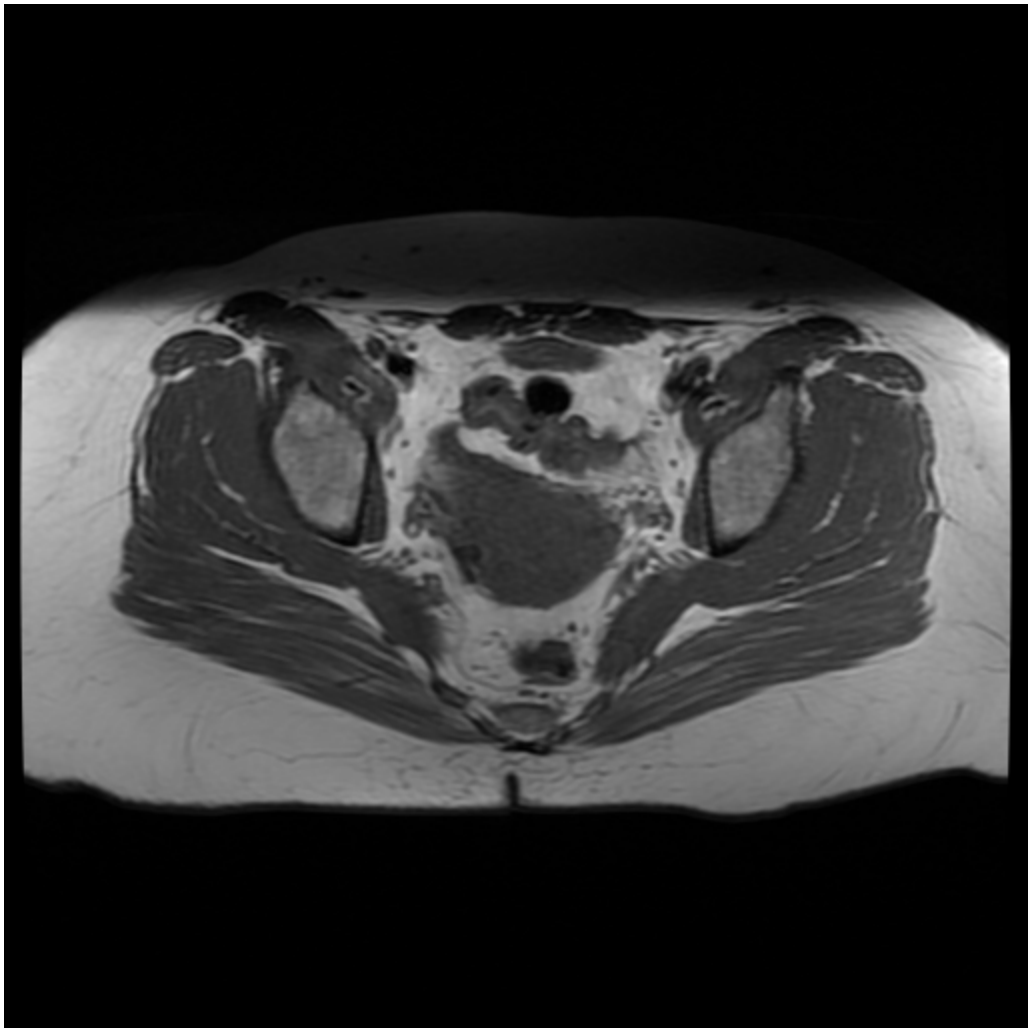

Axial T1 weighted image demonstrates a left type II sciatic nerve with some fibers coursing anterior and some coursing through the piriformis muscle.

Podium #33

DIAGNOSIS OF ISCHIOFEMORAL IMPINGEMENT BY A NOVEL ULTRASOUND TECHNIQUE

Yaron Berkowitz, MB BChir, MRCS, FRCR[1]; Simon Greenwood, MBChB, MSc, MRCP, FRCR[1]; Hatim Alabsi, MBBS[2]; Charis McNabney, MB BCh, BAO[1]; Darra Murphy, MB BCh, BAO, FRCPC[1]; Mark Cresswell, MB BCh, FRCR, FRCPC[1]
[1]St Paul's Hospital, Vancouver, BC, Canada; [2]King Abdulaziz University, Jeddah, Saudi Arabia
(Presented by: Yaron Berkowitz, MB BChir, MRCS, FRCR, St Paul's Hospital)

Purpose: Ischiofemoral impingement (IFI) is an under-recognised cause of posterior hip pain in the deep gluteal region. The etiology is poorly understood, but is related to narrowing of the ischiofemoral space (IFS). The normal IFS ranges from 19 – 35mm, and 12 – 22mm in IFI. The diagnosis is aided by magnetic resonance imaging (MRI).

IFS dimensions assessed by ultrasound have been shown to be equivalent to MRI. However, ultrasound offers the advantage of dynamic assessment of the space in various hip positions. We sought to establish the basis of a diagnostic sign on ultrasound that triggers symptoms, which will provide a useful test in diagnosing IFI.

Materials and Methods: A prospective study of patients presenting with a clinical suspicion of IFI over 4 months was completed with MRI and ultrasound; dynamic ultrasound of the IFS in various hip positions was performed, correlating with pain. The IFS was observed whilst patients triggered their pain, and sonographically guided deep palpation of the IFS to reproduce pain was assessed.

Results: Patients with MRI findings of IFI showed correlation to positive findings on dynamic ultrasound. The narrowest IFS correlated to triggering of pain and the IFS distances were equivalent to MRI. Focal sonographic palpation of the IFS reproducing symptoms was strongly supportive of the diagnosis.

Conclusion: In patients with clinically suspected IFI and with supportive MRI evidence, ultrasound can be used to dynamically correlate their symptoms with hip positions at which the IFS is at its narrowest, and reproduce symptoms by sonographically guided deep palpation of the IFS. Therefore we can establish which hip positions produce maximal narrowing, and provide information as to the range of symptomatic IFS distances. Dynamic ultrasound may prove to be a useful test in assessment of IFI, with similar sensitivity but higher specificity than MRI.

Modality % - Radiography / Fluoroscopy:	0
Modality % - CT:	0
Modality % - MRI:	20
Modality % - US:	80
Modality % - Nuclear Medicine:	0

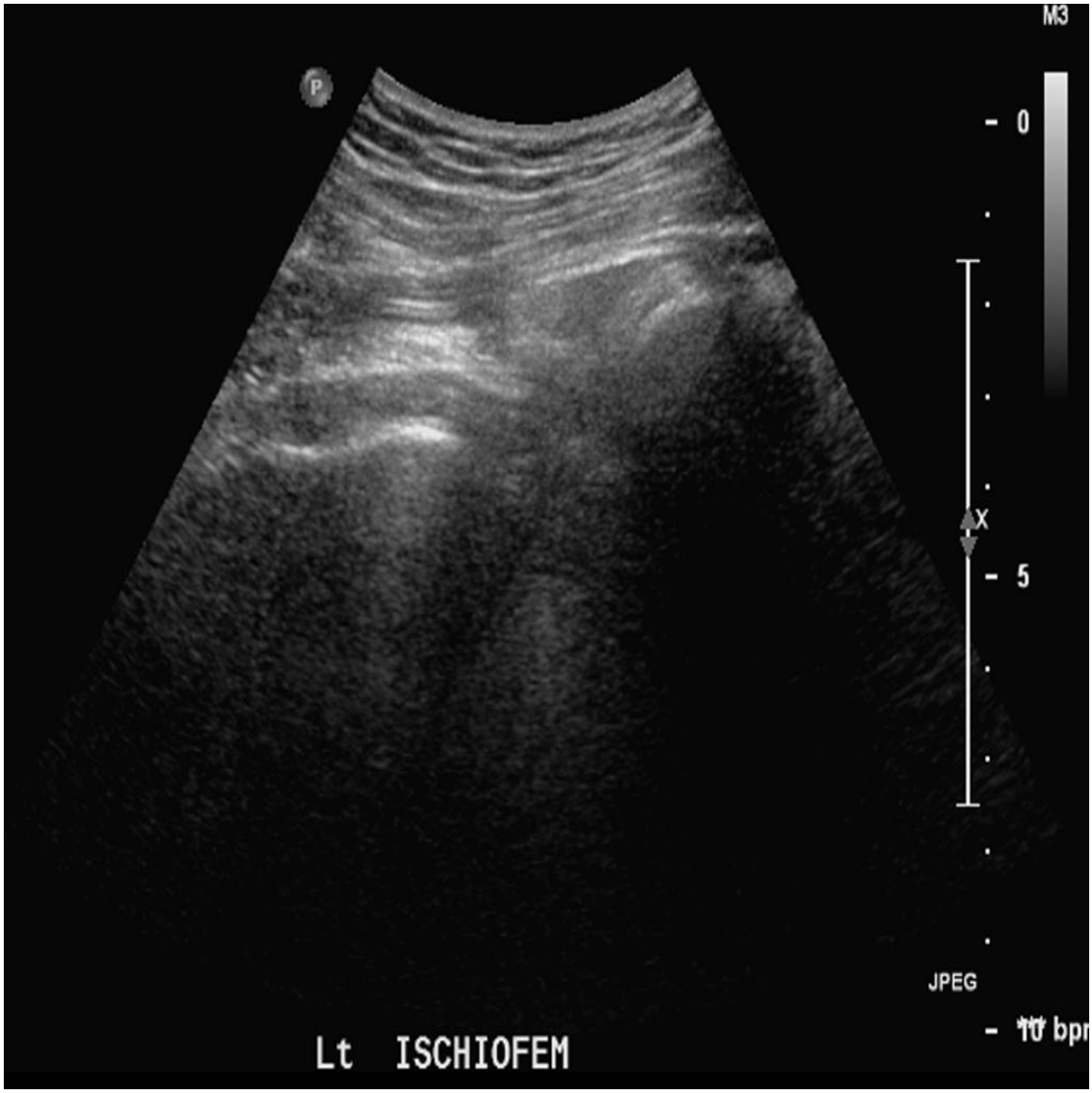

Ultrasound of the posterior left ischiofemoral space with the patient prone in internal hip rotation. The space is 24mm, and the patient is pain free.

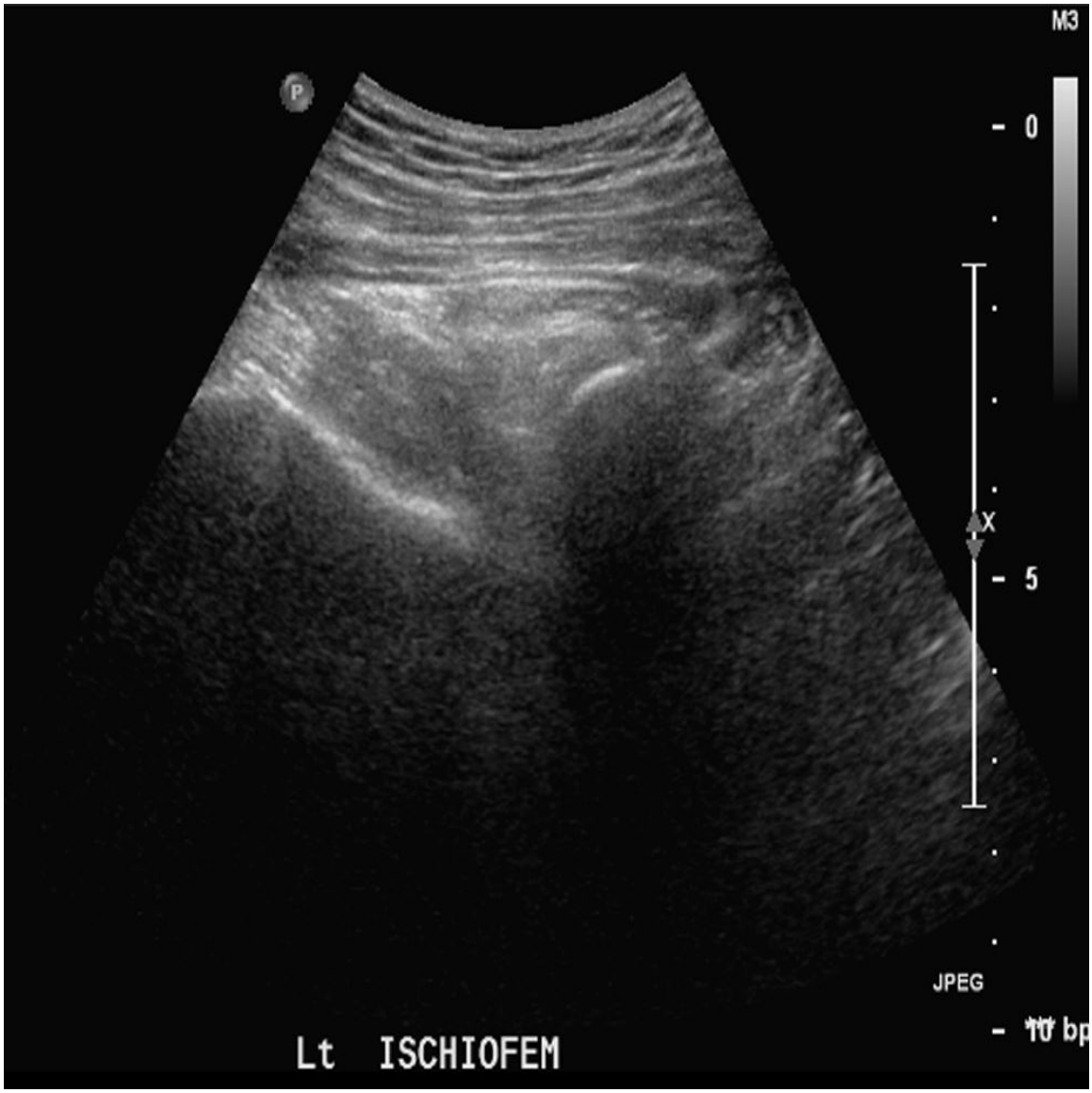

Ultrasound of the posterior left ischiofemoral space with the patient prone in external hip rotation. The space closes to 14mm, triggering the patient's pain.

Podium #34

BREAK FROM PLAY: INCIDENCE AND IMPLICATIONS OF FRACTURE IN CORE MUSCLE INJURY

Joseph Delic, MD; Andrew Ross, MD, MPH; Donna Blankenbaker, MD
University of Wisconsin Hospital & Clinics, Madison, WI, USA
(Presented by: Joseph Delic, MD, University of Wisconsin Hospital & Clinics)

Purpose: Core muscle injury (athletic pubalgia) is a well-known injury spectrum involving the pubic symphysis and rectus abdominis/adductor musculature. Osteitis pubis, muscle, tendon, and aponeurotic plate injuries are commonly described; however, we hypothesize that fracture of the adjacent pubic bones may be an under-recognized co-existing injury. Our aim was to identify the fracture incidence and associated injury patterns in patients with aponeurotic plate injuries.

Materials and Methods: This retrospective study had IRB approval and waived informed consent. 84 consecutive patients with athletic pubalgia protocol MRI showing aponeurotic plate injuries from March 2011 through August 2017 were independently analyzed by two musculoskeletal radiologists. Evaluation included presence/absence of: fracture; pubic symphysis osteophytes, sclerosis, marrow edema, and fluid; adductor and rectus abdominis myotendinous injury; and aponeurotic plate injury (location and size). Statistical analysis was performed with two-sided chi-squared, Fisher's exact, and Wilcoxon rank sum tests.

Results: The cohort included 84 patients (78 men and 6 women) with mean age of 34.9 years (16-66). Fracture incidence was 21.4% (18/84) including avulsion 4.76% (n=4), pubic body 15.48% (n=13), and pubic ramus 1.19% (n=1). A statistically significant association existed between adductor longus tendon (40%, p=0.012) and muscle (30%, p=0.047) strains and pubic body fracture. No association existed between the presence of fracture and measured size of the aponeurotic plate injury (range right mediolateral 5-25mm p=0.81, right craniocaudal 9-44mm p=0.69, left mediolateral 4-23mm p=0.79, and left craniocaudal 6-31 mm p=0.4).

Conclusion: Fractures occurred in 21.4% of our cohort with a wide range of core muscle injury patterns. The presence of fracture did not correlate with the size of the aponeurotic plate injury suggesting the injury mechanisms are associated but unique. These potentially under-recognized fractures may impact treatment strategy and further analysis of return to play time would help patient stratification.

Modality % - Radiography / Fluoroscopy:	0
Modality % - CT:	0
Modality % - MRI:	100
Modality % - US:	0
Modality % - Nuclear Medicine:	0

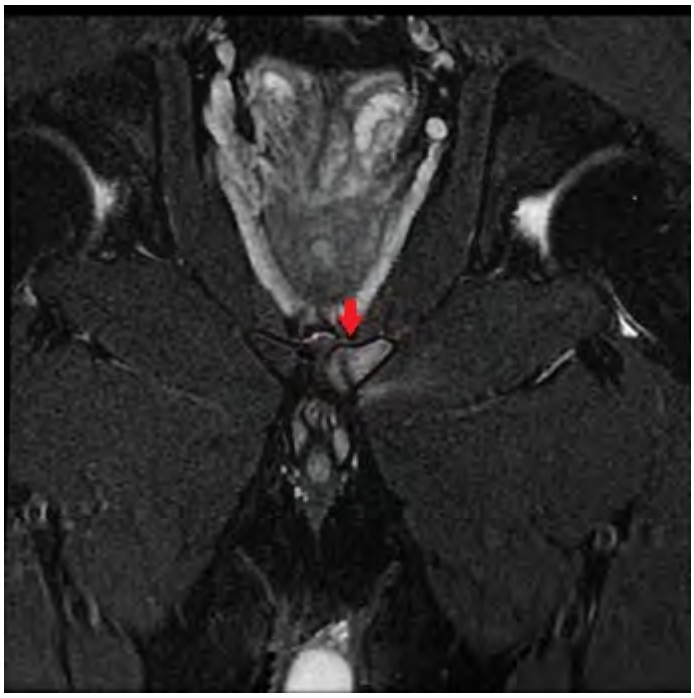

Axial PD and T2 fat saturated sequences demonstrate a vertically oriented hypo-intense fracture line through the left pubic body (red arrows) with marrow edema.

Podium #35

Effect of analytics driven custom worklists on musculoskeletal MRI interpretation times in an academic setting

Tony Wong, MD; Jonathan Kazam, MD; Michael Rasiej, MD
Columbia-Presbyterian Medical Center, New York, NY, USA
(Presented by: Tony Wong, MD, Columbia-Presbyterian Medical Center)

Purpose: To evaluate if use of analytics driven custom worklists can decrease musculoskeletal MRI interpretation times in an academic setting.

Materials and Methods: All MRIs signed by 3 radiologists (readers 1, 2, and 3) during the 2016 calendar year were queried. The interpretation time for each exam was calculated from times of initial exam view and report signing. Exclusion criteria: trainee contribution, no time stamps, or ≥ 45 min. interpretation time. Average interpretation times per body part were calculated for each reader for this baseline period.

Custom worklists were made based upon difference in relative interpretation speeds and used prospectively for a 7-day trial period. Exam interpretation times were then calculated (n = 168). Differences between the average times during the trial period vs. baseline and difference in volume distribution were calculated. A z-score was used to assess statistical significance of changes in speed.

Results: Difference between average interpretation times during trial period vs. baseline for all reader combinations (Readers 1&2, Readers 1&3, Readers 2&3): -12439 secs. (3 hrs. and 27 mins less) (Figure 1).

Reader 1 interpreted wrist exams (n=4) ~10 mins slower ($p = 0.01$) and Reader 3 interpreted C-spine exams (n = 7) ~9 mins faster ($p = 0.0048$) compared to baseline. No significant change in interpretation speed for all other body parts for all readers ($p \geq 0.05$).

Volume of exams interpreted during trial period that differed by ≥ 5% from individual baseline volume:

Reader 1: none

Reader 2: C-spine (+14%), L-spine (-9%), pelvis (+9%), hip (-7%), knee (-13%)

Reader 3: L-spine (+5%), elbow (+9%), hip (+10%), knee (-24%)

Conclusion: Analytics driven worklists may decrease overall MRI interpretation time in a multi-reader setting without significant alteration in individual speed, though a change in volume distribution is required.

Modality % - Radiography / Fluoroscopy:	0
Modality % - CT:	0
Modality % - MRI:	100
Modality % - US:	0
Modality % - Nuclear Medicine:	0

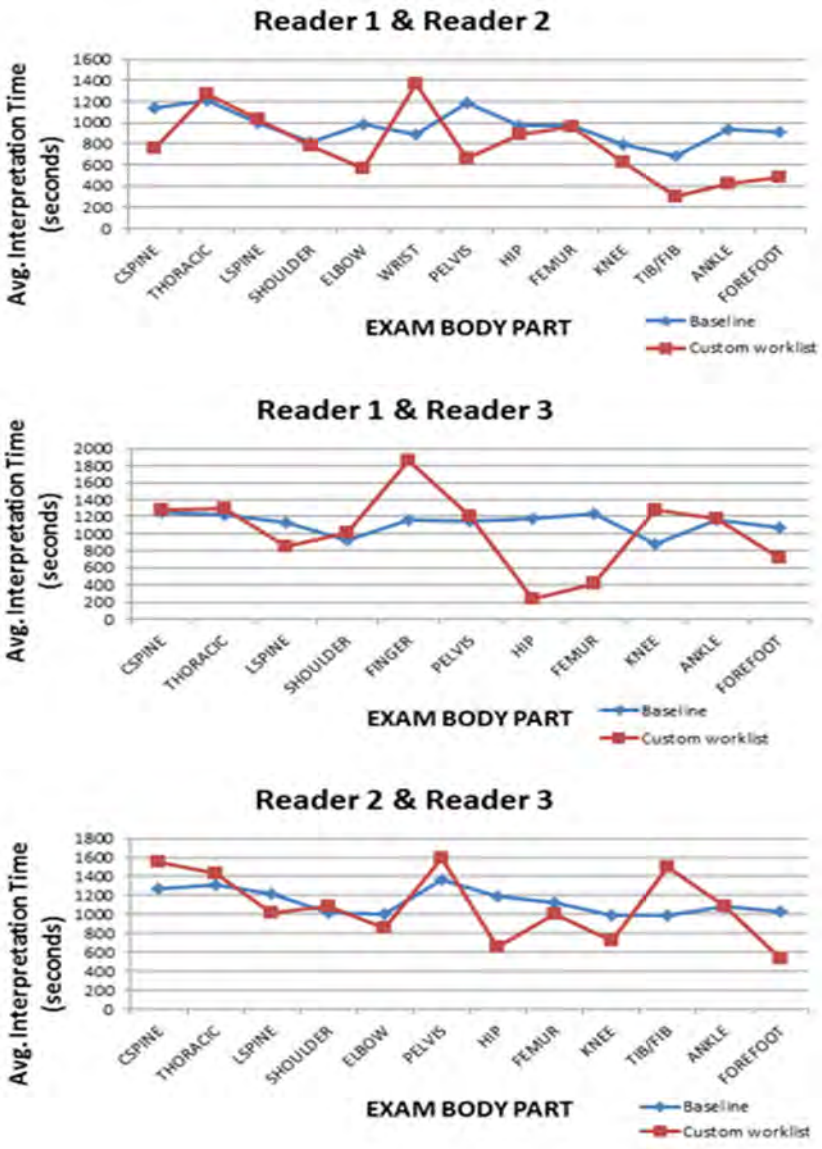

Average exam interpretation times for all reader combinations at baseline and with custom worklists

Podium #36

LOW DOSE METAL ARTIFACT REDUCTION CT IN ARTHROPLASTY IMAGING: A CADAVERIC AND CLINICAL STUDY

Naveen Subhas, MD, MPH[1]; Bong Jae Jun, PhD[1]; Eric Ricchetti, MD[1]; Nancy Obuchowski, PhD[1]; Andrew Primak, PhD[2]; Joseph Iannotti, MD, PhD[1]

[1]Cleveland Clinic, Cleveland, OH, USA; [2]Siemens Healthcare, Cleveland, OH, USA

(Presented by: Naveen Subhas, MD, MPH, Cleveland Clinic)

Purpose: To determine if a simulated low dose metal artifact reduction (MAR) CT technique is comparable to the clinical dose MAR technique for shoulder arthroplasty evaluation.

Materials and Methods: 2 cadavers and 10 patients with shoulder arthroplasties were scanned at clinical dose (140 kVp, 300 qrmAs). Cadavers were also scanned at half dose (140 kVp, 150 qrmAs). Images were reconstructed using a MAR CT algorithm (iMAR) at full dose and with a noise insertion algorithm (NIA) simulating 50% dose reduction. The difference in the standard deviation (SD) of regions of interest and streak artifact near the arthroplasty graded by 3 blinded readers (2 surgeons and 1 radiologist) between the actual half dose and simulated half dose cadaver scans were used to validate the NIA. Simulated half dose scans were then compared to full dose scans in patients by measuring the differences in implant position using a 3D software (OrthoVis) and readers' grading of periprosthetic radiolucency and streak artifact.

Results: The NIA was validated with a mean difference in SD between actual and simulated half dose methods of 2.42 HU with 95% CI of [1.4, 3.4] and no difference in the streak artifact grades in 13/18 (72.2%) comparisons in cadavers. In patients, the difference in the measurement of implant position between full and simulated half dose methods was within 1 degree or 1 mm in 149/150 (99.3%) measurements. The inter-reader agreement rates for grading radiolucency and streak artifact were also nearly identical when readers were using full dose (73.9% overall agreement, 133/180) or simulated half dose scans (73.3% overall agreement, 528/720).

Conclusion: A simulated half-dose MAR CT technique is comparable both quantitatively and qualitatively to a standard dose technique for shoulder arthroplasty evaluation and demonstrates the potential for reducing dose in arthroplasty imaging.

Modality % - Radiography / Fluoroscopy:	0
Modality % - CT:	100
Modality % - MRI:	0
Modality % - US:	0
Modality % - Nuclear Medicine:	0

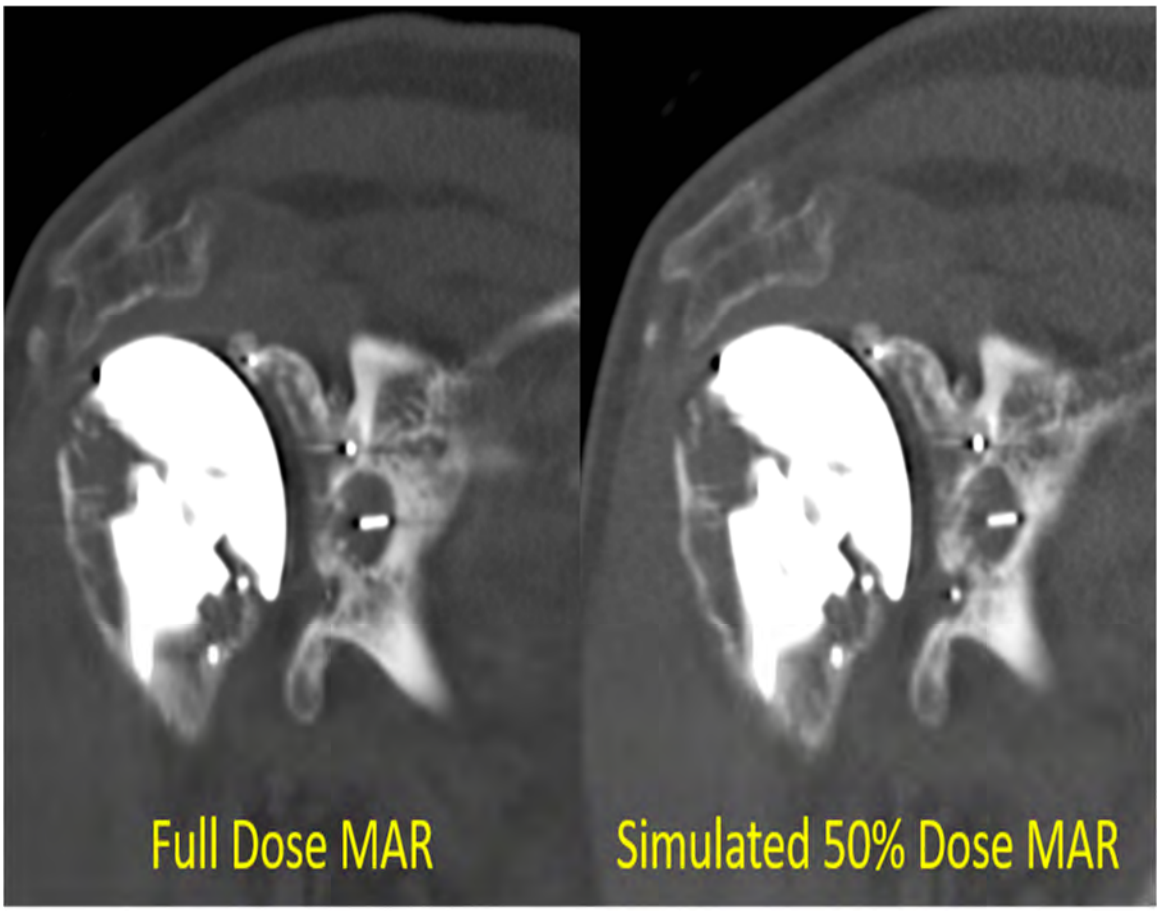

Full and simulated 50% dose coronal MAR (metal artifact reduction) CT images showing osteolysis around the central glenoid peg

Podium #37

Subchondral Insufficiency Fracture of the Knee (the old SONK): Novel MRI-Based Grading System and its Clinical Implication

Felix Gonzalez, MD[1]; Yara Younan, MD[1]; Johanness Roedl, MD[2]; Monica Umpierrez, MD[1]; Adam Singer, MD[1]; Gulshan Sharma, PhD, MPH[3]; Adam Zoga, MD[2]; William Morrison, MD[2]
[1]Emory University Dept. of Radiology, MSK Division, Atlanta, GA, USA; [2]Thomas Jefferson University Hospital, Philadelphia, PA, USA; [3]Cumming School of Medicine, Calgary, AB, Canada
(Presented by: Felix Gonzalez, MD, Emory University Dept. of Radiology, MSK Division)

Purpose: To propose an MRI grading system for subchondral insufficiency fracture of the knee (SIFK) and compare low-grade and high-grade lesions vs control.

Materials and Methods: A retrospective review of 50 patients with SIFK seen on initial MRI with a 6-12 months follow up exam. Four SIFK grades were used. Grade 1 represents subchondral edema, Grade 2 a subchondral fracture (SF), Grade 3 superimposed cystic changes, and Grade 4 early osteonecrosis. Grades 1-2 were considered low-grade (LG) and grades 3-4 high-grade (HG) lesions. The associations between LG and HG lesions and SIFK location/lesion size, BME, meniscal tears/ location and chondrosis were determined and compared to 50 age, gender-BMI matched controls.

Results: Our study consisted of 31 males and 19 females, with a mean age of 51.5±16(12-89). 78% of those had a LG SIFK while 22% had a HG lesion. The most common SIFK location was the medial femoral condyle (LG=61.5%; HG=100%). 61.5% of patients with LG SIFK had a medial mensical tear vs 100% with HG SIFK (p=0.01), with the majority of tears involving the posterior root attachment (LG=47.8%, HG=90.9%, p=0.03). Mod meniscal extrusion (3-5mm) was seen in the majority of LG SIFK with severe extrusion (>5mm) in the HG group. LG SIFK patients had significant subchondral marrow edema improvement, whereas the majority (72.8%) of HG lesions showed progression (p<0.001). Low-grade chondrosis was seen with LG lesions, while the majority of HG SIFK showed high-grade chondrosis (p=0.002). Compared to controls, there was a difference in the incidence of medial meniscal tears, tear location, degree of extrusion, and chondrosis location (p=0.025 and ps<0.001, respectively).

Conclusion: MRI-based SIFK grading shows that HG lesions demonstrate marrow edema progression, severe chondrosis and severe meniscal extrusion. LG SIFK shows resolution despite moderate meniscal extrusion.

Modality % - Radiography / Fluoroscopy:	0
Modality % - CT:	0
Modality % - MRI:	1
Modality % - US:	0
Modality % - Nuclear Medicine:	0

Podium #38

ULTRASOUND EVALUATION OF RADIAL NERVE PALSY ASSOCIATED WITH HUMERAL SHAFT FRACTURE TO GUIDE OPERATIVE VERSUS CONSERVATIVE TREATMENT

Mihra Taljanovic, MD, PhD; Melissa Esparza, MD; Lana Gimber, MD, MPH; Lisa Truchan, MD; Tyson Chadaz, MD; Christina Boulton, MD; Jason Wild, MD
University of Arizona HCS - Tucson, Tucson, AZ, USA
(Presented by: Mihra Taljanovic, MD, PhD, University of Arizona HCS - Tucson)

Purpose: Radial nerve palsies are commonly associated with humeral shaft fractures. The purpose of this study is to determine the effectiveness of ultrasound (US) at evaluating the condition of the radial nerve in the setting of humeral shaft fractures and determine if surgical management is needed.

Materials and Methods: A retrospective review of US studies in patients with radial nerve palsy associated with humeral shaft fractures was conducted. Twenty patients were identified who met inclusion criteria. Eight patients with US diagnosis of radial nerve laceration and/or entrapment underwent prompt ORIF of their humeral shaft fracture. One patient with US diagnosis of complete radial nerve laceration underwent additional surgery 6 weeks after injury with tendon transfer. Others were initially treated conservatively with 5 patients undergoing subsequent surgical treatment for other reasons unrelated to radial nerve palsy. Clinical, operative and US results were compared.

Results: Of 20 patients, 13 (65%) were male and 7(35%) female. Average age was 45 years. In 8 patients who underwent initial ORIF of their radial shaft fracture, US correctly diagnosed 1 complete radial nerve laceration, 1 partial radial nerve laceration with entrapment, 4 radial nerve entrapments, and one partial radial nerve entrapment which were all operatively confirmed. In one patient US failed to see the radial nerve at the fracture site which was proven to be complete transection at surgery. In 5 surgically treated patients without radial nerve entrapment or laceration, US diagnosis was concordant with surgical findings. In 6 patients who were treated conservatively, clinical follow-up showed complete or at least partial radial nerve recovery.

Conclusion: US provides accurate diagnosis of radial nerve injuries in patients with humeral shaft fractures and helps in treatment guidance.

Modality % - Radiography / Fluoroscopy:	0
Modality % - CT:	0
Modality % - MRI:	0
Modality % - US:	1
Modality % - Nuclear Medicine:	0

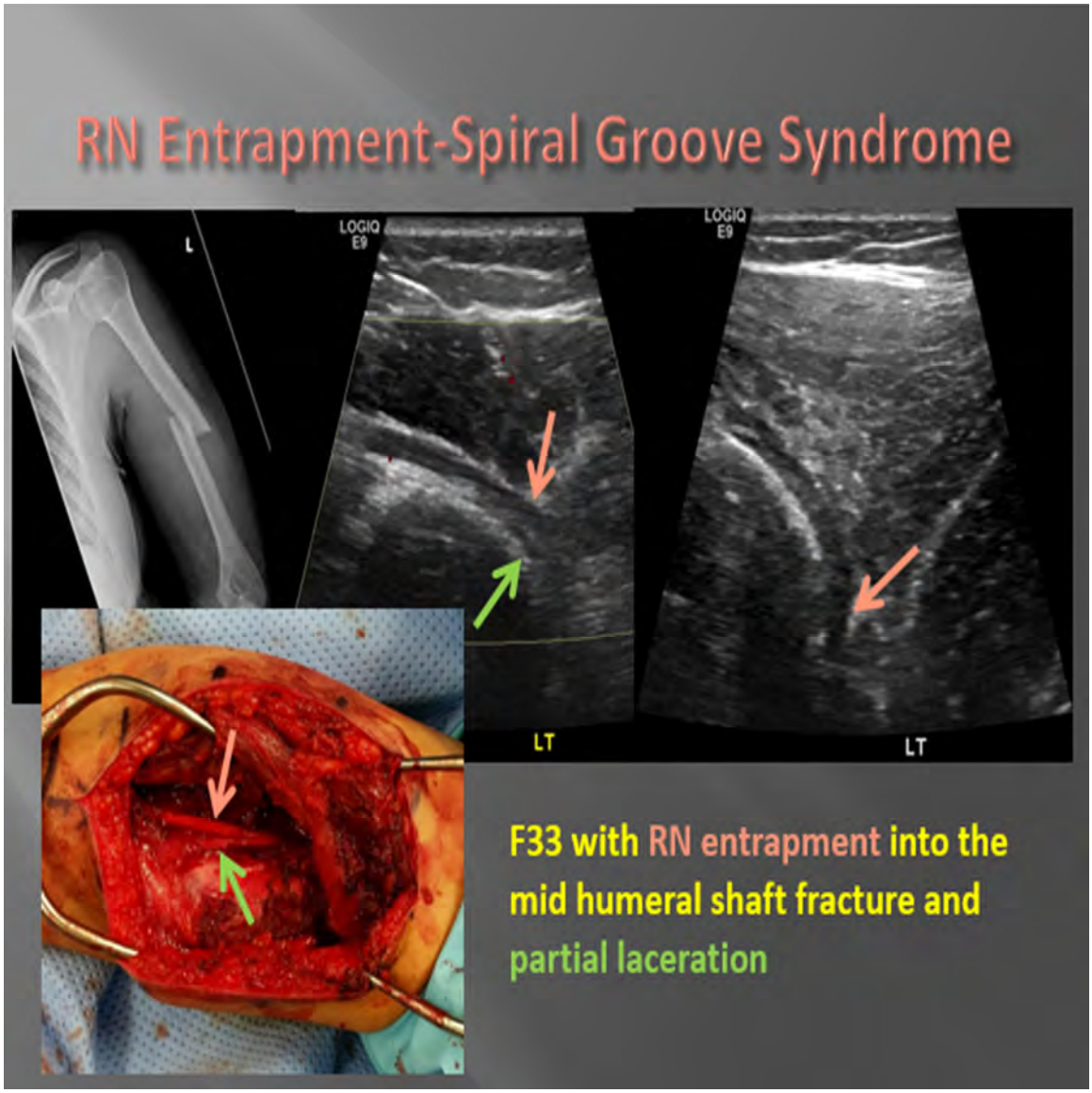

33-year-old female with humeral shaft fracture which caused radial nerve entrapment and partial laceration.

Podium #39

"OSTEITIS": HITHER, THITHER OR WITHER? PREDICTION OF OSTEOMYELITIS IN PATIENTS WITH EQUIVOCAL MRI FINDINGS

William Morrison, MD; Alessandra Sax, MD; Adam Zoga, MD; Johannes Roedl, MD; Jeffrey Belair, MD
Thomas Jefferson University Hospital, Philadelphia, PA, USA
(Presented by: William Morrison, MD, Thomas Jefferson University Hospital)

Purpose: We sought to examine MRI exams of the foot/ankle in diabetic patients with ulceration and equivocal findings for osteomyelitis (abnormal T2 signal without replacement of marrow fat) to determine findings that could help predict outcome.

Materials and Methods: Pedal MR imaging of 60 patients with ulcer and suspected osteomyelitis were examined. Inclusion criteria included diabetes, ulcer, initial MRI imaging with bone marrow edema (without replacement of marrow fat on T1w images) in proximity to an ulcer, and subsequent MRI imaging, biopsy or definitive surgery.

Ulcers were categorized based on size and distance to bone. Bone marrow edema was defined as T2fs and STIR hyperintensity. The ratio of marrow to fluid signal ROI measurements were obtained. Development of osteomyelitis was characterized by loss of the normal T1 marrow fat signal on subsequent MRI. Additional clinical variables that were analyzed include ESR, WBC count, surgical pathology, and treatment regimens.

Statistical analysis was performed.

Results: Of 60 MR exams, 27 showed resolution of marrow findings (no osteomyelitis, follow-up average 522 days) and 33 developed frank osteomyelitis (follow-up average 207 days). Ulcer size was 3.4 cm2 in the OM group versus 3.3 cm2 in the non-OM group. Average proximity to the underlying bone was 6mm in the OM group compared to 9mm in the non-OM group ($p<0.05$). The ROI of marrow signal intensity on T2fs/STIR averaged 65% relative to fluid in the OM group, and 44% in the non-OM group ($p<0.05$).

Conclusion: Both the ratio of marrow to fluid signal ROI of greater than 50% on T2fs/STIR imaging and the distance of the ulcer to the underlying bone were strong predictors for the development of osteomyelitis. This preliminary study will inform future efforts including logistic regression to generate risk ratios for additional MR imaging features.

Modality % - Radiography / Fluoroscopy:	0
Modality % - CT:	0
Modality % - MRI:	100
Modality % - US:	0
Modality % - Nuclear Medicine:	0

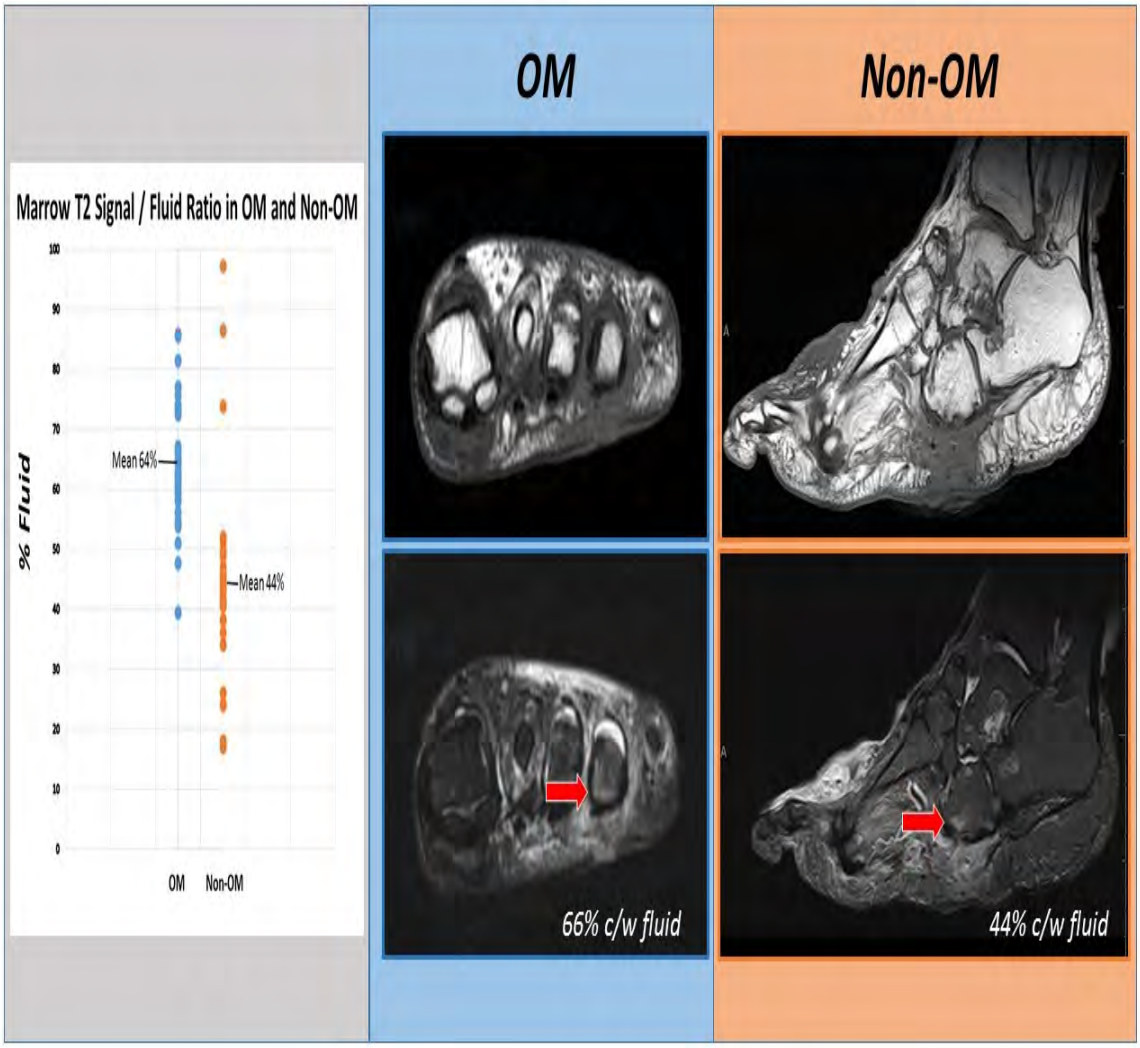

Distribution of marrow T2 signal / fluid signal ratio in patient with osteomyelitis (OM) and Non-OM outcome

Podium #40

BONE BRUISE VS. NON-DISPLACED FRACTURE AT MRI: A GRADING SYSTEM TO PREDICT RETURN TO PLAY

Jeffrey Belair, MD[1]; Adam Zoga, MD[1]; William Morrison, MD[1]; Roedl Johannes, MD[1]; Blake Bowden, MD[2]
[1]Thomas Jefferson University Hospital, Philadelphia, PA, USA; [2]Augusta University, Augusta, GA, USA
(Presented by: Jeffrey Belair, MD, Thomas Jefferson University Hospital)

Purpose: MRI is the modality of choice for diagnosing radiographically-occult traumatic osseous injuries. MRI criteria for diagnosing bone contusion versus non-displaced fracture are not well established. We propose an algorithm for grading osseous injury at MRI in a cohort of professional athletes, correlating MRI findings with return to play (RTP).

Materials and Methods: 30 lower extremity MRIs in 23 professional hockey players who sustained direct trauma and had normal radiographs were reviewed by 2 MSK radiologists blinded to clinical history. Bone marrow edema (BME) was graded as 1=patchy/ill-defined, 2=focal/mild, 3=focal/intense, 4=extensive/intense. Marrow replacement on T1-weighted sequences was documented, along with linear or curvilinear hypointensity. Presence of cortical breech, microtrabecular disruption, and soft tissue injury were also assessed. Location of osseous injury was categorized as weight-bearing, subenthesial, both, or neither. Concurrent CT examinations were reviewed in addition to MRI when available.

Results: Mean interval from injury to MRI was 1 day and mean interval to follow-up MR was 10 days. Mean RTP for athletes with linear T1-hypointensity at MRI was 11 days vs. 8 days for those without (α = .25, unpaired t-test). Mean RTP for athletes with a constellation of T1 marrow replacement and grade 3 BME in a weight-bearing location was 14 days vs. 4 days for those without this combination (α = .04). Subenthesial injuries had a slightly longer RTP without statistical significance. None of the cases examined demonstrated cortical breech, and all concurrently obtained CT examinations were negative for fracture. Majority of subjects with grade 1 BME had RTP within 2 days.

Conclusion: MRI is useful for grading bone bruise injuries and predicting RTP. MRI constellation of T1 marrow replacement and grade 3 BME in a weight-bearing location correlates with longer return to play than other MRI findings.

Modality % - Radiography / Fluoroscopy:	0
Modality % - CT:	10
Modality % - MRI:	90
Modality % - US:	0
Modality % - Nuclear Medicine:	0

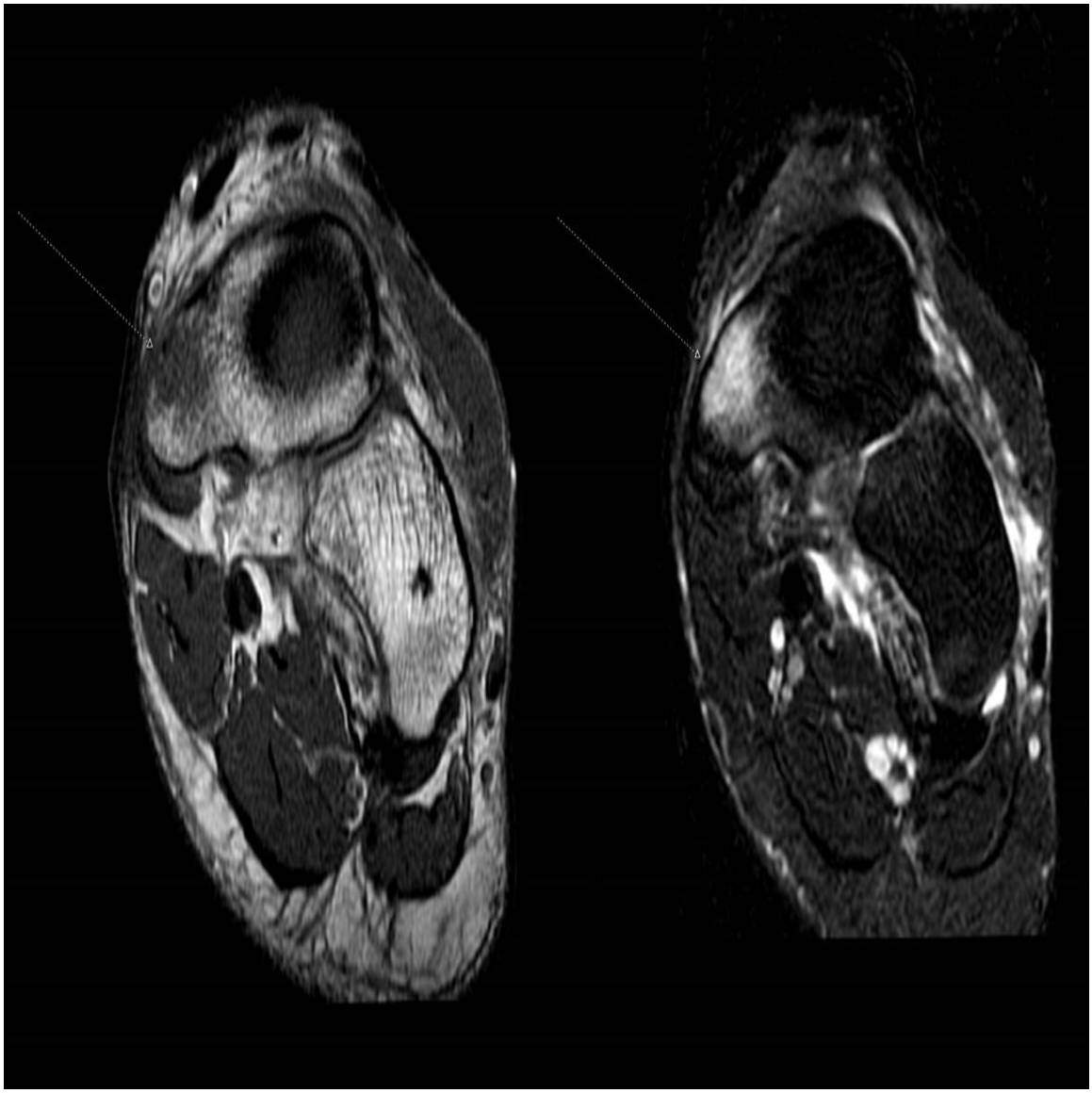

Short-axis T1 and T2 fat-suppressed images demonstrating grade 3 (focal/intense) bone marrow edema with T1 marrow replacement in the navicular of a professional hockey player.

Podium #41

EVALUATION OF ATRAUMATIC MUSCULOSKELETAL PAIN IN THE EMERGENCY DEPARTMENT BY DUAL ENERGY CT (DECT) WITH VIRTUAL NONCALCIUM APPLICATION FOR BONE MARROW EDEMA AND COLOR OVERLAY: BEYOND FRACTURES

E Garwood, MD; Soterios Gyftopoulos, MD; Emilio Vega, BS; Michael Mechlin, MD
NYU Medical Center/ Hospital for Joint Diseases Langone Medical Center, New York, NY, USA
(Presented by: E Garwood, MD, NYU Medical Center/ Hospital for Joint Diseases Langone Medical Center)

Purpose: To demonstrate the appearance of osseous pathologies other than traumatic bone marrow edema using DECT with virtual noncalcium application for bone marrow edema and color overlay in patients presenting acutely to the emergency department with atraumatic musculoskeletal pain.

Materials and Methods: This study was IRB approved and informed consent was waived. 166 consecutive patients presenting to the emergency department from 2/1/2017 - 7/1/2017 who underwent DECT (Somatom Force, Siemens) for musculoskeletal indications were retrospectively identified. CTs performed for the indication of trauma (n=113) were excluded. Post-processing was performed offline using a virtual noncalcium algorithm with color overlay (syngo.via; Siemans). Demographics were extracted from the electronic medical record. Descriptive statistics were performed.

Results: In the study period, 20 females and 31 males, average age 59 years (range 20-92) underwent 53 CTs. Indications for imaging were infection (n=28), postoperative pain (n=2), and atraumatic pain (n=23). 34 (64%) had only soft tissue findings or were negative. 19 (36%) demonstrated atraumatic osseous etiologies of pain including metastasis, primary bone tumor, osteomyelitis, and inflammatory or infectious arthropathy. The appearance of these etiologies with color overlay is illustrated. 15 (28%) underwent subsequent imaging with MRI, bone scan, or PET with concordant results and these correlates are shown.

Conclusion: DECT has emerged as a technology for detecting traumatic bone marrow edema. Bone marrow edema related to other, atraumatic etiologies including inflammatory arthropathy, tumor, and infection are also visually highlighted by this technique. In the emergent setting, DECT with virtual noncalcium subtraction and color overlay may be a useful adjunct to provide a visual aid for the detection or exclusion of marrow edema or a marrow infiltrating process in patients presenting with atraumatic musculoskeletal pain.

Modality % - Radiography / Fluoroscopy:	5
Modality % - CT:	90
Modality % - MRI:	5
Modality % - US:	0
Modality % - Nuclear Medicine:	0

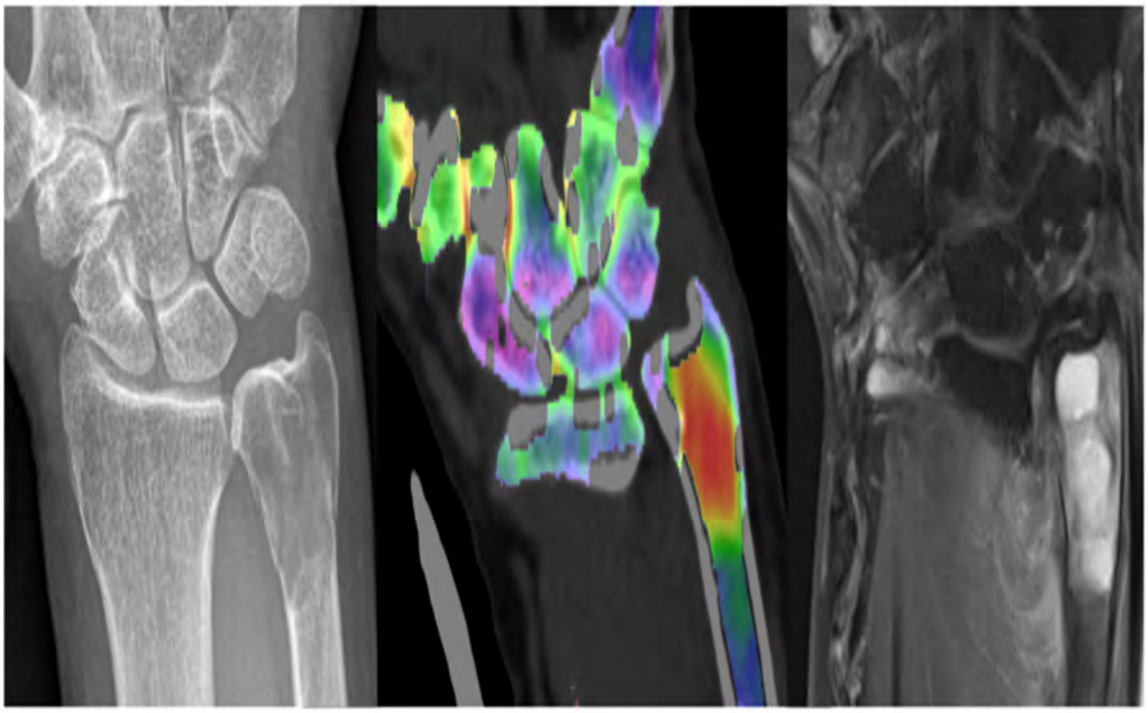

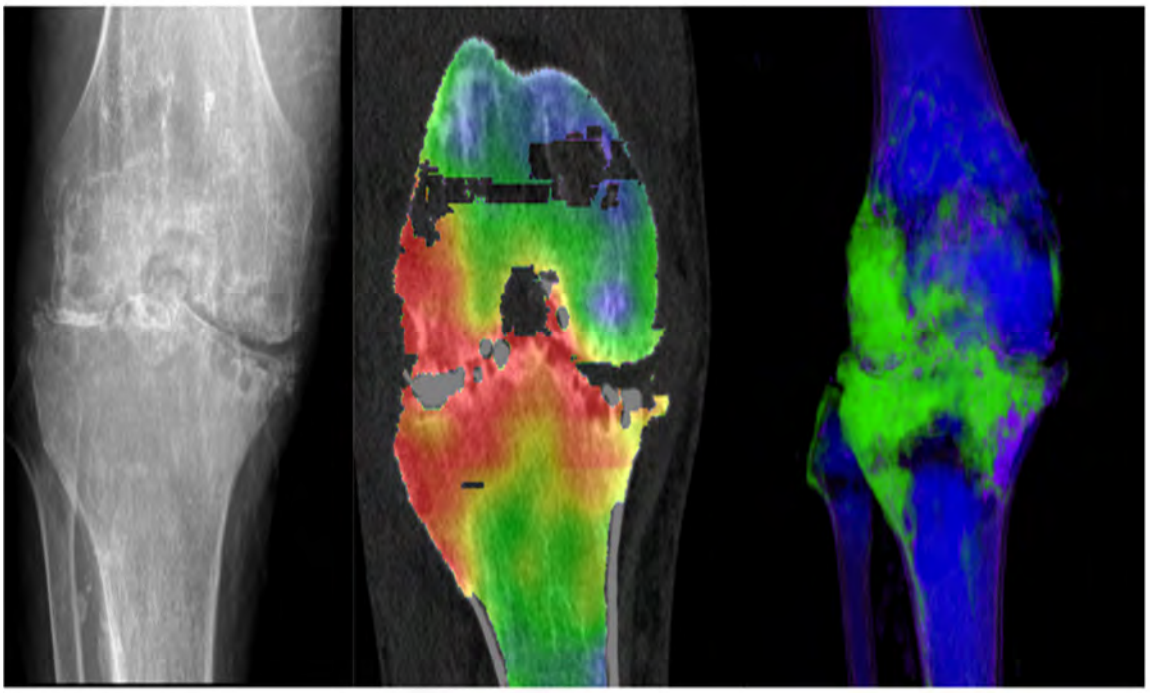

1. Primary bone tumor and pathologic fracture
2. Inflammatory arthropathy

WEDNESDAY

Society of Skeletal Radiology

41st Annual Meeting

March 25-28, 2018

Wednesday, March 28, 2018

7:00 a.m.–7:55 a.m. **Continental Breakfast**

7:00 a.m.–12:30 p.m. **Registration/Information Desk Open**

7:00 a.m.–10:30 a.m. **Exhibit Hall Open**

7:00 a.m.–10:30 a.m. **ePoster Session**

8:00 a.m.–10:00 a.m. **TUMOR**

Moderators: Behrang Amini, MD, PhD, Francesca D. Beaman, MD

8:00 a.m. #42 **QUANTITATIVE FUNCTIONAL AND METABLIC IMAGING FOR THE CHARACTERIZATION OF MALIGNANT TUMORS IN PATIENTS WITH NEUROFIBROMATOSIS TYPE 1**
Shivani Ahlawat, MD; Laura Fayad, MD
Johns Hopkins University, Baltimore, MD, USA
(Presented by: Shivani Ahlawat, MD, Johns Hopkins University)

8:15 a.m. #43 **BROWN ADIPOSE TISSUE AND CANCER ACTIVITY**
Miriam Bredella, MD; Stijn Bos, MS; Corey Gill, MS; Martin Torriani, MD
Mass General Hospital, Boston, MA, USA
(Presented by: Miriam Bredella, MD, Mass General Hospital)

8:30 a.m. #44 **MSK RADIOLOGY-PATHOLOGY CORRELATION: DOES WEEKLY REVIEW IMPROVE CARE?**
James Banks, MD; Hillary Garner, MD; Daniel Wessell, MD, PhD; Joseph Bestic, MD; Jeffrey Peterson, MD
Mayo Clinic Florida, Jacksonville, FL, USA
(Presented by: James Banks, MD, Mayo Clinic Florida)

8:45 a.m. #45 **ADVANCED IMAGING OF SPINDLE CELL LIPOMA**
James Jelinek, MD[1]; Alex Wu, MD[2]; Albert Aboulafia, MD[2]; Matthew Wallace, MD[2]; Mark Murphey, MD[3]; Dhruv Kumar, MD[1]; Robert Henshaw, MD[1]
[1]MedStar Washington Hospital Center, Washington D.C., DC, USA; [2]MedStar Franklin Square Hospital, Baltimore, MD, USA; [3]American Institute for Radiologic Pathology, Silver Spring, MD, USA
(Presented by: James Jelinek, MD, MedStar Washington Hospital Center)

9:00 a.m. #46 **ASSOCIATION OF PSOAS MUSCLE UPTAKE ON FDG PET/CT WITH PROGRESSION FROM SMOLDERING TO SYMPTOMATIC MULTIPLE MYELOMA**
Behrang Amini, MD, PhD[1]; Yves-Paul Nakache, BS[2]; Lorenzo Nardo, MD[2]; Elisabet Manasanch, MD[1]; Leon Lenchik, MD[3]; Robert Boutin, MD[2]
[1]The University of Texas M.D. Anderson Cancer Center, Houston, TX, USA; [2]University of California, Davis, Sacramento, CA, USA; [3]Wake Forest University School of Medicine, Lexington, NC, USA
(Presented by: Behrang Amini, MD, PhD, The University of Texas M.D. Anderson Cancer Center)

9:15 a.m. #47 **IMAGING FEATURES OF MUSCULOSKELETAL PLEOMORPHIC LIPOSARCOMA WITH PATHOLOGIC CORRELATION**
Michael Shvarts, MD[1]; James Jelinek, MD[2]; Mark Murphey, MD[1]; Mark Kransdorf, MD[3]
[1]American Institute for Radiologic Pathology, Silver Spring, MD, USA; [2]Medstar Washington Hospital Center, Washington, DC, USA; [3]Mayo Clinic, Phoenix, AZ, USA
(Presented by: Michael Shvarts, MD, American Institute for Radiologic Pathology)

9:30 a.m. #48 **CAN PRE-TREATMENT FDG-18 PET/CT PREDICT LOCAL CONTROL FOLLOWING SPINE STEREOTACTIC RADIOSURGERY**
Behrang Amini, MD, PhD[1]; Ethan Wang, HS[2]; Andrew Bishop, MD[1]; Jing Li, MD[1]; Laurence Rhines, MD[1]; Claudio Tatsui, MD[1]; Yeboa Debra, MD[1]; Amol Ghia, MD[1]
[1]The University of Texas M.D. Anderson Cancer Center, Houston, TX, USA; [2]The University of Texas at Austin, Austin, TX, USA
(Presented by: Behrang Amini, MD, PhD, The University of Texas M.D. Anderson Cancer Center)

9:45 a.m. #49 **UTILITY OF INTRAVENOUS CONTRAST FOR DETECTION OF RECURRENT SOFT TISSUE SARCOMAS ON MRI**
Behrang Amini, MD, PhD; Tamara Haygood, MD, PhD; Rajendra Kumar, MD; John Madewell, MD; Kevin McEnery, MD; Bilal Mujtaba, MD; William Murphy, II, MD; Wei Wei, MS; Colleen Costelloe, MD
The University of Texas M.D. Anderson Cancer Center, Houston, TX, USA
(Presented by: Behrang Amini, MD, PhD, The University of Texas M.D. Anderson Cancer Center)

10:00 a.m.–10:05 a.m. **CASE OF THE DAY**
Presenting Author: Nathaniel Meyer, MD

10:05 a.m.–10:30 a.m. **Break** - Visit the Exhibit Hall

10:30 a.m.–12:30 p.m. **LOWER EXTREMITY**
Moderators: Bethany Casagranda, DO, Peter Evangelista, MD

10:30 a.m. #50 **ULTRASOUND SHEAR WAVE ELASTOGRAPHY OF THE LATERAL ANKLE LIGAMENTS IN HEALTHY SUBJECTS AT REST AND STRESS**
Lana Gimber, MD, MPH[1]; L Latt, MD, PhD[1]; Chelsea Caruso, DO[1]; Andres Nuncio Zuniga[1]; Elizabeth Krupinski, PhD[2]; Tyson Chadaz, MD[1]; Mihra Taljanovic, MD, PhD[1]
[1]University of Arizona HCS - Tucson, Tucson, AZ, USA; [2]Emory University, Atlanta, GA, USA
(Presented by: Lana Gimber, MD, MPH, University of Arizona HCS - Tucson)

10:45 a.m. #51 **MUCOID DEGENERATION OF THE ACL: THE LIGAMENTOUS STRAIN HYPOTHESIS**
Andrew Wilmot, MD; Jeffrey Towers, MD
University of Pittsburgh Medical Center, Pittsburgh, PA, USA
(Presented by: Andrew Wilmot, MD, University of Pittsburgh Medical Center)

11:00 a.m. #52 **FULLY-AUTOMATED 10-MIN 3D TSE MRI OF THE PEDIATRIC KNEE**
Shivani Ahlawat, MD; Rushyuan Lee, MD; Jan Fritz, MD
Johns Hopkins University, Baltimore, MD, USA
(Presented by: Shivani Ahlawat, MD, Johns Hopkins University)

11:15 a.m. #53 **"SOCCER TOE": CHRONIC PHYSEAL INJURY OF THE FIRST METATARSAL**
Tal Laor, MD[1]; Andrew Schapiro, MD[2]
[1]Children's Hospital, Harvard University, Boston, MA, USA; [2]Cincinnati Children's Hospital, University of Cincinnati, Cincinnati, OH, USA
(Presented by: Tal Laor, MD, Children's Hospital, Harvard University)

11:30 a.m. #54 **T2 MAPPING OF ARTICULAR CARTILAGE OF THE NORMAL PEDIATRIC KNEE AT 3.0 T**
Hailey Allen, MD[1]; Fang Liu, PhD[2]; Richard Kijowski, MD[2]; Jie Nguyen, MD, MS[3]
[1]University of Utah Medical Center / SOM, Salt Lake City, UT, USA; [2]University of Wisconsin Hospital & Clinics, Madison, WI, USA; [3]Hospital for Special Surgery, New York, NY, USA
(Presented by: Hailey Allen, MD, University of Utah Medical Center / SOM)

11:45 a.m. #55 **CARVED IN BONE: "CALCANEAL CRESCENT" IN PATIENTS WITH AND WITHOUT PLANTAR FASCIITIS**

Palanan Siriwanarangsun, MD; Tim Finkenstaedt, MD; Sheronda Statum, MS; Won Bae, PhD; Christine Chung, MD
University of California, San Diego & Veterans Affairs Med Center, SD, San Diego, CA, USA
(Presented by: Palanan Siriwanarangsun, MD, University of California, San Diego & Veterans Affairs Med Center, SD)

12:00 p.m. #56 **3T MRI BASED BI-EXPONENTIAL T2 RELAXATION MEASUREMENT IN KNEE MENISCI**

Hamza Alizai, MD; Rahman Baboli, MS; Azadeh Sharafi, PhD; Gregory Chang, MD; Ravinder Regatte, PhD
NYU Medical Center/ Hospital for Joint Diseases Langone Medical Center, New York, NY, USA
(Presented by: Hamza Alizai, MD, NYU Medical Center/ Hospital for Joint Diseases Langone Medical Center)

12:15 p.m. #57 **EFFECT OF PERIMENISCAL SCARRING ON PREVENTION OF KNEE OSTEOARTHRITIS**

William Morrison, MD[1]; Vishal Desai, MD[2]; Adam Zoga, MD[1]; Johannes Roedl, MD[1]; Suzanne Long, MD[1]; Jeffrey Belair, MD[1]
[1]Thomas Jefferson University Hospital, Philadelphia, PA, USA; [2]Jefferson Radiology Musculoskeletal Radiology Fellowship, Philadelphia, PA, USA
(Presented by: William Morrison, MD, Thomas Jefferson University Hospital)

Related ePosters

TUMOR

Poster #38 **EARLY DETECTION OF METASTASES USING WHOLE-BODY MRI FOR INITIAL STAGING AND ROUTINE FOLLOW-UP OF MYXOID LIPOSARCOMA**
Thomas Powell, MB,BCh., BAO, FFR(RSCI); Natalia Gorelik, MD; Santhosh Reddy, MBBS, MRCP, FRCR; Robert Turcotte, MD, FCRSC; Krista Goulding, MD, MPH, FRCSC; Sungmi Jung, MD, FRCPC; Thierry Alcindor, MD, MSc
McGill University, Montreal, QC, Canada

Poster #39 **Round Cell Component of Myxoid Liposarcoma: Can We Identify these Concerning Areas on Imaging?**
Lien Senchak, MD[1]; Mark Murphey, MD[2]; Michael Shvarts, MD[2]; James Jelinek, MD[3]; Mark Kransdorf, MD[4]
[1]Walter Reed National Military Medical Center, Bethesda, MD, USA; [2]American Institute for Radiologic Pathology, Silver Spring, MD, USA; [3]Medstar Washington Hospital Center, Washington, DC, USA; [4]Mayo Clinic, Phoenix, AZ, USA

Poster #40 **IMAGING APPEARANCE OF WELL DIFFERENTIATED LIPOSARCOMAS WITH MYXOID STROMA**
Yoav Morag, MD; Corrie Yablon, MD; Jon Jacobson, MD; Monica Brigido, MD; David Lucas, MD
University of Michigan Medical Center, Ann Arbor, MI, USA

Poster #41 **TUMOR INDUCED OSTEOMALACIA, A REVIEW OF 5 CASES**
LEE KATZ, MD; Kirsten Cooper, MD
Yale University School of Medicine, New Haven, CT, USA

Poster #42 **DISTRIBUTION OF FEMORAL SHAFT METASTATSES; IMPLICATIONS FOR PET/CT SCANNING**
Michael Mulligan, MD
University of Maryland School of Medicine, Baltimore, MD, USA

Poster #51 **OPTIMIZING BONE MARROW LESION DETECTION USING DUAL ENERGY CT: A PHANTOM STUDY**
Ramya Srinivasan[1], Hsu-Cheng Huang[2], Yuxin Sun[1], Stefanie Weinstein[1], Lynne Steinbach[1], Benjamin Yeh[1]
[1]University of California San Francisco; [2]Taipei City Hospital, Taipei, Taiwan

LOWER EXTREMITY

Poster #43 **COMPARISON OF DIAGNOSTIC ULTRASOUND AND MRI IN THE EVALUATION OF THE PERONEAL TENDON INJURIES IN CORRELATION WITH OPERATIVE FINDINGS**
Mihra Taljanovic, MD, PhD; Lana Gimber, MD, MPH; Aamir Ahmad, MS; Tyson Chadaz, MD; L Latt, MD, PhD
University of Arizona HCS - Tucson, Tucson, AZ, USA

Poster #44 **Assessing Obesity by Correlating BMI to Subcutaneous Fat Measurement on Axial Knee MRIs**
Felix Gonzalez, MD[1]; Ricardo Hernandez, BS[2]; Yara Younan, MD[1]; Adam Singer, MD[1]; Gulshan Sharma, PhD, MPH[3]; Michael Mulligan, MD[4]; Monica Umpierrez, MD[1]
[1]Emory University Dept. of Radiology, MSK Division, Atlanta, GA, USA; [2]Philadelphia College of Osteopathic Medicine, Suwanee, GA, USA; [3]Cumming School of Medicine, Calgary, AB, Canada; [4]University of Maryland School of Medicine, baltimore, MD, USA

Poster #45 **IMPROVED QUALITY OF KNEE RADIOGRAPHS IN A MULTI-CENTER PRACTICE AFTER INTRODUCTION OF A STANDARDIZED POSITIONING FRAME**
Faysal Altahawi, MD; Carl Winalski, MD; Erika Schneider, PhD; Morgan Jones, MD; Spindler Kurt, MD; Schils Jean, MD
The Cleveland Clinic Foundation, Cleveland, OH, USA

Related ePosters

Poster #46 **WEIGHT-BEARING DIGITAL TOMOSYNTHESIS OF FOOT/ANKLE ARTHRITIS: COMPARISON TO RADIOGRAPHY AND SIMULATED WEIGHT-BEARING CT**

Xue Cunningham, MD[1]; Alan Leung, MD[2]; Jennifer Favinger, MD[2]; Daniel Hippe, MS[2]; Alice Ha, MD[2]
[1]Wake Forest University School of Medicine, Winston-Salem, NC, USA; [2]University of Washington / Harborview Medical Center, seattle, WA, USA

Poster #47 **LADY OR GENTLEMAN: SEX DIFFERENCES IN BONY AND CARTILAGE STRUCTURES OF THE KNEE**

Laura Fayad, MD, MS; Lauren Pringle, MD
Johns Hopkins University, Baltimore, MD, USA

Poster #48 **IMAGING OF ANKLE IMPINGEMENT SYNDROMES**

Gary LiMarzi, MD; Omar Khan, MD; Yashesh Shah, MD; Corrie Yablon, MD
University of Michigan Medical Center, Ann Arbor, MI, USA

Poster #49 **“CYCLOPS-LIKE" LESION RELATED TO MUCOID DEGENERATION OF THE ACL**

Maria Bedoya, MD[1]; Andrew Chi, MD[1]; Christian Barrera, MD[2]; Yiftah Beer, MD[3]; Nogah Shabshin, MD, MBA, BSC[1]
[1]Hospital of University of Pennsylvania, Philadelphia, PA, USA; [2]Children's Hospital of Philadelphia, Philadelphia, PA, USA; [3]Assaf Harofeh Medical Center, Zeriffin, Israel

Poster #50 **GETTING TO YOUR FEET: MR IMAGING OF FOREFOOT PAIN: WHAT THE PRACTICING RADIOLOGIST NEEDS TO KNOW**

Richard Leake, MD; Sarah Stilwill, MD; Chris Hanrahan, MD, PhD
University of Utah Medical Center / SOM, Salt Lake City, UT, USA

Podium #42

QUANTITATIVE FUNCTIONAL AND METABLIC IMAGING FOR THE CHARACTERIZATION OF MALIGNANT TUMORS IN PATIENTS WITH NEUROFIBROMATOSIS TYPE 1

Shivani Ahlawat, MD; Laura Fayad, MD
Johns Hopkins University, Baltimore, MD, USA
(Presented by: Shivani Ahlawat, MD, Johns Hopkins University)

Purpose: To determine the utility of quantitative metrics obtained from functional (magnetic resonance (MR) imaging using diffusion weighted imaging (DWI) and apparent diffusion coefficient (ADC) mapping) versus metabolic (^{18}F-fluoro-deoxy-glucose positron-emission-tomography/computed tomography (^{18}F-FDG-PET/CT) imaging in patients with Neurofibromatosis type 1(NF1) for the characterization of peripheral nerve sheath tumors (PNSTs) as benign or malignant.

Materials and Methods: This IRB–approved, HIPAA–compliant study retrospectively reviewed imaging of 55 indeterminate PNSTs in 22 patients with NF1. Imaging included anatomic (unenhanced T1, fluid-sensitive, contrast-enhanced T1-weighted) MR sequences, functional (DWI (b-values 50, 400, 800s/mm^2) and ADC mapping) MR sequences and ^{18}F-FDG-PET/CT imaging. Anatomic (size, morphology, signal), functional (minimum ADC values) and metabolic (maximum standard uptake values (SUVmax)) imaging characteristics were recorded. ADC values were correlated with SUVmax. Using histological correlation for all MPNSTs and histology or clinical and/or imaging stability >12 months for benign lesions as reference standards, diagnostic accuracy for each metric was calculated.

Results: Of 55 PNSTs, there were 17(31%) malignant and 38(69%) benign PNSTs (including 3 atypical PNSTs). Benign PNSTS were overall smaller than MPNSTs (largest diameter(cm) 4.5$\pm$1.9 v. 8.2$\pm$3, p=0.014). Benign PNSTS had higher ADCmin ($\times10^{-3}$mm^2/s) than MPNSTs (1.6$\pm$ 0.5 v. 0.6$\pm$0.2, p<0.0001) and lower SUVmax than MPNST (3.2$\pm$1.7 v. 8.3$\pm$4, p<0.0001). ADCmin correlated inversely with SUVmax (correlation coefficient r=-0.62 (p<0.0001, 95%CI:-0.76to-0.43). Two discordant PNSTs (elevated SUVmax and normal ADC) were histopathologically proven to be atypical. For perfect sensitivity of 100% using threshold values of ADCmin$\leq$1 or SUVmax<3.2, DWI yielded specificity of 87% (95%CI 72-96%) while ^{18}F-FDG-PET/CT offered specificity of 74% (95%CI 57-87%).

Conclusion: Although both quantitative metabolic and functional imaging offer high sensitivity for the characterization of PNSTs as malignant, functional MR imaging using DWI/ADC mapping offers increased specificity and maybe a more useful modality in the characterization of atypical PNSTs.

Modality % - Radiography / Fluoroscopy:	0
Modality % - CT:	0
Modality % - MRI:	50
Modality % - US:	0
Modality % - Nuclear Medicine:	50

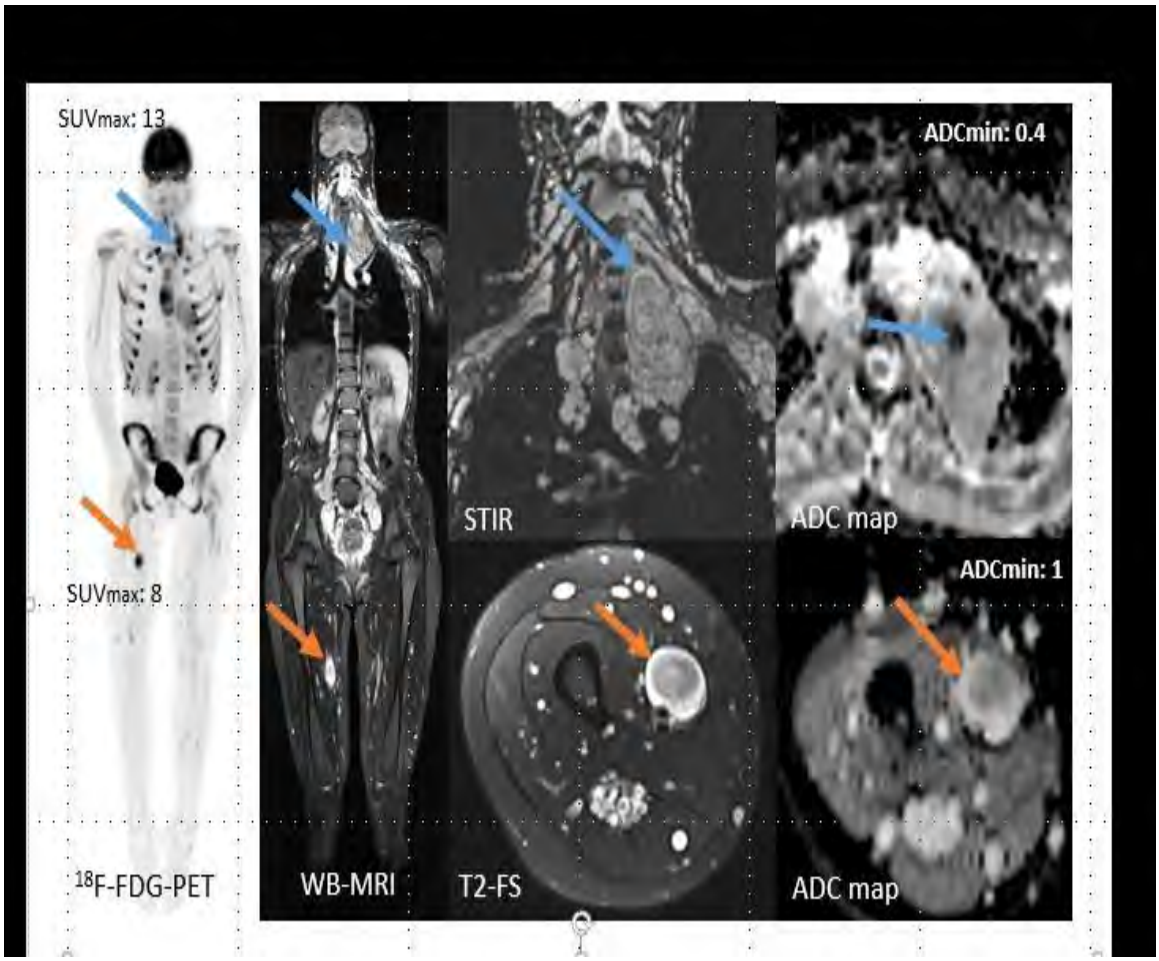

18 year-old with NF1 with mediastinal MPNST (elevated SUVmax and decreased ADCmin) and benign right leg PNST (elevated SUVmax but ADC value>1.0×10−3 mm2/s).

Podium #43

BROWN ADIPOSE TISSUE AND CANCER ACTIVITY

Miriam Bredella, MD; Stijn Bos, MS; Corey Gill, MS; Martin Torriani, MD
Mass General Hospital, Boston, MA, USA
(Presented by: Miriam Bredella, MD, Mass General Hospital)

Purpose: Adipose tissue plays an important role in the development and progression of cancer. White adipose tissue (WAT) stores energy and becomes dysfunctional in obesity, which predetermines to cardiometabolic disease and cancer. Brown adipose tissue (BAT) is metabolically active and is characterized by high mitochondrial content and high vascularity. Recent studies have indicated a potential role of BAT in breast cancer progression. The purpose of our study was to determine the role of BAT in cancer activity.

Materials and Methods: Our study group comprised 142 patients (121 f, 21 m; mean age: 49±16 yrs) who underwent F18-FDG PET/CT for staging or surveillance of malignant neoplasms and who were BAT-positive on PET/CT. BAT volume by PET/CT and abdominal fat and paraspinous muscle cross sectional areas (CSA) by CT were assessed. Groups with and without active malignant disease on PET/CT were compared using a 2-sided paired t-test. Linear correlation analyses between BAT and measures of body composition were performed.

Results: There were 62 patients (54 f, 8 m) who had active malignant disease on PET/CT and 80 patients (67 f, 13 m) without active malignancy (no abnormal FDG activity). Groups were similar in age and BMI ($p>0.4$), abdominal and muscle CSA ($p>0.3$). Patients who had active malignant disease on PET/CT had higher BAT volume compared to patients without active malignancy (24±6 vs 12±2 cm^3, $p=0.009$). In patients without active malignancy, BAT was associated with BMI and abdominal fat ($r= 0.56$ to 0.58, $p<0.0001$) while there were no such associations in patients with active malignancy ($p>0.2$). No associations between BAT and age or muscle CSA were found ($p>0.1$).

Conclusion: BAT activity is greater in patients with active malignancy compared to age and BMI-matched BAT positive patients without active malignancy, suggesting a possible role of BAT in cancer progression.

Modality % - Radiography / Fluoroscopy:	0
Modality % - CT:	100
Modality % - MRI:	0
Modality % - US:	0
Modality % - Nuclear Medicine:	100

Podium #44

MSK RADIOLOGY-PATHOLOGY CORRELATION: DOES WEEKLY REVIEW IMPROVE CARE?

James Banks, MD; Hillary Garner, MD; Daniel Wessell, MD, PhD; Joseph Bestic, MD; Jeffrey Peterson, MD
Mayo Clinic Florida, Jacksonville, FL, USA
(Presented by: James Banks, MD, Mayo Clinic Florida)

Purpose: To determine the frequency of musculoskeletal (MSK) biopsy patients with pathology results that were discordant with the imaging findings and to reduce the number of undetected discordant results to zero by December 2017.

Materials and Methods: A retrospective review was performed of all MSK biopsies from 7/1/2016 to 6/30/2017 to determine the frequency of discordant and non-diagnostic results. Beginning August 1, 2017, MSK radiologists reviewed in consensus the imaging and pathology results of patients who had undergone a MSK biopsy the prior week. Following review, an addendum with the pathology results, the radiology-pathology concordance or discordance and a follow-up recommendation were added to each patient's biopsy report. In cases of discordance, ordering physicians were also notified directly. The time to acknowledgement of biopsy results and time to order entry of the next followup step were compared between patients before and after August 2017.

Results: Of 212 cases evaluated, 24% were non-neoplastic, 16% were benign, 31% were primary malignancies, and 28% were metastases. 3/212 (1%) of the biopsy samples were non-diagnostic, of which all were followed appropriately. There were clinical notes specifically acknowledging biopsy results with assessment and plans in all 125 patients with biopsy-proven malignancies compared to 84/87 patients with benign/non-neoplastic results. There was a mean duration of 4.26 days between the pathology report and a clinical note describing the plan. 6/212 (3%) of diagnostic quality specimens were determined to be discordant, 3 of which were followed appropriately. After the initiation of weekly reviews, all discordant cases were acted upon appropriately.

Conclusion: Radiology-pathology correlation for biopsy results is essential. Despite being a National Cancer Institute designated cancer center, suboptimal follow-up was arranged for 3/6 discordant biopsy results in the past year. Following the establishment of a weekly review, all discordant and non-diagnostic cases had timely appropriate follow-up.

Modality % - Radiography / Fluoroscopy:	3
Modality % - CT:	19
Modality % - MRI:	52
Modality % - US:	6
Modality % - Nuclear Medicine:	31

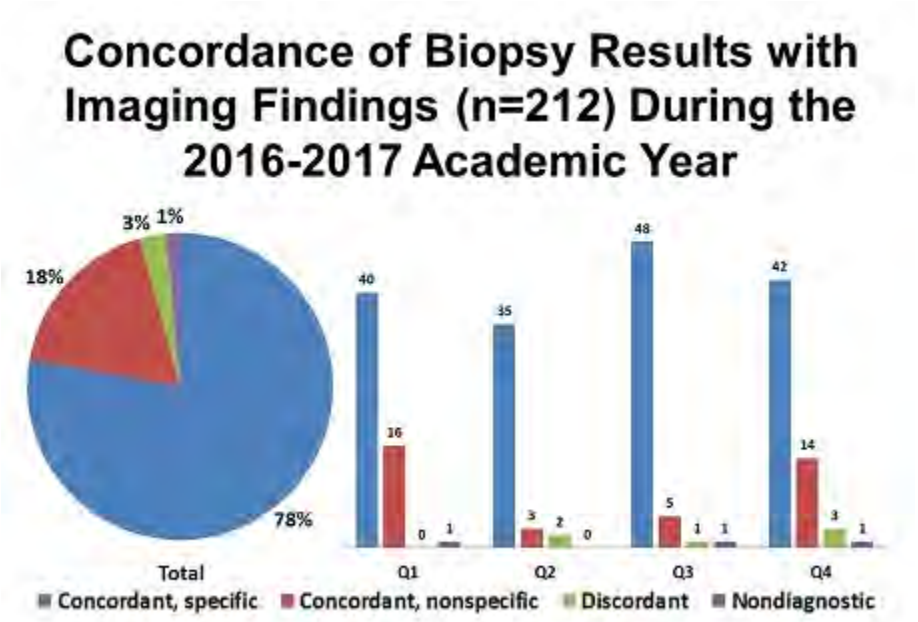

Figure 2: Pie graph results of radiology-pathology correlation and bar graph results of radiology-pathology correlation for each quarter of the academic year 2016-2017.

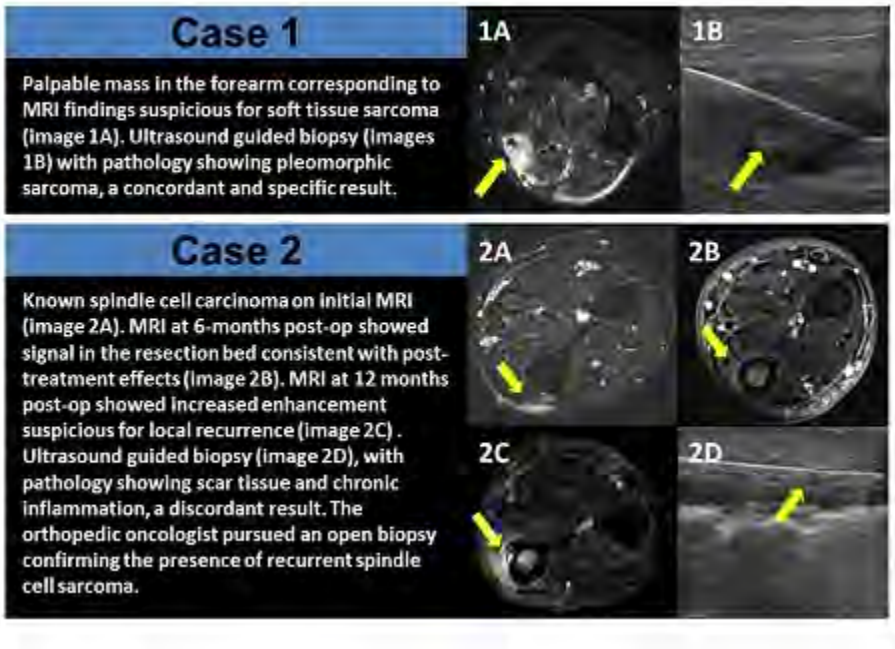

Figure 1: Example cases of radiology-pathology concordance (case 1) and discordance (case 2).

Podium #45

Advanced Imaging of Spindle Cell Lipoma

James Jelinek, MD[1]; Alex Wu, MD[2]; Albert Aboulafia, MD[2]; Matthew Wallace, MD[2]; Mark Murphey, MD[3]; Dhruv Kumar, MD[1]; Robert Henshaw, MD[1]
[1]MedStar Washington Hospital Center, Washington D.C., DC, USA; [2]MedStar Franklin Square Hospital, Baltimore, MD, USA; [3]American Institute for Radiologic Pathology, Silver Spring, MD, USA
(Presented by: James Jelinek, MD, MedStar Washington Hospital Center)

Purpose: To evaluate the varied imaging appearance of spindle cell lipoma and correlate with pathologic findings.

Materials and Methods: We retrospectively evaluated the MR and CT imaging findings of 25 pathologically proven spindle cell lipoma (SCL) from two orthopedic oncology practices. Evaluation included patient demographics, size, anatomic location, compartment location, and imaging features on MR (N=23) and CT (N=7). Imaging features evaluated included margins, percentage visible fat, MR signal characteristics and enhancement (N=14).

Results: Patient ages ranged from 18 to 80 years with an average age of 58. Males were affected more than twice as frequently as females (M=17, F=8). The most common locations included flank/paraspinal (24%), neck (20%), shoulder (16%), and foot/ankle (12%). SCL were most common in the subcutaneous fat (52%) as compared to an intermuscular (32%) or intramuscular (16%) location. SCL ranged in size from 2cm up to a maximal dimension of 10 cm with an average greatest dimension of 5.2 cm. Five lesions (20%) contained no visible fat on CT or MR and the diagnosis was strongly questioned by referring surgeons. Four (16%) had 50% or less fat content. The remainder of lesions (64%) had 75-100% fat by MR or CT. Only 5 of 25 (20%) had an appearance of a typical lipoma. On MRI 80% demonstrated varying degrees of hyperintensity on T2-weighted sequences. Peritumoral edema was noted in 8 of 23 (35%) cases. All SCL which had contrast MRI studies (N=14) demonstrated some degree of enhancement with 4 (28%) showing marked enhancement, 5 (36%) showing minimal and 5 (36%) moderate enhancement.

Conclusion: Conclusion:Spindle cell lipomas have a considerably variable imaging appearance and may have minimal or no visible fat on MR or CT. Furthermore enhancement is seen in all cases. The imaging appearance may mimic an atypical lipomatous tumor / liposarcoma.

Modality % - Radiography / Fluoroscopy:	0
Modality % - CT:	20
Modality % - MRI:	80
Modality % - US:	0
Modality % - Nuclear Medicine:	0

Podium #46

ASSOCIATION OF PSOAS MUSCLE UPTAKE ON FDG PET/CT WITH PROGRESSION FROM SMOLDERING TO SYMPTOMATIC MULTIPLE MYELOMA

Behrang Amini, MD, PhD[1]; Yves-Paul Nakache, BS[2]; Lorenzo Nardo, MD[2]; Elisabet Manasanch, MD[1]; Leon Lenchik, MD[3]; Robert Boutin, MD[2]
[1]The University of Texas M.D. Anderson Cancer Center, Houston, TX, USA; [2]University of California, Davis, Sacramento, CA, USA; [3]Wake Forest University School of Medicine, Lexington, NC, USA
(Presented by: Behrang Amini, MD, PhD, The University of Texas M.D. Anderson Cancer Center)

Purpose: Sarcopenia, as assessed on CT, has been associated with poor prognosis in patients with symptomatic multiple myeloma. Functional imaging with 18F-FDG PET/CT of muscle has not been used in the assessment of myeloma patients. We sought to determine association of body composition with prognosis in patients with smoldering myeloma.

Materials and Methods: Consecutive patients with smoldering myeloma and FDG PET/CT at asymptomatic phase made up the study population. Mean CT attenuation and area were manually measured on PACS by a single investigator blinded to outcomes data. Muscle and adipose measures were made at T12, L4, femoral neck, and mid thigh. Secondary indices included: Thoracic and lumbar muscle index and density, and skeletal muscle gauge and radiographic density ratio at T12, L4, femoral neck, and mid thigh. SUVmean of muscle, retroperitoneal fat, and bone was measured at the L4 level (Fig 1) on a PET/CT viewer. Progression-free survival (PFS) by patient group (based on quartiles) was estimated using Kaplan-Meier method. Cox proportional hazard model was used to associate risk factors with PFS.

Results: 73 patients were included in the study. On PET, Lowest quartile of psoas uptake was associated with worse PFS. None of the CT indices was associated with PFS. On PET, uni- and multi-variate analysis found an association between worse PFS and low mean psoas uptake as well as high M-protein and female sex. The lowest quartile of muscle SUVmean compared to the 2nd, 3rd, and 4th quartiles had hazard ratios for earlier PFS of 0.055 (95% CI: 0.013-0.241), 0.1 (95% CI: 0.031-0.319), and 0.09 (95%CI: 0.024-0.333), respectively (Fig.2).

Conclusion: SUV measurements can be easily obtained during routine interpretation of FDG PET/CTs and may provide added value to imaging performed as standard of care.

Modality % - Radiography / Fluoroscopy:	0
Modality % - CT:	50
Modality % - MRI:	0
Modality % - US:	0
Modality % - Nuclear Medicine:	50

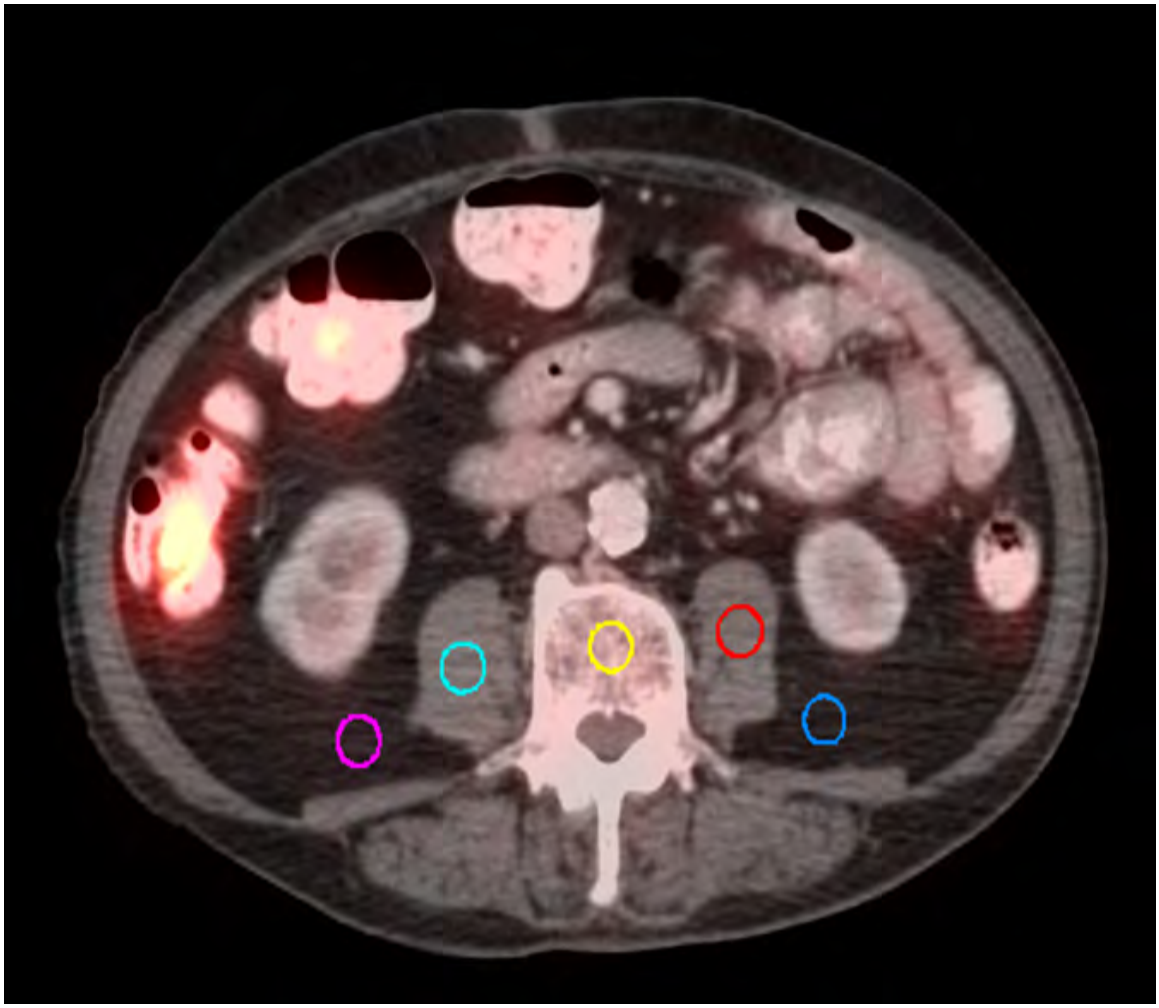

Muscle, fat, and bone SUV regions of interest at L4.

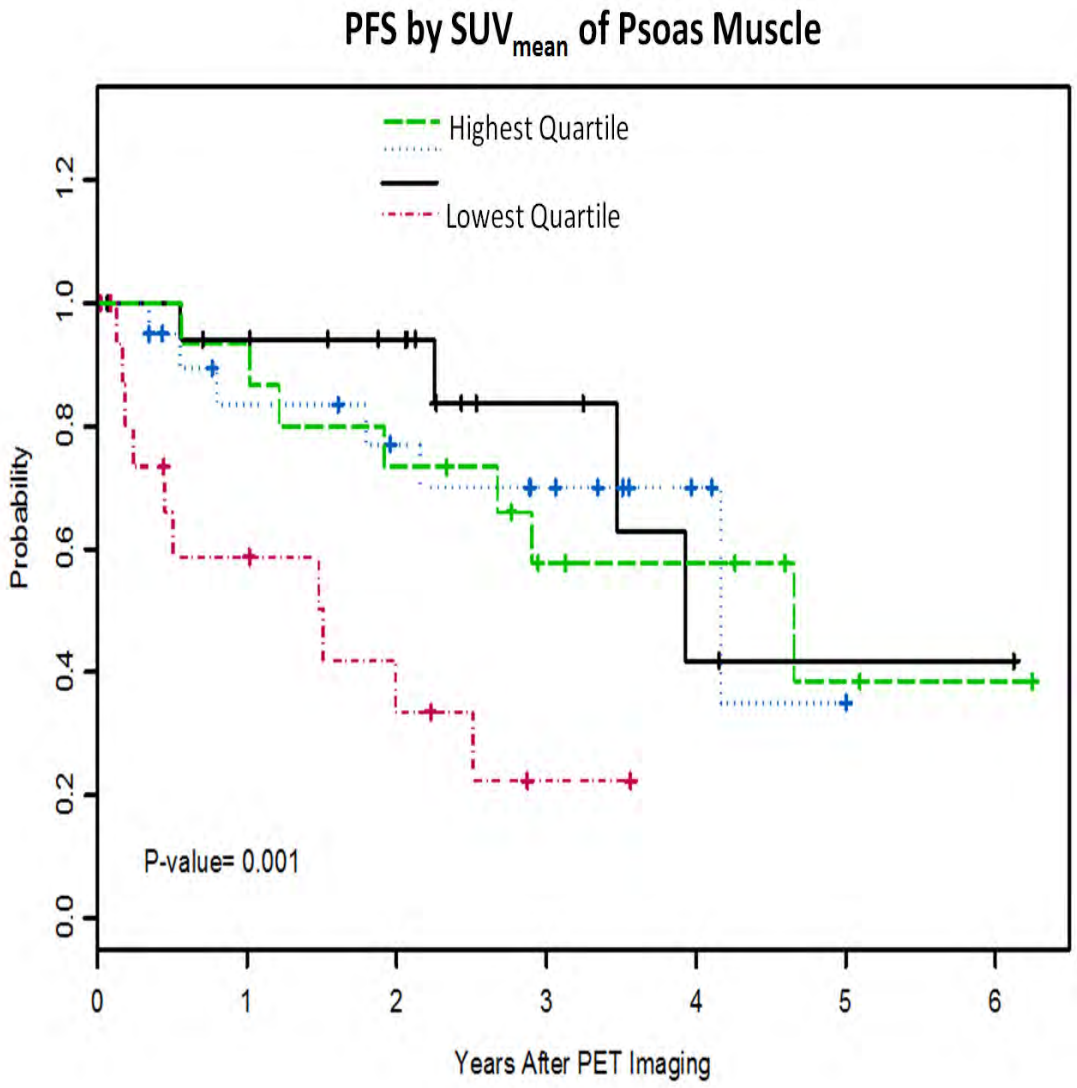

Lowest quartile of muscle SUVmean had improved PFS compared to the other quartiles.

Podium #47

Imaging Features of Musculoskeletal Pleomorphic Liposarcoma with Pathologic Correlation

Michael Shvarts, MD[1]; James Jelinek, MD[2]; Mark Murphey, MD[1]; Mark Kransdorf, MD[3]
[1]American Institute for Radiologic Pathology, Silver Spring, MD, USA; [2]Medstar Washington Hospital Center, Washington, DC, USA; [3]Mayo Clinic, Phoenix, AZ, USA
(Presented by: Michael Shvarts, MD, American Institute for Radiologic Pathology)

Purpose: To describe the radiologic appearance of musculoskeletal pleomorphic liposarcoma with pathologic correlation.

Materials and Methods: We retrospectively reviewed 17 pathologically confirmed cases of pleomorphic liposarcoma. Radiologic studies were reviewed by three musculoskeletal radiologists with agreement by consensus and included radiographs(n=8), CT(n=9), and MRI(n=10). Evaluation included patient demographics, lesion location/size, presence and character of intralesional fat and intrinsic characteristics on CT and MRI.

Results: Patient ages ranged from 40-83 years with an average age of 58. There was a female predominance(58%) in our series. Presenting symptoms included pain(58%) and an enlarging mass(71%). Lesions were most frequent in an intramuscular muscular location(65%), and the thigh(58%) and lower leg(18%). Tumors had an average lesion size of 9 x 9 x 15 cm.

Radiographs demonstrated a nonspecific soft tissue mass(100%). On CT, 67% of lesions contained fat, which was less 25% of the volume of the lesion in 75% of these cases. Following contrast administration, tumors demonstrated mild(33%) to marked(67%) enhancement with peripheral nodular pattern in all cases (100%).

On MRI, all tumors were well defined. On T1, the majority of lesions were low-to-intermediate signal intensity(90%). On T2, lesions were low to intermediate signal in 80% of cases. Heterogeneity was seen in all cases on both T1 and T2 weighed imaging. Hemorrhage was apparent in 60% of tumors. Fat was identified in 80% of lesions, most commonly subtle and less than 25% of tumor volume in 80%.

Conclusion: Pleomorphic liposarcomas demonstrated certain characteristics which help distinguish these tumors from other soft tissue sarcomas, specifically the presence of intralesional fat by CT or MR(76%) which was usually subtle, in an otherwise nonspecific intramuscular mass.

Modality % - Radiography / Fluoroscopy:	15
Modality % - CT:	30
Modality % - MRI:	55
Modality % - US:	0

Modality % - Nuclear Medicine:

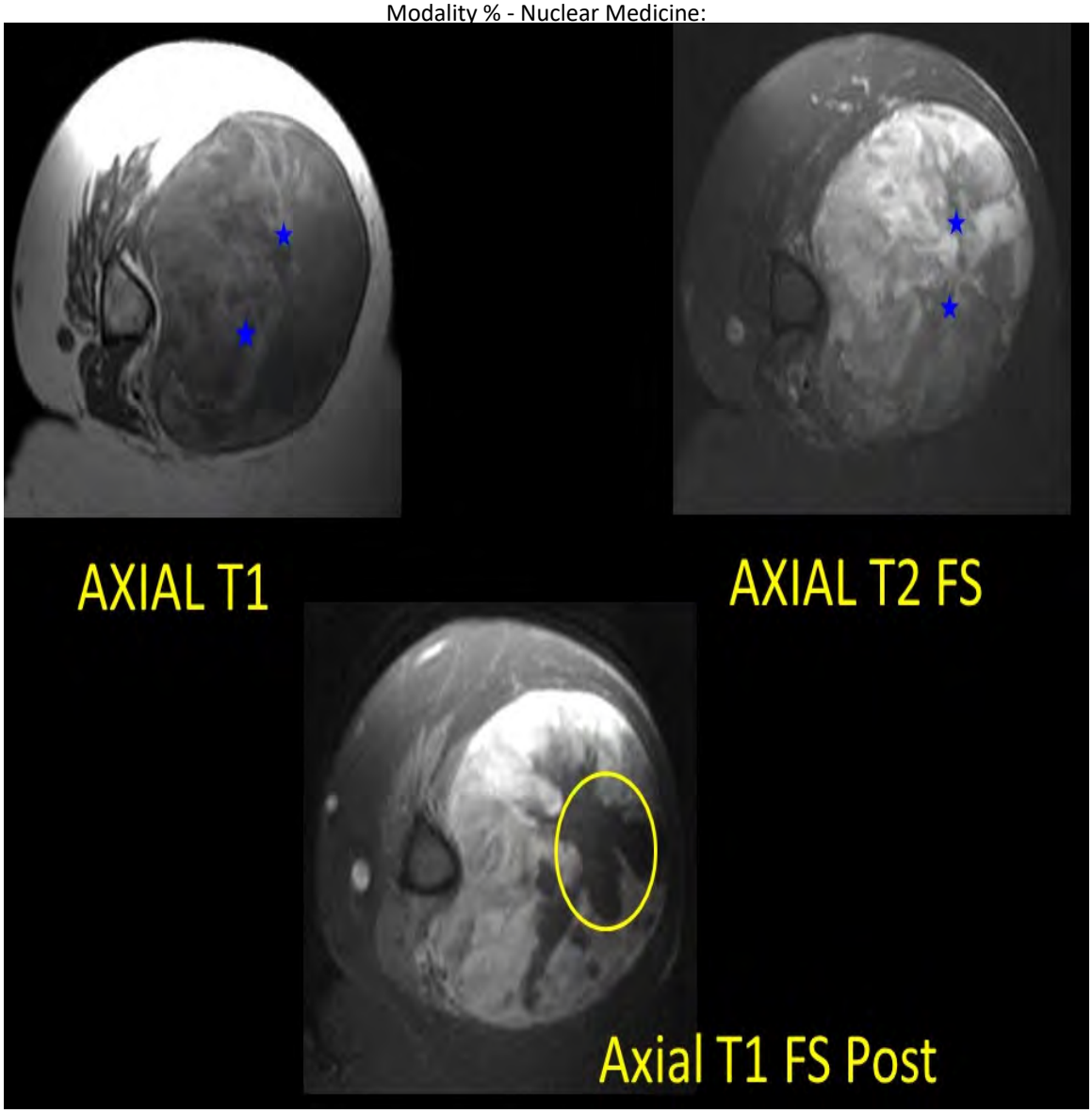

Selected images of an upper extremity pleomorphic liposarcoma.
Blue stars: Areas of subtle fat
Yellow Circle: area of necrosis

Podium #48

CAN PRE-TREATMENT FDG-18 PET/CT PREDICT LOCAL CONTROL FOLLOWING SPINE STEREOTACTIC RADIOSURGERY

Behrang Amini, MD, PhD[1]; Ethan Wang, HS[2]; Andrew Bishop, MD[1]; Jing Li, MD[1]; Laurence Rhines, MD[1]; Claudio Tatsui, MD[1]; Yeboa Debra, MD[1]; Amol Ghia, MD[1]

[1]The University of Texas M.D. Anderson Cancer Center, Houston, TX, USA; [2]The University of Texas at Austin, Austin, TX, USA

(Presented by: Behrang Amini, MD, PhD, The University of Texas M.D. Anderson Cancer Center)

Purpose: To determine whether pre-treatment Standardized Uptake Value (SUV) of spine lesions on 18-F FDG PET/CT scans can be used to predict local recurrence of spinal metastases following spine stereotactic radiosurgery (SSRS).

Materials and Methods: 446 patients treated with SSRS from 1/6/2014 to 6/30/2017 at a tertiary cancer center were reviewed. The study population consisted of 41 patients who had received a PET/CT within 30 days prior to SSRS and had more than six months of follow-up post-SSRS. SUVmax of the lesions was measured. Local control was determined through MRI and/or PET/CT follow-up. Kaplan-Meier curves were constructed for survival analysis.

Results: There was no statistically significant difference in the SUVmax of lesions that exhibited local failure versus those that did not ($p>0.05$). Lesions with SUVmax between the 33rd and 66th percentile had significantly improved local control compared to those with lower ($p=0.0002$) and higher ($p=0.009$) SUVs. Using this middle range of SUVs to detect local failure yielded sensitivity of 57%, specificity of 81% and positive and negative likelihood ratios of 3.1 and .53, respectively

Conclusion: Lesions with intermediate SUVmax (5.6-8.6) in our population had significantly worse local control rates compared to those with lower and higher SUVmax. SUVmax can be moderately specific for detecting lesions that will exhibit local failure following SSRS, but is not sensitive for detecting local failure.

Modality % - Radiography / Fluoroscopy:	0
Modality % - CT:	0
Modality % - MRI:	20
Modality % - US:	0
Modality % - Nuclear Medicine:	76

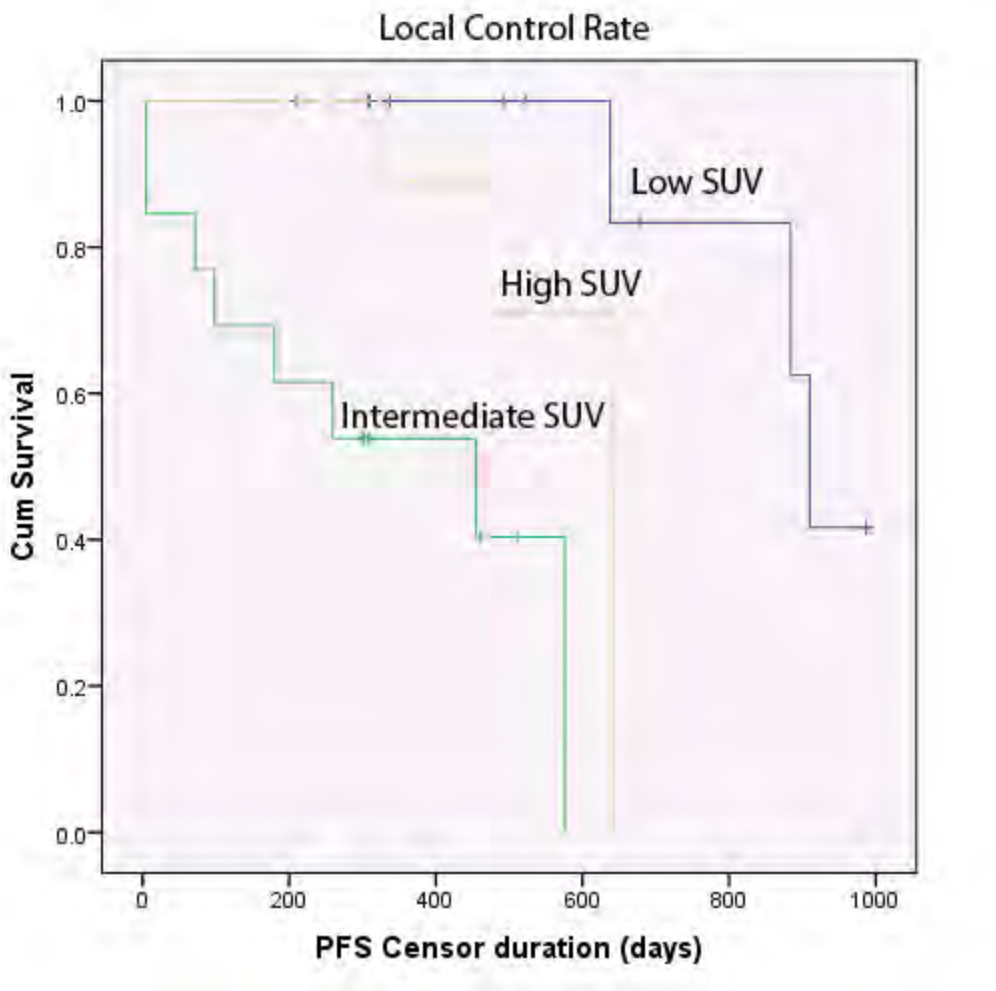

Intermediate SUVmax (green) had worse local control compared lower (blue) and higher (yellow) SUVmax

Podium #49

UTILITY OF INTRAVENOUS CONTRAST FOR DETECTION OF RECURRENT SOFT TISSUE SARCOMAS ON MRI

Behrang Amini, MD, PhD; Tamara Haygood, MD, PhD; Rajendra Kumar, MD; John Madewell, MD; Kevin McEnery, MD; Bilal Mujtaba, MD; William Murphy, II, MD; Wei Wei, MS; Colleen Costelloe, MD
The University of Texas M.D. Anderson Cancer Center, Houston, TX, USA
(Presented by: Behrang Amini, MD, PhD, The University of Texas M.D. Anderson Cancer Center)

Purpose: To determine the utility of gadolinium-based contrast administration in detection of recurrent soft tissue sarcomas.

Materials and Methods: Retrospective database search in patients with soft tissue sarcomas of the extremity and body wall yielded 69 patients with locally recurrent disease confirmed by pathology. The control group consisted of cases in the same patients at a different time point without recurrent disease, but with postoperative findings (e.g., seroma, hematoma, and granulation tissue), resulting in 63 age- and gender-matched controls. Six musculoskeletal radiologists at a tertiary cancer center with a mean of 30 years of experience were blinded to the pathology results and asked to review the 132 randomized MRI studies and determine if recurrence was present on a 5-point scale. Images in the axial plane were presented to each reader in 3 different groups with a minimum of 2 weeks between each set: 1) T1 pre-contrast + T2 (T1T2), 2) T1 pre-contrast + T1-post-contrast (T1T1-Post), and 3) T1 pre-contrast + T2 + T1-post contrast (T1T2T1-Post). No consensus readings occurred. Sensitivity and specificity were calculated using McNemar's test.

Results: Mean sensitivity was 54%, 70%, and 71% for the T1T2, T1T1-Post, and T1T2T1-Post groups, respectively. Mean specificity was 92%, 94%, and 97% for the same groups, respectively. Readers interpreting the image sets with contrast (T1T1-Post and T1T2T1-Post) had significantly higher sensitivity for detection of recurrence than when interpreting the non-contrast (T1T2) images ($p = 0.001$ and 0.008, respectively). There was no significant difference in sensitivity between the T1T2T1-Post and T1T1-Post ($p = 0.65$). There was no significant difference in specificity between the 3 groups ($p > 0.05$).

Conclusion: Gadolinium based intravenous contrast administration results in improved sensitivity for detection of locally recurrent soft tissue sarcomas.

Modality % - Radiography / Fluoroscopy:	0
Modality % - CT:	0
Modality % - MRI:	100
Modality % - US:	0
Modality % - Nuclear Medicine:	0

Podium #50

ULTRASOUND SHEAR WAVE ELASTOGRAPHY OF THE LATERAL ANKLE LIGAMENTS IN HEALTHY SUBJECTS AT REST AND STRESS

Lana Gimber, MD, MPH[1]; L Latt, MD, PhD[1]; Chelsea Caruso, DO[1]; Andres Nuncio Zuniga[1]; Elizabeth Krupinski, PhD[2]; Tyson Chadaz, MD[1]; Mihra Taljanovic, MD, PhD[1]
[1]University of Arizona HCS - Tucson, Tucson, AZ, USA; [2]Emory University, Atlanta, GA, USA
(Presented by: Lana Gimber, MD, MPH, University of Arizona HCS - Tucson)

1. **Purpose:** Define ultrasound (US) shear wave elastography (SWE) velocity values of the anterior talofibular (ATFL) and calcaneofibular ligaments (CFL) in young healthy males at rest and stress.
2. Evaluate for inter-observer variability in SWE velocities of the ATFL and CFL in the same subjects.

Materials and Methods: Twenty three healthy male subjects with no history of prior ankle injury were included in the study. After the grey-scale US examination, the bilateral ankles including 46 ATFL and 46 CFL during rest were evaluated using US SWE independently by two musculoskeletal radiologists. SWE for each of the ligaments was repeated three times by both radiologists. SWE was then performed during manually applied stress by an orthopaedic surgeon. SWE of each of the ligaments was performed by a single radiologist three times during stress. Three ROIs in each of the ligaments were placed in similar locations and the mean velocity value was calculated. The results were then compared.

Results: Subject mean age was 29.8 years (sd=5.2; range 20-40) and all were right foot dominant. There was no significant correlation between SWE measurements and age, with no difference based on laterality. A significant difference in mean velocities between ATFL at rest versus stress was seen (2.09 m/s vs 3.21 m/s; $p<0.001$), in addition to mean velocities in CFL at rest versus stress (1.99 m/s vs 3.42 m/s; $p<0.0001$). Bland-Altman plot demonstrated good inter-observer agreement between the two radiologists.

Conclusion: We defined normal US SWE velocity values for the ATFL and CFL with significantly increased velocities for both ligaments with applied stress. In this study, US SWE showed promising results as a reproducible method to reflect changes in ankle ligament stiffness.

Modality % - Radiography / Fluoroscopy:	8
Modality % - CT:	0
Modality % - MRI:	0
Modality % - US:	100
Modality % - Nuclear Medicine:	0

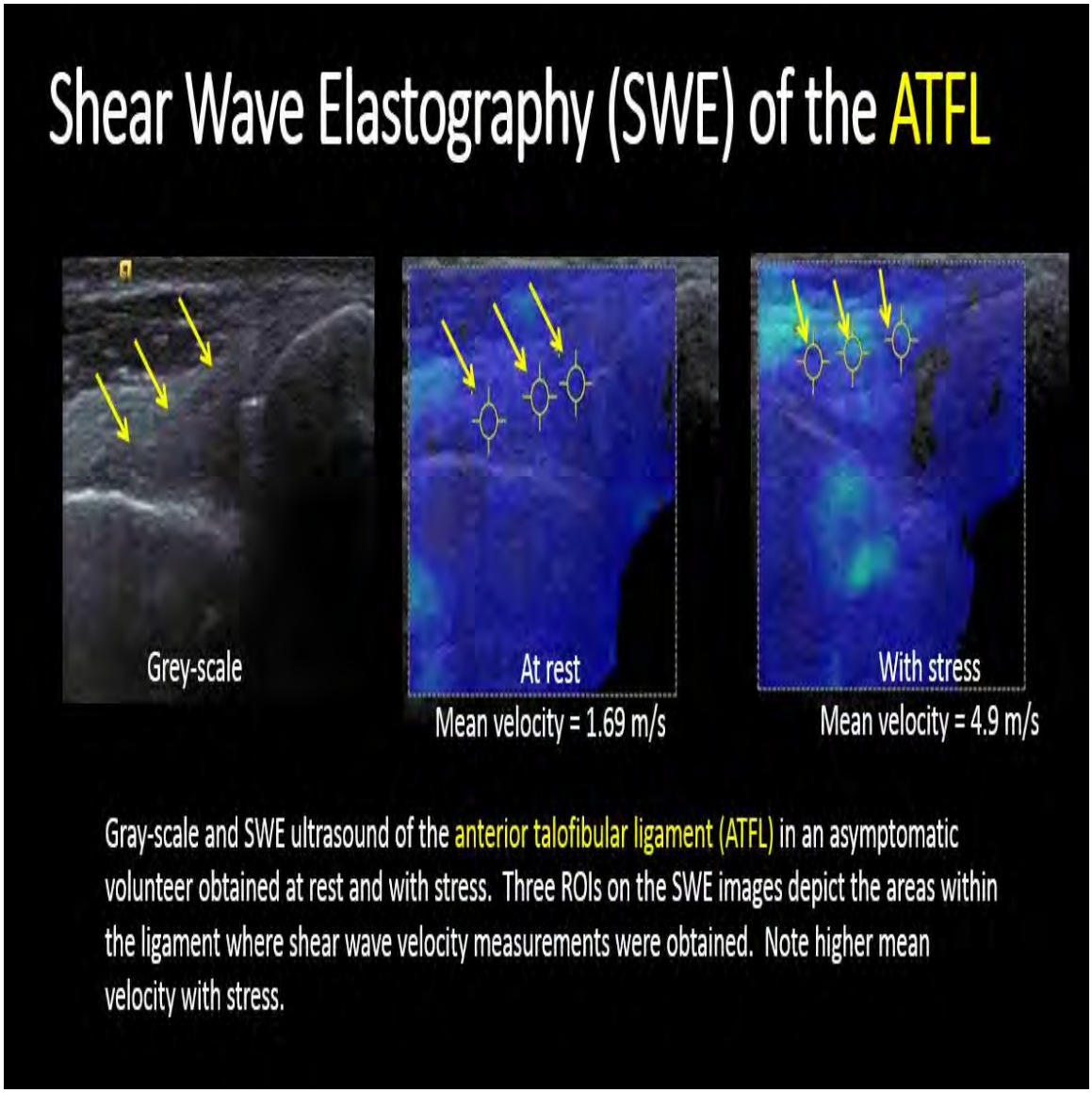

Gray-scale and shear wave ultrasound of the anterior talofibular ligament in an asymptomatic volunteer obtained at rest and with stress.

Podium #51

MUCOID DEGENERATION OF THE ACL: THE LIGAMENTOUS STRAIN HYPOTHESIS

Andrew Wilmot, MD; Jeffrey Towers, MD
University of Pittsburgh Medical Center, Pittsburgh, PA, USA
(Presented by: Andrew Wilmot, MD, University of Pittsburgh Medical Center)

Purpose: Mucoid degeneration of the ACL is commonly encountered on knee MRI. We present a novel theory on its etiology, based upon retrospective review of knee MRIs obtained in patients before and after its development.

Materials and Methods: Radiologic reports for MRI of the knee from 2013 through 2017 were searched for the term "mucoid degeneration." Reports and images from 758 MRIs of the knee were reviewed. Cases of mucoid degeneration in which an earlier MRI of the ipsilateral knee was available formed our patient population. Exclusion criteria included previous surgery to the ACL and inflammatory arthritis. The earliest and the latest MRI in each patient were reviewed in consensus, with grading of the ACL, PCL, MCL, menisci, posterior medial corner (PMC), cartilage, and bursae.

Results: The final population consisted of 38 patients, 13 females and 25 males, with average age of 59 (range: 37-76). The average length between earliest and latest MRI was 68 months (range 1-173). In 4 patients the ACL was normal on initial MRI, 22 showed mild strain, and 12 showed moderate to advanced strain. On the latest MRI all demonstrated moderate to advanced ACL strain. Medial meniscal tears were present on initial MRI in 32 patients, including all 4 with normal ACL and 21 of 22 with mild strain. Chondrosis averaged 1.9 and 2.8 on earliest and latest MRI, graded on a scale of 1 to 4. 29 patients had SMTCL bursitis on earliest MRI. The PMC demonstrated varying degrees of abnormality in all cases.

Conclusion: Medial meniscal tears, PMC pathology and SMTCL bursitis commonly precede mucoid degeneration of the ACL. The authors hypothesize that muciod degeneration most commonly results from chronic ACL strain related to altered biomechanics secondary to impaired function of the medial meniscus and its static and dynamic stabilizers.

Modality % - Radiography / Fluoroscopy:	0
Modality % - CT:	0
Modality % - MRI:	100
Modality % - US:	0
Modality % - Nuclear Medicine:	0

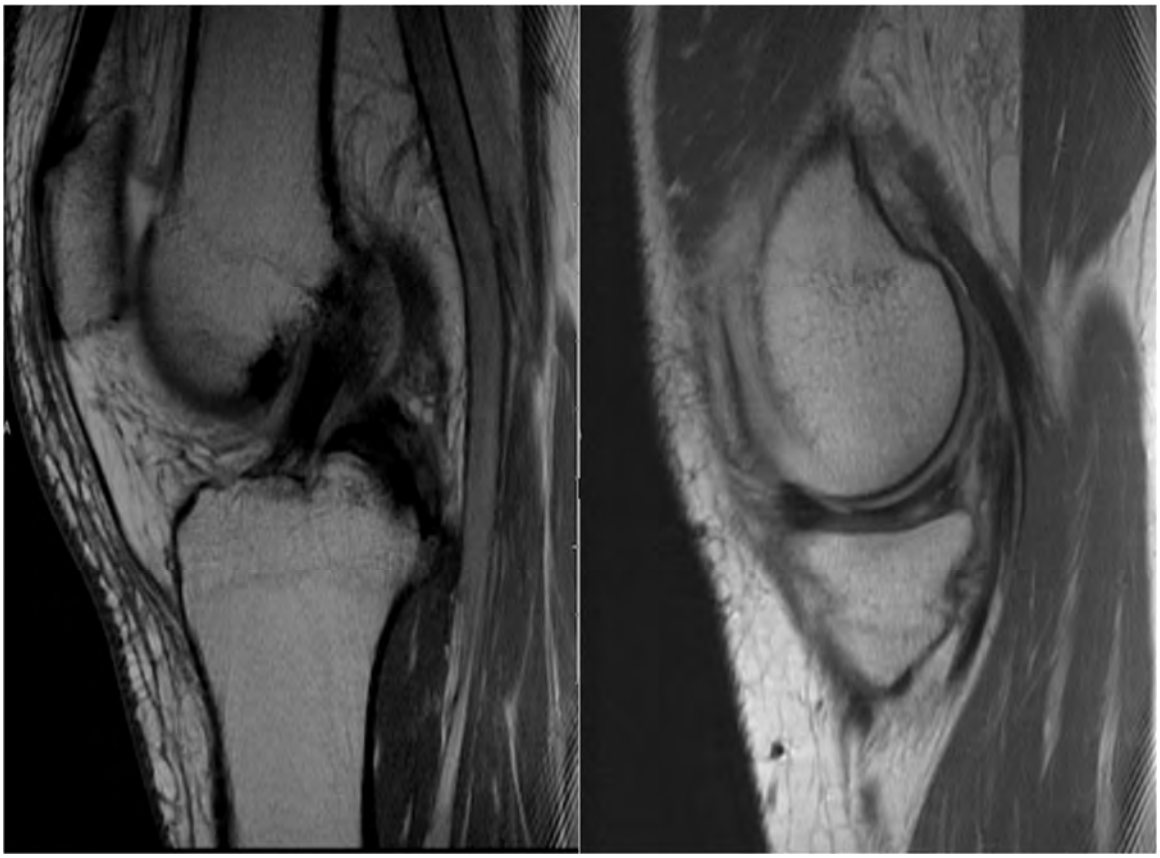

Sagittal PD Images from 2010 demonstrate normal caliber and signal intensity of the ACL and a horizontal tear of the medial meniscus.

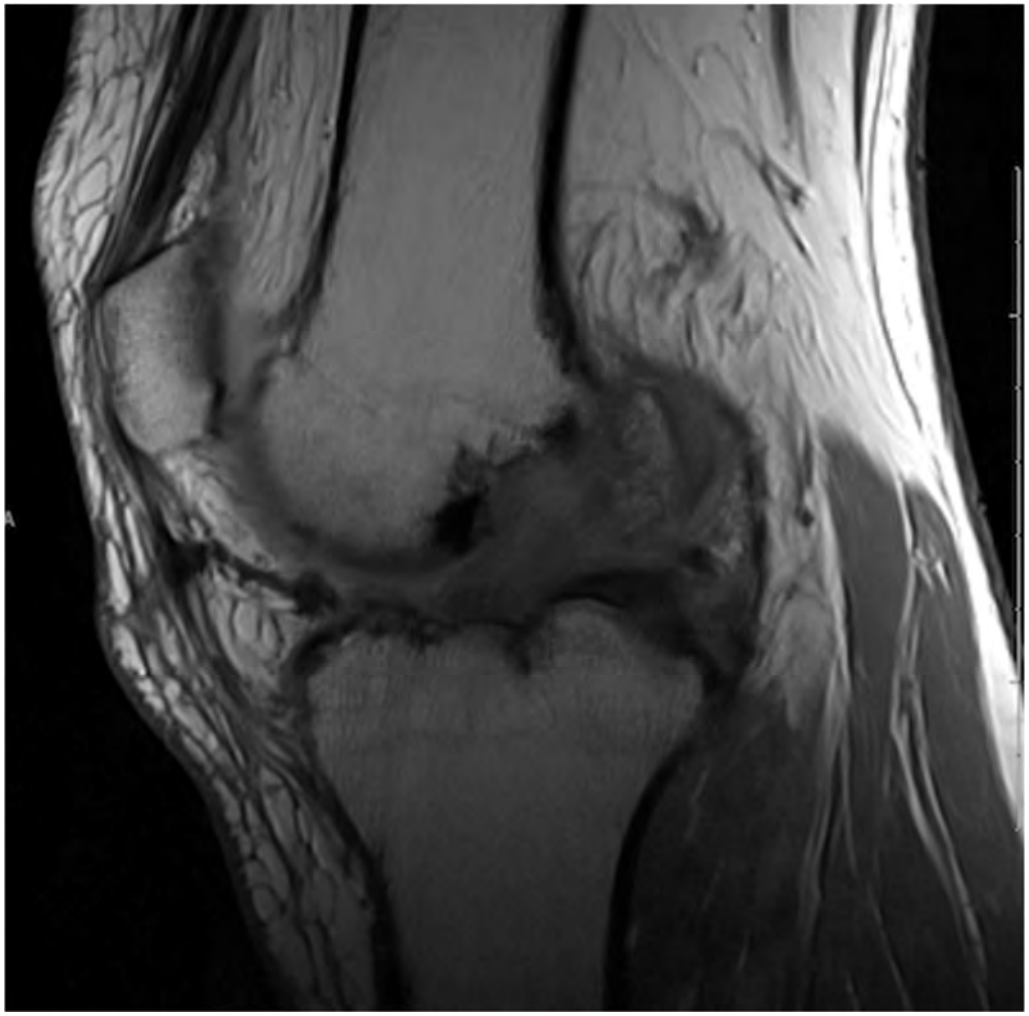

Sagittal PD image from 2016 MRI in the same patient demonstrates advanced mucoid degeneration of the ACL.

Podium #52

FULLY-AUTOMATED 10-MIN 3D TSE MRI OF THE PEDIATRIC KNEE

Shivani Ahlawat, MD; Rushyuan Lee, MD; Jan Fritz, MD
Johns Hopkins University, Baltimore, MD, USA
(Presented by: Shivani Ahlawat, MD, Johns Hopkins University)

Purpose: To prospectively assess the arthroscopy-based diagnostic performance of fully-automated, high-resolution 3D TSE MRI of the knee for the diagnosis of internal derangement in children and adolescents.

Materials and Methods: Following IRB approval and informed consent, 60 symptomatic subjects (38 boys, 22 girls; mean age=11years; age range, 2–16years) underwent 3T MRI of the knee using one-button-push protocol comprised of gradient echo-based scout algorithm, which automatically aligned and executed 0.5mm isotropic intermediate-weighted and 0.6mm isotropic fat-suppressed T2SPAIR 3D CAIPIRINHA SPACE sequence prototypes (Acquisition time=9:39 min). Two musculoskeletal radiologists independently evaluated the imaging including image quality using 5-point Likert scales, the presence or absence of discoid menisci and osteochondral dissecans lesions, meniscal tears and anterior/posterior cruciate ligament tears and cartilage defects (intact vs. partial-thickness v. full-thickness). Arthroscopic assessment, performed within 37(1-143) days of MRI, used the same criteria. Interreader agreements and diagnostic performance (sensitivity/specificity/positive predictive value/negative predictive value(PPV)/area under the Receiver Operating Characteristic curve) was calculated with arthroscopy as reference standard.

Results: The fully-automated, 10-min 3D TSE MRI protocol was completed in all 60 subjects. The image quality was rated good or very good in 53/60(88%) and adequate in 7/60(12%) cases (kappa=0.728). There were 10 (prevalence=10%) discoid lateral menisci (83%/100%/100%/98%/0.92) (kappa=1.0). There were 15(25%) medial meniscal tears (93%/93%/82%/98%/0.93) (kappa=0.882) and 21(35%) lateral meniscal tears (95%/90%/83%/97%/0.92) (kappa=0.861). There were 16 (27%) anterior cruciate ligament tears (100%/95%/89%/100%/0.98) (kappa=0.960). There were 2(3%) posterior cruciate ligament tears and 5(8%) medial femur osteochondritis dissecans lesions (100%/100%/100%/100%/1.0, respectively) (kappa=1.0, respectively). There were a total of 48(13%) cartilage defects (60%/97%/74%/94%/0.79) (kappa=0.730), of which 41 were partial-thickness (sensitivity=54%; PPV=100%) and 7 were full-thickness (sensitivity=100%; PPV=100%) defects.

Conclusion: A fully-automated 3D TSE MRI protocol using CAIPIRINHA SPACE enables high-resolution MRI of the pediatric knee in under 10 minutes with high diagnostic accuracy for meniscal, ligamentous and cartilage abnormalities.

Modality % - Radiography / Fluoroscopy:	0
Modality % - CT:	3
Modality % - MRI:	100
Modality % - US:	0
Modality % - Nuclear Medicine:	0

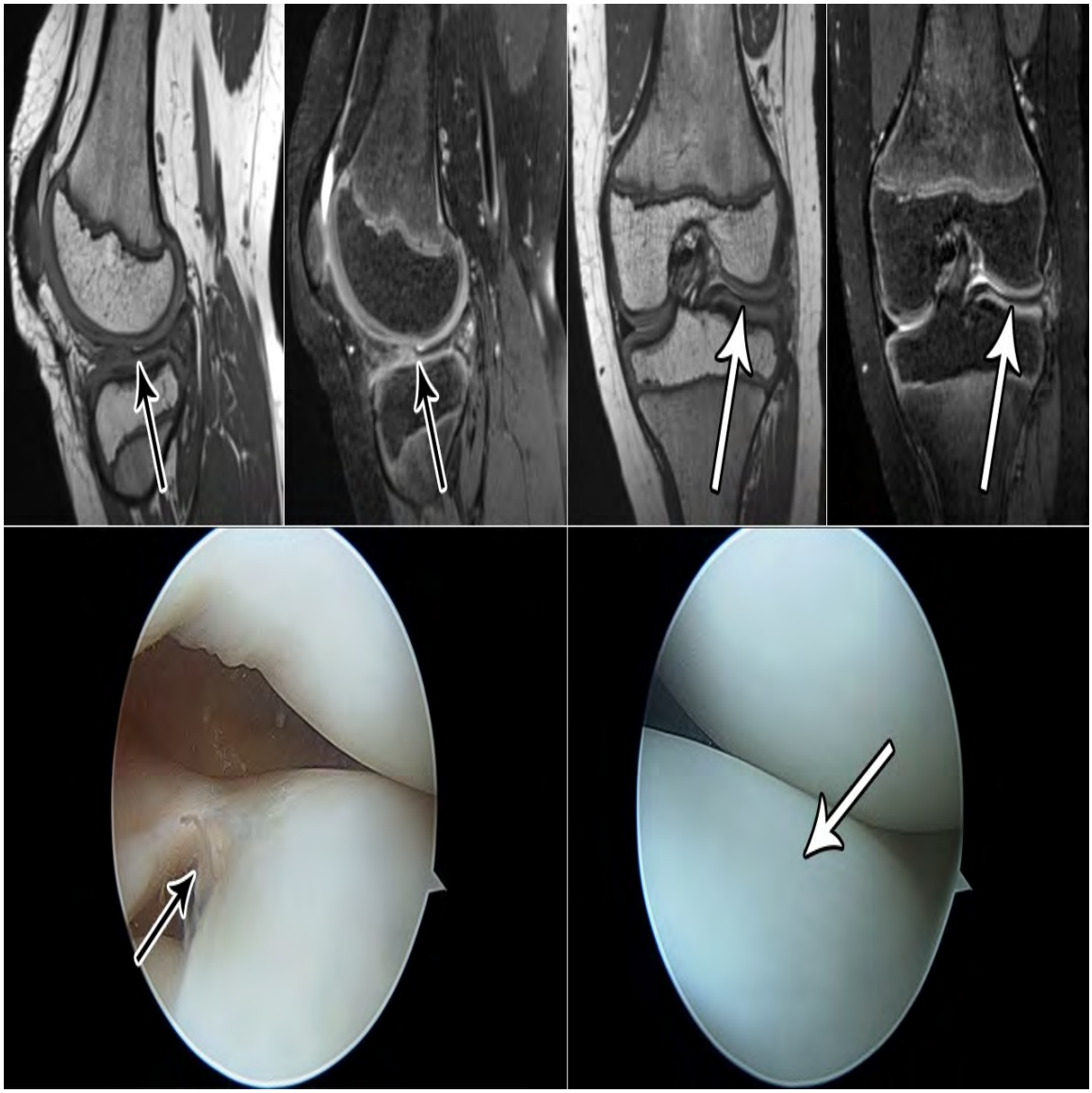

Figure 1.3D CAIPIRINHA SPACE MR images and arthroscopy demonstrate a discoid lateral meniscus (arrows, right images) with tear near the intercondylar notch (arrows, right images).

Podium #53

"SOCCER TOE": CHRONIC PHYSEAL INJURY OF THE FIRST METATARSAL

Tal Laor, MD[1]; Andrew Schapiro, MD[2]
[1]Children's Hospital, Harvard University, Boston, MA, USA; [2]Cincinnati Children's Hospital, University of Cincinnati, Cincinnati, OH, USA
(Presented by: Tal Laor, MD, Children's Hospital, Harvard University)

Purpose: Although considered a relatively safe sport for children, there is a substantial rate of soccer-related injuries. Most injuries are acute, but chronic overuse-type stress is increasingly identified. Therefore, our purpose is to describe the postulated mechanism and imaging appearance of chronic stress injury of the first metatarsal physis in skeletally immature soccer players.

Materials and Methods: Using a database search engine, children imaged for foot pain with the term “soccer” in the clinical history were evaluated initially, excluding those with a discrete traumatic episode or a fracture described on imaging. For the remaining patients, any available imaging was reviewed for physeal patency, and if present, for physeal widening of the great toe metatarsal. For those children ultimately included in the study group, demographics and medical records were reviewed. Location of widening within the physis (divided into quadrants), signal characteristics on MR imaging when available, and interval change on follow-up imaging when available, was recorded.

Results: Eight skeletally immature soccer players (5 girls, 3 boys, ages 9-13 years, mean 11 years, 10 months) were included. Six patients had both radiographs and MRI exams; 2 had radiographs only. Four physes were wide across the entire metatarsal, 3 had dorsal widening only, and one had plantar medial physeal sparing. None showed plantar physeal widening only. All widened physes retained physeal signal intensity, and one had a punctate focus of abnormally hyperintense T2-weighted signal. Of 4 children with follow-up imaging, 3 showed persistent radiographic physeal widening 1-8 months after initial presentation. The remaining child showed interval fusion.

Conclusion: Similar to chronic physeal stress changes in other locations, the first metatarsal in soccer players also may be affected. Recognition of this entity in growing children may explain their presenting pain and guide conservative treatment to allow for eventual return to sport.

Modality % - Radiography / Fluoroscopy:	75
Modality % - CT:	0
Modality % - MRI:	25
Modality % - US:	0
Modality % - Nuclear Medicine:	0

Fig 1A. Eleven-year-old soccer player with foot pain and widening of the lateral aspect of the first metatarsal physis (arrow).

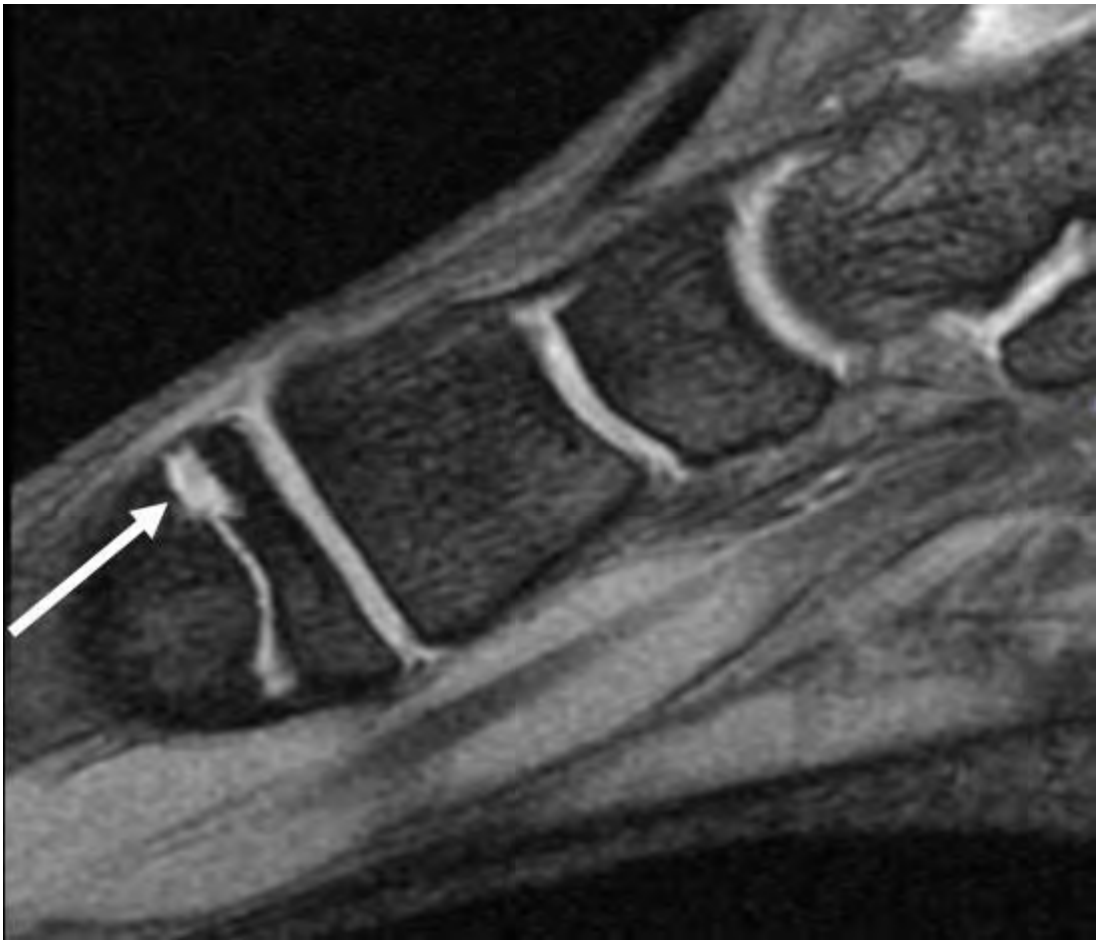

Fig 1B. Sagittal GRE image shows focal physeal widening (arrow) of the dorsal aspect of the first metatarsal with signal intensity similar to unaffected physis.

Podium #54

T2 MAPPING OF ARTICULAR CARTILAGE OF THE NORMAL PEDIATRIC KNEE AT 3.0 T

Hailey Allen, MD[1]; Fang Liu, PhD[2]; Richard Kijowski, MD[2]; Jie Nguyen, MD, MS[3]
[1]University of Utah Medical Center / SOM, Salt Lake City, UT, USA; [2]University of Wisconsin Hospital & Clinics, Madison, WI, USA; [3]Hospital for Special Surgery, New York, NY, USA
(Presented by: Hailey Allen, MD, University of Utah Medical Center / SOM)

Purpose: To use T2 relaxation time mapping to evaluate microstructural differences in cartilage of the normal pediatric knee using a 3.0-T magnetic resonance (MR) system and to establish sex, age/maturation, and weight/body mass index (BMI)-specific references.

Materials and Methods: This IRB-approved, HIPAA-compliant retrospective study was performed on 76 knees without internal derangement from 72 subjects (43 girls, mean age 13.0 years, range 3-18 years; 29 boys, mean age 12.5 years, range 3-18 years). Subjects underwent routine 3.0-T MR knee protocol with T2 mapping sequence. Semi-automated quantitative T2 mapping of epiphyseal cartilage was performed using MatLab. Global and regional T2 values were compared with sex, age, skeletal maturation, weight and BMI. Wilcoxon rank sum and Kruskal-Wallis tests were used to analyze subgroups and Spearman's rank correlation (ρ) for continuous variables. A linear regression model was used to analyze the relationship of T2 with age, weight, and BMI.

Results: Regional differences existed within the tibial plateau, with T2 values measuring lower than its respective femoral condyle ($p<0.001$). Moderate negative correlation existed between T2 values and age (global Spearman's ρ -0.65) with a significant decrease in T2 with progressive skeletal maturation (slope = - 0.86 ms/year, $p< 0.001$). There was no significant difference between males and females ($p=0.53$). Correlation was slightly stronger with weight (global Spearman's ρ -0.67, slope -0.66 ms/10 kilogram) than BMI (global Spearman's ρ -0.53).

Conclusion: Cartilage T2 values decreased with increasing age, progressive maturation, and increasing weight. This likely reflects differences in micro-structural organization in response to physiologic maturation and mechanical stress. This technique offers a reproducible, semi-automated assessment of knee epiphyseal cartilage. Once normal pediatric cartilage parameters are understood, these techniques can be used to assess pathological conditions with the aim of aiding in early diagnosis and monitoring treatment response.

Modality % - Radiography / Fluoroscopy:	0
Modality % - CT:	0
Modality % - MRI:	100
Modality % - US:	0
Modality % - Nuclear Medicine:	0

Sagittal T2 mapping magnetic resonance (MR) image obtained at 3.0-Tesla. A three-point radial line method was used to subdivide the cartilage into 8 anatomic subregions.

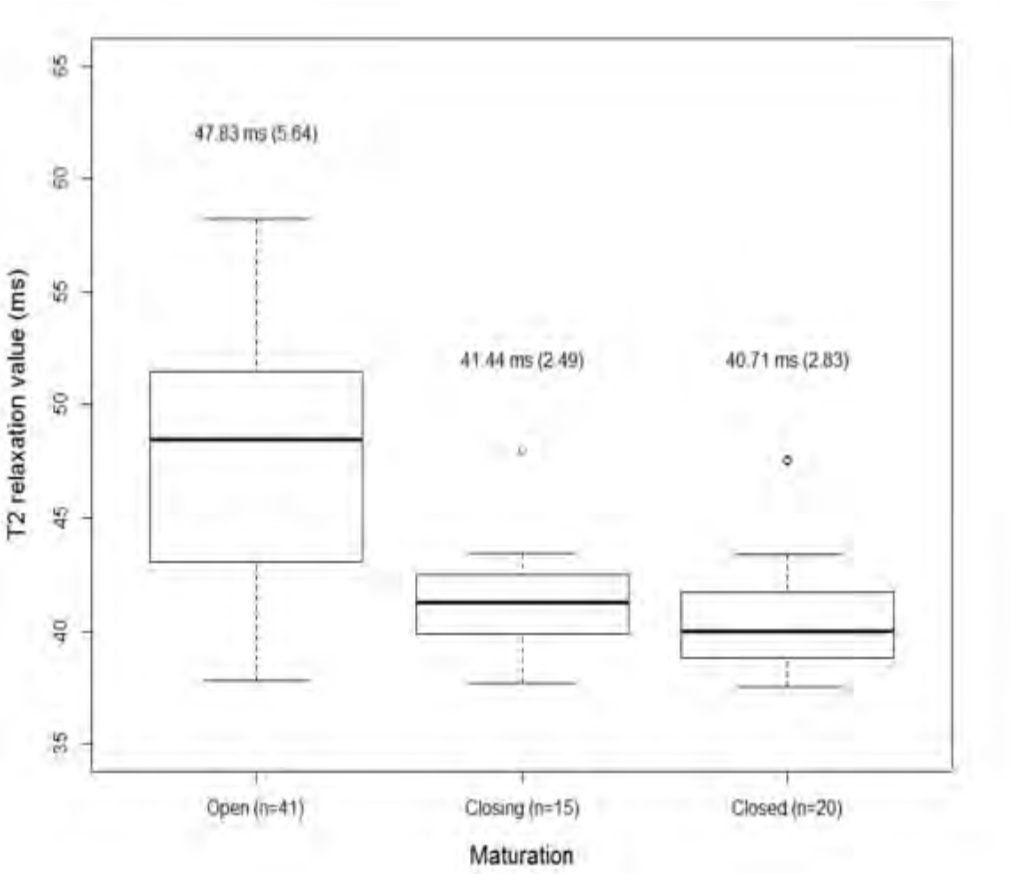

Cartilage T2 values decrease with skeletal maturation (p

Podium #55

Carved in bone: "calcaneal crescent" in patients with and without plantar fasciitis

Palanan Siriwanarangsun, MD; Tim Finkenstaedt, MD; Sheronda Statum, MS; Won Bae, PhD; Christine Chung, MD
University of California, San Diego & Veterans Affairs Med Center, SD, San Diego, CA, USA
(Presented by: Palanan Siriwanarangsun, MD, University of California, San Diego & Veterans Affairs Med Center, SD)

Purpose: The crescent-shaped trabeculae bundle ("calcaneal crescent") within the calcaneal tuberosity may represent a structural adaption to tensile forces between the Achilles tendon and plantar fascia. We investigate the significance difference of the calcaneal crescent in patients with plantar fasciitis, relative to controls.

Materials and Methods: MR images of 37 patients referred for work-up of foot/ankle pain were retrospectively evaluated in this IRB–approved study. Patients were assigned to two groups: (A) patients without pathology of Achilles-calcaneal-plantar (ACP) system (n=15, age 47±15 years, body-mass-index (BMI) 23.7±3.5) and (B) patients with clinical signs and/or MRI findings of plantar fasciitis (n=22, age 54±10 years, BMI 28.8±7.0).

The thickness (mm) and cross-sectional area (CSA, mm^2) of the Achilles tendon, calcaneal crescent and plantar fascia were measured on non-fat saturated PD images. The volume (cm^3) of entire crescent was measured using OsiriX on sagittal PD Cube images. Additionally, mean thickness (mm) and signal-to-noise ratio (SNR) of the calcaneal crescent was calculated using custom MATLAB software. ANOVA was performed to evaluate the difference between the various measurements with BMI as covariate. Partial correlation adjusted for BMI was used to assess relationship between the different measurements.

Results: Patients with plantar fasciitis had a significantly greater CSA and volume of the calcaneal crescent as well as a lower SNR (CSA: 100 mm^2 vs 74 mm^2, p=0.042; volume: 3.1 cm^3 vs. 2.0 cm^3, p=0.016; SNR: 8.9 vs. 10.1, p=0.049). In addition, the CSA of the Achilles tendon was positively correlated with the CSA (r=0.59, p=0.004) and volume (r=0.58, p=0.005) of the calcaneal crescent. Furthermore, the mean thickness of the calcaneal crescent was positively correlated with the maximum thickness (r=0.5, p=0.02) and CSA (r=0.52, p=0.012) of the plantar fascia.

Conclusion: Assessment of calcaneal crescent may provide useful insight about biomechanical etiology of plantar fasciitis.

Modality % - Radiography / Fluoroscopy:	0
Modality % - CT:	0
Modality % - MRI:	100
Modality % - US:	0
Modality % - Nuclear Medicine:	0

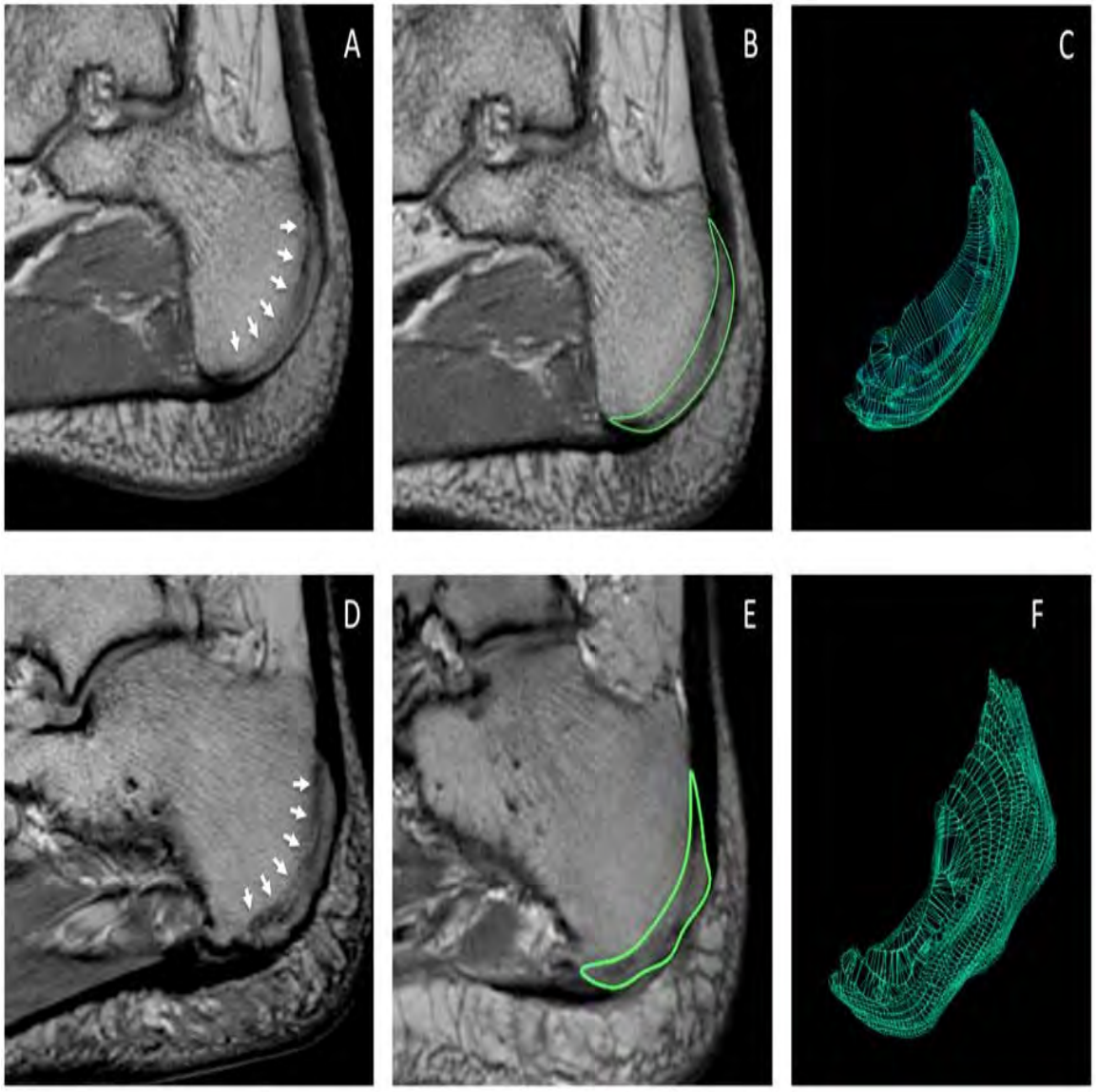

MR of healthy volunteer (A, B and C) and plantar fasciitis pateint (D, E and F). Image A and D (sagittal PD) calcaneal crescent (arrows).

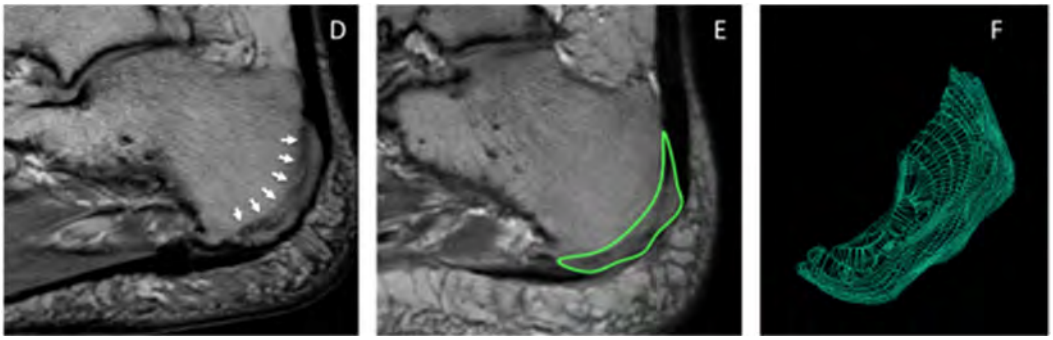

Image B and F show approach for the volumetric measurement (ROI). Image C and F are wireframe 3D volume rendering

Podium #56

3T MRI BASED BI-EXPONENTIAL T2 RELAXATION MEASUREMENT IN KNEE MENISCI

Hamza Alizai, MD; Rahman Baboli, MS; Azadeh Sharafi, PhD; Gregory Chang, MD; Ravinder Regatte, PhD
NYU Medical Center/ Hospital for Joint Diseases Langone Medical Center, New York, NY, USA
(Presented by: Hamza Alizai, MD, NYU Medical Center/ Hospital for Joint Diseases Langone Medical Center)

Purpose: To evaluate biexponential T2 relaxation mapping of human knee menisci in vivo in clinically feasible scan times

Materials and Methods: The study was approved by the Institutional Review Board and informed consent was obtained from eight 8 healthy volunteers (4 male & 4 female, mean age 30±4 years, mean weight 63±15 kg). T2-weighted MRI of the knee was acquired using a Siemens Prisma 3T MRI scanner. A 3D Turbo-Flash sequence was modified to enable T2-weighted imaging at 10 different echo times. Ten meniscal regions of interest were assessed: the red and white zones of the anterior and posterior horns, and the body of both the medial and lateral menisci. Series of T2-weighted images were fitted using mono- and biexponential models with two- and four- parametric nonlinear approaches, respectively.

Results: Biexponential relaxation of T2 was detected in the knee menisci in 10 regions of interest in all eight healthy volunteers. Global short/long relaxation components of T2 were estimated to be 6.1 / 57.2 msec with corresponding fractions of 65.16% / 34.84%, respectively. The global monoexponential relaxation of T2 was measured to be 19.8 msec. Significant differences were observed in T2 relaxation between different regions of interest.

Conclusion: Biexponential relaxation of T2 was observed in the human menisci in vivo. The short and long components are thought to be related to the tightly bound and loosely bound macromolecular water compartments respectively. These preliminary results of biexponential T2 analysis could potentially be used to increase the specificity for detection of early meniscal degeneration by measuring different water compartments and their fractions.

Modality % - Radiography / Fluoroscopy:	0
Modality % - CT:	0
Modality % - MRI:	100
Modality % - US:	0
Modality % - Nuclear Medicine:	0

Podium #57

EFFECT OF PERIMENISCAL SCARRING ON PREVENTION OF KNEE OSTEOARTHRITIS

William Morrison, MD[1]; Vishal Desai, MD[2]; Adam Zoga, MD[1]; Johannes Roedl, MD[1]; Suzanne Long, MD[1]; Jeffrey Belair, MD[1]
[1]Thomas Jefferson University Hospital, Philadelphia, PA, USA; [2]Jefferson Radiology Musculoskeletal Radiology Fellowship, Philadelphia, PA, USA
(Presented by: William Morrison, MD, Thomas Jefferson University Hospital)

Purpose: To investigate the protective effect of perimeniscal scarring on prevention of knee osteoarthritis in patients with meniscal tear.

Materials and Methods: A retrospective review was performed for patients with medial meniscal tear on initial MRI who had a follow-up knee MRI after at least 6 months. Categorization of meniscal tear/extrusion and grading of chondrosis was performed. Analysis was repeated on follow-up MRI, as well as presence of intermediate signal in the perimeniscal recess and surrounding tissues.

Results: 43 patients were included in the study with a median follow-up of 19 months. 20 (53%) had stability of chondrosis, with no significant difference in age, gender, study indication, or tear complexity compared to the group with worsening chondrosis (23 patients, 47%). Perimeniscal intermediate signal was found in 17 patients (85%) without progressive chondrosis, of which only 1 had moderate meniscal extrusion. In comparison, 7 patients (30%) had perimeniscal intermediate signal in the worsening chondrosis group, all of which had moderate to severe meniscal extrusion. Excluding patients with extrusion as an etiology for the signal, 13 out of 14 patients (93%) in the stable chondrosis group developed perimeniscal scarring, compared to 0 out of 6 for the worsening chondrosis group.

Conclusion: Perimeniscal scarring appears to have a chondroprotective effect in patients with meniscal tear.

Modality % - Radiography / Fluoroscopy:	0
Modality % - CT:	0
Modality % - MRI:	100
Modality % - US:	0
Modality % - Nuclear Medicine:	0

Initial MRI with medial meniscal tear
(no abnormal signal in the meniscal recesses)

Follow-up MRI in 20 months:
Development of perimeniscal scarring; stable chondrosis

Example of perimeniscal scarring in subgroup of patients without progression of chondrosis.

ePOSTERS

Society of Skeletal Radiology

41st Annual Meeting

March 25-28, 2018

ePoster* Complete Listing

**As these sessions are not moderated, ePosters are not CME accredited*

Location: Exhibit Hall

Sunday, March 24, 2018 .....7:00 a.m. – 4:30 p.m.

Monday, March 25, 2018.....7:00 a.m. – 12:30 p.m.

Tuesday, March 26, 2018.....7:00 a.m. – 12:30 p.m.

Wednesday, March 27, 2018 .....7:00 a.m. – 10:30 a.m.

ePoster Complete Listing

**As these sessions are not moderated, ePosters are not CME accredited*

EMERGING TECHNOLOGIES

Poster #1

WHOLE BODY (WB)-MRI WITH 3D VOLUMETRIC SEQUENCES AND ISOTROPIC RESOLUTION: A METHOD FOR FAST AND HIGH RESOLUTION WHOLE BODY IMAGING

Shivani Ahlawat, MD; Jaishri Blakeley; Mike Jacobs, PhD; Laura Fayad, MD, MS
Johns Hopkins University, Baltimore, MD, USA

Poster #2

Some New Angles on the Magic Angle: What MSK Radiologists Know and Don't Know

Michael Richardson, MD[1]; Behrang Amini, MD, PhD[2]; Todd Richards, PhD[1]
[1]University of Washington / Harborview Medical Center, Seattle, WA, USA; [2]The University of Texas M.D. Anderson Cancer Center, Houston, TX, USA

Poster #3

QUANTITATIVE ASSESSMENT OF CHANGE IN UPPER EXTREMITY MUSCLE STIFFNESS FOLLOWING FLUID INJECTION USING SHEAR WAVE ELASTOGRAPHY

O. Nwawka, MD; Shivi Duggal, MD; Bin Lin, MS; Nicholas Gutierrez, MD; Theodore Miller, MD
Hospital for Special Surgery, New York, NY, USA

Poster #4

3D PRINTING MAKES AN IMPOSSIBLE CASE POSSIBLE

Carissa White, MD; Marc-Anthony Lecky; David Nelson; Mauricio Silva, MD; Anthony Scaduto, MD
David Geffen School of Medicine at UCLA, Los Angeles, CA, USA

Poster #5

CLINICALLY RELEVANT RADIOLOGICAL INSIGHTS PROVIDED BY EN FACE MICROSCOPIC VISUALIZATION OF EROSIONS COMPLICATING ARTHRITIS, GRANULOMATOUS DISEASE, NEOPLASIA AND VASCULAR DISEASE

Bruce Rothschild, MD
West Virginia University School of Medicine, Morgantown, WV, USA

UPPER EXTREMITY

Poster #7

Superior Capsular Reconstruction for Irreparable Rotator Cuff Tears: Imaging Features and Complications

Pamela Walsh, MD; Mohammad Samim, MD; Luis Beltran, MD
NYU Medical Center/ Hospital for Joint Diseases Langone Medical Center, New York, NY, USA

Poster #8

GENDER DIFFERENCES IN GLENOID REMODELING IN GLENOHUMERAL DEGENERATIVE JOINT DISEASE

Christopher Peters, MD; Anna Zajicek, MD; Christopher Peters, MD; Kent Rinehart, MD; Matthew Teusink, MD
University of Nebraska Medical Center, Omaha, NE, USA

Poster #9

Os Subscapulare: imaging findings and clinical relevance

Alex Bergman, MD[1]; Hilary Umans, MD[2]; Jonathan Ticker, MD[3]
[1]Jacobi Medical Center, Bronx, NY, USA; [2]Lenox Hill Radiology and Imaging Associates, New York, NY, USA; [3]Orlin and Cohen Orthopedic Associates, Merrick, NY, USA

Poster #10

"Reducing" Radiologists' Anxiety about Carpal Instability

Jonelle Petscavage-Thomas, MD, MPH; Eric Walker, MD; Weaver Kesler, MD
Penn State Milton S. Hershey Medical Center, Hershey, PA, USA

Poster #11 **FOOSH Injuries of the Elbow with an Emphasis on Posterolateral Elbow Instability: A Multimodality Pictorial Review.**
Christopher Nall, MD; Robert Colvin, DO; Shashin Doshi, MD
Beaumont Health System, Royal Oak, MI, USA

Poster #12 **RADIOLOGIC EVALUATION OF ABNORMALITIES OF THE STERNUM AND STERNOCLAVICULAR JOINTS**
Sailaja Yadavalli, MD, PhD; Jason Esterle, MD; Christopher Nall, MD
Beaumont Health System, Royal Oak, MI, USA

INTERVENTION/POSTOPERATIVE

Poster #13 **CT GUIDED CORE NEEDLE BONE BIOPSY IN THE WORKUP OF OSTEOMYELITIS: DIAGNOSTIC YIELD AND EFFECT ON PATIENT CARE.**
Donald von Borstel, DO; Cameron Smith, DO; Gregory Bradley, DO; Sindhura Alapati, MD
Oklahoma State University Medical Center, Tulsa, OK, USA

Poster #14 **THE POSTOPERATIVE MRI: IS IT TUMOR RECURRENCE OR NODULAR SCAR?**
Lana Gimber, MD, MPH[1]; Samuel Oats, MD[1]; Lea MacKinnon, MD[1]; Mihra Taljanovic, MD, PhD[1]; James Warneke, MD[1]; Matthew Seidel, MD, MS[1]; Laura Fayad, MD[2]
[1]University of Arizona HCS - Tucson, Tucson, AZ, USA; [2]Johns Hopkins University, Baltimore, MD, USA

Poster #15 **CURRENT TRENDS IN MODALITY SELCETION FOR IMAGE-GUIDED MUSCULOSKELETAL PROCEDURES:FACTORS THAT INFLUENCE ULTRASOUND VERUS NON-ULTRASOUND UTILIZATION**
Judah Goldschmiedt, MD; Danielle Williams, MD; Chaitanya Shilagani, DO
Westchester Medical Center, Valhalla, NY, USA

Poster #16 **UTILITY OF CORE NEEDLE BIOPSY TO DIFFERENTIATE ANEURYSMAL BONE CYST FROM TELANGIECTATIC OSTEOSARCOMA**
Benjamin Levine, MD; Vishal Hedge, MD; Kambiz Motamedi, MD; Leanne Seeger, MD; Scott Nelson, MD; Nicholas Bernthal, MD
University of California, Los Angeles, Los Angeles, CA, USA

Poster #17 **DIAGNOSTIC YIELD OF ULTRASOUND GUIDED AND CT GUIDED SOFT TISSUE LESION BIOPSIES**
Kambiz Motamedi, MD; Kim Lee, MD; Benjamin Levine, MD; Leanne Seeger, MD
David Geffen School of Medicine at UCLA, Los Angeles, CA, USA

Poster #18 **ULTRASOUND-GUIDED ASPIRATION OF INTRAMUSCULAR HEMATOMAS: EFFICACY AND RELATIONSHIP TO SONOGRAPHIC APPEARANCE**
Edward Yoon, MD; Theodore Miller, MD; Susan Lee, MD
Hospital for Special Surgery, New York, NY, USA

Poster #19 **COMPARISON BETWEEN IMAGE-GUIDED AND LANDMARK-BASED GLENOHUMERAL JOINT INJECTIONS FOR THE TREATMENT OF ADHESIVE CAPSULITIS: A COST-EFFECTIVENESS STUDY**
Soterios Gyftopoulos, MD, MS[1]; Valentino Abballe, MD[1]; Mandeep Virk, MD[1]; James Koo, PhD[1]; Heather Gold, PhD[1]; Naveen Subhas, MPH, MD[2]
[1]NYU Medical Center/ Hospital for Joint Diseases Langone Medical Center, New York, NY, USA; [2]Cleveland Clinic, Cleveland, OH, USA

Poster #20 **CLINICAL AND PATIENT-REPORTED OUTCOMES AFTER IMAGE-GUIDED INTRA-ARTICULAR THERAPEUTIC HIP INJECTIONS: A RETROSPECTIVE STUDY**
William Walter, MD[1]; Craig Bearison, BS[2]; James Slover, MD, MS[1]; Heather Gold, PhD[1]; Soterios Gyftopoulos, MD, MSc[1]
[1]NYU Medical Center/ Hospital for Joint Diseases Langone Medical Center, New York, NY, USA; [2]New York University School of Medicine, New York, NY, USA

Poster #21 **EFFICACY OF INTRA-ARTICULAR HIP STEROID INJECTION AND SUBSEQUENT SURGERY**
Benjamin Levine, MD; Wilson Lai; Kambiz Motamedi, MD; Leanne Seeger, MD; Sharon Hame, MD
University of California, Los Angeles, Los Angeles, CA, USA

Poster #22 **VALUE OF PRE-OPERATIVE FLUOROSCOPIC-GUIDED SUBTALAR ARTHROGRAPHY**
Richard Walker, MD, FRCPC; Rachael Da Cunha, MD, FRCSC; Jason Boubalos, MD; Tara Heric, RN; Jeremy Lamothe, MD, PhD, FRCSC; Ian Le, MD, FRCSC
University of Calgary, Calgary, AB, Canada

HIP/PELVIS

Poster #23 **MRI OF THE LUMBOSACRAL PLEXUS: WHAT THE PRACTICING RADIOLOGIST NEEDS TO KNOW**
Hailey Allen, MD; Megan Mills, MD; Miriam Peckham, MD; Lubdha Shah, MD; Kent Sanders, MD; Sarah Stilwill, MD
University of Utah Medical Center / SOM, Salt Lake City, UT, USA

Poster #25 **MUSCLE BULK DIFFERENCES IN FAI AND HIP INSTABILITY VERSUS CONTROLS**
Avneesh Chhabra, MD
University of Texas Southwestern Medical Center at Dallas, Flowermound, TX, USA

Poster #26 **A COMPREHENSIVE REVIEW OF PROXIMAL FEMORAL FRACTURES AND THEIR COMPLICATIONS**
Kimia Kani, MD[1]; Hyojeong Mulcahy, MD[2]; Jack Porrino, MD[2]; Felix Chew, MD[2]
[1]University of Maryland School of Medicine, Baltimore, MD, USA; [2]University of Washington / Harborview Medical Center, Seattle, WA, USA

TRAUMA/MISCELLANEOUS

Poster #27 **ULTRASOUND FOR THE EVALUATION OF RADIAL NERVE PATHOLOGY: CORRELATION TO MRI FINDINGS**
Edward Yoon, MD; O. Nwawka, MD
Hospital for Special Surgery, New York, NY, USA

Poster #28 **UTILITY OF MRI IN EVALUATING FOR OSTEOMYELITIS IN PATIENTS WITH CELLULITIS**
Devon Klein, MD[1]; Brian Lee, MD[2]; Hariklia Bezhani, DPM[1]; Guillaume Stoffels, MS, MA[1]
[1]Lenox Hill Hospital, Northwell Health, New York, NY, USA; [2]Beth Israel Deaconess Medical Center Harvard Med School, Boston, MA, USA

Poster #29 **MUSCLE EDEMA - RECOGNIZING PATTERNS AND ASSOCIATED CAUSES**
Sailaja Yadavalli, MD, PhD; Michael Hierl, MD; David Marcantonio, MD
Beaumont Health System, Royal Oak, MI, USA

Poster #30 **CALCIUM HYDROXYAPATITE DEPOSITION DISEASE: A MULTI-MODALITY REVIEW FOR THE PRACTICING RADIOLOGIST AND RADIOLOGIST IN TRAINING, WITH EMPHASIS ON CLINICAL PRESENTATION, PATHOGENESIS AND IMAGING APPEARANCE.**
Jason Esterle, MD; David Marcantonio, MD; Christopher Nall, MD
Beaumont Health System, Royal Oak, MI, USA

Poster #31 **REVIEW AND UPDATE ON IMAGING OF CHEST WALL INJURIES**
Kimia Kani, MD[1]; Hyojeong Mulcahy, MD[2]; Jack Porrino, MD[2]; Felix Chew, MD[2]
[1]University of Maryland School of Medicine, Baltimore, MD, USA; [2]University of Washington / Harborview Medical Center, Seattle, WA, USA

Poster #32 **EVALUATION OF GADOLINIUM DEPOSITION IN THE BRAIN FOLLOWING MAGNETIC RESONANCE ARTHROGRAM**
Lauren Ladd, MD; Krish Singhal, MD; Mark Frank, MD, MBA; Stephen Kralik, MD
Indiana University, Indianapolis, IN, USA

Poster #33 **MRI INTERPRETATION RATHER THAN TISSUE DIAGNOSIS DETERMINES ACUTE OSTEOMYELITIS MANAGEMENT: ONE INSTITUTION'S EXPERIENCE**

Josephina Vossen, MD, PhD; Peter Haar, MD, MS; Curtis Hayes, MD; Michael Perone, MD; Kevin Hoover, MD, PhD
Virginia Commonwealth University Medical Center, Richmond, VA, USA

Poster #34 **PERIOSTEAL THICKENING AS THE ONLY VISUALIZED SIGN OF OSTEONECROSIS ON RADIOGRAPHS.**

Josephina Vossen, MD, PhD; Candice Kim, BS; Peter Haar, MD, PhD; Curtis Hayes, MD; Kevin Hoover, MD, PhD
Virginia Commonwealth University Medical Center, Richmond, VA, USA

Poster #35 **THE INCIDENCE, ONSET AND DISTRIBUTUION OF CRYSTAL DEPOSITION WITHIN THE CERVICAL SPINE**

Eric Walker, MD[1]; Dylan Simmons, DO[2]; Joshua Tice, MD[3]; Jonelle Petscavage-Thomas, MPH, MD[1]
[1]Penn State Milton S. Hershey Medical Center, Hershey, PA, USA; [2]Emory University Dept. of Radiology, MSK Division, Atlanta, GA, USA; [3]West Reading Radiology Associates, West Reading, PA, USA

Poster #36 **DAY OF WEEK, SITE OF SERVICE, AND PATIENT COMPLEXITY DISPARITIES IN MUSCULOSKELETAL MRI INTERPRETATIONS BY RADIOLOGISTS VS. NON-RADIOLOGISTS**

Paige Sharp, MD[1]; Richard Duszak, Jr., MD[1]; Wenyi Wang, MA[2]; Danny Hughes, PhD[2]; Neil Lall, MD[3]; Paul Harkey, MD[1]
[1]Emory University Dept. of Radiology, Atlanta, GA, USA; [2]Harvey L. Neiman Health Policy Institute, Reston, VA, USA; [3]Ochsner Health System, New Orleans, LA, USA

Poster #37 **Imaging Features of Calciphylaxis**

Ryan Franke, MD; Mark Kransdorf, MD; Michael Fox, MD; F. Chivers, MD; Jonathan Flug, MD
Mayo Clinic, Phoenix, AZ, USA

TUMOR

Poster #38 **EARLY DETECTION OF METASTASES USING WHOLE-BODY MRI FOR INITIAL STAGING AND ROUTINE FOLLOW-UP OF MYXOID LIPOSARCOMA**

Thomas Powell, MB,BCh., BAO, FFR(RSCI); Natalia Gorelik, MD; Santhosh Reddy, MBBS, MRCP, FRCR; Robert Turcotte, MD, FCRSC; Krista Goulding, MD, MPH, FRCSC; Sungmi Jung, MD, FRCPC; Thierry Alcindor, MD, MSc
McGill University, Montreal, QC, Canada

Poster #39 **Round Cell Component of Myxoid Liposarcoma: Can We Identify these Concerning Areas on Imaging?**

Lien Senchak, MD[1]; Mark Murphey, MD[2]; Michael Shvarts, MD[2]; James Jelinek, MD[3]; Mark Kransdorf, MD[4]
[1]Walter Reed National Military Medical Center, Bethesda, MD, USA; [2]American Institute for Radiologic Pathology, Silver Spring, MD, USA; [3]Medstar Washington Hospital Center, Washington, DC, USA; [4]Mayo Clinic, Phoenix, AZ, USA

Poster #40 **IMAGING APPEARANCE OF WELL DIFFERENTIATED LIPOSARCOMAS WITH MYXOID STROMA**

Yoav Morag, MD; Corrie Yablon, MD; Jon Jacobson, MD; Monica Brigido, MD; David Lucas, MD
University of Michigan Medical Center, Ann Arbor, MI, USA

Poster #41 **TUMOR INDUCED OSTEOMALACIA, A REVIEW OF 5 CASES**

LEE KATZ, MD; Kirsten Cooper, MD
Yale University School of Medicine, New Haven, CT, USA

Poster #42 **DISTRIBUTION OF FEMORAL SHAFT METASTATSES; IMPLICATIONS FOR PET/CT SCANNING**
Michael Mulligan, MD
University of Maryland School of Medicine, Baltimore, MD, USA

Poster #51 **OPTIMIZING BONE MARROW LESION DETECTION USING DUAL ENERGY CT: A PHANTOM STUDY**
Ramya Srinivasan[1], Hsu-Cheng Huang[2], Yuxin Sun[1], Stefanie Weinstein[1], Lynne Steinbach[1], Benjamin Yeh[1]
[1]University of California San Francisco; [2]Taipei City Hospital, Taipei, Taiwan

LOWER EXTREMITY

Poster #43 **COMPARISON OF DIAGNOSTIC ULTRASOUND AND MRI IN THE EVALUATION OF THE PERONEAL TENDON INJURIES IN CORRELATION WITH OPERATIVE FINDINGS**
Mihra Taljanovic, MD, PhD; Lana Gimber, MD, MPH; Aamir Ahmad, MS; Tyson Chadaz, MD; L Latt, MD, PhD
University of Arizona HCS - Tucson, Tucson, AZ, USA

Poster #44 **Assessing Obesity by Correlating BMI to Subcutaneous Fat Measurement on Axial Knee MRIs**
Felix Gonzalez, MD[1]; Ricardo Hernandez, BS[2]; Yara Younan, MD[1]; Adam Singer, MD[1]; Gulshan Sharma, PhD, MPH[3]; Michael Mulligan, MD[4]; Monica Umpierrez, MD[1]
[1]Emory University Dept. of Radiology, MSK Division, Atlanta, GA, USA; [2]Philadelphia College of Osteopathic Medicine, Suwanee, GA, USA; [3]Cumming School of Medicine, Calgary, AB, Canada; [4]University of Maryland School of Medicine, baltimore, MD, USA

Poster #45 **IMPROVED QUALITY OF KNEE RADIOGRAPHS IN A MULTI-CENTER PRACTICE AFTER INTRODUCTION OF A STANDARDIZED POSITIONING FRAME**
Faysal Altahawi, MD; Carl Winalski, MD; Erika Schneider, PhD; Morgan Jones, MD; Spindler Kurt, MD; Schils Jean, MD
The Cleveland Clinic Foundation, Cleveland, OH, USA

Poster #46 **WEIGHT-BEARING DIGITAL TOMOSYNTHESIS OF FOOT/ANKLE ARTHRITIS: COMPARISON TO RADIOGRAPHY AND SIMULATED WEIGHT-BEARING CT**
Xue Cunningham, MD[1]; Alan Leung, MD[2]; Jennifer Favinger, MD[2]; Daniel Hippe, MS[2]; Alice Ha, MD[2]
[1]Wake Forest University School of Medicine, Winston-Salem, NC, USA; [2]University of Washington / Harborview Medical Center, seattle, WA, USA

Poster #47 **LADY OR GENTLEMAN: SEX DIFFERENCES IN BONY AND CARTILAGE STRUCTURES OF THE KNEE**
Laura Fayad, MD, MS; Lauren Pringle, MD
Johns Hopkins University, Baltimore, MD, USA

Poster #48 **IMAGING OF ANKLE IMPINGEMENT SYNDROMES**
Gary LiMarzi, MD; Omar Khan, MD; Yashesh Shah, MD; Corrie Yablon, MD
University of Michigan Medical Center, Ann Arbor, MI, USA

Poster #49 **“CYCLOPS-LIKE" LESION RELATED TO MUCOID DEGENERATION OF THE ACL**
Maria Bedoya, MD[1]; Andrew Chi, MD[1]; Christian Barrera, MD[2]; Yiftah Beer, MD[3]; Nogah Shabshin, MD, MBA, BSC[1]
[1]Hospital of University of Pennsylvania, Philadelphia, PA, USA; [2]Children's Hospital of Philadelphia, Philadelphia, PA, USA; [3]Assaf Harofeh Medical Center, Zeriffin, Israel

Poster #50 **GETTING TO YOUR FEET: MR IMAGING OF FOREFOOT PAIN: WHAT THE PRACTICING RADIOLOGIST NEEDS TO KNOW**
Richard Leake, MD; Sarah Stilwill, MD; Chris Hanrahan, MD, PhD
University of Utah Medical Center / SOM, Salt Lake City, UT, USA

Poster #1

WHOLE BODY (WB)-MRI WITH 3D VOLUMETRIC SEQUENCES AND ISOTROPIC RESOLUTION: A METHOD FOR FAST AND HIGH RESOLUTION WHOLE BODY IMAGING

Shivani Ahlawat, MD; Jaishri Blakeley; Mike Jacobs, PhD; Laura Fayad, MD, MS
Johns Hopkins University, Baltimore, MD, USA
(Presented by: Shivani Ahlawat, MD, Johns Hopkins University)

Purpose: To describe the feasibility of WB-MRI 3D-volumetric anatomic (T1/STIR) and functional (DWI) sequences with isotropic resolution, applied to patients with NF syndromes.

Materials and Methods: WB-MRI, performed in 10 subjects with NF at 3T, included coronal STIR (TR/TE=6640/84, matrix=256x256, slice thickness(SL)=2 mm), T1 and contrast-enhanced T1 (TR/TE=0.88/2/43, matrix=256×256, SL=2 mm), and DWI/ADC mapping (TR/TE=4100/70, b-values=50, 400, 800 s/mm2, SL=5mm) of the whole body (FOV50×50cm2). All sequences were performed with isotropic resolution. Two readers reviewed all imaging for quality of original acquisition and MPR views using a semiquantiative scale (1=>75% artifacts, 2=25-75% artifacts, 3=< 25% artifacts, 4=no artifact) and presence and character of peripheral lesions. Lesion size and MRI features (signal intensity, heterogeneity, enhancement characteristics, and ADC values) were recorded. Descriptive statistics were reported.

Results: Diagnostic quality for anatomic 3D-sequences was highest (mean score of 4, 3.9 and 3.8, respectively). Mean DWI quality score was 2.6. A total of 223 lesions were detected and 128 lesions were characterized, with mean size of 3.1 cm. Lesions were characterized as PNSTs (97%(124/128)) or cysts (3%(4/128)) based on enhancement. The majority of PNSTs were solitary (97%(120/124)) while 3%(4/124) were plexiform. PNSTs were homogeneously T1 isointense(100%), heterogeneously STIR hyperintense (19%(23/124)) and enhanced heterogeneously(81%(101/124)) with target sign in 77%(95/124) and tail sign in 35%(43/124). By DWI, tumor ADC values(×10-3mm2/s) were variable, with range of 1.7+0.5 to 2.7+0.5. In one subject, there was malignant degeneration of a PNST(minimum ADC 0.4).

Conclusion: WB-MRI with anatomic and functional 3D-volumetric sequences of isotropic resolution is feasible with high quality, for detection (assessment of tumor burden) and characterization. Functional sequences (with DWI/ADC mapping and contrast administration) specifically provide information regarding tumor character and biology (malignant degeneration), and the distinction of peripheral tumors from perineural cysts.

Modality % - Radiography / Fluoroscopy:	0
Modality % - CT:	0
Modality % - MRI:	100
Modality % - US:	0
Modality % - Nuclear Medicine:	0

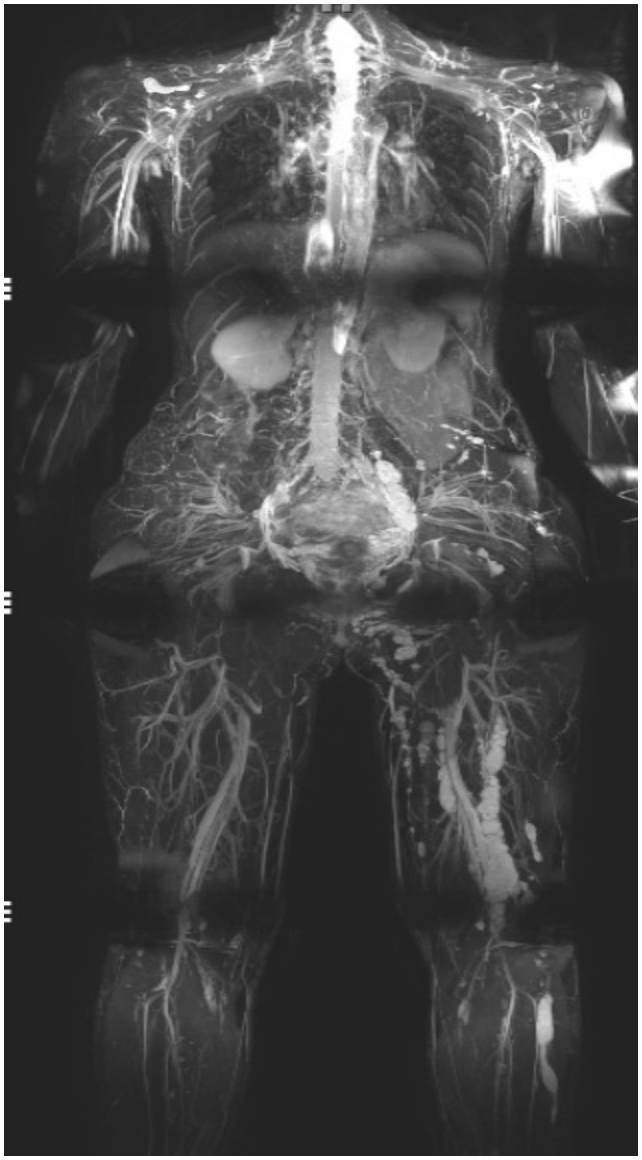

33 year old man with segmental schwannomatosis localized to the left pelvis and lower extremity

Poster #2

Some New Angles on the Magic Angle: What MSK Radiologists Know and Don't Know

Michael Richardson, MD[1]; Behrang Amini, MD, PhD[2]; Todd Richards, PhD[1]
[1]University of Washington / Harborview Medical Center, Seattle, WA, USA; [2]The University of Texas M.D. Anderson Cancer Center, Houston, TX, USA
(Presented by: Michael Richardson, MD, University of Washington / Harborview Medical Center)

Purpose: We created an interactive teaching module to give our residents hands-on experience with a simulated ankle tendon changing its angle in a magnetic field. This simulator allows one to adjust T2 and TE values with slider controls and then see real-time changes in tendon signal intensity. This module's behavior surprised us and forced us to correct several of our own misconceptions about magic angle effects (MAE). From conversations with colleagues, we began to suspect such misconceptions might be common among other clinical musculoskeletal (MSK) radiologists.

Materials and Methods: We surveyed the members of the Society of Academic Bone Radiologists as to which pulse sequences, imaging parameters, tissue types and angles to the B0 field were most likely to produce MAE.

Results: Survey respondents were well-aware that MAE are strongly dependent on TE, and that they commonly present on T1W, FSE and PD sequences. However, they were less aware that MAE may also appear on T2W, STIR and DWI sequences. They were well-aware of MAE effects in tendons, ligaments and cartilage, but less aware that MAE also appear in entheses, peripheral nerves and intervertebral discs. Our MAE simulator demonstrated that for low values of TE, significant MAE can occur over a much wider angular range than we had suspected, in some cases between 30--80°. Our survey respondents greatly underestimated this angular range.

Conclusion: Collagen-containing tissues may exhibit dramatically increased signal intensity when oriented at 55° from the main magnetic field. Such MAE were first reported in clinical MR images of tendons imaged with spin-density sequences. Since then, MAE have been reported in a variety of other pulse sequences and in a number of other MSK structures. MSK radiologists tend to underestimate the variety of situations in which significant MAE may be seen.

Modality % - Radiography / Fluoroscopy:	0
Modality % - CT:	0
Modality % - MRI:	100
Modality % - US:	0
Modality % - Nuclear Medicine:	0

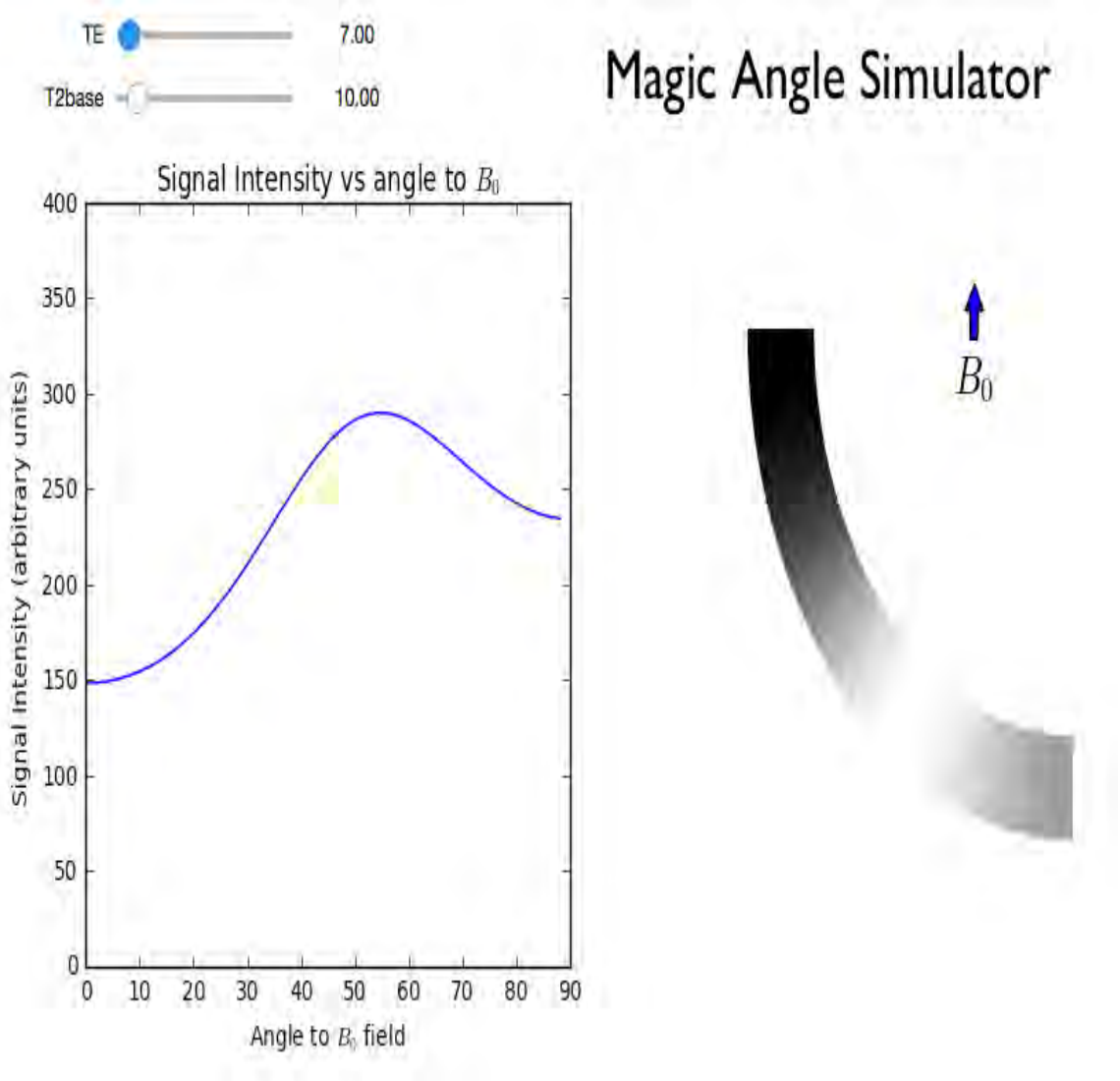

Figure 1. Magic angle effect demonstrated in a simulated ankle tendon.

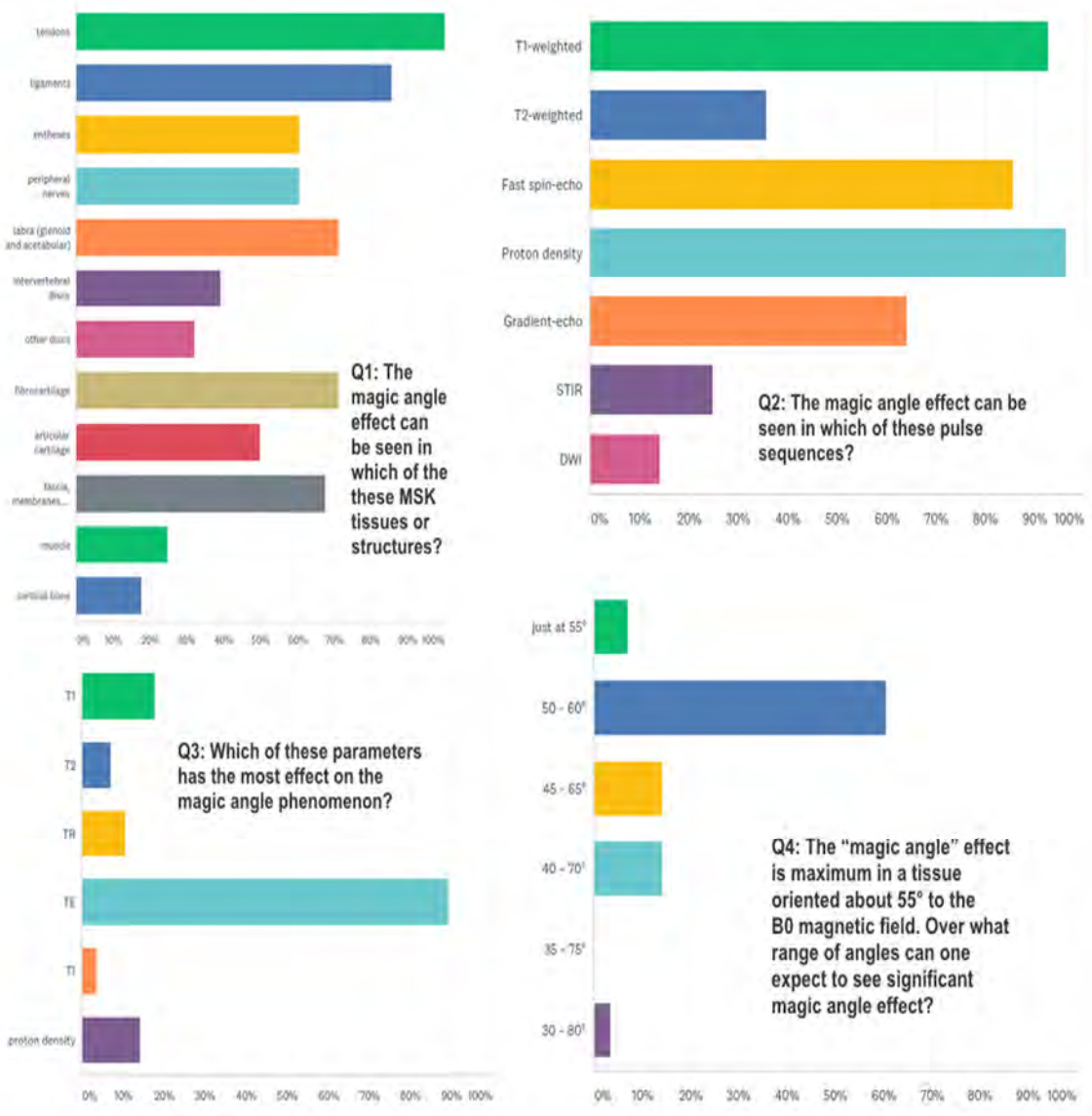

Figure 2. Survey responses to four magic angle questions.

Poster #3

QUANTITATIVE ASSESSMENT OF CHANGE IN UPPER EXTREMITY MUSCLE STIFFNESS FOLLOWING FLUID INJECTION USING SHEAR WAVE ELASTOGRAPHY

O. Nwawka, MD; Shivi Duggal, MD; Bin Lin, MS; Nicholas Gutierrez, MD; Theodore Miller, MD
Hospital for Special Surgery, New York, NY, USA
(Presented by: O. Nwawka, MD, Hospital for Special Surgery)

Purpose: An immediate change in shear wave elastography (SWE)-measured muscle stiffness can be seen following intramuscular injection of saline-reconstituted botulinum toxin (BTX), but it is unclear whether the cause is saline or BTX. The purpose of this pilot study is to quantitatively assess for change in muscle stiffness following intramuscular saline injection using SWE.

Materials and Methods: 30 muscles [lateral deltoid (LD), biceps brachii (BB), brachialis, pronator teres (PT), flexor carpi radialis (FCR), flexor carpi ulnaris (FCU)] from 5 fresh frozen cadaveric upper extremity specimens were assessed. Under sonographic guidance, 5 mL (FCR, FCU, PT) or 10 mL (LD, brachialis, BB) of saline were injected into each muscle belly. Using a LOGIC E9 ultrasound system (GE Healthcare, Waukesha, WI), pre- and post-injection muscle belly thickness (MT) (mm) and SWE (kPa) measurements were obtained. Paired t-test was used to assess for post-injection change in mean SWE measurements. Pearson correlation coefficients were calculated to look for correlation between SWE measurements and MT.

Results: All muscles demonstrated a decrease in the mean SWE value post injection (Figure 1), ranging from 12.02 kPa to 21.64 kPa (Figure 2). The mean muscle stiffness decrease was statistically significant in the LD and brachialis muscles ($p=0.01$). Mean pre-injection SWE measurements in all muscles except the FCU moderate to strong correlation with MT.

Conclusion: Following saline injection, a decrease in upper extremity muscle stiffness is detected using SWE. Moderate to strong correlations suggest a relationship between MT and SWE. These findings may serve as precursor to broader quantitative evaluation of edema-related muscle pathology.

Modality % - Radiography / Fluoroscopy:	0
Modality % - CT:	0
Modality % - MRI:	0
Modality % - US:	100
Modality % - Nuclear Medicine:	0

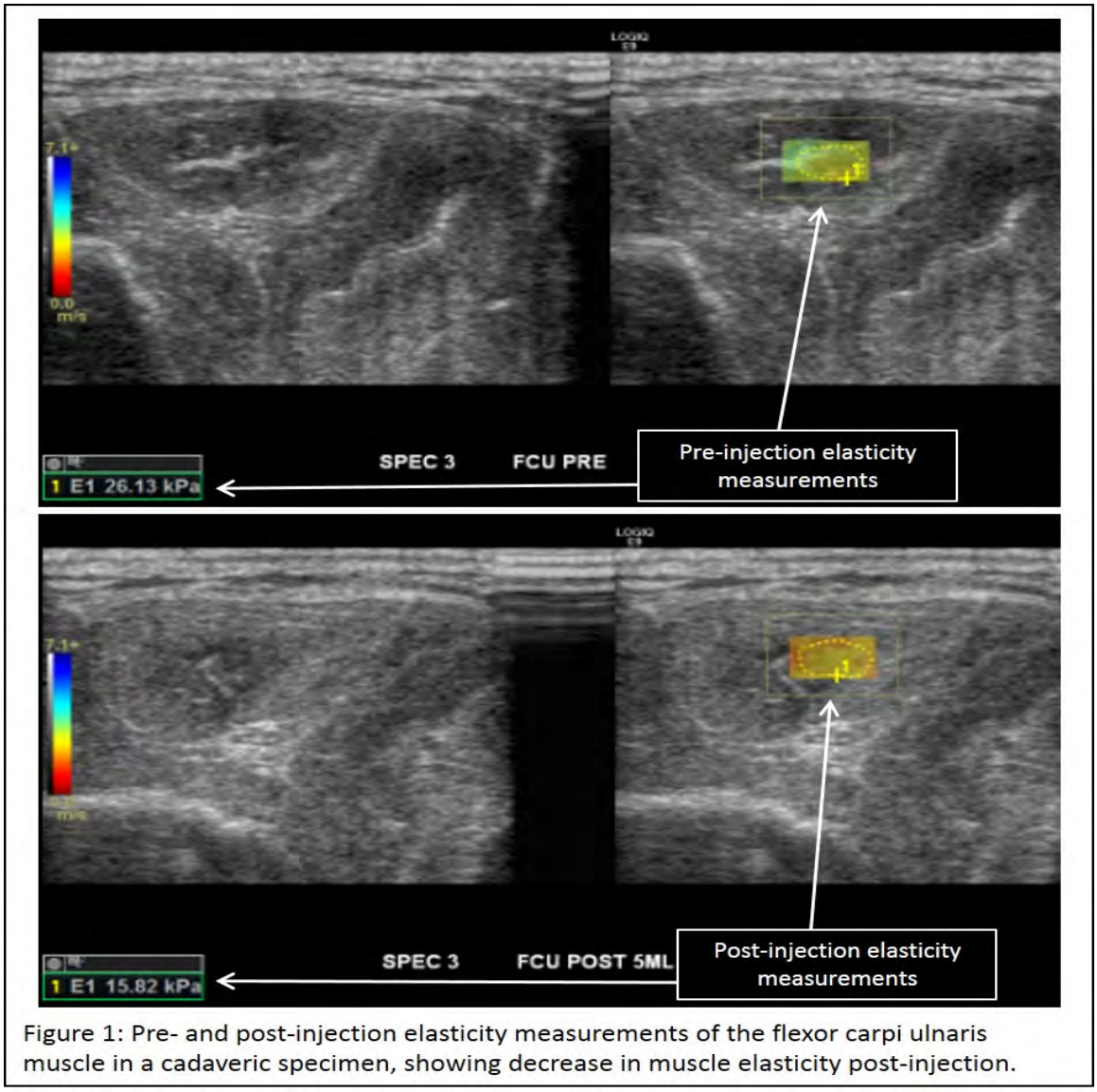

Figure 1: Pre- and post-injection elasticity measurements of the flexor carpi ulnaris muscle in a cadaveric specimen, showing decrease in muscle elasticity post-injection.

Figure 1: Pre- and post-injection elasticity measurements of the flexor carpi ulnaris muscle in a cadaveric specimen, showing decrease in muscle elasticity post-injection.

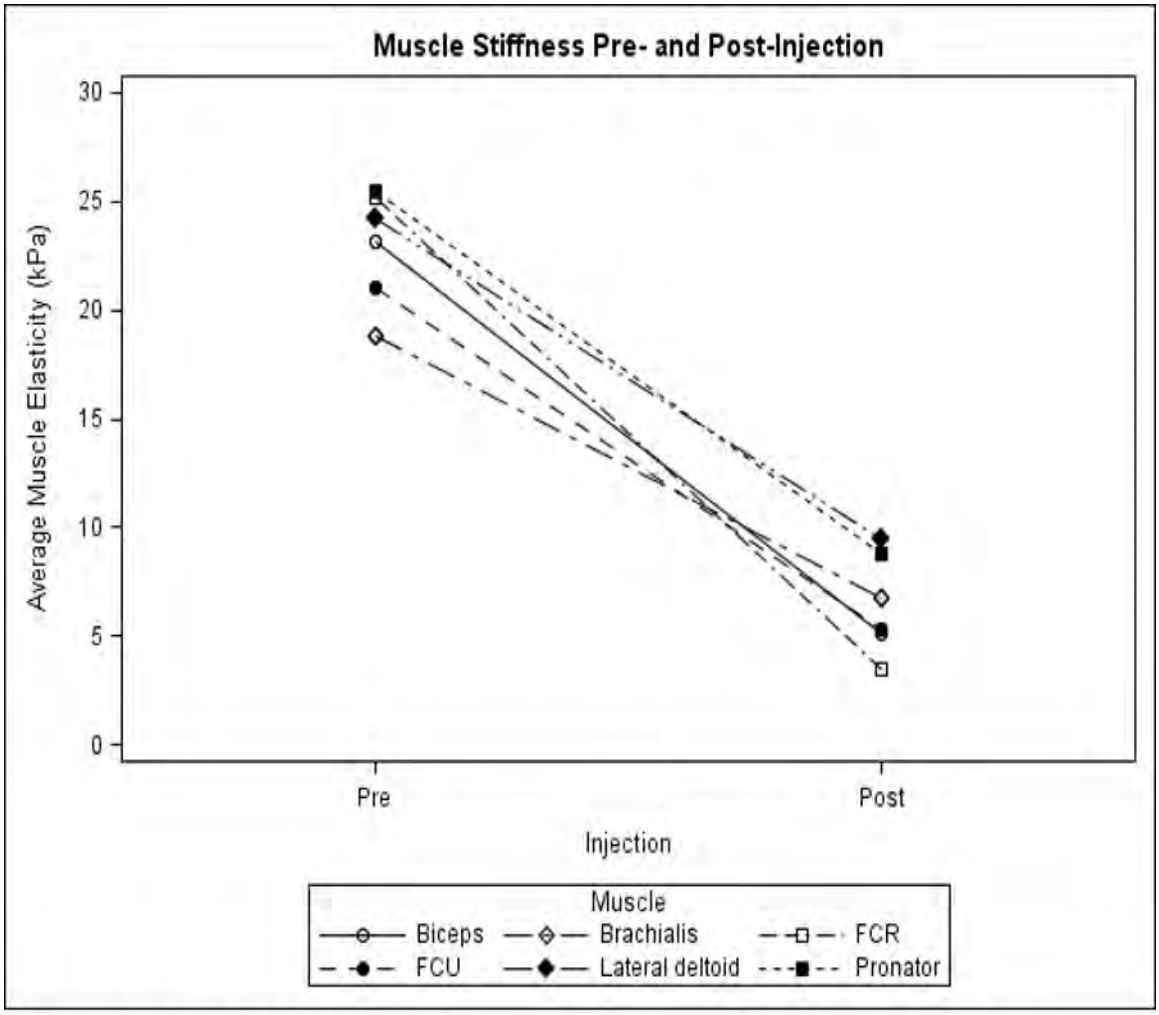

Figure 2. Pre- and Post-injected average SWE values for each muscle depicting change in muscle stiffness.

Figure 2. Pre- and Post-injected average SWE values for each muscle depicting change in muscle stiffness.

Poster #4

3D PRINTING MAKES AN IMPOSSIBLE CASE POSSIBLE

Carissa White, MD; Marc-Anthony Lecky; David Nelson; Mauricio Silva, MD; Anthony Scaduto, MD
David Geffen School of Medicine at UCLA, Los Angeles, CA, USA
(Presented by: Carissa White, MD, David Geffen School of Medicine at UCLA)

Purpose: To illustrate how 3D printing of complex musculoskeletal cases can add value to patient care.

Materials and Methods: A 13-year-old female presented with a complex fracture malunion of her left distal humerus, resulting in locked full extension at the elbow joint. Radiographs demonstrated a deformity so severe that it was deemed inoperable. A CT scan of the patient's left elbow was reconstructed to 1.5 mm slices and segmented using Mimics software (Materialise). The resulting .stl file was then exported into 3-matic (Materialise) for mesh optimization. A tubular connector was designed between the radial head and the distal humerus to maintain anatomical relationships of the printed parts. The model was 3D printed in polyamide.

Results: After receiving the model, the orthopedic surgeons were able to better understand the deformity and formulate a surgical plan to correct the alignment and restore range of motion at the joint. However, when mock surgery was attempted on the model, the degree of rotation of the medial and lateral epicondyles necessitated by the initial surgical plan was shown to be too dangerous, carrying a high risk of neurovascular injury. Nonetheless, using real-time feedback from the model, the surgeons were able to design an alternative, safer procedure. The patient successfully underwent the redesigned surgery to correct the distal humeral malalignment and place her elbow in 70 degrees of flexion, allowing for a more functional position of the arm and enabling use of her left hand.

Conclusion: 3D printing significantly changed clinical management of a complex life-limiting pediatric elbow deformity not once, but twice. Enhanced 3D visualization afforded by the model made the previously inoperable case operable, while a practice procedure on the model allowed for hands-on feasibility testing and refinement of the surgical plan.

Modality % - Radiography / Fluoroscopy:	50
Modality % - CT:	50
Modality % - MRI:	0
Modality % - US:	0
Modality % - Nuclear Medicine:	0

Pre-operative PA, oblique and lateral radiographs of the patient's left elbow (above), compared with a similar view of the 3D printed model (below)

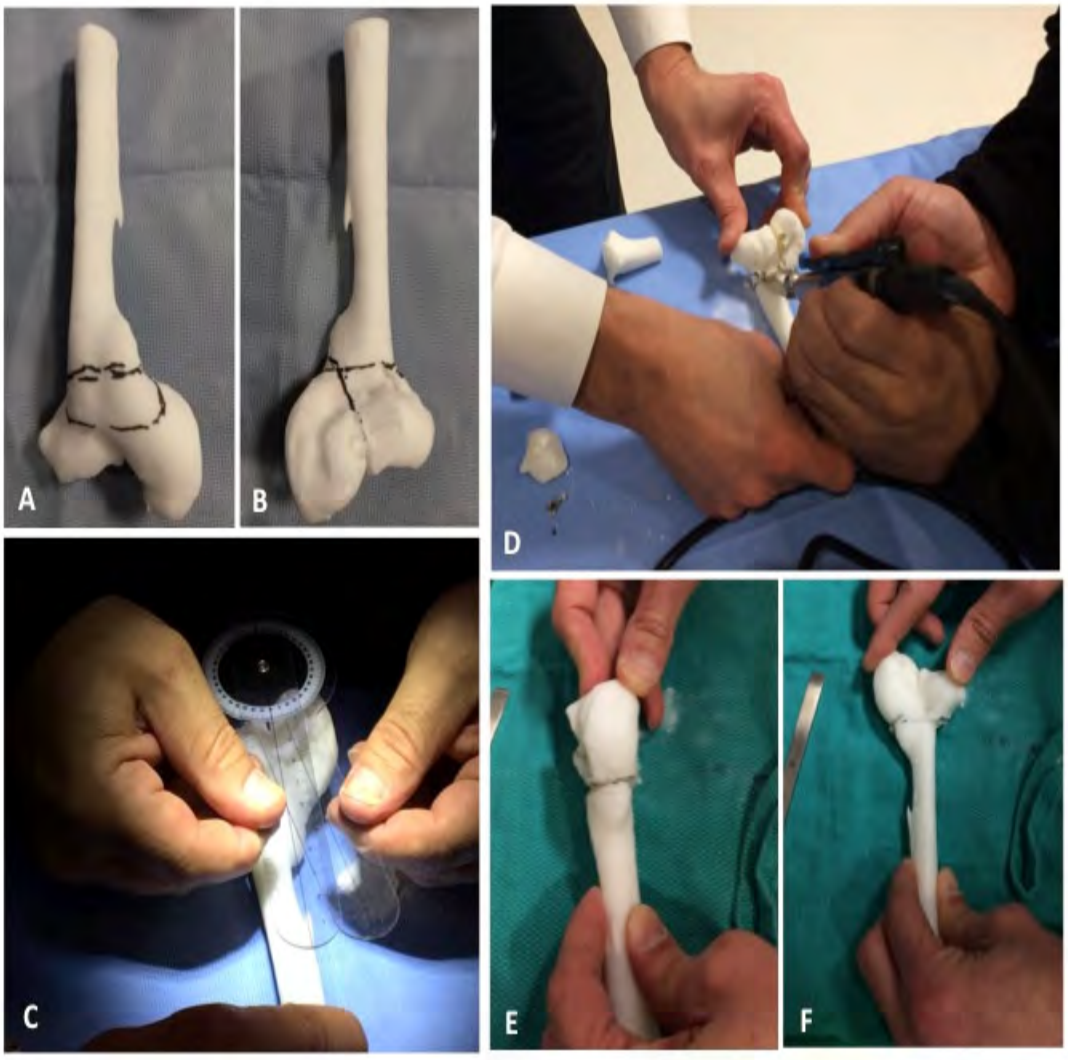

(A,B) Model with planned osteotomies drawn in marker
(C) Measuring angulation and (D) cutting the model
(E,F) Model in anatomic alignment after the osteotomies

Poster #5

CLINICALLY RELEVANT RADIOLOGICAL INSIGHTS PROVIDED BY EN FACE MICROSCOPIC VISUALIZATION OF EROSIONS COMPLICATING ARTHRITIS, GRANULOMATOUS DISEASE, NEOPLASIA AND VASCULAR DISEASE

Bruce Rothschild, MD
West Virginia University School of Medicine, Morgantown, WV, USA
(Presented by: Bruce Rothschild, MD, West Virginia University School of Medicine)

Purpose: Radiologic and macroscopic examination of joints provides perspectives, but is limited in resolution. The purpose of this study is to bridge the resolution gap by utilizing direct articular surface microscopy, to provide and anatomical explanation for radiologically and macroscopically observed articular defects.

Materials and Methods: Surface microscopy at 50 to 200x magnification was utilized to examine macroscopically recognized articular surface defects in individuals in the Hamann-Todd and Terry human skeletal collections with previously verified diagnoses of rheumatoid arthritis, spondyloarthropathy, juvenile inflammatory arthritis, calcium pyrophosphate deposition disease, gout, metastatic cancer, multiple myeloma, non-granulomatous infection, pyogenic and granulomatous infection in the form of fungal disease and tuberculosis, histiocytosis and sickle cell anemia. The appearance of the defects in these disorders was characterized as to border regularity, shape, evidence of pressure changes, sclerosis, remodeling and periosteal reaction.

Results: Erosions related to RA ae sharply defined fronts of resorption, without microscopic evidence of surface remodeling or reactive new bone formation; spondyloarthropathy and juvenile inflammatory arthritis, well-defined fronts of resorption with remodeling and reactive new bone formation; gout, sharply defined with new bond formation from pressure on surrounding bone; calcium pyrophosphate deposition disease, ill-defined with fragmentation and shedding; sickle cell anemia, sharply defined with retained fragments; metastatic cancer, ill-defined with occasional sclerosis; multiple myeloma, sharply defined uniform expansion independent of bone density; histiocytosis, sharply defined with periosteal reaction; pyogenic infection, ill-defined with filigree internal and periosteal reaction; tuberculosis, sharply defined with basal sclerosis; and fungal disease, sharply defined with expansion independent of bone density producing pressure erosion and slight periosteal reaction.

Conclusion: Epi-illumination microscopy provides clearer characterization of bone alteration and allows new criteria for discrimination among the common erosive varieties of arthritis.

Modality % - Radiography / Fluoroscopy:	25
Modality % - CT:	0
Modality % - MRI:	0
Modality % - US:	0
Modality % - Nuclear Medicine:	0

Poster #7

Superior Capsular Reconstruction for Irreparable Rotator Cuff Tears: Imaging Features and Complications

Pamela Walsh, MD; Mohammad Samim, MD; Luis Beltran, MD
NYU Medical Center/ Hospital for Joint Diseases Langone Medical Center, New York, NY, USA
(Presented by: Pamela Walsh, MD, NYU Medical Center/ Hospital for Joint Diseases Langone Medical Center)

Purpose: Superior Capsular Reconstruction (SCR) is a recent surgical procedure for irreparable massive rotator cuff tears, which can be challenging to evaluate on postoperative MRI, especially assessing for graft failure. Our purpose is to report MRI features of SCR and complications.

Materials and Methods: Digital database retrospective query was performed to identify SCR cases. Clinical data was reviewed with attention to postoperative pain as correlates for graft failure. Postoperative MRI studies were reviewed with attention to 1) humeral head position 2) graft detachment 3) suture anchor placement 4) graft position 5) muscle atrophy.

Results: 6 patients (3 women, 3 men, ages 55-71, mean 63, median 62) imaged 1-10 months after SCR were evaluated. One patient underwent SCR revision after imaging demonstrated failure of the first repair. Of the 7 SCR procedures, 5/7 reported shoulder pain postoperatively, 3 demonstrated superior translation of the humeral head greater than 10 mm above the superior glenoid and detachment of the allograft from either the glenoid or humeral insertion. 6/7 cases had two glenoid anchors placed in the posterosuperior quadrant of the glenoid with corresponding allograft coursing over the posterosuperior aspect of the humeral head. All patients had at least grade III supraspinatus atrophy and at least grade II infraspinatus atrophy. Other complications included dislodged suture anchor into the deltoid and tear of the graft from an infraspinatus myotendinous anastomosis. Two patients did not report postoperative pain and showed intact grafts with the superior aspect of the humeral head no more than 7 mm above the superior glenoid on postoperative MRI.

Conclusion: Following SCR, signs of graft failure include postoperative pain, high riding humeral head greater than 10 mm, and graft detachment on postoperative MRI.

Modality % - Radiography / Fluoroscopy:	0
Modality % - CT:	0
Modality % - MRI:	100
Modality % - US:	0
Modality % - Nuclear Medicine:	0

70 year old female status post Superior Capsular Reconstruction. No reported post-operative pain.

70-year-old female status post superior capsular reconstruction. No reported post-operative pain with intact capsular reconstruction.

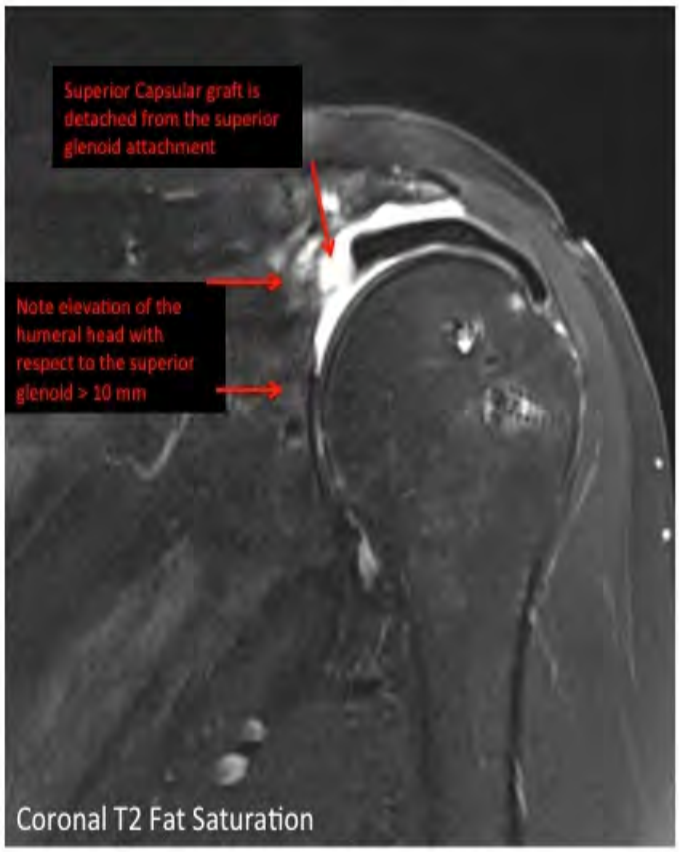

59 year old male status post Superior Capsular Reconstruction Revision with post-operative pain and loss of range of motion.

59 year-old-man status post superior capsular reconstruction revision with post-operative pain and loss of range of motion with failure of the capsular reconstruction.

Poster #8

GENDER DIFFERENCES IN GLENOID REMODELING IN GLENOHUMERAL DEGENERATIVE JOINT DISEASE

Christopher Peters, MD; Anna Zajicek, MD; Christopher Peters, MD; Kent Rinehart, MD; Matthew Teusink, MD
University of Nebraska Medical Center, Omaha, NE, USA
(Presented by: Christopher Peters, MD, University of Nebraska Medical Center)

Purpose: To review underlying bony anatomical variance of the shoulder, particularly the glenoid, between males and females. To discuss how the underlying difference in glenoid development between males and females may contribute to hardware failure in patients receiving arthroplasty, mainly failure secondary to mismatch between glenoid component and native glenoid anatomy. To provide valuable information on how recognizing differences in patterns of remodeling between sexes on imaging can assist in constructing glenoid hardware, and potentially reduce hardware failure.

Materials and Methods: A retrospective medical record review to characterize gender differences in glenoid wear rates in patients with advanced glenohumeral osteoarthritis. Pre-arthroplasty CT measurements focusing on glenoid version, inclination, vault depth, volume and glenoid morphology performed on patients who subsequently underwent anatomic total shoulder arthroplasties. Subjects included (N=140) will have had total shoulder arthroplasty surgery by one surgeon at our institution within the last 4 years. Measurements are compared between males and females using the independent sample t-test. The association of categorical patient characteristics with gender is evaluated using Fishers exact test. All tests are 2-sided and a p-value < 0.05 is considered statistically significant.

Results: We hypothesize that females tend to remodel the glenoid concentrically and medially, whereas males tend to remodel the glenoid posteriorly with increased retroversion.

Conclusion: Data comparing glenohumeral morphology and wear secondary to osteoarthritis between sexes could provide valuable insight for glenohumeral hardware design. Continued research evaluating glenoid osteoarthritis patterns between males and females is needed, especially since glenoid failure and loosening is a well-known complication of a total shoulder arthroplasty.

Modality % - Radiography / Fluoroscopy:	0
Modality % - CT:	100
Modality % - MRI:	0
Modality % - US:	0
Modality % - Nuclear Medicine:	0

Poster #9

Os Subscapulare: imaging findings and clinical relevance

Alex Bergman, MD[1]; Hilary Umans, MD[2]; Jonathan Ticker, MD[3]
[1]Jacobi Medical Center, Bronx, NY, USA; [2]Lenox Hill Radiology and Imaging Associates, New York, NY, USA; [3]Orlin and Cohen Orthopedic Associates, Merrick, NY, USA
(Presented by: Alex Bergman, MD, Jacobi Medical Center)

Purpose: To describe the "Os Subscapulare" and report its correlation with subscapularis tendon tear and long head biceps tendon (LHBT) pathology.

Materials and Methods: Retrospective review of arthroscopy images and operative notes (1 surgeon, 2009-2017) yielded 7 shoulders (all male 44-64 years) with an OS embedded in the subscapularis tendon.

MRI (five 1.5T, one 0.3T) and radiographs were reviewed in six. MRI report only was available in one (0.3T MRI). MRI were reviewed for: OS dimensions, subscapularis and supra-/infraspinatus tendon tear, and LHBT pathology. Radiographs were reviewed. Sensitivity of findings were assessed.

Results: Arthroscopy findings- 7 subscapularis tendons tears: all full thickness (FT), 3 complete. 6 supraspinatus tears: 4 repaired, 3 concomitant tear and repair of the infraspinatus. LHBT: 7 tears (2 ruptured, 5 partial thickness (PT) with 3 subluxed); treated with tenotomy (3) or tenodesis (2).

Radiographs- 6/6 visible on axillary, 1/6 visible in all views.

MRI findings (6)- LHBT tear: 4 (2 PT), intact/dislocated (1), intact/located (1); Subscapularis tendon: FT tear (4, 2 complete), PT (1) and intact (1). Sensitivity for accurate detection of Subscapularis, Supra-/Infraspinatus and LHBT pathology: 60%, 100% and 80%, respectively. Diagnosis of 4 True Positive subscapularis tears: 1 low confidence. 2 False Negative mis-diagnosed with intermediate-high degree of confidence.

MRI report only (1 shoulder, 0.3T), did not mention the OS or the subscapularis; on re-review the OS was identified and the subscapularis tendon was reported as partially torn (arthroscopy proven complete tear).

Conclusion: An OS is reliably visible on axillary radiographs and all MRI. The OS is an important imaging surrogate for full thickness subscapularis tear and clinically significant LHBT pathology.

Modality % - Radiography / Fluoroscopy:	5
Modality % - CT:	0
Modality % - MRI:	95
Modality % - US:	0
Modality % - Nuclear Medicine:	0


T1-w
PD-fat sat

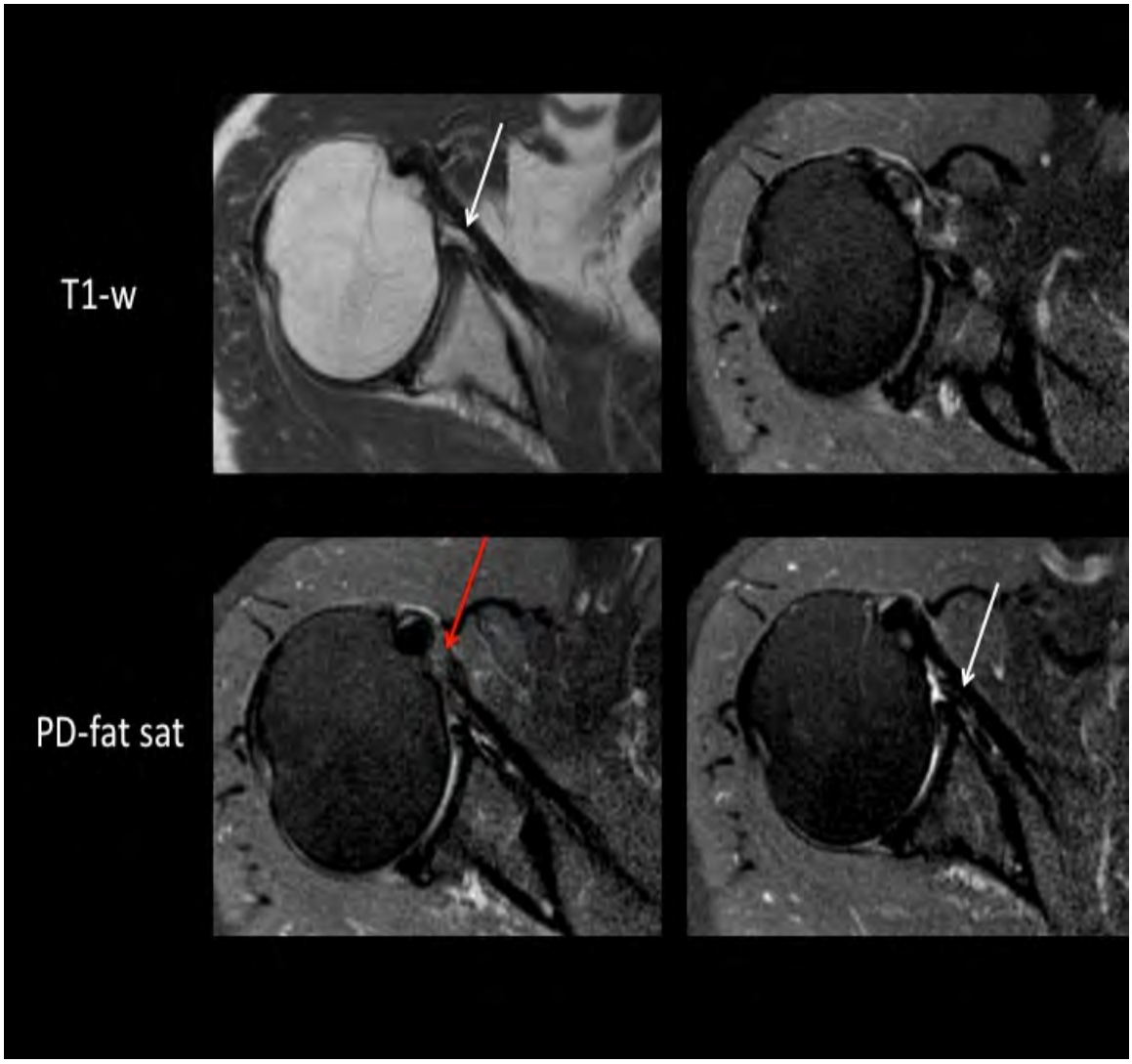

OS visible in Axillary radiograph only and T1-w MRI (white arrows). True positive subscapular tear (red arrow). MRI false negative for LHBT tear and subluxation.

Poster #10

"Reducing" Radiologists' Anxiety about Carpal Instability

Jonelle Petscavage-Thomas, MD, MPH; Eric Walker, MD; Weaver Kesler, MD
Penn State Milton S. Hershey Medical Center, Hershey, PA, USA
(Presented by: Jonelle Petscavage-Thomas, MD, MPH, Penn State Milton S. Hershey Medical Center)

Purpose: The carpus is the key transmitter of force between the forearm and the hand and provides the foundation for maximum hand function. Disruption of the normal carpal alignment resulting in instability can be clinically subtle yet result in significant arthritis and loss of normal hand and wrist function. Imaging is key to detecting early signs of instability and providing a diagnosis and surgical plan when physical examination is limited due to pain and tenderness.

- **Materials and Methods:** Review normal carpal anatomy on radiographs
- Discuss column, row, and combined column-row theories of carpal kinematics
- Illustrate normal cross-sectional imaging of intrinsic and extrinsic ligaments of the carpus
- Show how to measure the scapholunate (SL) and capitolunate (CL) angles
- Review patterns of carpal instability on radiographs and cross-sectional imaging

Results: Posteroanterior, oblique, and lateral radiographs will be used to review normal osseous anatomy, including joint space parallelism, the three carpal arcs, scaphoid, lunate, and capitate axes, and normal scapholunate and capitolunate angles. The dorsal and volar extrinsic ligaments and the intrinsic scapholunate and lunatotriquetral ligament anatomy will be reviewed. The following pathologies will be discussed: dorsal intercalated segment instability (DISI), volar intercalated segmental instability (VISI), perilunate dislocation, midcarpal dislocation, lunate dislocation, rotary subluxation of the scaphoid, and scapholunate advanced collapse (SLAC).

Conclusion: Recognition of subtle abnormalities in carpal alignment on radiographs is important to providing diagnosis of patients with carpal instability and preventing significant functional loss and arthritis. After reviewing this exhibit, the learner will understand normal and abnormal imaging appearance and measurements of the carpus.

Modality % - Radiography / Fluoroscopy:	65
Modality % - CT:	15
Modality % - MRI:	15
Modality % - US:	5

Modality % - Nuclear Medicine: 

Lateral radiograph of the wrist shows abnormal scapholunate angle of 82 degrees. This is a finding in DISI.

Poster #11

FOOSH Injuries of the Elbow with an Emphasis on Posterolateral Elbow Instability: A Multimodality Pictorial Review.

Christopher Nall, MD; Robert Colvin, DO; Shashin Doshi, MD
Beaumont Health System, Royal Oak, MI, USA
(Presented by: Christopher Nall, MD, Beaumont Health System)

Purpose: To review and reinforce important multimodality imaging findings and injury patterns which can indicate high morbidity elbow injuries in patients who have fallen on an outstretched hand. These diagnoses include: posterolateral elbow instability, medial collateral ligament injuries, radial head and neck fractures, Essex-Lopresti fracture-dislocation, coronoid process fractures, distal humeral fractures, olecranon process fractures, elbow dislocation, and Monteggia fracture and dislocation. These diagnoses have specific imaging findings and injury patterns that are important to recognize to limit overall morbidity.

Materials and Methods: Cases performed at a large tertiary care medical center will be reviewed and high morbidity FOOSH-type elbow injuries will be collected. This exhibit will review the classic clinical presentation and multimodality imaging findings associated with these cases. Important imaging findings and injury patterns will be highlighted in a case-based format with an emphasis on posterolateral elbow instability.

Results: FOOSH injuries of the elbow are common traumatic injuries with specific anatomic and morphologic patterns that are important to recognize to decrease overall morbidity. This exhibit will provide a multimodality pictorial review of these types of cases to sharpen the diagnostic ability of both practicing radiologists and radiologists in training.

Conclusion: FOOSH injuries of the elbow are commonly encountered in typical daily practice. Diagnosis of these injuries based on specific anatomic and morphologic patterns is important to ensure early treatment and to decrease morbidity.

Modality % - Radiography / Fluoroscopy:	20
Modality % - CT:	20
Modality % - MRI:	60
Modality % - US:	0
Modality % - Nuclear Medicine:	0

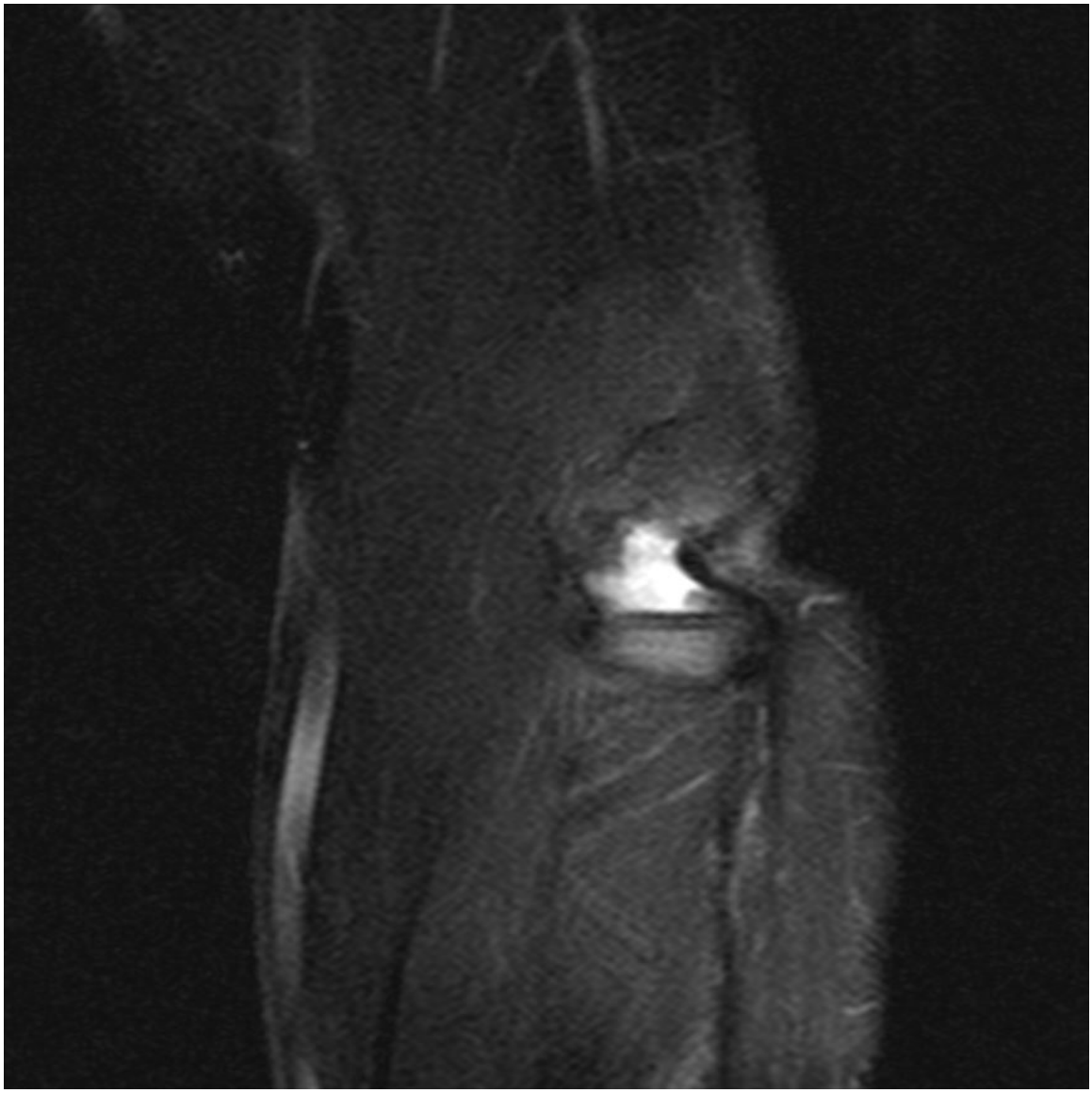

Chronic radial collateral ligament injury.

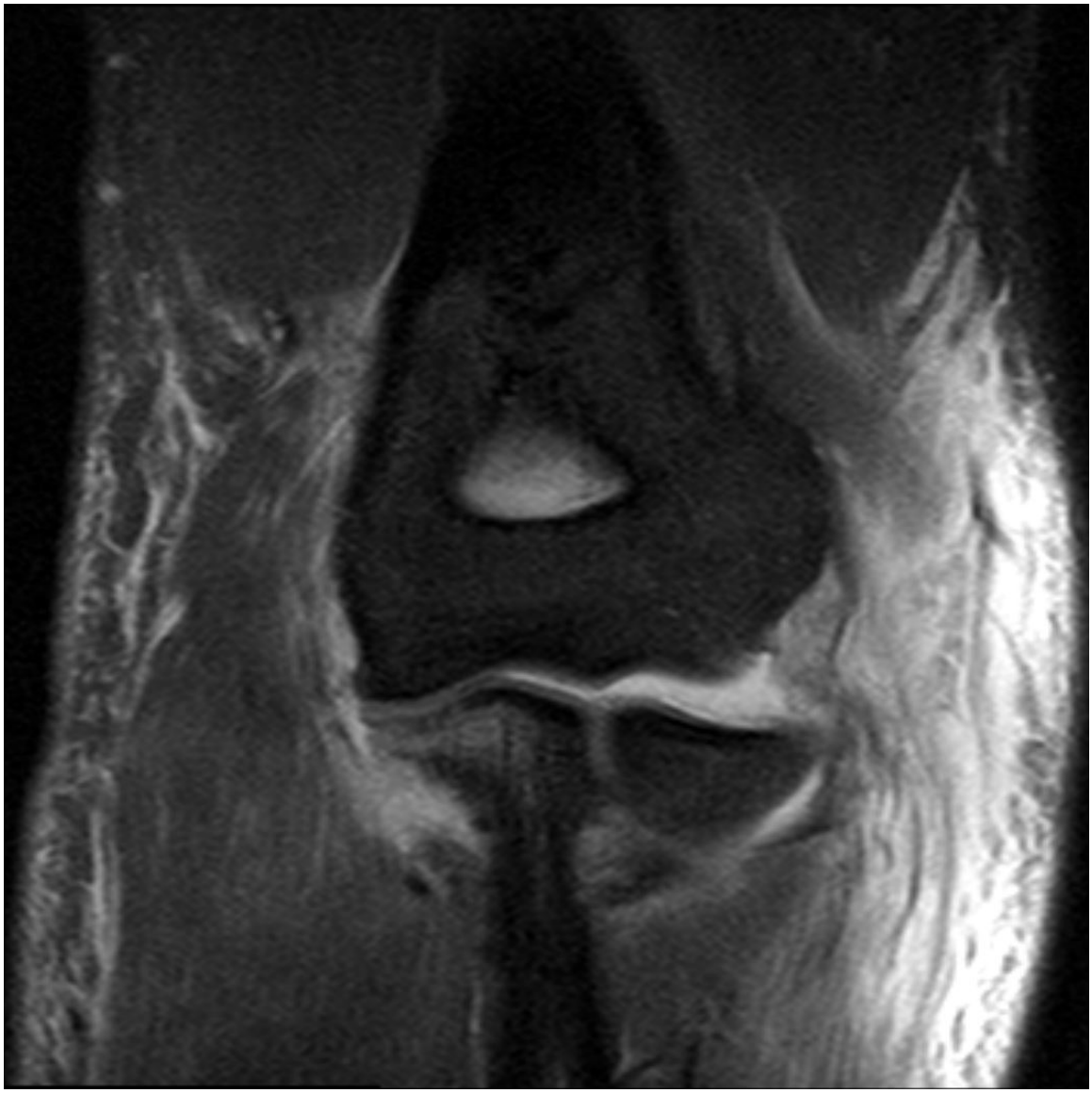

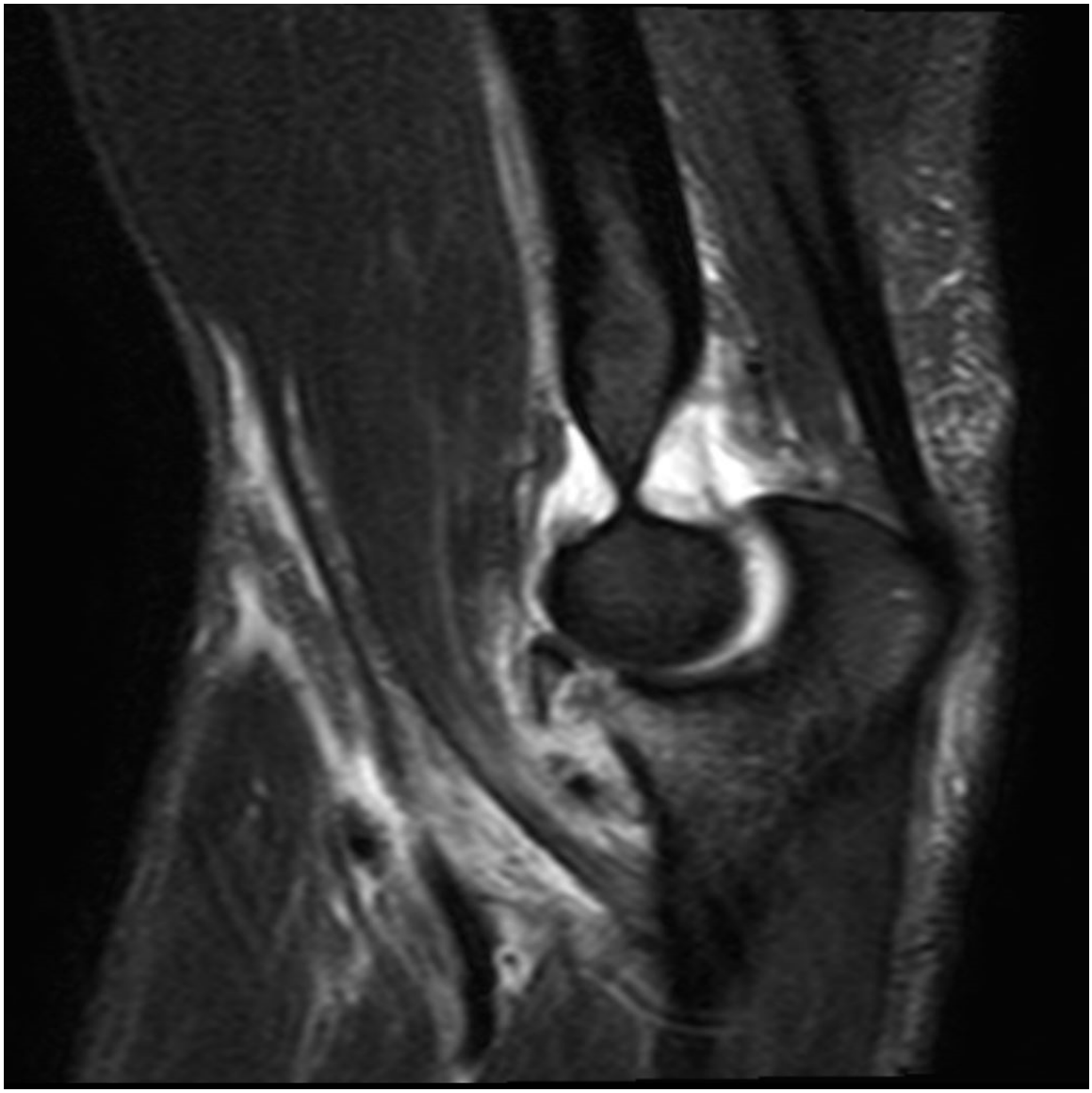

PLRI injury with coronoid process fracture.

Poster #12

RADIOLOGIC EVALUATION OF ABNORMALITIES OF THE STERNUM AND STERNOCLAVICULAR JOINTS

Sailaja Yadavalli, MD, PhD; Jason Esterle, MD; Christopher Nall, MD
Beaumont Health System, Royal Oak, MI, USA
(Presented by: Sailaja Yadavalli, MD, PhD, Beaumont Health System)

Purpose: The exhibit will review normal anatomy, congenital anomalies and pathologic conditions that involve the sternum and sternoclavicular joints. Although these structures are included daily on countless radiologic studies, they are often given only a perfunctory glance by radiologists. The close proximity of these anterior chest wall structures to vital mediastinal organs makes it important for radiologists to be familiar with acute and chronic processes that may involve them. A missed diagnosis may lead to significant morbidity and mortality such as with mediastinitis or traumatic injury of adjacent vessels.

Materials and Methods: The exhibit will first review the complex normal anatomy of the sternoclavicular joint and sternum and some of the commonly seen congenital or developmental anomalies. Following this, using a case based approach, we will present imaging findings related to various pathologic conditions that may affect the sternum and sternoclavicular joints. The presentation will also discuss optimal imaging techniques and include radiographs, CT, MRI and ultrasound images. Where relevant interventional techniques will also be discussed.

Results: Sternum and sternoclavicular joints are often injured in anterior chest wall trauma and should be reviewed with great care as abnormalities may be subtle, easily overlooked or evident only on sagittal reformatted CT images. The sternoclavicular joint is a synovial joint and may be affected by inflammatory arthritides. Distinguishing between inflammatory processes, osteoarthrosis and infections affecting the joint may sometimes be difficult and need additional clinical information or joint aspiration. Awareness of postoperative complications that may follow mediastinal surgery is important to avoid significant morbidity and mortality. Tumors involving the sternum are most often metastasis and malignant.

Conclusion: Familiarity with different abnormalities affecting the sternoclavicular joint and sternum and optimal imaging techniques is important in making an accurate diagnosis where findings may be subtle and easily overlooked.

Modality % - Radiography / Fluoroscopy:	10
Modality % - CT:	70
Modality % - MRI:	10
Modality % - US:	10
Modality % - Nuclear Medicine:	0

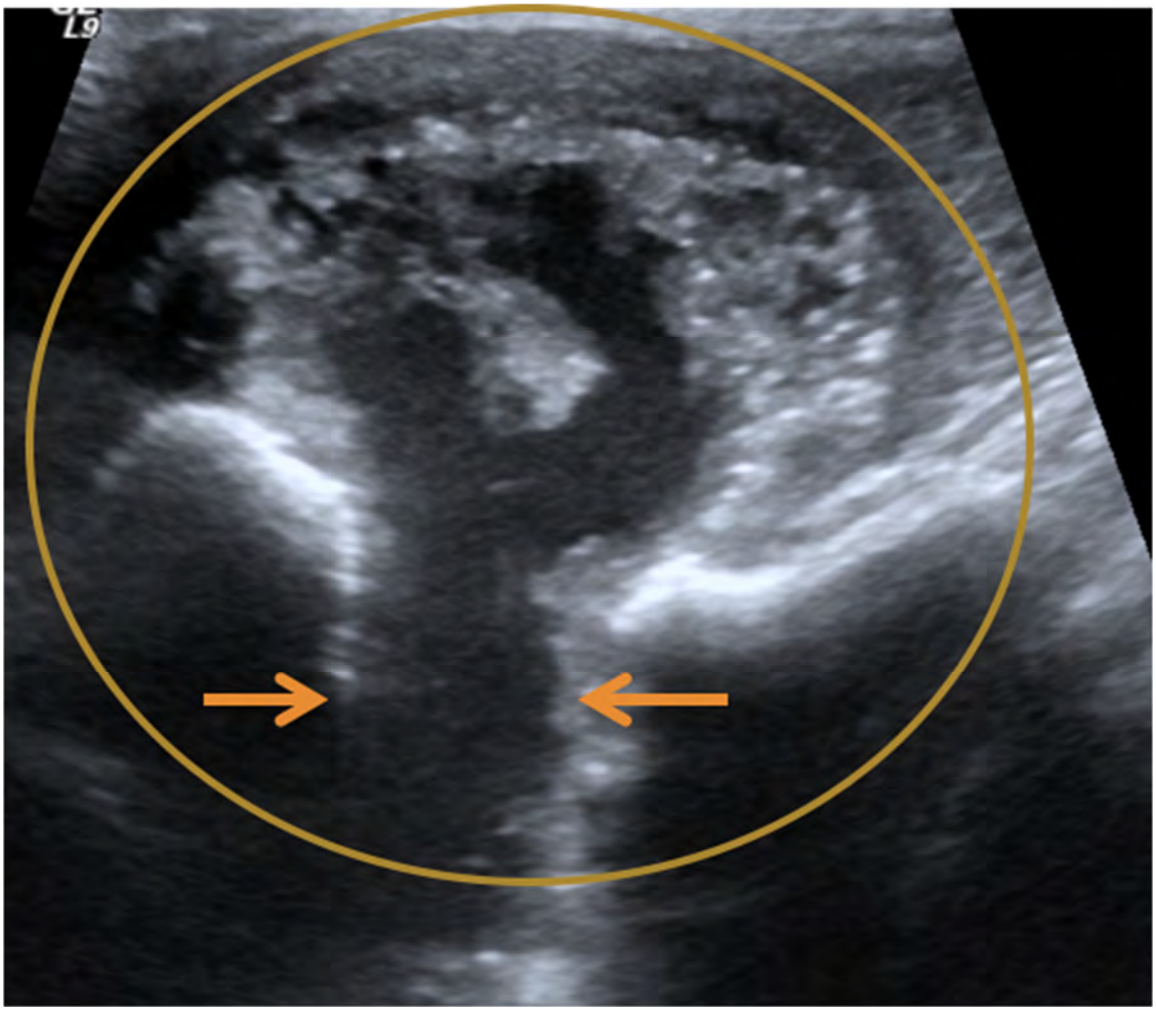

Sternoclavicular joint mass- fluid collection with destruction of manubrium is seen by CT and US. Diagnosis of chronic S.Aureus infection made after aspiration.

Note dehiscence of sternum seen on scout and axial CT images. Findings on axial image show patient's increased risk for developing mediastinitis.

Poster #13

CT GUIDED CORE NEEDLE BONE BIOPSY IN THE WORKUP OF OSTEOMYELITIS: DIAGNOSTIC YIELD AND EFFECT ON PATIENT CARE.

Donald von Borstel, DO; Cameron Smith, DO; Gregory Bradley, DO; Sindhura Alapati, MD
Oklahoma State University Medical Center, Tulsa, OK, USA
(Presented by: Donald von Borstel, DO, Oklahoma State University Medical Center)

Purpose: To examine the overall diagnostic yield of bone biopsy in the setting of osteomyelitis and its role in management.

Materials and Methods: A retrospective review of 35 bone biopsies performed by a single institution for suspected osteomyelitis. Data collected and analyzed from these cases included biopsy location, culture and pathology results, preoperative MRI impressions, and antibiotic therapy prior to and after culture. Culture was presented as negative or positive and used as the primary outcome for diagnostic yield. Nine of the thirty-five cases were excluded from analysis due to incomplete culture results or unknown use of antibiotics. A total of twenty-six cases were included in the final analysis.

Results: Of the 26 cases reviewed from our institution, 30.8% were diagnostic of an organism on culture. Of the 8 positive cases, 6 had change in antibiotic therapy based on the bone culture results. Of the 8 cases with positive bone culture results, 6 had identical wound culture results. There was no change in long-term broad-spectrum antibiotic therapy in 16 of 26 cases. MRI positive findings for osteomyelitis showed a statistically significant association with antibiotic therapy ($p = 0.0004$) versus nonsignificance of culture positive results ($p = 0.428$). Statistical analysis performed with Microsoft Excel version 15.38.

Conclusion: From our study, appendicular image-guided biopsy is a relatively low-yield procedure, approximately 31% had positive culture results. In most cases bone biopsy plays a minor role in overall diagnosis and treatment, as approximately 70% of biopsies were negative with no change in overall treatment. Based on our review, MRI appears adequate to diagnose osteomyelitis with little value added when biopsy was performed. This calls into question whether an invasive biopsy and sedation is worth the cost and clinical risk to the patient.

Modality % - Radiography / Fluoroscopy:	25
Modality % - CT:	22
Modality % - MRI:	50
Modality % - US:	0
Modality % - Nuclear Medicine:	6

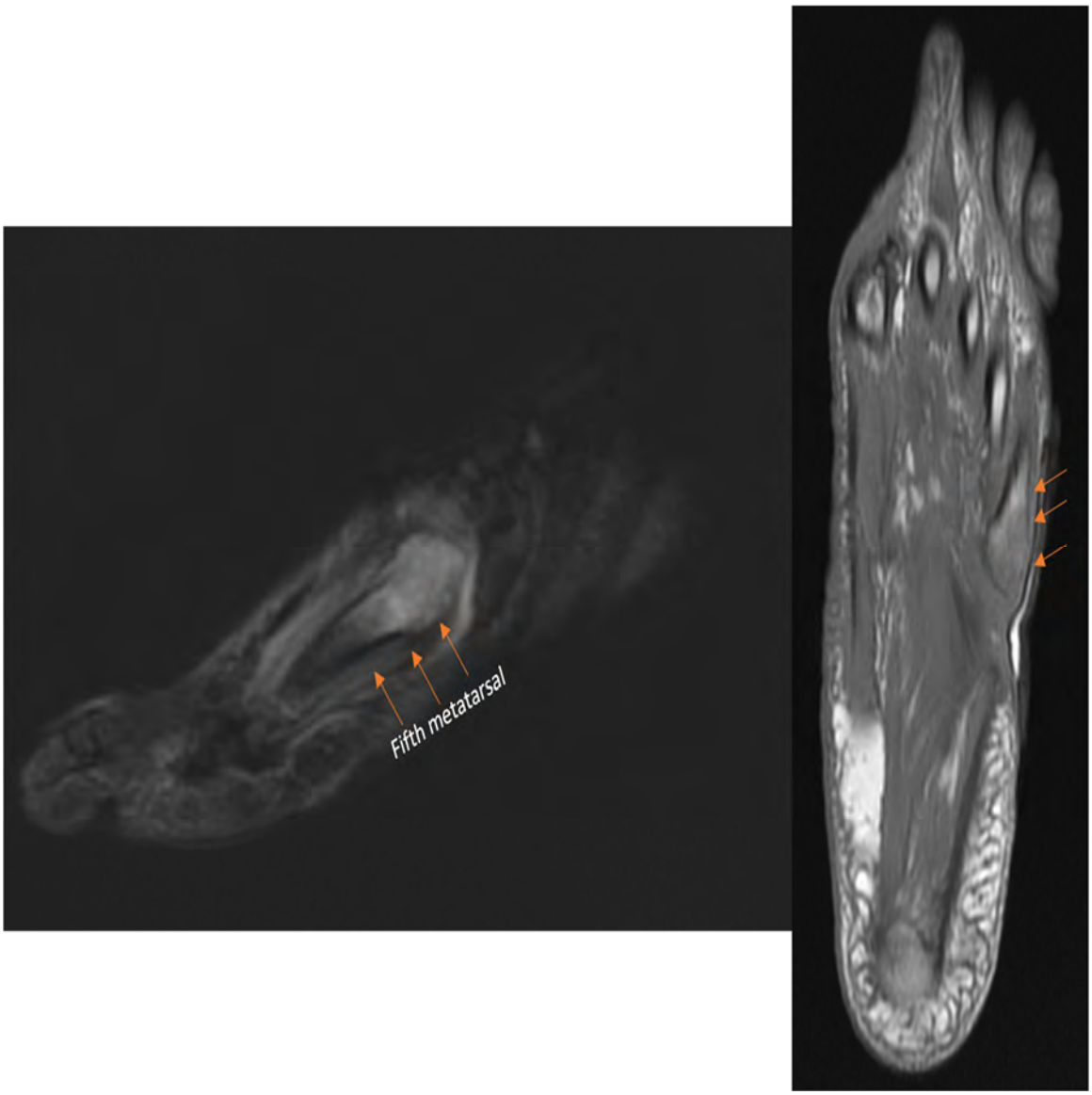

Sagittal STIR and Coronal T1-weighted images showing STIR-hyperintense and T1-hypointense marrow signal compatible with osteomyelitis.

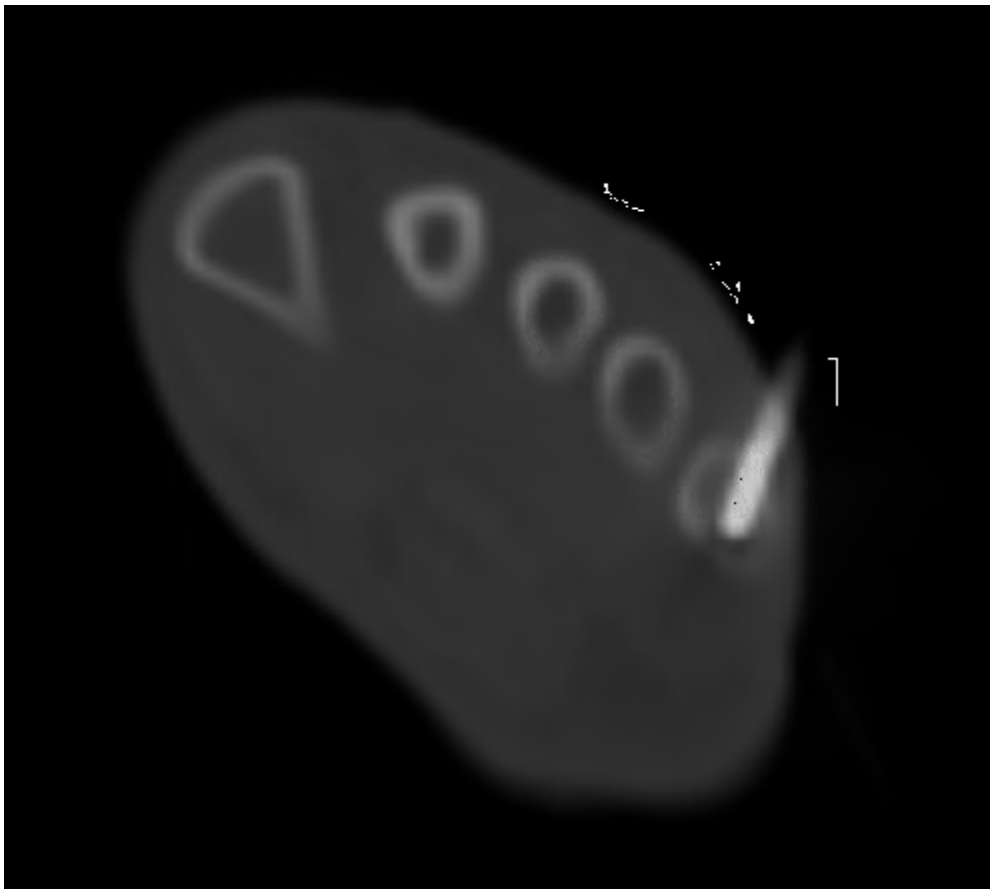

Axial intraoperative image displaying the biopsy needle within the fifth metatarsal base. This was diagnosed as osteomyelitis on the pre-procedural MRI.

Poster #14

THE POSTOPERATIVE MRI: IS IT TUMOR RECURRENCE OR NODULAR SCAR?

Lana Gimber, MD, MPH[1]; Samuel Oats, MD[1]; Lea MacKinnon, MD[1]; Mihra Taljanovic, MD, PhD[1]; James Warneke, MD[1]; Matthew Seidel, MD, MS[1]; Laura Fayad, MD[2]

[1]University of Arizona HCS - Tucson, Tucson, AZ, USA; [2]Johns Hopkins University, Baltimore, MD, USA

(Presented by: Lana Gimber, MD, MPH, University of Arizona HCS - Tucson)

Purpose: Magnetic resonance (MR) imaging is a routine part of postoperative surveillance in sarcoma patients. However, postsurgical inflammation/scarring can make it difficult to distinguish between postsurgical nodular scar versus tumor recurrence on MR images. In institutions where functional MR imaging is not routinely performed, these patients may undergo biopsy or short interval follow up imaging. This work-in-progress study helps to define routine MR characteristics which may assist radiologists in distinguishing postoperative nodular scar versus soft tissue sarcoma recurrence.

Materials and Methods: Patients with musculoskeletal sarcoma and MR imaging with T1-weighted, T2-weighted, and contrast-enhanced sequences after surgical resection were included retrospectively. Images were evaluated by a musculoskeletal radiologist for size, location, tissue layer, and MR features (signal intensity, heterogeneity, margin, and perilesional characteristics) of the nodular scar or recurrence on each sequence. Characteristics of nodular scar (defined by stability or histology) were compared with recurrence (defined histologically).

Results: Of 178 MR studies evaluated, 18 had sarcoma recurrence while 27 had nodular scars. Mean age of subjects was 45.7 years (range 3-91 years). Recurrences were significantly larger than nodular scars (mean=5.8 cm versus 2.3 cm; p=0.001). No significant difference was seen with location and tissue layer in addition to MR characteristics such as signal intensity and heterogeneity. More recurrent masses were identified on both T1 and T2-W images (p=0.002 and p=0.002). Nodular scars were more likely to show poorly-defined margins on T1 and T2-W images (p=0.004 and p=0.013) in addition to ill-defined perilesional enhancement (p=0.012) compared to recurrences.

Conclusion: MR features more strongly associated with sarcoma recurrence in the soft tissues included a larger size and more identifiable mass on noncontrast sequences. Alternatively, features associated with postoperative nodular scar included more poorly defined margins and ill-defined perilesional enhancement.

Modality % - Radiography / Fluoroscopy:	0
Modality % - CT:	0
Modality % - MRI:	100
Modality % - US:	0
Modality % - Nuclear Medicine:	0

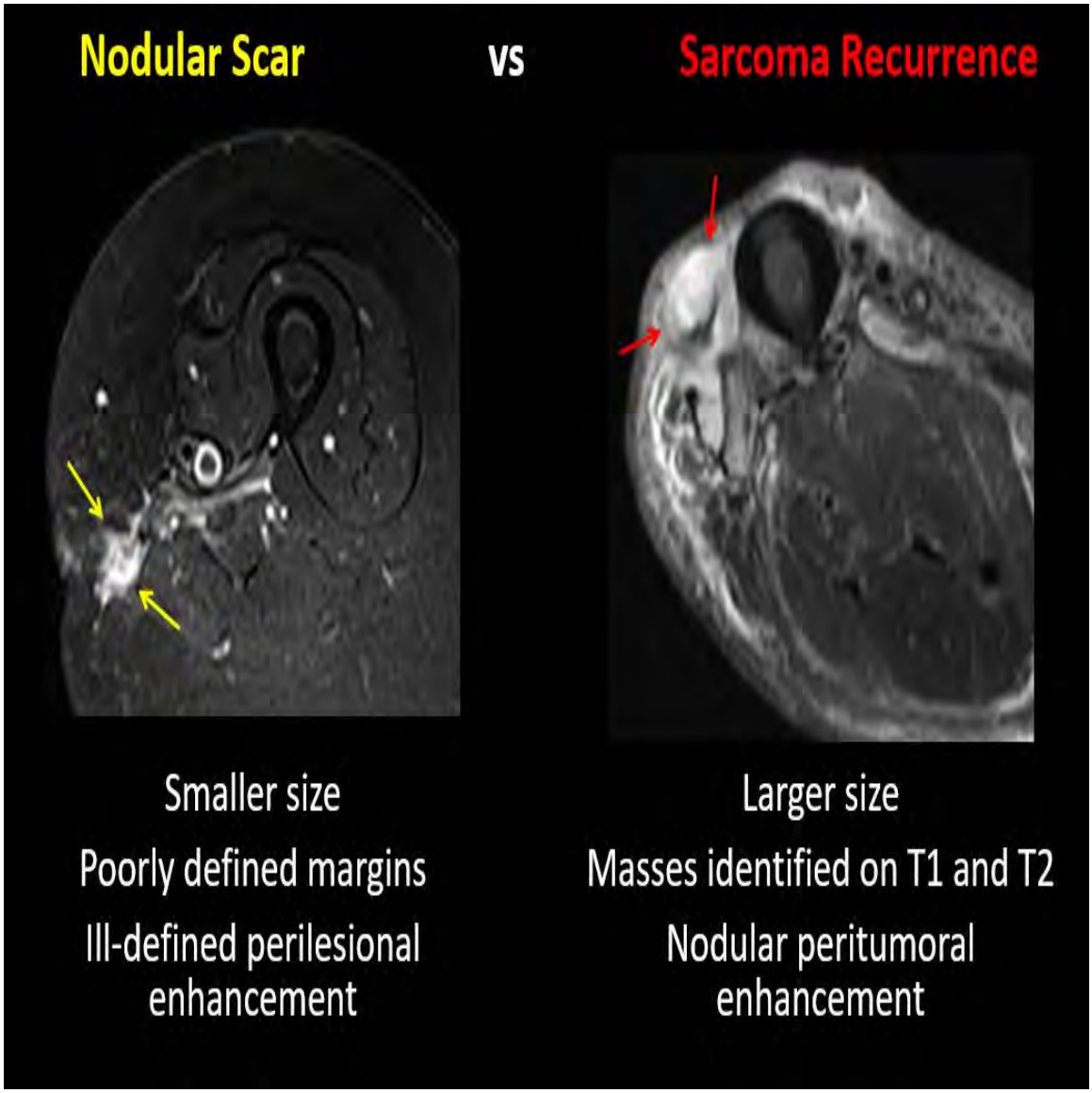

Routine MR features which may assist radiologists in distinguishing postoperative nodular scar versus soft tissue sarcoma recurrence.

Poster #15

CURRENT TRENDS IN MODALITY SELCETION FOR IMAGE-GUIDED MUSCULOSKELETAL PROCEDURES:FACTORS THAT INFLUENCE ULTRASOUND VERUS NON-ULTRASOUND UTILIZATION

Judah Goldschmiedt, MD; Danielle Williams, MD; Chaitanya Shilagani, DO
Westchester Medical Center, Valhalla, NY, USA
(Presented by: Judah Goldschmiedt, MD, Westchester Medical Center)

Purpose: To determine and describe current trends in selection of imaging modality for image-guided musculoskeletal procedures.

Materials and Methods: An anonymous online questionnaire was sent to members of the Society of Skeletal Radiology, inquiring about current patterns in clinical practice related to image guided and therapeutic joint injections. Shoulder and hip joints were chosen as clinical examples and were evaluated separately in relationship to several variables such as clinical practice experience, type(s) of subspecialty training, practice setting and modality chosen.

Results: In general, respondents seemed to strongly favor the use of fluoroscopy over ultrasound across studied variables (years in clinical practice, practice setting) for both shoulder and hip joint injections. Statistically significant differences in the proportion of ultrasound utilization was only observed with hip injections when compared across practice settings (academic, hybrid, and private practice; p=0.03), with ultrasound being performed at hybrid practice models at a rate of 16% (9/57). Otherwise, the proportion of ultrasound utilization did not differ across years of clinical experience or practice setting, when evaluated as independent variables or together.

Conclusion: Despite substantial support for the expansion of ultrasound as a desired guidance modality for musculoskeletal interventions, the majority of image guided shoulder and hip joint injections were primarily performed utilizing fluoroscopy. This may be a reflection of a deficiency in training or limited ultrasound availability in the reported academic, private practice or hybrid setting. Efforts to promote ultrasound training and implementation would be considered a worthwhile endeavor in order to promote this paradigm going forward.

Modality % - Radiography / Fluoroscopy:	85
Modality % - CT:	2
Modality % - MRI:	0
Modality % - US:	13
Modality % - Nuclear Medicine:	0

Practice Set	Years of Pra	Fluoroscop	Ultrasound	Total	Fisher Exact
Academic					p=0.94
n=166	0-5	43 (91)	4 (9)	47	
	6-10	38 (91)	4 (9)	42	
	11-20	35 (95)	2 (5)	37	
	>21	37 (93)	3 (7)	40	
Hybrid					p= 0.37
n=57	0-5	4 (67)	2 (33)	6	
	6-10	15 (83)	3 (17)	18	
	11-20	17 (94)	1(6)	18	
	>21	12 (80)	3 (20)	15	
Private					p=0.31
n=121	0-5	19 (86)	3 (14)	22	
	6-10	35 (95)	2 (5)	37	
	11-20	37 (97)	1 (3)	38	
	>21	22 (92)	2 (8)	24	

Tabulation of modality used by practice setting and clinical experience, shoulder injection only

Practice Set	Years of Pra	Fluoroscop	Ultrasound	Total	Fisher Exact
Academic					p=0.94
n=166	0-5	43 (91)	4 (9)	47	
	6-10	38 (91)	4 (9)	42	
	11-20	35 (95)	2 (5)	37	
	>21	37 (93)	3 (7)	40	
Hybrid					p= 0.37
n=57	0-5	4 (67)	2 (33)	6	
	6-10	15 (83)	3 (17)	18	
	11-20	17 (94)	1(6)	18	
	>21	12 (80)	3 (20)	15	
Private					p=0.31
n=121	0-5	19 (86)	3 (14)	22	
	6-10	35 (95)	2 (5)	37	
	11-20	37 (97)	1 (3)	38	
	>21	22 (92)	2 (8)	24	

Tabulation of modality used by practice setting and clinical experience, hip injection only

Poster #16

UTILITY OF CORE NEEDLE BIOPSY TO DIFFERENTIATE ANEURYSMAL BONE CYST FROM TELANGIECTATIC OSTEOSARCOMA

Benjamin Levine, MD; Vishal Hedge, MD; Kambiz Motamedi, MD; Leanne Seeger, MD; Scott Nelson, MD; Nicholas Bernthal, MD
University of California, Los Angeles, Los Angeles, CA, USA
(Presented by: Benjamin Levine, MD, University of California, Los Angeles)

Purpose: Telangiectatic osteosarcoma (TOS) and aneurysmal bone cysts (ABC) have similar clinical and imaging characteristics, yet completely different treatment algorithms. Obtaining pathologic diagnosis prior to definitive surgery is therefore critical. While there is acceptance of core needle biopsy (CNB) for evaluation of solid tumors, the current standard for diagnosis of ABC remains open surgical biopsy. Historically, there has been hesitation to use CNB for the diagnosis of ABC due mainly to concerns regarding its reliability in procuring cystic tissue. The purpose of this study was to evaluate: 1) the accuracy of CNB in differentiating ABC from TOS, and 2) the effectiveness of CNB as the initial procedure for suspected ABC.

Materials and Methods: Following IRB approval, a retrospective review of our pathology database (1990-2016) was performed using search criteria “aneurysmal bone cyst” and “telangiectatic osteosarcoma”. All cases were reviewed for the presence of an image guided CNB. CNB results were considered “effective” if they yielded pathology sufficient to proceed with definitive surgery without requiring open biopsy. CNB results were considered “accurate” if they were both effective and yielded pathology that matched the definitive surgical pathology.

Results: 92 CNB cases were identified during the study period. 19 cases were excluded due to absence of available final surgical pathology results. Of the 73 included cases, 81% (59/73) were effective. Of these effective cases, 93% (55/59) were accurate. Sensitivity and specificity for CNB was 89% and 100%, respectively. PPV was 1.00 and NPV was 0.82. There were no CNB related complications.

Conclusion: CNB is safe and highly accurate for distinguishing ABC from TOS. CNB is effective in guiding definitive surgical management without requiring additional open surgical biopsy. CNB should be used as the initial procedure of choice to distinguish ABC from TOS.

Modality % - Radiography / Fluoroscopy:	40
Modality % - CT:	25
Modality % - MRI:	25
Modality % - US:	10

Modality % - Nuclear Medicine: 

14 year old with a lytic lesion in the proximal tibia.

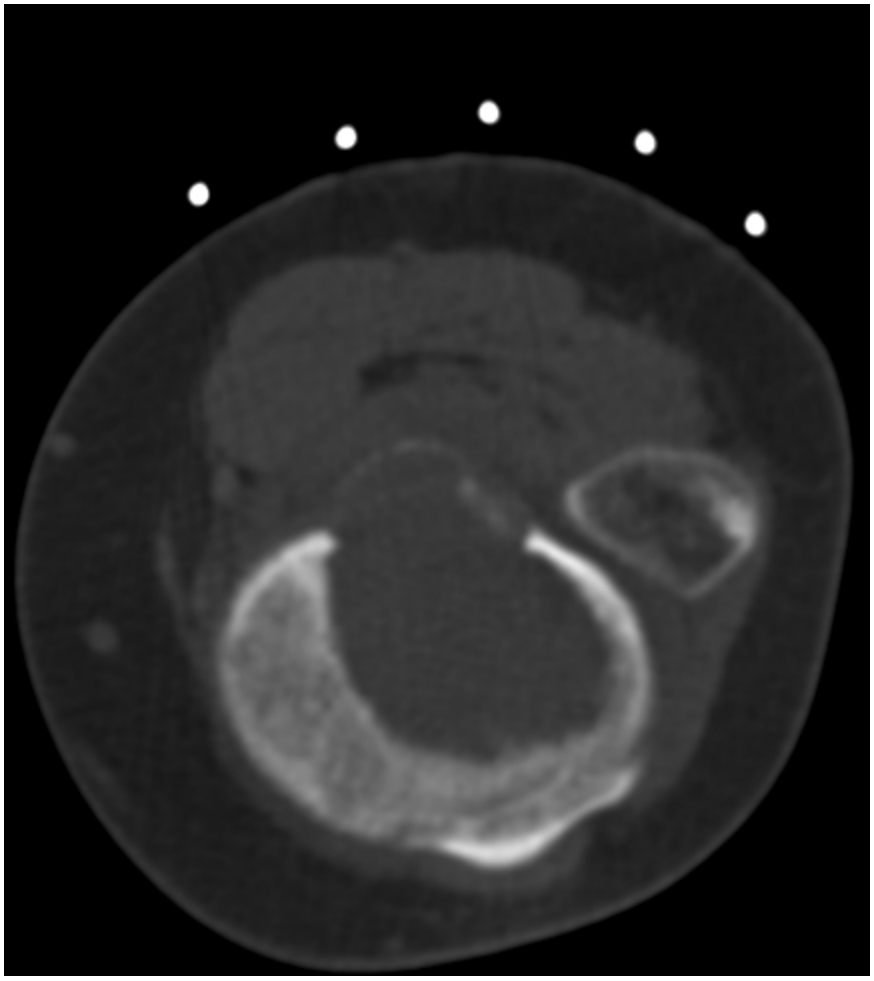

14 year old with CT showing the mildly expansile lytic lesion. Core needle biopsy revealed telangiectatic osteosarcoma.

Poster #17

DIAGNOSTIC YIELD OF ULTRASOUND GUIDED AND CT GUIDED SOFT TISSUE LESION BIOPSIES

Kambiz Motamedi, MD; Kim Lee, MD; Benjamin Levine, MD; Leanne Seeger, MD
David Geffen School of Medicine at UCLA, Los Angeles, CA, USA
(Presented by: Kambiz Motamedi, MD, David Geffen School of Medicine at UCLA)

Purpose: Our aim was to determine which factors may influence diagnostic yield of soft tissue lesion biopsies. Ultrasound (US) guided and computed tomography (CT) guided biopsies were analyzed.

Materials and Methods: A retrospective review of 100 consecutive US-guided soft tissue biopsies and 50 consecutive CT-guided soft tissue biopsies performed at a single institution in one year. Lesion location, size (0 to > 9 cm), fattiness (< or> 50%), depth (0 to > 4 cm), benignity/malignancy, and echotexture were collected. A biopsy was considered diagnostic, if it provided a clear pathologic diagnosis or was useful in guiding further clinical management.

Results: Diagnostic yields for US-guided, CT-guided, and both US and CT guided biopsies were 85%, 90%, and 87%, respectively.

US-guided biopsies: 73% (11/15) of the nondiagnostic biopsies were benign lesions. A malignant lesion was less likely to be nondiagnostic (OR: 0.3 CI: 0.2 – 0.4; $p < 0.05$)). Lesion depth, fattiness, echotexture, or position did not have a significant effect on diagnostic yield.

CT-guided biopsies: 80% (4/5) of the nondiagnostic biopsies were benign lesions and benign lesions were more likely to produce nondiagnostic results (OR: 0.3 CI: 0.2 – 0.4, $p = 0.00$).

Diagnostic yields between CT and US guided biopsies were not statistically different ($p = 0.7$). There were baseline statistical significant differences in distribution of lesion depths and sizes between CT and US. Fattiness did not significantly affect overall diagnostic yield for CT and US biopsies combined ($p = 0.18$).

Conclusion: With CT or US guidance, benign lesion biopsies are more likely to be nondiagnostic. Echotexture has no effect on diagnostic yield for US guided biopsies. There was no significant difference in diagnostic yield was detected between the two modalities.

Modality % - Radiography / Fluoroscopy:	0
Modality % - CT:	40
Modality % - MRI:	5
Modality % - US:	55

Modality % - Nuclear Medicine: 

CT guided biopsy of a fatty tumor. The nodular portion was targeted which was a myxoid liposarcoma.

US guided biopsy of a peripheral nerve sheath tumor. This was a schwannoma.

Poster #18

ULTRASOUND-GUIDED ASPIRATION OF INTRAMUSCULAR HEMATOMAS: EFFICACY AND RELATIONSHIP TO SONOGRAPHIC APPEARANCE

Edward Yoon, MD; Theodore Miller, MD; Susan Lee, MD
Hospital for Special Surgery, New York, NY, USA
(Presented by: Edward Yoon, MD, Hospital for Special Surgery)

Purpose: To evaluate the safety and efficacy of ultrasound-guided aspiration of intramuscular hematomas. To determine whether the sonographic appearance of intramuscular hematomas correlates with ease of aspiration.

Materials and Methods: An IRB waiver-approved, retrospective search of our radiology database was conducted using key words "hematoma" and "aspiration" between 1/1/2008 – 9/28/2017, performed by a single senior musculoskeletal radiologist specializing in musculoskeletal ultrasound. Procedure notes were reviewed to evaluate the following parameters: location, echogenicity on ultrasound, aspiration amount, aspirate consistency/quality, whether lavage was performed, needle gauge, immediate complications, and amount of decompression. Decompression was categorized as minimal (<25% decompression), mild (25-50%), moderate (50-75%), and complete (>75%). The medical record was reviewed to determine response to therapy and presence of long term complications.

Results: The cohort comprised 67 patients (32 F, 16-80 years) who had undergone ultrasound-guided hematoma aspiration, with no immediate complications. 47 patients returned for follow-up or other orthopedic/rheumatologic treatment. 23/47 patients returned for hematoma-specific follow up, with none reporting infection and all reporting symptomatic relief. One patient presented with hematoma re-accumulation after 2 weeks; repeat aspiration resulted in complete decompression. Decompression ranged from: minimal (6), mild (5), moderate (11), and complete (45). Of the completely decompressed hematomas, 6 (13%) were anechoic on ultrasound, 23 (47%) heterogeneously hypoechoic, and 18 (40%) complex. Needles used ranged from 13- to 20-gauge. Hematoma location included the arm, thigh, knee, calf, foot, and abdomen. Lavage was performed on 34 (50.7%) hematomas, with saline or lidocaine, when initial aspiration was unsuccessful secondary to clot/viscous blood; yielding 100% improved decompression.

Conclusion: Ultrasound-guided intramuscular hematoma aspiration is a safe and effective treatment. Sonographic appearance of the hematoma does not correlate to ease of aspiration/degree of decompression.

Modality % - Radiography / Fluoroscopy:	0
Modality % - CT:	0
Modality % - MRI:	0
Modality % - US:	100
Modality % - Nuclear Medicine:	0

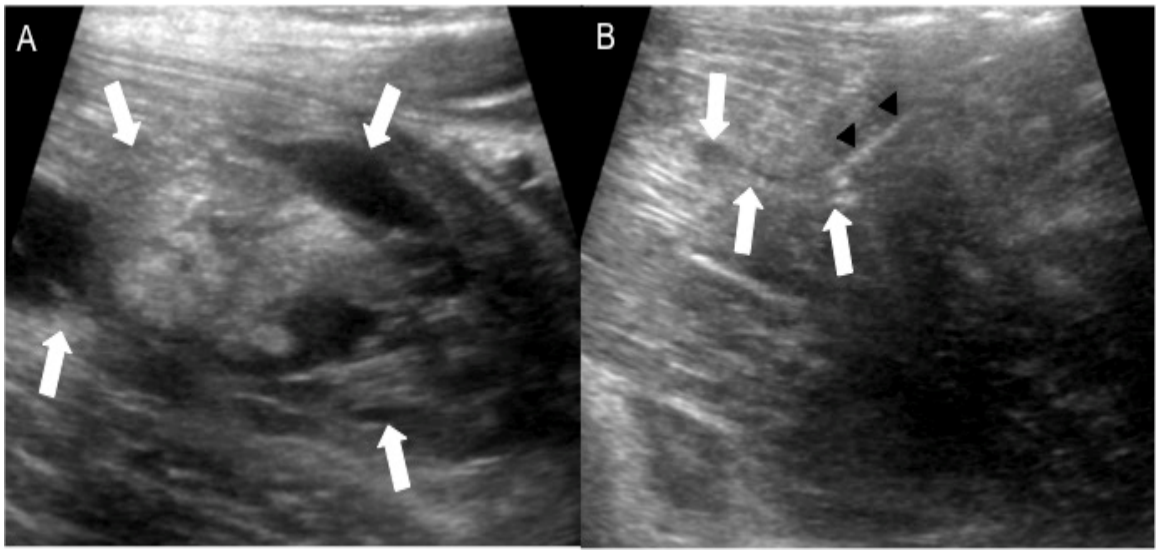

A. Complex intramuscular hematoma (arrows) of the pectineus demonstrates anechoic and hyperechoic regions. B. Aspiration with 13-gauge trochar needle (arrowheads) yielded complete decompression.

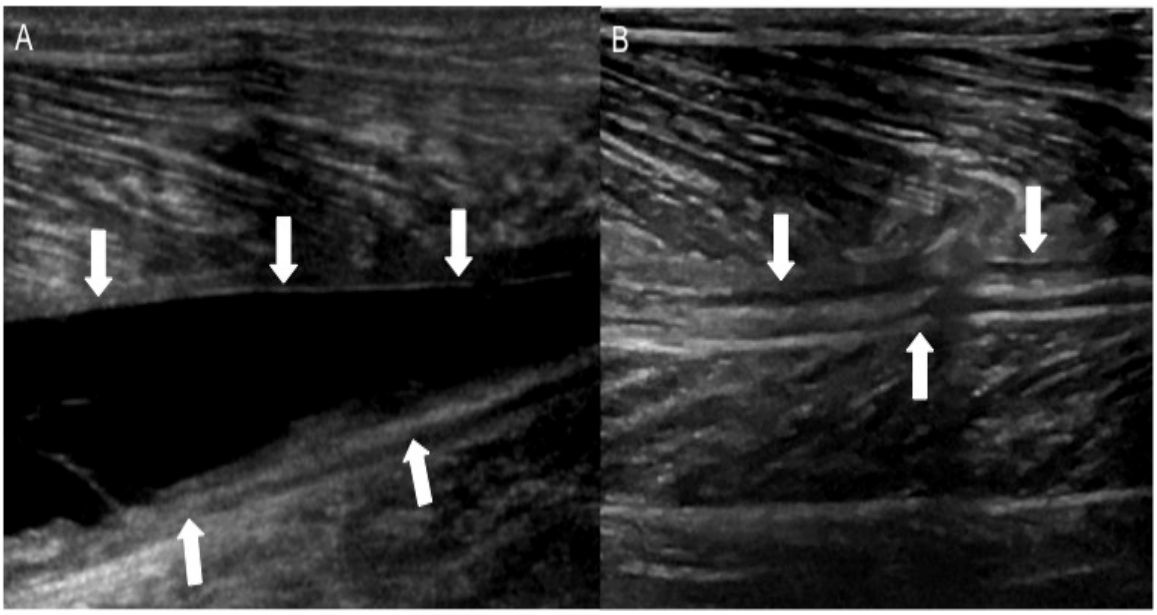

A. Simple, anechoic hematoma (arrows) at the myotendinous junction of the medial head of the gastrocnemius. B. Aspiration with 16-gauge needle yielded complete decompression.

Poster #19

COMPARISON BETWEEN IMAGE-GUIDED AND LANDMARK-BASED GLENOHUMERAL JOINT INJECTIONS FOR THE TREATMENT OF ADHESIVE CAPSULITIS: A COST-EFFECTIVENESS STUDY

Soterios Gyftopoulos, MD, MS[1]; Valentino Abballe, MD[1]; Mandeep Virk, MD[1]; James Koo, PhD[1]; Heather Gold, PhD[1]; Naveen Subhas, MPH, MD[2]

[1]NYU Medical Center/ Hospital for Joint Diseases Langone Medical Center, New York, NY, USA; [2]Cleveland Clinic, Cleveland, OH, USA

(Presented by: Soterios Gyftopoulos, MD, MS, NYU Medical Center/ Hospital for Joint Diseases Langone Medical Center)

Purpose: To determine the value of landmark-based and image-guided intra-articular steroid injections for the initial treatment of a population with the clinical diagnosis of adhesive capsulitis (AC).

Materials and Methods: Decision analytic model from the healthcare system perspective for 50-year-old patients with a history and physical examination findings consistent with AC to evaluate the incremental cost-effectiveness of three techniques to administer intra-articular steroid into the glenohumeral joint: landmark-based (blind), ultrasound guided (UG), and fluoroscopy-guided (FG). Comprehensive literature search and expert opinion provided input data on cost, probability and utility estimates. The primary effectiveness outcome was quality-adjusted life years (QALYs). Costs were estimated in 2017 U.S. dollars.

Results: UG injections were the dominant strategy for our base case, as it was the least costly ($1279) and most effective (.4096 QALYs) of the three options. Our model was sensitive to the probabilities of getting the steroid into the joint using blind, UG, and FG techniques, and UG and blind costs. Two-way sensitivity analyses demonstrated that UG injections were favored over blind and FG injections over a range of reasonable probabilities and costs. [a1] Probabilistic sensitivity analysis demonstrated that UG injections were cost-effective in 44% of simulations compared to 34% for blind injections and 22% for FG injections, and over a wide range of willingness-to-pay thresholds.

Conclusion: UG injections are the most cost-effective option for the steroid-based treatment of patients with adhesive capsulitis. Blind and FG injections can also be cost-effective options when performed by a clinician who is likely to accurately administer the medication into the correct location.

Modality % - Radiography / Fluoroscopy:	50
Modality % - CT:	0
Modality % - MRI:	0
Modality % - US:	50
Modality % - Nuclear Medicine:	0

Poster #20

CLINICAL AND PATIENT-REPORTED OUTCOMES AFTER IMAGE-GUIDED INTRA-ARTICULAR THERAPEUTIC HIP INJECTIONS: A RETROSPECTIVE STUDY

William Walter, MD[1]; Craig Bearison, BS[2]; James Slover, MD, MS[1]; Heather Gold, PhD[1]; Soterios Gyftopoulos, MD, MSc[1]
[1]NYU Medical Center/ Hospital for Joint Diseases Langone Medical Center, New York, NY, USA; [2]New York University School of Medicine, New York, NY, USA
(Presented by: William Walter, MD, NYU Medical Center/ Hospital for Joint Diseases Langone Medical Center)

Purpose: Patient-reported outcomes (PROs) are uncommonly and inconsistently measured for image-guided therapeutic procedures. Our study measures PROs before and after image-guided intra-articular hip injections to better define their value in hip pain management, and correlates outcomes with patient factors.

Materials and Methods: At a large academic center, 2,748 patients responded to surveys, including EQ5D, EQ5D-QOL, and the hip disability and osteoarthritis outcome score (HOOS), administered between 10/5/2011 and 8/10/2017, totaling 18,869 surveys. Retrospective review included 75 randomly selected patients' surveys, electronic medical records, and PACS images. Pre- and post-injection scores were compared and patient factors recorded, including age, BMI, and osteoarthritis severity (Tönnis classification). Time to repeat injection and hip surgery were recorded. Statistical methods included Wilcoxon signed rank test to assess score differences, and Spearman correlation and Mann-Whitney tests to assess correlation with patient and injection-specific factors.

Results: Seventeen patients completed surveys within 3 months prior to injection and post-injection surveys within 3-6 months after their first hip injection. The mean change in EQ5D scores (Δx=-0.045) was statistically significant (p=0.010). A positive correlation between age and ΔEQ5D-QOL (r=0.49, p=0.045) was found. No other significant differences in outcomes or correlations between survey score change and patient gender, BMI, osteoarthritis severity, or imaging modality were detected.

Conclusion: Our preliminary findings demonstrate a small, statistically significant decrease in EQ5D scores among patients receiving therapeutic hip injections at 3-6 months post injection. We will augment this preliminary data by review of the remaining 2,673 patients to increase statistical power to detect significant differences in outcomes or correlation with other predictive factors. This study emphasizes the importance of systematic, organized PROs research, an increasingly important tool for radiologists to remain effective custodians of the interventions we offer in the age of value-based care.

Modality % - Radiography / Fluoroscopy: 50
Modality % - CT: 0
Modality % - MRI: 0
Modality % - US: 50
Modality % - Nuclear Medicine: 0

		Pre		Post		Change	
Test	N	Mean±SD	IQR	Mean±SD	IQR	Mean±SD	p
EQ5D	17	0.676±0.18	0.24	0.631±0.19	0.36	-0.045±0.10	**0.010***
EQ5D_QOL	17	72.18±16.79	21.50	73.588±13.17	15.50	1.412±14.79	0.970
HOOS	11	54.27±17.67	17.80	55.655±19.94	25.60	1.382±9.54	0.849

The number of survey scores (N) and the mean, standard deviation (SD), and inter-quartile range (IQR) of each survey pre- and post-injection are shown as well as the changes in score with corresponding p-values.
*Indicates a significant p-value (<0.05), calculated by the Wilcoxon test.

Table 1. Pre- and post-injection outcomes scores for image-guide therapeutic hip injections

Poster #21

EFFICACY OF INTRA-ARTICULAR HIP STEROID INJECTION AND SUBSEQUENT SURGERY

Benjamin Levine, MD; Wilson Lai; Kambiz Motamedi, MD; Leanne Seeger, MD; Sharon Hame, MD
University of California, Los Angeles, Los Angeles, CA, USA
(Presented by: Benjamin Levine, MD, University of California, Los Angeles)

Purpose: Intra-articular hip steroid injections are widely used as an initial alternative to hip surgery. Identifying patient characteristics that could predict injection response is useful for guiding treatment management. Our study aimed to determine the duration of pain relief from fluoroscopic guided intra-articular hip steroid injections and the rate of subsequent hip surgery.

Materials and Methods: Following IRB approval, fluoroscopic-guided intra-articular hip injections performed at a single institution between January 2010 and December 2012 were reviewed. Response based on medical record review was divided into three groups: no relief, moderate response (<2 weeks of pain relief), and excellent response (>2 weeks of pain relief). Presence of hip surgery performed within 2 years following injection was collected. Data regarding age, gender, duration of symptoms, body mass index (BMI), radiographic Tönnis grade, and injection response were collected.

Results: 109 injections in 100 patients were analyzed. 18% (20/109) showed no response, 52% (57/109) showed moderate response, and 29% (32/109) showed excellent response. There was no significant correlation between injection response and age, Tönnis grade, BMI, or duration of symptoms. 49% of all patients had hip surgery within 2 years after initial injection. There was a significant association between higher Tönnis grades and higher surgery rates. There was no association between injection response and surgery rates.

Conclusion: The majority of patients obtain less than 2 weeks pain relief following fluoroscopic guided intra-articular hip steroid injection, based on this study. Gender, age, BMI, duration of symptoms, and radiographic severity of osteoarthritis do not predict injection response. Surgical rates within 2 years following hip steroid injection across all groups are relatively high, suggesting intra-articular hip steroid injections do not have a long-term effect.

Modality % - Radiography / Fluoroscopy:	100
Modality % - CT:	0
Modality % - MRI:	0
Modality % - US:	0
Modality % - Nuclear Medicine:	0

71 yo female, Tonnis grade 2 osteoarthritis

71 yo female who had moderate response to steroid injection and total hip arthroplasty within 2 years after injection.

Poster #22

VALUE OF PRE-OPERATIVE FLUOROSCOPIC-GUIDED SUBTALAR ARTHROGRAPHY

Richard Walker, MD, FRCPC; Rachael Da Cunha, MD, FRCSC; Jason Boubalos, MD; Tara Heric, RN; Jeremy Lamothe, MD, PhD, FRCSC; Ian Le, MD, FRCSC
University of Calgary, Calgary, AB, Canada
(Presented by: Richard Walker, MD, FRCPC, University of Calgary)

Purpose: We report a single centre experience incorporating fluoroscopic-guided diagnostic and therapeutic subtalar arthrography in the pre-operative assessment of patients with subtalar osteoarthritis (OA) undergoing consideration for surgical arthrodesis.

Materials and Methods: Patients with symptomatic subtalar arthritis presenting for pre-operative assessment by an orthopedic foot and ankle surgeon were recruited from January 2014 through June 2016. All subjects completed an American Orthopedic Foot & Ankle Society (AOFAS) Hindfoot Score, baseline 50-foot walk time test and pain score on visual analogue scale (VAS). Subjects subsequently underwent fluoroscopic-guided subtalar injection using an anterolateral approach performed by a single musculoskeletal radiologist. Procedural time, fluoroscopy time, number of attempts, procedural success, and communication with regional articulations or soft-tissue extravasation was recorded. 10-minutes following the procedure the 50-foot walk time test and VAS pain score were recorded.

Results: 21 subjects were enrolled in the study, with one subject undergoing 2 ipsilateral injections and another 3 ipsilateral injections. 6 subjects were excluded resulting in 18 procedures in 15 subjects for analysis. The average age was 51 years and the right foot was symptomatic in 9 subjects. The most common aetiology was post-traumatic OA (60%), the average duration of symptoms 8.5 years (range 1 to 40), and the average AOFAS Hindfoot Score was 49.3 (range: 17 to 79). The subtalar arthrogram was successful on the first attempt in 89% of cases, and 94% overall. Average fluoroscopy time was 0.99 minutes and overall procedural time 11.3 minutes. The VAS pain score decreased 2.2 from baseline following the injection and the 50-foot walk time test decreased by 6.1 seconds. No procedural complications were recorded.

Conclusion: In our experience, diagnostic subtalar arthrography using an anterolateral approach can be reliably performed in patients with symptomatic subtalar OA and is an important adjunctive tool when considering subtalar arthrodesis.

Modality % - Radiography / Fluoroscopy:	100
Modality % - CT:	0
Modality % - MRI:	0
Modality % - US:	0
Modality % - Nuclear Medicine:	0

Poster #23

MRI OF THE LUMBOSACRAL PLEXUS: WHAT THE PRACTICING RADIOLOGIST NEEDS TO KNOW

Hailey Allen, MD; Megan Mills, MD; Miriam Peckham, MD; Lubdha Shah, MD; Kent Sanders, MD; Sarah Stilwill, MD
University of Utah Medical Center / SOM, Salt Lake City, UT, USA
(Presented by: Hailey Allen, MD, University of Utah Medical Center / SOM)

Purpose: To prepare radiology residents and aid the practicing radiologist in interpreting pathology encountered on MR imaging of the lumbosacral plexus.

Materials and Methods: The learner will be presented with a structured approach to identifying the key anatomic structures of the lumbosacral plexus on MR images, as well as a suggested search pattern for sequences obtained as part of a dedicated lumbosacral neurogram protocol. Upon completion of the exhibit, the learner should be proficient in recognizing the direct and indirect MR findings of commonly encountered lumbosacral plexus pathology.

A. **Results:** Lumbosacral Plexus Normal Anatomy and Important Variants
B. Lumbosacral Plexus MRI Protocol Review
C. Systematic MRI search pattern
D. Case based imaging review of the following topics, including distinguishing MR imaging features of each entity, with direct and indirect imaging findings.
    a. Trauma
    b. Infectious and Inflammatory Pathology
    c. Congenital
    d. Tumor and Tumor-Like Conditions

Conclusion: A robust understanding of anatomy in combination with a systematic sequence-based approach to MRI interpretation is key to the identification and characterization of pathology involving the lumbosacral plexus.

Modality % - Radiography / Fluoroscopy:	0
Modality % - CT:	0
Modality % - MRI:	100
Modality % - US:	0
Modality % - Nuclear Medicine:	0

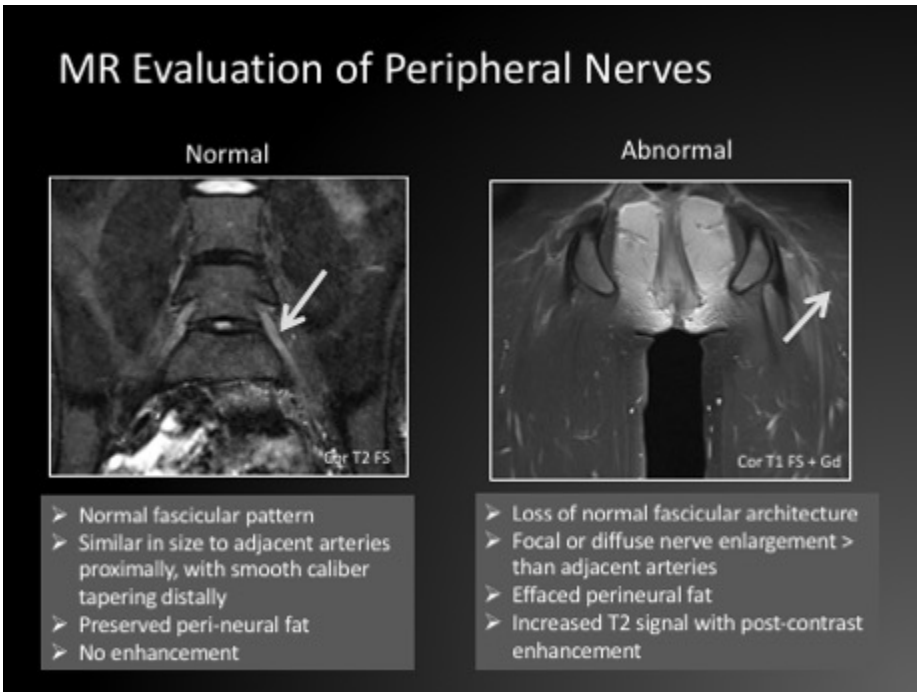

MRI Evaluation of Peripheral Nerves: Normal and Abnormal

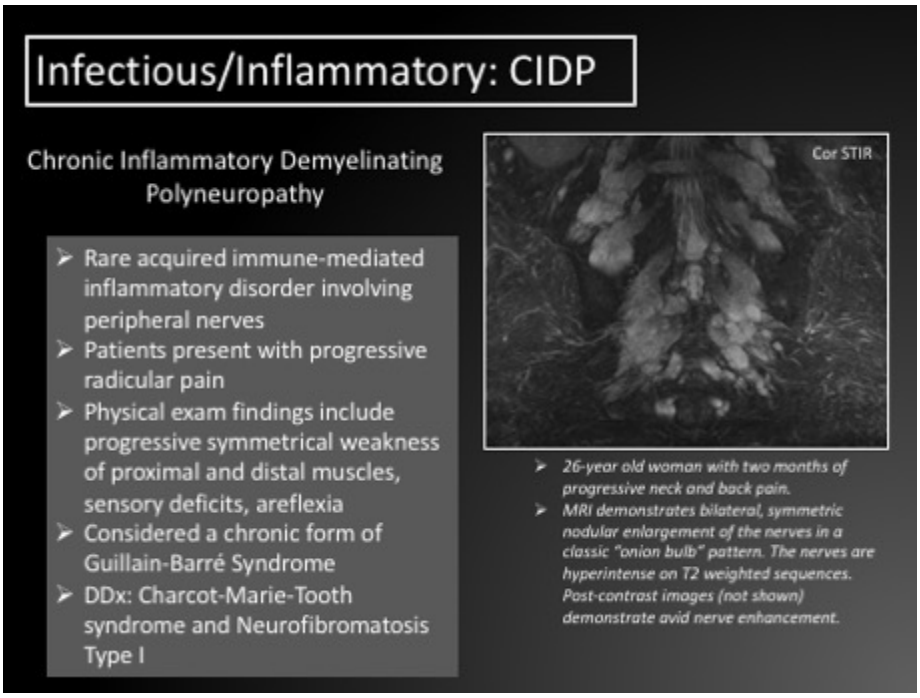

Infectious/Inflammatory Pathology: Chronic Inflammatory Demyelinating Polyneuropathy

Poster #25

MUSCLE BULK DIFFERENCES IN FAI AND HIP INSTABILITY VERSUS CONTROLS

Avneesh Chhabra, MD
University of Texas Southwestern Medical Center at Dallas, Flowermound, TX, USA
(Presented by: Avneesh Chhabra, MD, University of Texas Southwestern Medical Center at Dallas)

Purpose: Evaluate differences in muscle perimeter and area in patients with FAI, dysplasia and controls.

Materials and Methods: Patients with 3DCT between 2012 and 2017 and a final diagnosis of hip dysplasia or FAI were chosen and compared with controls. All scans were analyzed for muscle bulk in the iliopsoas, rectus femoris, gluteus medius and gluteus minimus. Mean differences were compared between control, instability, and impingement groups using analysis of variance model. Tukey adjustment and ROC analysis was used.

Results: 25 cases of FAI (age= 31+/-7.4), 16 cases of dysplasia (age= 29.9 +/-9.0), and 38 controls (age= 41.7 +/- 7.8) were analyzed. Control patients had significantly lower gluteus medius perimeter (p=0.032), psoas area (p=0.028), gluteus minimus perimeter (p=0.004), rectus femoris area (p=0.014) and rectus femoris perimeter (p=0.036) than impingement cases. Patients with impingement had higher gluteus medius perimeters (p=0.003) and gluteus minimus perimeters (p=0.043) than those with instability. Controls had smaller muscle measurements in all four muscles measured, though not all were significant. Abnormal hips of FAI cases had smaller muscle areas when compared to the contralateral normal hips, though none reached statistical significance. Abnormal hips of dysplasia had smaller muscle areas in the iliopsoas than the contralateral normal hips, though this did not reach statistical significance. Rectus femoris had the highest AUC for detecting impingement/instability from control subjects (AUC=0.64).

Conclusion: Muscle analysis was able to quantify differences between patients with FAI, dysplasia and controls. Perhaps this could indicate either a muscle imbalance contributing to the pathology or that the mild muscle atrophy stems from the painful symptoms and decreased use in the pathological hip. If muscle atrophy is present before hip pathology, this could present a way for physicians to encourage strength training to avoid future complications in FAI including both surgery and osteoarthritis.

Modality % - Radiography / Fluoroscopy:	5
Modality % - CT:	95
Modality % - MRI:	0
Modality % - US:	0
Modality % - Nuclear Medicine:	0

Poster #26

A COMPREHENSIVE REVIEW OF PROXIMAL FEMORAL FRACTURES AND THEIR COMPLICATIONS

Kimia Kani, MD[1]; Hyojeong Mulcahy, MD[2]; Jack Porrino, MD[2]; Felix Chew, MD[2]
[1]University of Maryland School of Medicine, Baltimore, MD, USA; [2]University of Washington / Harborview Medical Center, Seattle, WA, USA
(Presented by: Kimia Kani, MD, University of Maryland School of Medicine)

Purpose: Hip fractures are most common in the elderly. Early detection and correct imaging classification of hip fractures are prerequisites to early appropriate therapy. The risk of death and major morbidity is significantly increased in the elderly with hip fractures, especially with delayed treatment.

Materials and Methods: Educational goals:

1. Describe pertinent proximal femoral anatomy (with a focus on vascular anatomy)
2. Categorize proximal femoral fractures (PFFs)
3. Recognize the different imaging patterns of traumatic versus stress fractures in each location
4. Describe the most common treatment oriented classifications (along with their underlying rationale) for the different types of PFFs

Recognize the roles of different imaging modalities in prereduction, postreduction and post-surgical stages of patient management

Results: Key issues:

1. Intracapsular PFFs (femoral head; subcapital and transcervical femoral neck fractures) can potentially compromise femoral head blood flow
2. Avascular necrosis and nonunion are the primary concerns for intracapsular PFFs
3. Acute fracture instability and malunion are the primary concerns for extracapsular PFFs
4. Femoral head fracture-dislocations are most commonly classified based on morphology of femoral head fracture and presence or absence of femoral neck or acetabular fractures
5. Femoral neck fractures are commonly classified on prereduction imaging in the elderly (Garden classification) and on postreduction imaging in younger adults (Pauwels system)
6. The most common classification system of intertrochanteric fractures is based on location and direction of fracture line along with degree of comminution and displacement of the fracture fragments
7. Insufficiency fractures usually demonstrate typical morphologic features and locations in each of the femoral head, neck and subtrochanteric regions

Conclusion: Early detection and correct imaging classification of hip fractures is necessary for appropriate early treatment and decreased complication rates.

Modality % - Radiography / Fluoroscopy:	60
Modality % - CT:	20
Modality % - MRI:	20
Modality % - US:	0
Modality % - Nuclear Medicine:	0

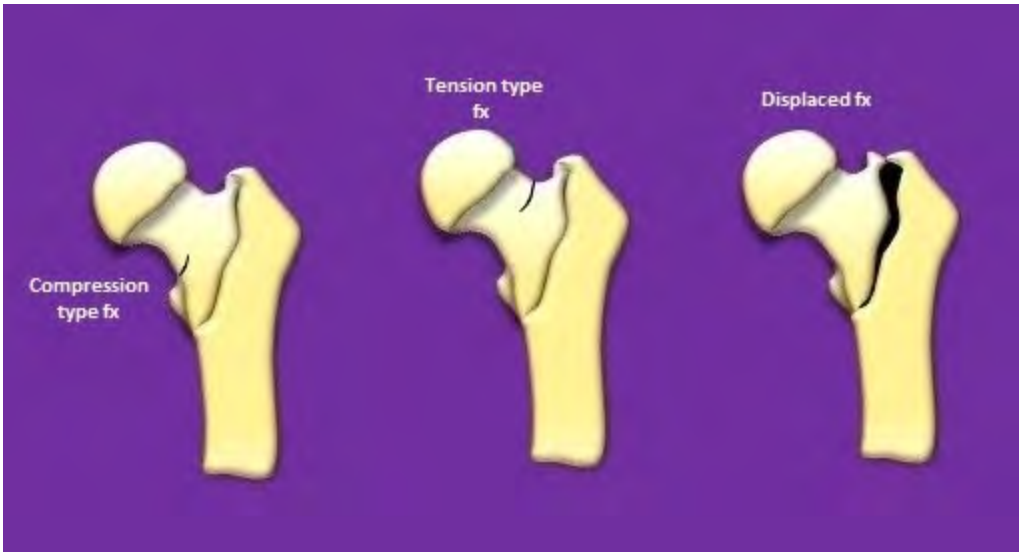

Fig. 1: Femoral neck stress fractures
Fig. 2: Atypical subtrochanteric insufficiency fracture

Poster #27

ULTRASOUND FOR THE EVALUATION OF RADIAL NERVE PATHOLOGY: CORRELATION TO MRI FINDINGS

Edward Yoon, MD; O. Nwawka, MD
Hospital for Special Surgery, New York, NY, USA
(Presented by: Edward Yoon, MD, Hospital for Special Surgery)

Purpose: MRI and ultrasound are both modalities of choice to evaluate for peripheral nerve pathology. There are few small studies that have compared MRI and US for peripheral nerve pathology, demonstrating comparable sensitivity and specificity. Our study aims to specifically compare US assessment of radial nerve pathology to MRI.

Materials and Methods: Following IRB approval, search of our institution's radiology information system was performed between 7/1/2014-6/30/2017 using the search terms "radial nerve ultrasound". From the search yield, examinations with concurrent peripheral nerve MRI and EMG-confirmed radial neuropathy were selected. These reports were reviewed to assess for concordance with MRI findings.

Results: Out of 62 ultrasound examinations, 42 had concurrent MRI of the radial nerve performed at our institution, and EMG-confirmed radial neuropathy. 31 cases demonstrated concordance between US and MRI findings. Reasons for discordance included poor visualization of the radial nerve on MRI due to adjacent metallic hardware, and detection of radial nerve enlargement due to contralateral side imaging comparison on US. Of the 42 patients, 31 had concurrence between the MRI and Ultrasound findings. Of note, MRI reports were shown to describe muscle denervation effects more frequently than US.

Conclusion: Our findings show that US and MRI demonstrate good concordance in the evaluation of radial neuropathy. Additional benefits conferred by ultrasound are related to decreased susceptibility to metallic artifact, and ease of contralateral side imaging for comparison of nerve size. MRI appears to be able to more readily detect denervation change in radial nerve innervated muscles.

Modality % - Radiography / Fluoroscopy:	0
Modality % - CT:	0
Modality % - MRI:	47
Modality % - US:	50
Modality % - Nuclear Medicine:	0

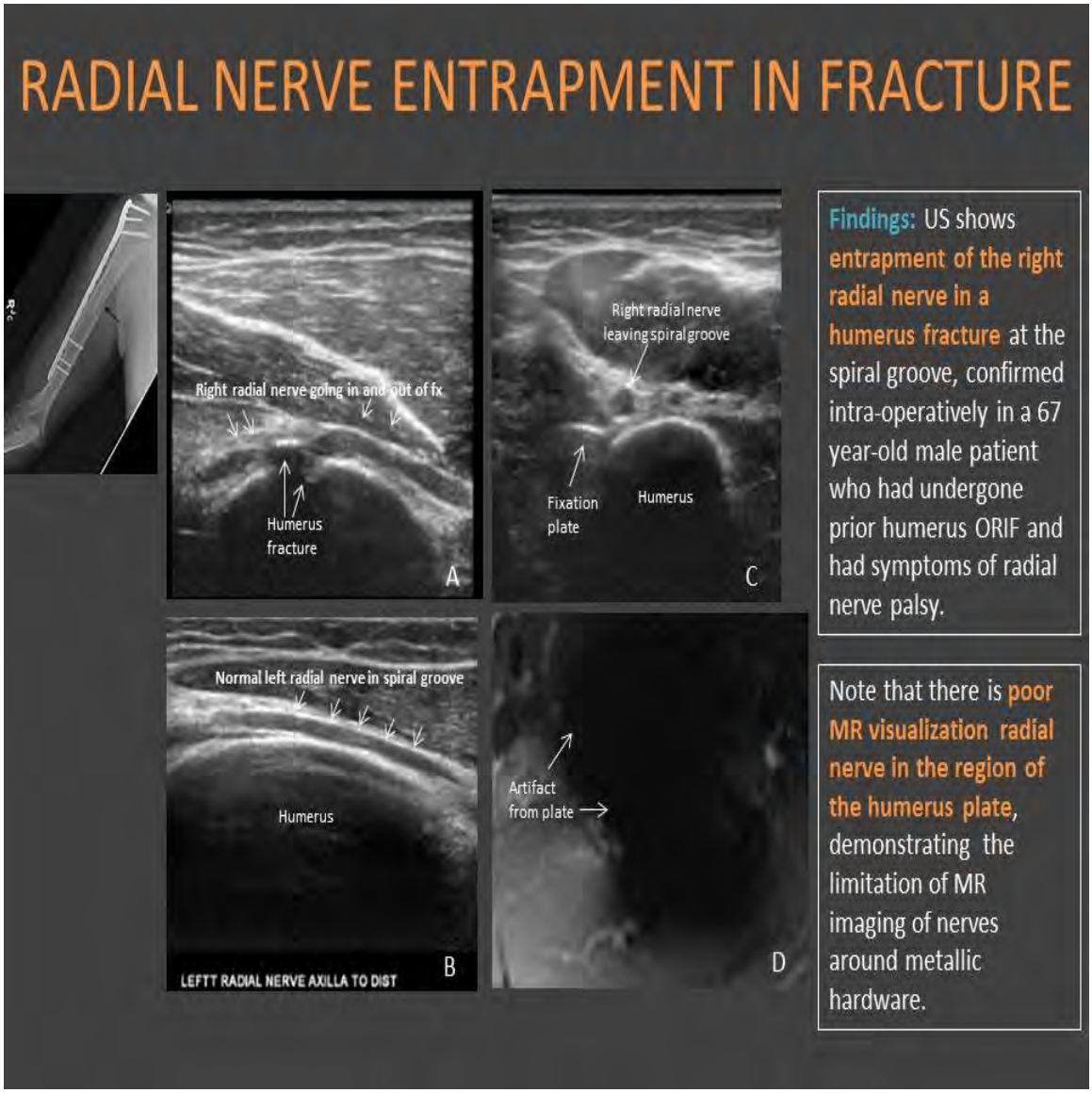

Figure 1: Radial nerve entrapment in humerus fracture.

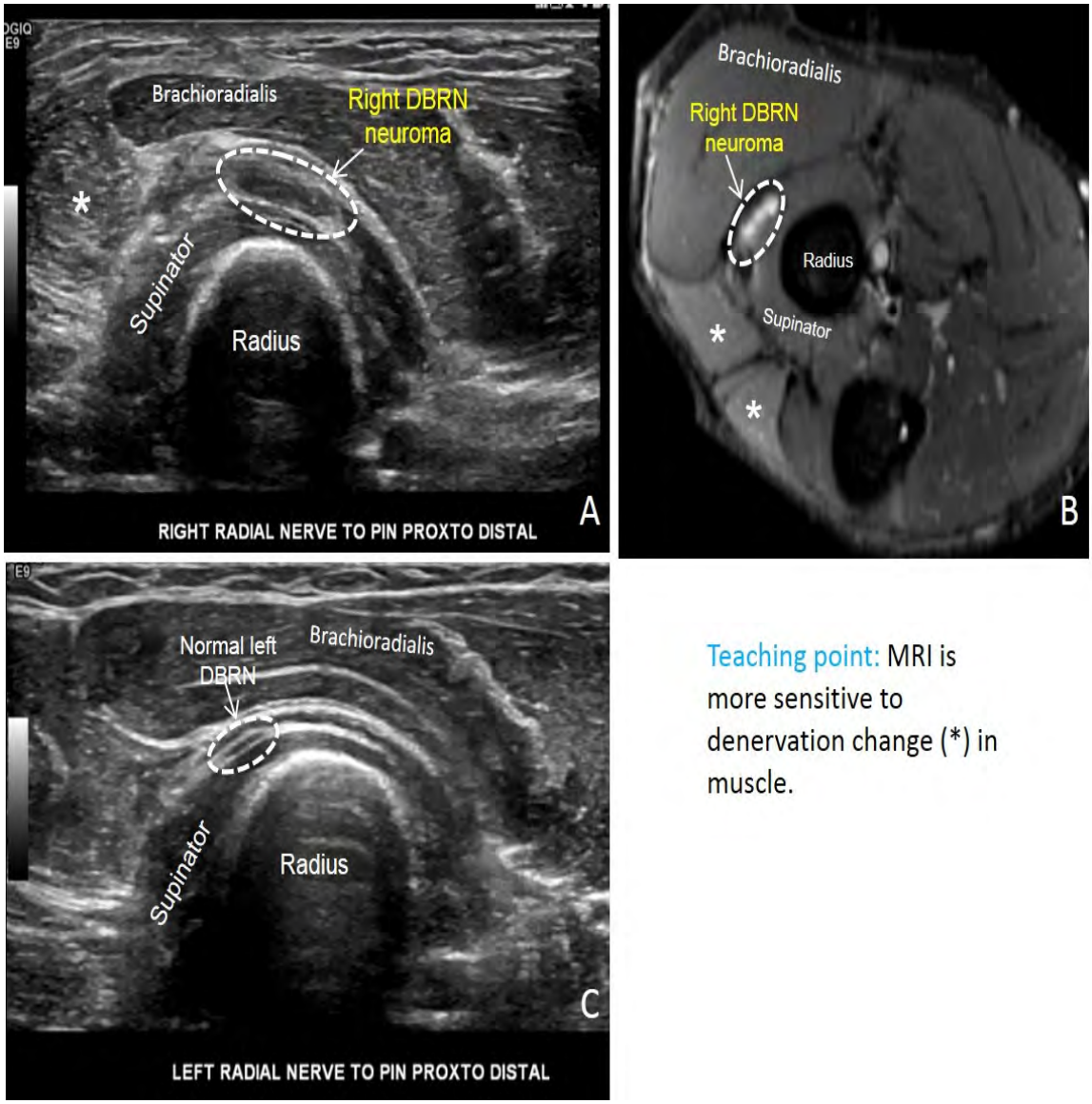

Figure 2: Deep branch of the radial nerve neuroma on US and MRI.

Poster #28

UTILITY OF MRI IN EVALUATING FOR OSTEOMYELITIS IN PATIENTS WITH CELLULITIS

Devon Klein, MD[1]; Brian Lee, MD[2]; Hariklia Bezhani, DPM[1]; Guillaume Stoffels, MS, MA[1]
[1]Lenox Hill Hospital, Northwell Health, New York, NY, USA; [2]Beth Israel Deaconess Medical Center Harvard Med School, Boston, MA, USA
(Presented by: Devon Klein, MD, Lenox Hill Hospital, Northwell Health)

Purpose: To assess the rates of OM in patients presenting with cellulitis with or without clinical features such as skin ulcers, comorbitiies and patient demographics.

Materials and Methods: We reviewed all MRIs of the lower extremity prerformed for evaluation of OM in patients with cellulitis over a 5 year periord. Only adult patients,were included. This resulted in 488 MRI examinations. 47 examinations were excluded.

The MRI reports were reviewed, looking for the presence or absence of osteomyelitis, abscess, and ulceration. Demographic information collected from the EMR included age, sex, diagnosis of diabetes, hyperlipidemia/ atherosclerotic disease, and/or peripheral vascular disease.

Univariable analyses were conducted to identify factors that might be associated with OM. A multivariable analysis, based on a logistic regression model, was carried out to determine which factors were associated with OM, when all proposed factors were considered simultaneously.

Results: Of the 441 included cases, 170 (39%) established a diagnosis of OM on the basis of the MRI findings. 236 (54%) had demonstrable ulceration on MRI, 66 (15%) had an abscess and 307 (70%) had the diagnosis of cellulitis by MRI.

Those with MRI findings of OM (170) and those without (271), there was no statistical difference for variables such as age ($p = 0.40$), laterality ($p = 0.69$), reporting physician ($p = 0.14$), patient class ($p= 0.19$). ,There was a statistically significant difference in rates of OM by gender, $p=0.0003$ in patietnts with diabietes,($p<0001$), hyperlipidemia/atherosclerotic disease ($p=0.001$ and those with ulceration by MRI ($p<0.0001$). No difference in rates of OM could be found in patients with documented PVD ($p=0.78$).

Conclusion: The perception that uncomplicated cellulitis often leads to underlying OM is not supported by this study.

Modality % - Radiography / Fluoroscopy:	0
Modality % - CT:	0
Modality % - MRI:	100
Modality % - US:	0
Modality % - Nuclear Medicine:	0

Sag STIR imaging demostrates ulceration at plantar tip of hallux. The marrow of the distal phalanx is diffuesely replaced by signal hyperintensity

On T1 weighted imaging the marrow fat is replaced by hypointense signal and lss of the cortical margins is more conspicuous.

Poster #29

MUSCLE EDEMA - RECOGNIZING PATTERNS AND ASSOCIATED CAUSES

Sailaja Yadavalli, MD, PhD; Michael Hierl, MD; David Marcantonio, MD
Beaumont Health System, Royal Oak, MI, USA
(Presented by: Sailaja Yadavalli, MD, PhD, Beaumont Health System)

Purpose: The focus of the exhibit is to provide an educational review of edema patterns seen in muscles on Magnetic Resonance Imaging (MRI) due to various causes, correlating them with associated findings within the muscles or adjacent structures and with relevant clinical history in order to make an accurate diagnosis.

Materials and Methods: The exhibit will utilize a case based format to review muscle edema patterns and distribution that may be seen on MRI due to various clinical entities including, but not limited to, infectious, inflammatory and neoplastic processes, trauma and nerve injuries. Description of additional pathology within the muscles and adjacent structures will also be included in the discussion. Where needed clinical history and data will also be highlighted to illustrate how these may help in making a diagnosis or in narrowing the differential. The discussion will also include the benefits of utilizing intravenous contrast or other imaging modalities such as radiography, ultrasound or CT when appropriate.

Results: Muscle edema is often seen on MRI in everyday practice. The cause of the edema signal may not be readily apparent, resulting in delayed or wrong diagnosis or unnecessary intervention. Many causes of muscle edema may be recognized by the pattern and distribution such as with denervation injuries. Recognizing associated findings such as in the cases of myositis ossificans and correlating with radiographs or CT may be important in making the correct diagnosis. Distinguishing between boundaries of a tumor and related reactive edema is important in the staging process. These are just a few examples of cases that will be presented in the exhibit.

Conclusion: Awareness and understanding of edema patterns in muscles on MRI and knowledge of associated findings are important for the Radiologist to make an accurate diagnosis and avoid delay in treatment or unnecessary interventions.

Modality % - Radiography / Fluoroscopy:	5
Modality % - CT:	5
Modality % - MRI:	85
Modality % - US:	5

Modality % - Nuclear Medicine:

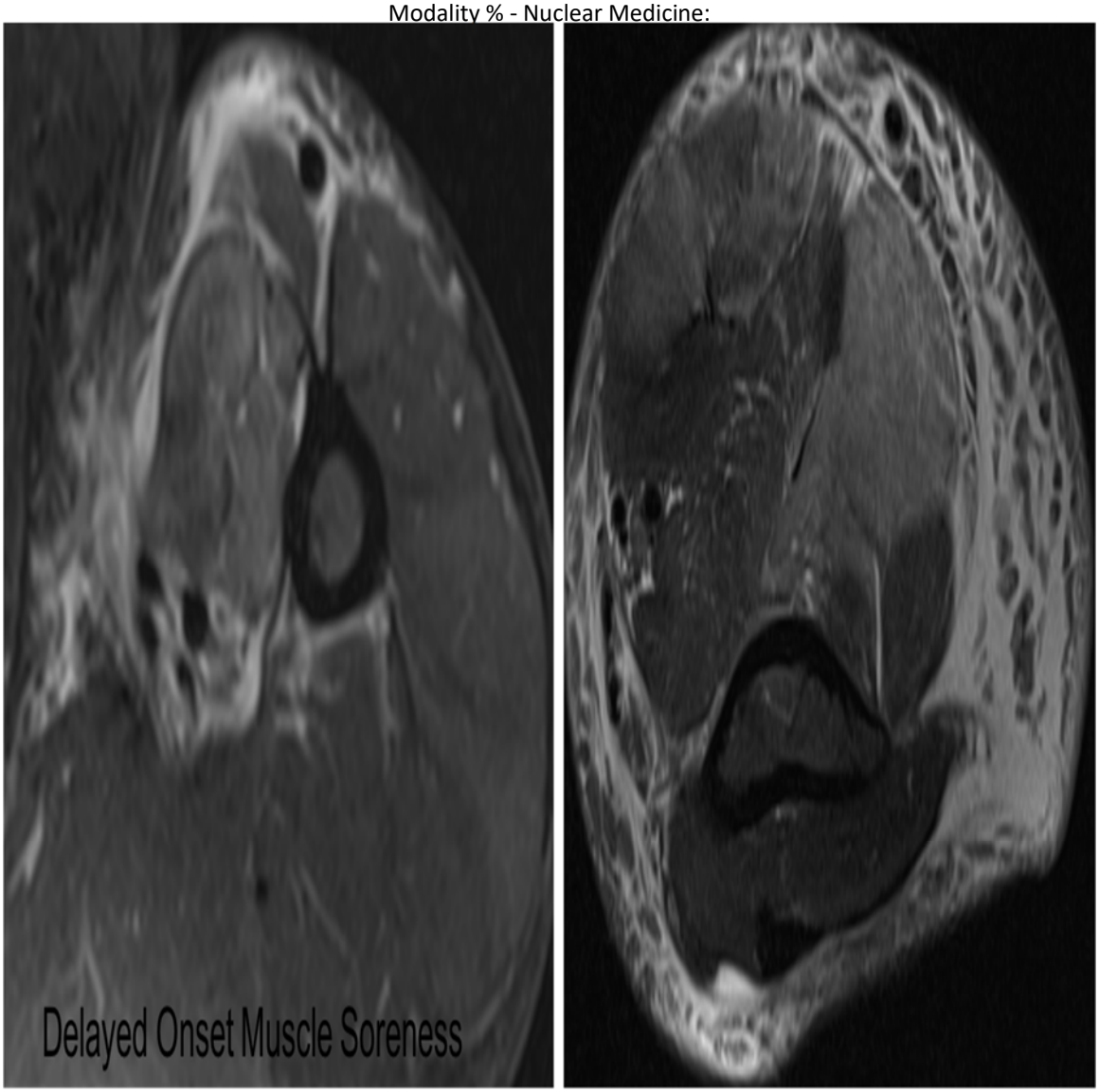

Figure 1: T2 FS Axial: Upper arm edema developed in a construction worker a few days after lifting weights and breaking cement the next day.

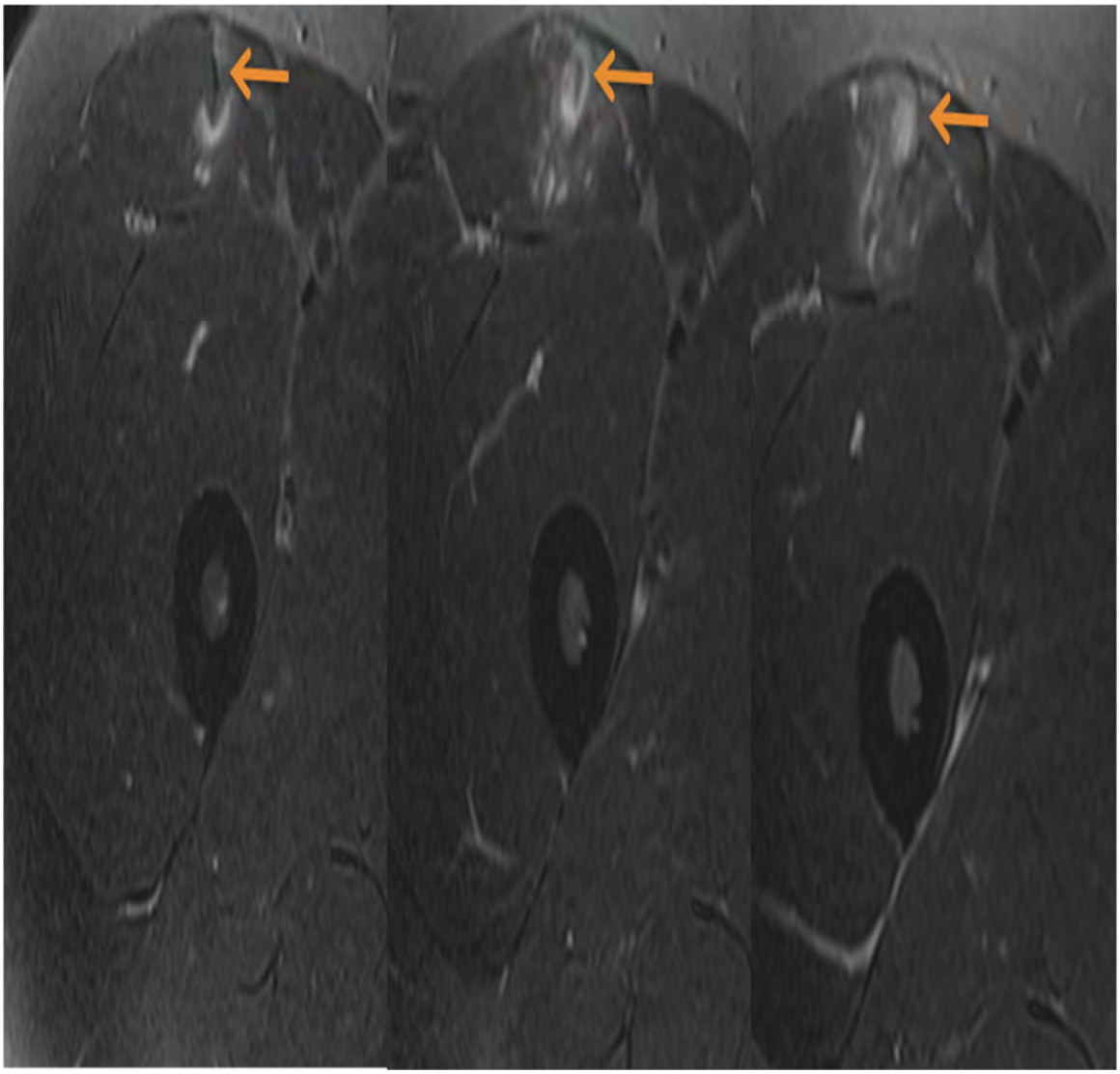

Figure 2: T2 FS Axial: Edema in the rectus femoris muscle secondary to intramuscular degloving injury.

Poster #30

CALCIUM HYDROXYAPATITE DEPOSITION DISEASE: A MULTI-MODALITY REVIEW FOR THE PRACTICING RADIOLOGIST AND RADIOLOGIST IN TRAINING, WITH EMPHASIS ON CLINICAL PRESENTATION, PATHOGENESIS AND IMAGING APPEARANCE.

Jason Esterle, MD; David Marcantonio, MD; Christopher Nall, MD
Beaumont Health System, Royal Oak, MI, USA
(Presented by: Jason Esterle, MD, Beaumont Health System)

Purpose: To review and highlight the calcium hydroxyapatite deposition disease (HADD) spectrum, which includes calcific tendinitis, periarticular hydroxyapatite deposition, and hydroxyapatite induced arthritis. The multi-modality imaging appearance of HADD will be highlighted at commonly encountered locations, including the hip and shoulder. This exhibit will provide a useful and relevant review of the clinical presentation and pathogenesis of HADD, including the three described phases of HADD, and also will discuss imaging based treatment options and outcomes. Pertinent differential diagnostic considerations will be reviewed, with an emphasis on features of HADD that may help distinguish this entity from other aggressive processes, with the goal of avoiding unnecessary patient imaging, intervention and morbidity.

Materials and Methods: This exhibit will review the clinical presentation and multi-modality imaging appearance of HADD across its three described phases using a practical, case-based approach, with the goal of educating the practicing radiologist and radiologist in training to facilitate early and accurate recognition of this common condition. Mimics of HADD also will be briefly discussed in order to highlight relevant differential diagnoses.

Results: Calcium hydroxyapatite is the most common pathologic calcification in the body and must be recognized by the practicing radiologist and radiologist in training. This exhibit will provide education regarding common sites of occurrence, multimodality imaging appearance, and pertinent differential diagnostic consideration of HADD.

Conclusion: Calcium hydroxyapatite deposition disease occurs at multiple periarticular locations around the body and is commonly encountered at imaging, often with an imaging appearance that may resemble aggressive processes such as infection, trauma and neoplasm. An increased understanding of the HADD spectrum will help the practicing radiologist and radiologist in training recognize this entity and therefore eliminate unnecessary further imaging, intervention and morbidity.

Modality % - Radiography / Fluoroscopy:	25
Modality % - CT:	5
Modality % - MRI:	50
Modality % - US:	20
Modality % - Nuclear Medicine:	0

AP radiograph of the left shoulder demonstrates soft tissue calcification along the expected course of the rotator cuff tendons, consistent with calcium hydroxyapatite crystal deposition.

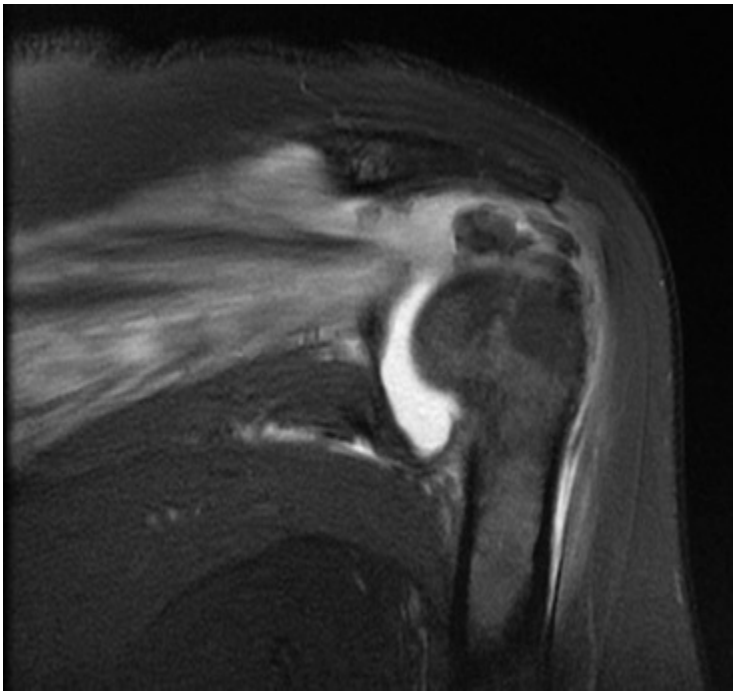

Coronal fluid sensitive MR image of the left shoulder demonstrates focal low signal within the distal infraspinatus tendon, diffuse infraspinatus muscle edema and joint effusion.

Poster #31

REVIEW AND UPDATE ON IMAGING OF CHEST WALL INJURIES

Kimia Kani, MD[1]; Hyojeong Mulcahy, MD[2]; Jack Porrino, MD[2]; Felix Chew, MD[2]
[1]University of Maryland School of Medicine, Baltimore, MD, USA; [2]University of Washington / Harborview Medical Center, Seattle, WA, USA
(Presented by: Kimia Kani, MD, University of Maryland School of Medicine)

Purpose: Chest wall injuries may be overlooked in the acute setting due to their frequent association with more pressing life-threatening injuries. Severity of chest wall injuries varies: some injuries may be inherently life-threatening, while others may predispose to long term complications, particularly if overlooked.

1. Become familiar with the spectrum of chest wall injuries, with a focus on improving diagnosis in the acute setting
2. Recognize the potentially associated life-threatening injuries and long-term complications of chest wall injuries

Materials and Methods: Educational goals:

1. Recognize the imaging spectrum of osteoarticular chest wall injuries, with emphasis on features that affect management
2. Identify the imaging spectrum of pectoralis muscle and other chest wall muscle injuries
3. Describe the potential life-threatening complications of some chest wall injuries
4. Recognize the potential long-term complications of chest wall injuries
5. Describe the preferred treatment options for different types of chest wall injuries

Results: Key issues:

The following will be discussed:

1. Sternal, clavicular, scapular and rib fractures: spectrum (with emphasis on pertinent imaging features), classification, treatment and complications
2. Sternoclavicular dislocation, manubriosternal dislocation, AC joint separation, floating shoulder, scapulothoracic dissociation: spectrum (with emphasis on pertinent imaging features), classification, treatment and complications
3. Imaging of pectoralis major and other chest wall muscle injuries

Conclusion: Chest wall injuries comprise a wide spectrum of injuries. These injuries may be overlooked in the acute setting. Awareness of the imaging spectrum of chest wall injures is important to improve the diagnosis and management of these conditions.

Modality % - Radiography / Fluoroscopy:	50
Modality % - CT:	25
Modality % - MRI:	21
Modality % - US:	4
Modality % - Nuclear Medicine:	0

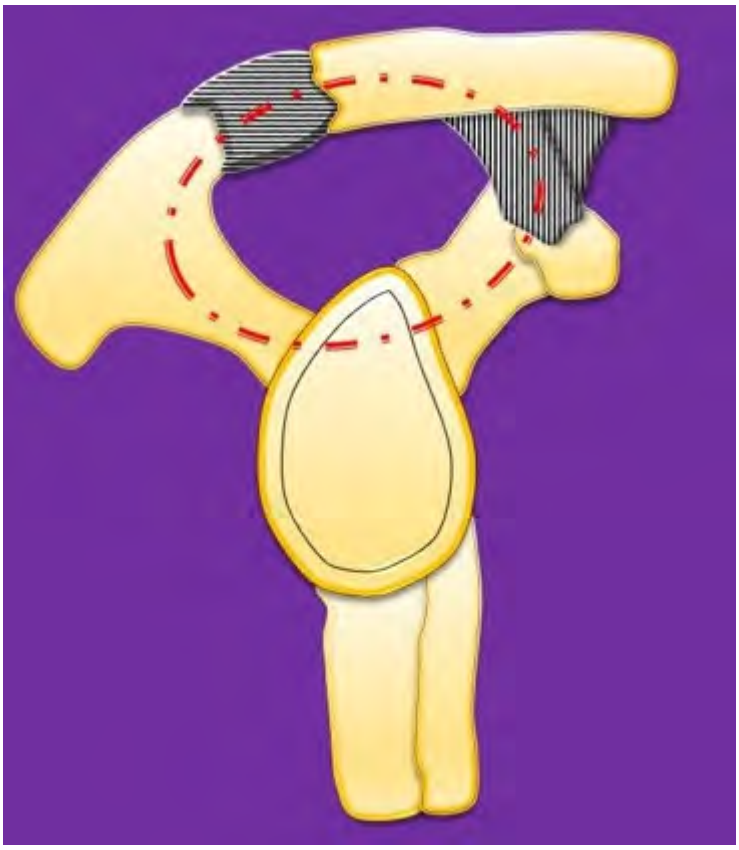

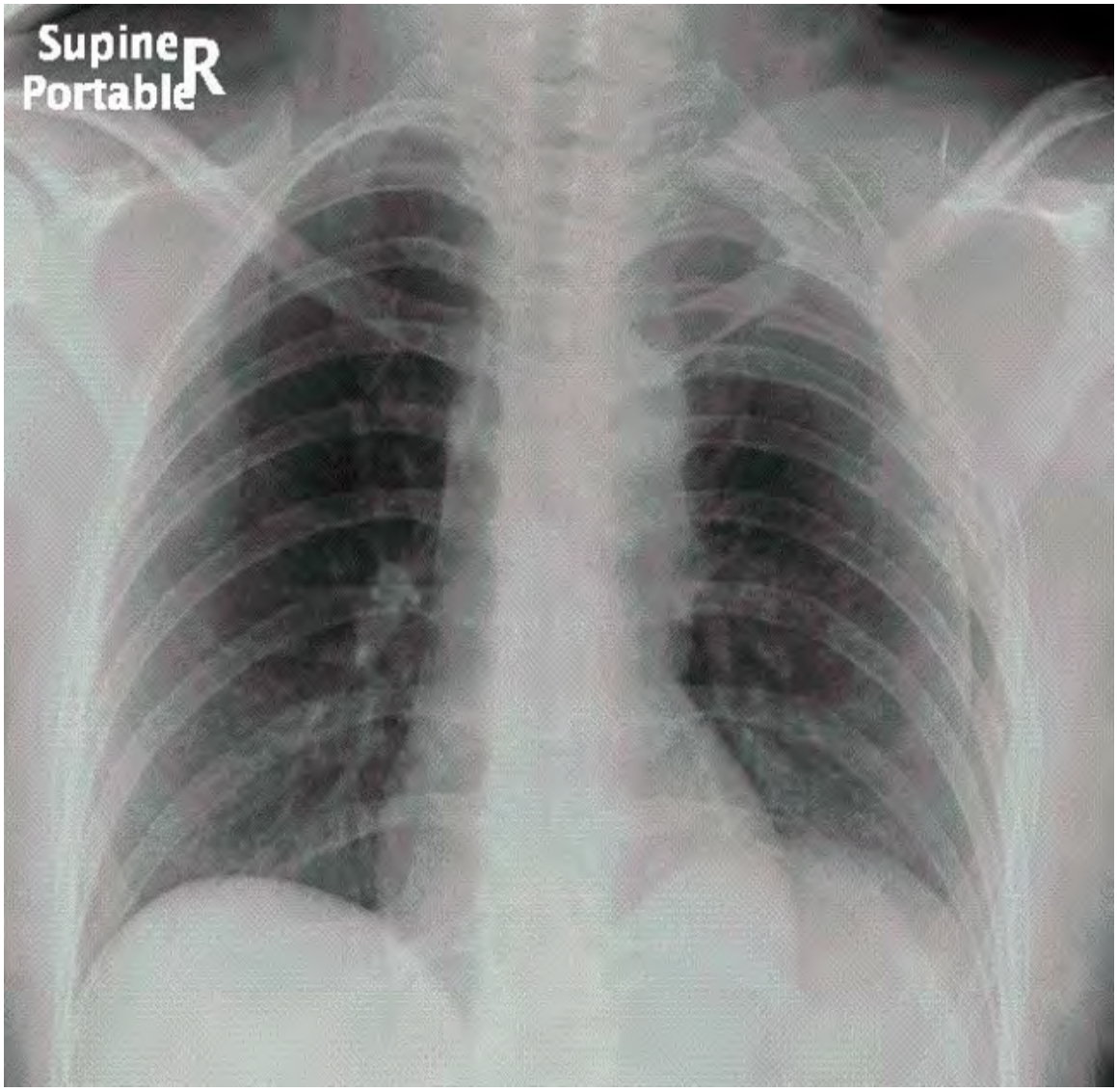

Fig. 1: Superior shoulder suspensory complex
Fig. 2: Left sided scapulothoracic dissociation

Poster #32

EVALUATION OF GADOLINIUM DEPOSITION IN THE BRAIN FOLLOWING MAGNETIC RESONANCE ARTHROGRAM

Lauren Ladd, MD; Krish Singhal, MD; Mark Frank, MD, MBA; Stephen Kralik, MD
Indiana University, Indianapolis, IN, USA
(Presented by: Lauren Ladd, MD, Indiana University)

Purpose: While there has been significant investigation into the deposition of gadolinium in the brains of patients receiving intravenous gadolinium, there is little research concerning non-intravenous uses of gadolinium, specifically of musculoskeletal magnetic resonance (MR) arthrograms. Although small in volume, intra-articular administration is an off-label use of gadolinium, necessitating careful scrutiny for patient safety. Thus, we investigated the relationship between intra-articular gadolinium administration during MR arthrogram and the presence of intracranial gadolinium deposition on subsequent brain MRI.

Materials and Methods: Following institutional review board approval, a retrospective study was performed on patients without prior history of gadolinium exposure who underwent MR arthrogram from 2006-2016 followed by a non-contrast brain MR examination. A reader placed regions of interest (ROIs) within bilateral dentate nucleus (DN), bilateral globus pallidi (GP), bilateral thalami, bilateral middle cerebral peduncle (MCP), and central pons (CP) on T1-weighted sequences. The left and right ROIs were averaged, and ratios of signal intensity were calculated for DN/MCP, DN/CP, GP/MCP, GP/CP, thalamus/MCP, and thalamus/CP. Similar ROIs and ratios were performed for age-matched controls with history of brain MRI and no prior gadolinium exposure. T-testing was used to compare signal intensity ratios between subjects and controls.

Results: A total of 33 patients met the inclusion criteria over the ten-year period analyzed and were compared to 34 control subjects. The average patient age was 45.1 +/- 18.5 years in the subject group and 45.2 +/- 18.0 years in the control group. The median time interval between MR arthrogram to brain MRI was 934 days. There was no significant difference between subject and control signal intensity for DN/MCP (p=0.4430), DN/CP (p=0.3245), GP/MCP (p=0.1654), GP/Pons (p=0.1134), Thalami/MCP (p=0.3694), and Thalami/Pons (p=0.2038).

Conclusion: MR arthrogram does not appear to be associated with detectable gadolinium deposition within the brain.

Modality % - Radiography / Fluoroscopy:	0
Modality % - CT:	0
Modality % - MRI:	100
Modality % - US:	0
Modality % - Nuclear Medicine:	0

Poster #33

MRI INTERPRETATION RATHER THAN TISSUE DIAGNOSIS DETERMINES ACUTE OSTEOMYELITIS MANAGEMENT: ONE INSTITUTION'S EXPERIENCE

Josephina Vossen, MD, PhD; Peter Haar, MD, MS; Curtis Hayes, MD; Michael Perone, MD; Kevin Hoover, MD, PhD
Virginia Commonwealth University Medical Center, Richmond, VA, USA
(Presented by: Josephina Vossen, MD, PhD, Virginia Commonwealth University Medical Center)

Purpose: Characteristic MRI signal changes are often used as a proxy for tissue diagnosis in cases of suspected pedal osteomyelitis (OM). This study was designed to determine the effect of MRI interpretation on management of suspected acute pedal OM.

Materials and Methods: Retrospective analysis was conducted on 127 foot MRI exams from 108 patients with a clinical question of OM from 11/7/2012 to 5/3/2014. MRI examinations with or without the characteristic imaging findings of acute OM (OM+/OM-) were interpreted by one of three subspecialty-trained musculoskeletal radiologists. Clinical management immediately prior to and following interpretation of the MRI exam was confirmed from review of the patient's electronic health record. Bone biopsy was not obtained for confirmation on these patients. The standard treatment regimen used by the infectious disease (ID) specialists at our institution for acute osteomyelitis was 4-6 weeks intravenous (IV) antibiotic therapy or maintenance of IV antibiotics until surgical debridement or amputation. Soft tissue infection was treated by antibiotic therapy for 14 days or fewer, change from IV to oral administration of antibiotics, or discontinuation of antibiotics.

Results: Of the 127 foot MRI examinations on patients clinically suspected of having osteomyelitis, 75 were OM+ and 52 were OM-. Treatment for acute osteomyelitis immediately following MRI interpretation of OM+ was found in 71/75 (95%) of the exams. Treatment for soft tissue infection immediately following MRI interpretation of OM- was found in 47/52 (90%).

Conclusion: In patients suspected of having osteomyelitis at a tertiary care center, clinical management immediately following MRI interpretation was concordant with the imaging diagnosis at a rate of 95% when positive for acute osteomyelitis and 90% when negative for acute osteomyelitis.

Modality % - Radiography / Fluoroscopy:	0
Modality % - CT:	0
Modality % - MRI:	100
Modality % - US:	0
Modality % - Nuclear Medicine:	0

Poster #34

PERIOSTEAL THICKENING AS THE ONLY VISUALIZED SIGN OF OSTEONECROSIS ON RADIOGRAPHS.

Josephina Vossen, MD, PhD; Candice Kim, BS; Peter Haar, MD, PhD; Curtis Hayes, MD; Kevin Hoover, MD, PhD
Virginia Commonwealth University Medical Center, Richmond, VA, USA
(Presented by: Josephina Vossen, MD, PhD, Virginia Commonwealth University Medical Center)

Purpose: The term osteonecrosis translates to bone death and is used to describe the spectrum of pathological and radiological changes occurring within bone as a result of ischemia. Periosteal reaction is observed in a wide variety of benign, malignant and systemic conditions, as well as during periods of normal growth and in response to injury. The aim of the study was to evaluate the presence of periosteal thickening on radiographs in patient with MRI proven osteonecrosis.

Materials and Methods: Imaging examinations of MRIs in 77 patients with MRI proven osteonecrosis and comparison radiographs were retrospectively reviewed. Imaging evaluation included an assessment of presence of osteonecrosis on MRI, periosteal reaction on radiograph and location of bone infarct. Patients with osteonecrosis in the epiphysis were excluded.

Results: Lesions were located in the metaphysis and/or diaphysis around the knee in 70% (54/77), around the ankle in 16% (12/77), around the hip in 8% (6/77) and around the shoulder in 6% cases (5/77). Periosteal reaction was observed in 21% (16/77). Within this group with periosteal reaction, in 50% (8/16) of cases periosteal reaction was the only sign of osteonecrosis seen on the radiographs. All cases with periosteal reaction were located around the knee.

Conclusion: We demonstrated in a group of patients with osteonecrosis, that periosteal reaction can be present, and in some cases can be the only sign seen on radiographs.

Modality % - Radiography / Fluoroscopy:	50
Modality % - CT:	0
Modality % - MRI:	50
Modality % - US:	0
Modality % - Nuclear Medicine:	0

Poster #35

THE INCIDENCE, ONSET AND DISTRIBUTUION OF CRYSTAL DEPOSITION WITHIN THE CERVICAL SPINE

Eric Walker, MD[1]; Dylan Simmons, DO[2]; Joshua Tice, MD[3]; Jonelle Petscavage-Thomas, MPH, MD[1]
[1]Penn State Milton S. Hershey Medical Center, Hershey, PA, USA; [2]Emory University Dept. of Radiology, MSK Division, Atlanta, GA, USA; [3]West Reading Radiology Associates, West Reading, PA, USA
(Presented by: Eric Walker, MD, Penn State Milton S. Hershey Medical Center)

Purpose: To examine the incidence, age of onset and distribution of crystal deposition withing the cervical spine.

Materials and Methods: We retrospectively reviewed 170 cervical spine computed tomography (CT) examinations obtained in the emergency department. CT studies were reviewed by three musculoskeletal radiologists with agreement by consensus. Evaluation included patient age and evaluation for crystal deposition. Locations evaluated included the transverse ligament, the anterior longitudinal ligament, the posterior longitudinal ligament, the longus colli, the annulus fibrosis, the nucleus pulposus, the facet joints, the ligamentum flavum, the interspinous ligament, and the supraspinal ligament.

Results: Patients between one and 39 years-of-age (76) demonstrated no crystal deposition. Crystal deposition was noted in seven of 31 patients (22.6%) between the ages of 40 and 49, five of 11 patients (45.5%) between the ages of 50 and 59, nine of 18 patients (50%) between the ages of 60 and 69, 11 of 12 patients (91.7%) between the ages of 80 and 89, and 11 of 11 patients (100%) between the ages of 90 and 99. The most common locations in patients with crystal deposition include the annulus fibrosis (96.0%), the nucleus pulposus (76.5%), the facet joints (37.3%), the transverse ligament (33.3%), the ligamentum flavum (19.6%), the posterior longitudinal ligament (15.7%), the interspinous ligaments (5.9%) and the longus colli and supraspinus ligament (both 3.9%).

Conclusion: Crystal deposition in the cervical spine is more prevalent at higher patient age. The annulus fibrosis is the most common location of deposition.

Modality % - Radiography / Fluoroscopy:	0
Modality % - CT:	76
Modality % - MRI:	0
Modality % - US:	0
Modality % - Nuclear Medicine:	0

Crystals within the annulus fibrosis (arrowhead) and nucleus pulposus (curved arrow).

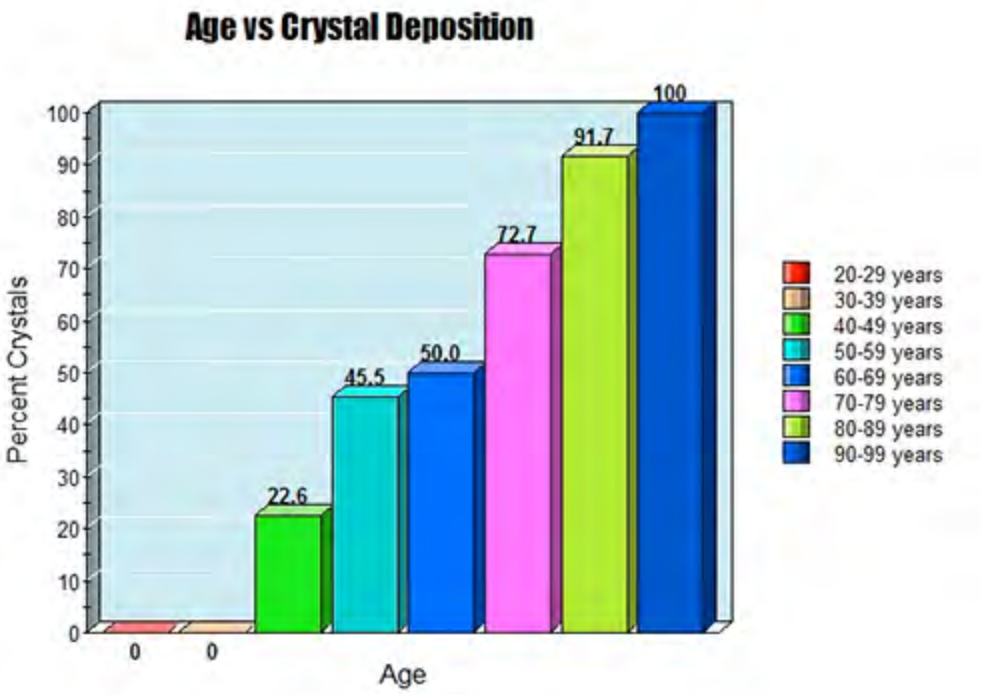

Percent prevalence of crystal deposition versus age of the patient.

Poster #36

DAY OF WEEK, SITE OF SERVICE, AND PATIENT COMPLEXITY DISPARITIES IN MUSCULOSKELETAL MRI INTERPRETATIONS BY RADIOLOGISTS VS. NON-RADIOLOGISTS

Paige Sharp, MD[1]; Richard Duszak, Jr., MD[1]; Wenyi Wang, MA[2]; Danny Hughes, PhD[2]; Neil Lall, MD[3]; Paul Harkey, MD[1]
[1]Emory University Dept. of Radiology, Atlanta, GA, USA; [2]Harvey L. Neiman Health Policy Institute, Reston, VA, USA; [3]Ochsner Health System, New Orleans, LA, USA
(Presented by: Paige Sharp, MD, Emory University Dept. of Radiology)

Purpose: While the majority of musculoskeletal MRI examinations are interpreted by radiologists, many non-radiologists provide interpretation services as well. We aimed to study day-of-week (weekday vs. weekend), site of service, and patient complexity differences between radiologists and non-radiologists interpreting lower extremity MRIs on Medicare beneficiaries.

Materials and Methods: Using research identifiable file carrier claims data for a 5% random sample of Medicare fee-for-service beneficiaries nationwide from 2012 to 2014, we identified all claims for lower extremity joint MRI examinations. Services were classified by specialty of billing physician, day of week of service, and site of service. Patient complexity scores were assigned to all patients using calculated Charlson Comorbidity Indices (CCI). Chi-square analysis was performed to test statistical significance.

Results: Of all 125,800 lower extremity joint MSK examinations in the 5% sample, 118,295 (94%) were performed on a weekday and 7,505 (6%) on a weekend. Of weekday examinations for which a provider specialty could be identified, radiologists interpreted 85,991 (83.3%) and non-radiologists 17,260 (16.7%). Of weekend examinations, radiologists interpreted 6,212 (92.8%) and non-radiologists 485 (7.2%). Radiologists interpreted 6,499 (99%) of examinations in the inpatient hospital and emergency department setting vs. 51 (1%) for non-radiologists. Of the most clinically complex patients (CCI ≥ 3), radiologists interpreted 4,228 (90.2%) examinations vs. 461 (9.8%) for non-radiologists. All inter-specialty differences were statistically significant ($p<0.001$).

Conclusion: Radiologists interpret the large majority of lower extremity joint MRI examinations in the Medicare population. Compared with non-radiologists, radiologists disproportionately provide services on weekends, in the highest acuity sites of service, and on the most clinically complex patients. Future pay-for-performance metrics should focus on such parameters to promote patient access and minimize disparities.

Modality % - Radiography / Fluoroscopy:	0
Modality % - CT:	0
Modality % - MRI:	100
Modality % - US:	0
Modality % - Nuclear Medicine:	0

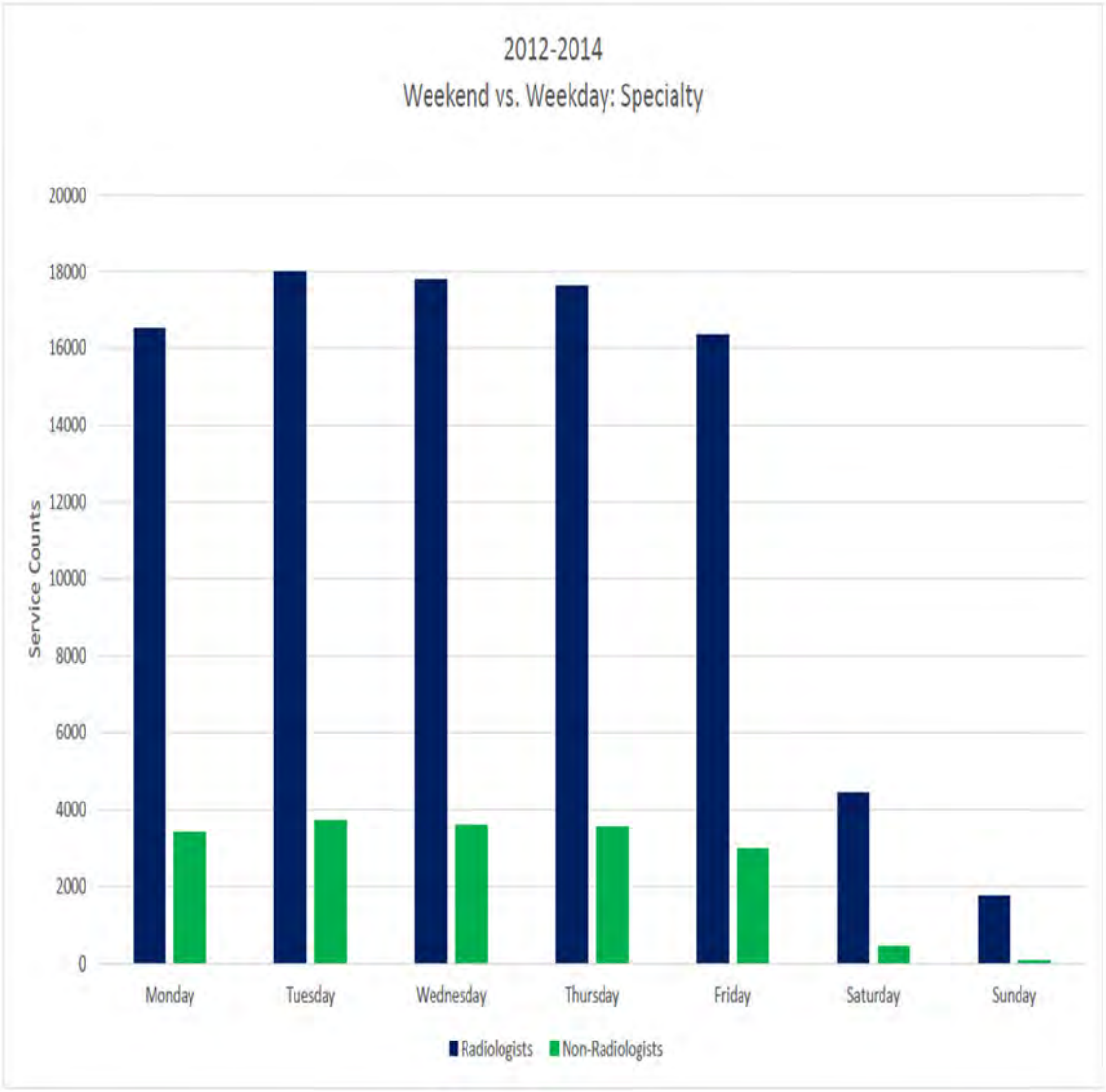

Weekend vs. Weekday: Specialty

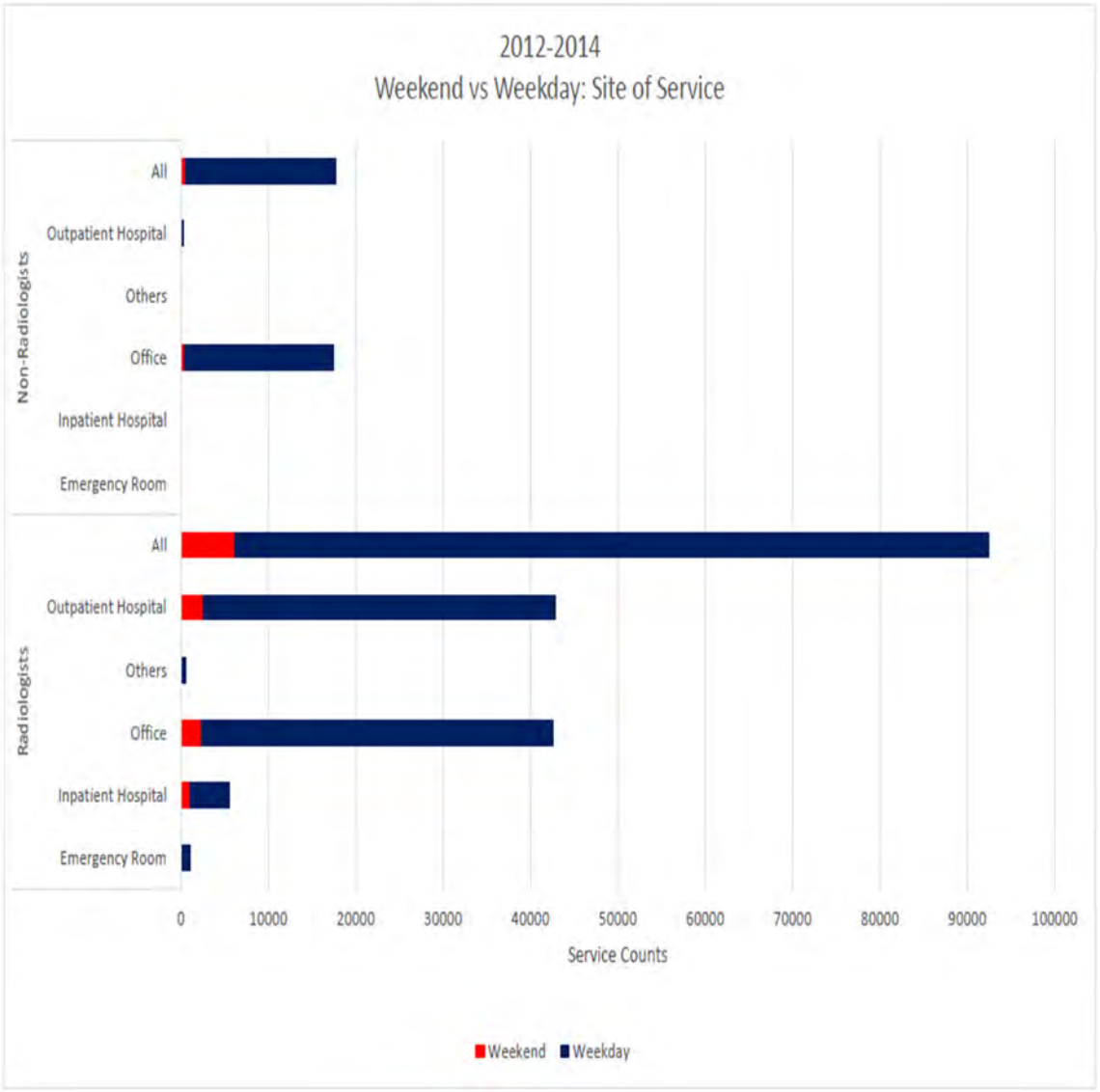

Weekend vs. Weekday: Site of Service

Poster #37

Imaging Features of Calciphylaxis

Ryan Franke, MD; Mark Kransdorf, MD; Michael Fox, MD; F. Chivers, MD; Jonathan Flug, MD
Mayo Clinic, Phoenix, AZ, USA
(Presented by: Ryan Franke, MD, Mayo Clinic)

Purpose: Background: Calciphylaxis is an uncommon condition most commonly found in patients with end-stage renal disease, estimated to affect up to 4% of that population. Typical clinical presentation includes ischemia and necrosis of the skin, soft tissues, and organs with small vessel vascular calcifications visible on imaging exams. Because of its association with infection and organ failure, mortality rates as high as 60-80% have been reported. We reviewed our experience with the imaging features of 11 patients with calciphylaxis to identify the imaging feature characteristic of the uncommon entity.

Materials and Methods: We retrospectively reviewed all available records in our institutional electronic pathology report data base for all patients with a diagnosis of "calciphylaxis." A total of 43 patients were identified. All pathology reports and imaging studies for these patients were reviewed. Study group inclusion criteria required: (a) definitive pathological diagnosis of calciphylaxis or findings "strongly suggestive" of calciphylaxis and (b) imaging studies (radiographs, CT, bone scan and/or US) of the area of the biopsy.

Results: The study group included 11 patients, four men and seven women, with and average age of 52 years (range 37-77 years). Imaging studies reviewed included radiographs (all patients), CT (5 patients) and bone scan (2 patients). The dominant imagine feature was fine small vessel vascular calcification within the subcutaneous adipose tissue just deep to the skin. This was seen well on both radiographic and CT examinations. Skin thickening and varying amounts of associated panniculitis immediately adjacent to the skin were well seen on CT, although less well-delineated on radiographs. Ill-defined increased tracer accumulation was readily identified on bone scintigraphy.

Conclusion: Imaging findings demonstrating extensive fine small vessel vascular calcification within the subcutaneous adipose tissue just deep to the skin with associated skin thickening and panniculitis are highly characteristic of calciphyaxis.

Modality % - Radiography / Fluoroscopy:	50
Modality % - CT:	39
Modality % - MRI:	0
Modality % - US:	0
Modality % - Nuclear Medicine:	10

Radiograph showing the fine small vessel clarifications best seen along the posterior inferior heel.

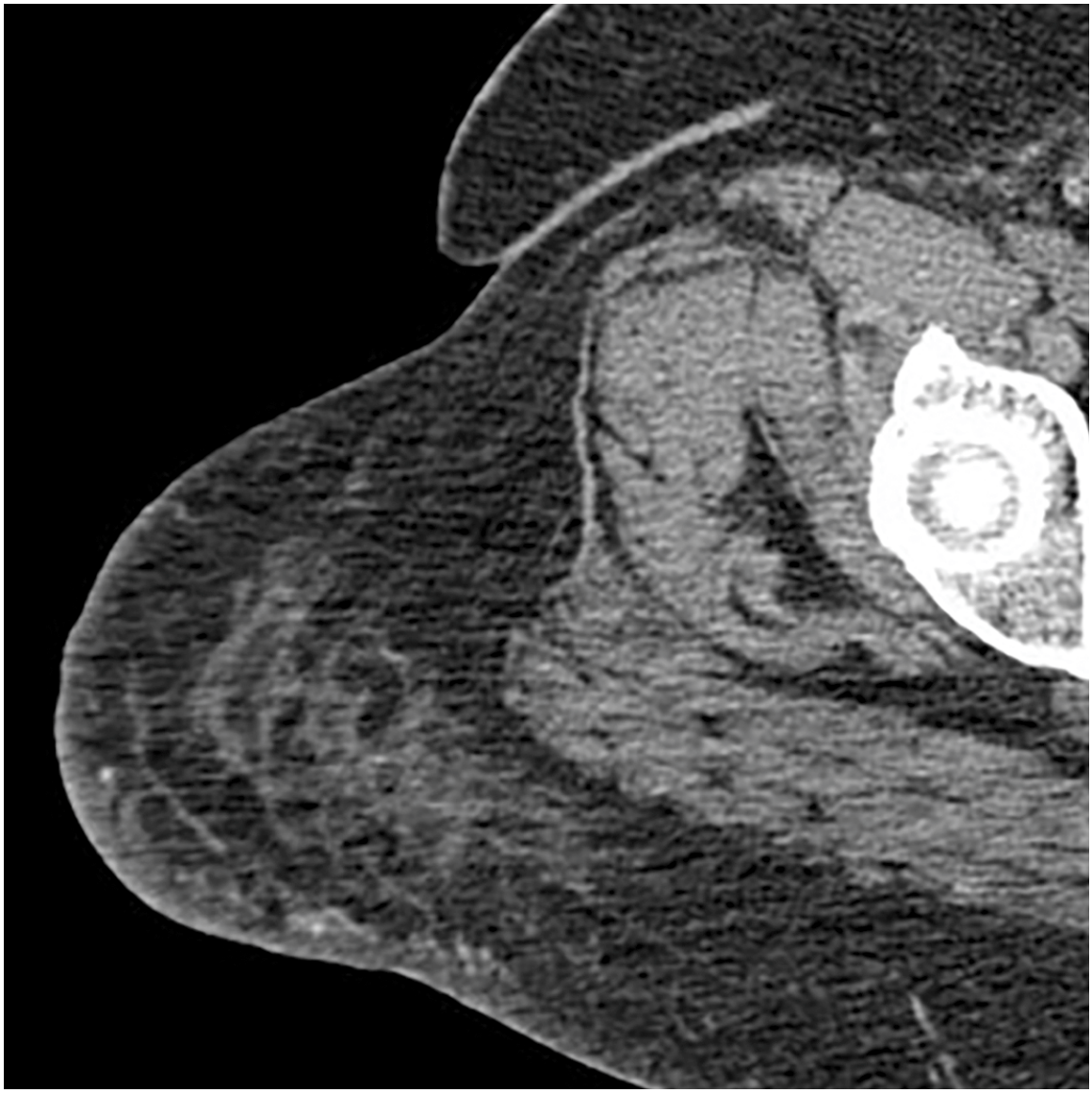

CT showing the small vascular calcification with mild skin thickening and panniculitis.

Poster #38

EARLY DETECTION OF METASTASES USING WHOLE-BODY MRI FOR INITIAL STAGING AND ROUTINE FOLLOW-UP OF MYXOID LIPOSARCOMA

Thomas Powell, MB,BCh., BAO, FFR(RSCI); Natalia Gorelik, MD; Santhosh Reddy, MBBS, MRCP, FRCR; Robert Turcotte, MD, FCRSC; Krista Goulding, MD, MPH, FRCSC; Sungmi Jung, MD, FRCPC; Thierry Alcindor, MD, MSc
McGill University, Montreal, QC, Canada
(Presented by: Thomas Powell, MB,BCh., BAO, FFR(RSCI), McGill University)

Purpose: To define the role of whole body MRI (WBMRI) for initial staging and routine follow-up of myxoid liposarcoma (MLS).

Materials and Methods: A retrospective review of all the patients with MLS who underwent WBMRI for initial staging and routine follow-up at our institution between October 1, 2006 and September 30, 2016 was performed. Patient demographics, clinical presentation, imaging findings, tumor histology and occurrence and location of metastatic disease were recorded. Thirty-three patients who underwent a total of 150 WBMRI examinations were included in the study.

Results: Nine patients (27%) were diagnosed with metastases between 0 and 60 months (mean 17 months) from the histopathological diagnosis of the primary tumor. The initial site of metastatic disease was extrapulmonary in all patients. Only two patients developed pulmonary metastases, which were diagnosed by CT chest 9 and 29 months after the first discovery of extrapulmonary metastases. The first metastasis was diagnosed by WBMRI in 7 patients (78%), by thoracic CT in 1 patient, and by abdominal CT in 1 patient. Eight of nine patients were asymptomatic at the time of diagnosis of the metastases. In 7 patients (78%), WBMRI demonstrated metastases included within the field of view of, but occult on a contemporaneous CT scan.

Conclusion: Our 10-year institutional experience demonstrates that the use of WBMRI for initial staging and routine follow-up of patients with MLS facilitates early detection of extrapulmonary metastases, before the onset of clinical symptoms and pulmonary metastases. WBMRI depicts extrapulmonary metastases that are often occult on CT scans. The current surveillance strategies are insufficient for screening for extrapulmonary MLS metastases.

Modality % - Radiography / Fluoroscopy:	0
Modality % - CT:	15
Modality % - MRI:	80
Modality % - US:	0
Modality % - Nuclear Medicine:	5

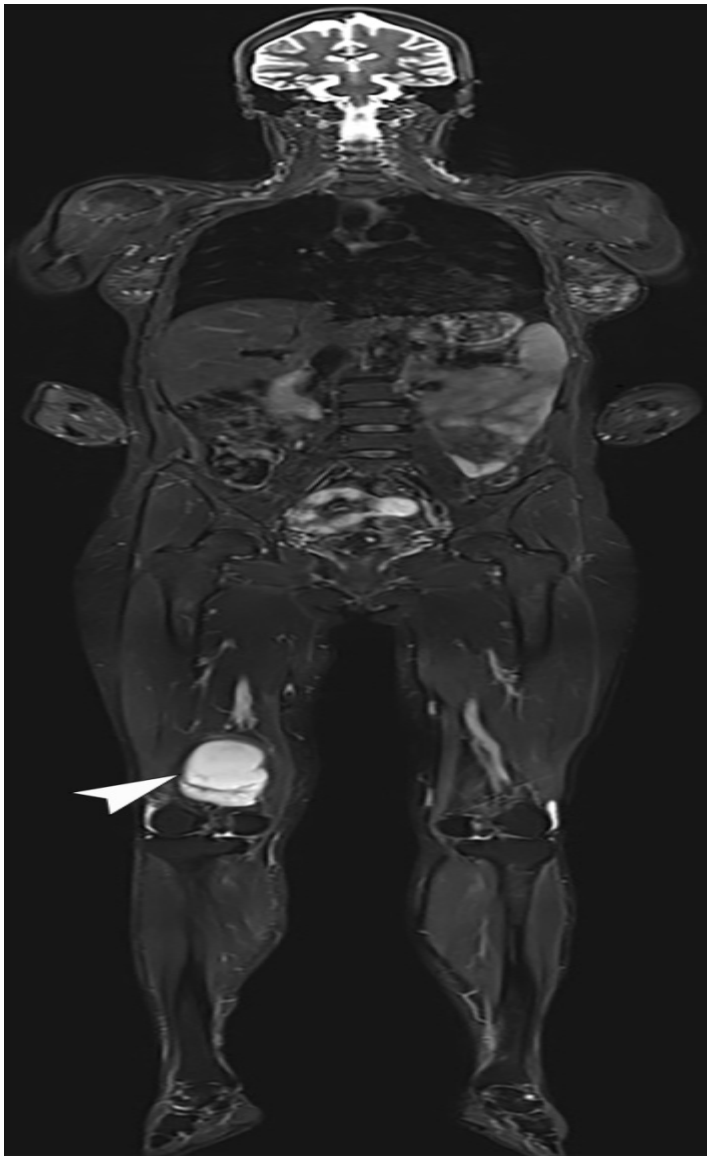

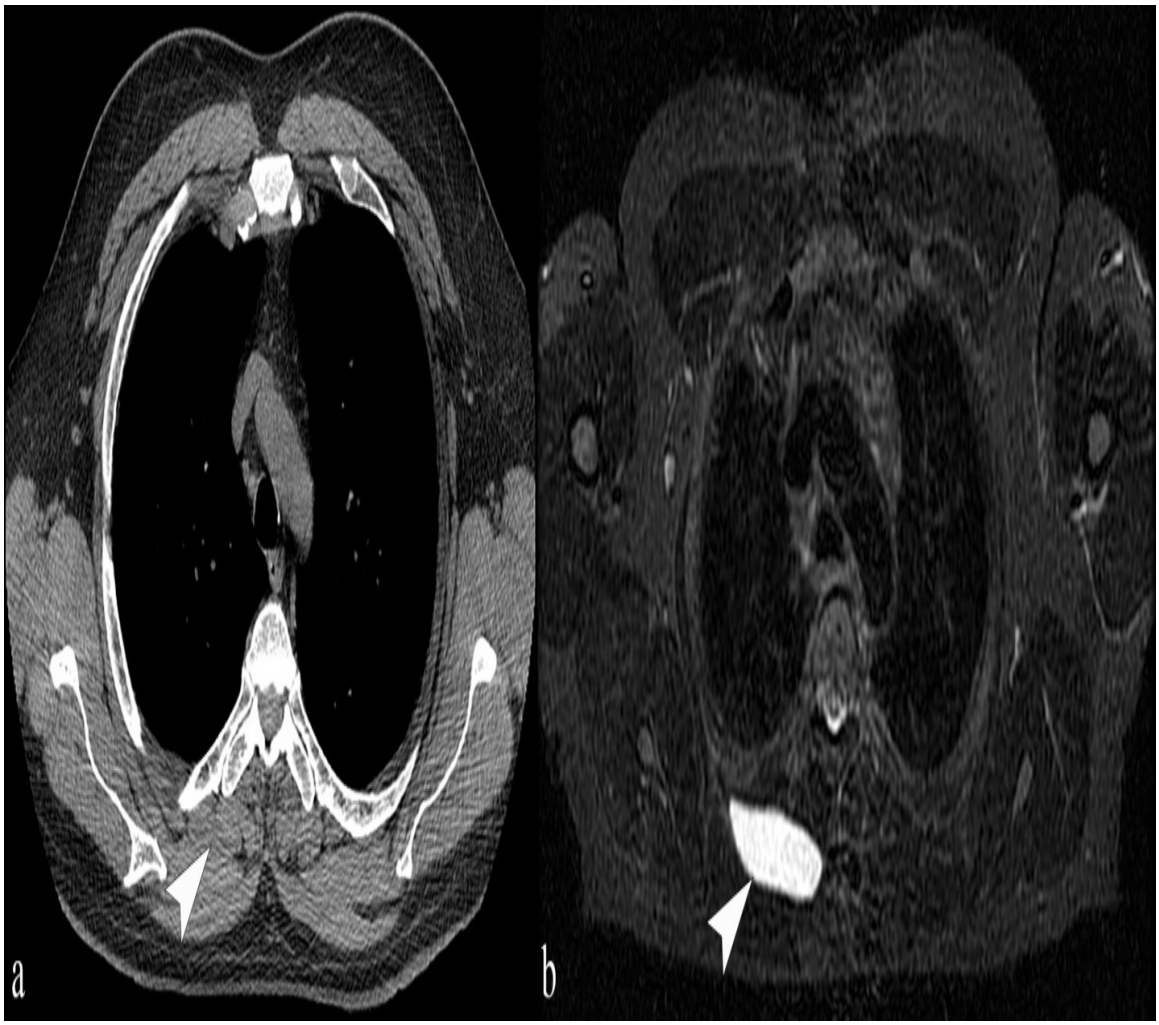

Fig. 1. Example of a staging WBMRI showing a right thigh primary MLS and no metastases.
Fig. 2. Posterior chest wall metastasis occult on CT.

Poster #39

Round Cell Component of Myxoid Liposarcoma: Can We Identify these Concerning Areas on Imaging?

Lien Senchak, MD[1]; Mark Murphey, MD[2]; Michael Shvarts, MD[2]; James Jelinek, MD[3]; Mark Kransdorf, MD[4]
[1]Walter Reed National Military Medical Center, Bethesda, MD, USA; [2]American Institute for Radiologic Pathology, Silver Spring, MD, USA; [3]Medstar Washington Hospital Center, Washington, DC, USA; [4]Mayo Clinic, Phoenix, AZ, USA
(Presented by: Lien Senchak, MD, Walter Reed National Military Medical Center)

Purpose: To determine whether pathologically confirmed round cell components of myxoid liposarcoma can be detected on imaging.

Materials and Methods: We retrospectively reviewed 14 pathologically confirmed cases of myxoid liposarcoma with round cell components. Radiographs(n=8), CT(n=6), and MRI (n=12) were reviewed by three musculoskeletal radiologists with agreement by consensus. Evaluation included patient demographics/history, lesion location/size, presence/character of intralesional fat, and intrinsic characteristics on CT/MRI. Higher grade round cell components were identified as focal higher areas of attenuation on CT or areas of mildly higher T1/lower T2 signal or diffuse focal enhancement.

Results: Patient age range 37-68 years(average 51) with a mild male predominance(57%). An intermuscular location was most common(78%). Tumors were most frequent in the thigh (71%) and lower leg (21%). The average lesion measured 7.5x9x15 cm.

Radiographs demonstrated either nonspecific soft tissue mass or fullness(87%). On CT, all tumors were defined masses, and contained fat (83%), although less than 10% by volume(100%).

On MRI, all tumors were well defined lesions and most commonly low to intermediate signal(88%) on T1 weighting. On T2 weighted images, the tumors demonstrated predominantly high(90%) or intermediate(10%) signal. Hemorrhage was apparent in 10% of tumors. Fat was identified in 75% of lesions, usually less than 10% of neoplasm volume(89%).

Areas suggesting significant round cell components were seen on CT in 17% of cases and on MR in 55% of cases.

Conclusion: A significant round cell component within myxoid liposarcoma, representing high grade foci, may commonly be identified on MR(55%). These areas are seen as focal, mildly increased T1 signal/decreased T2 signal, or areas of focal enhancement, relative to the myxoid regions of the lesion. These round cell components are important to detect and target at biopsy as they are associated with worsened prognosis and may alter therapy.

Modality % - Radiography / Fluoroscopy:	5
Modality % - CT:	25
Modality % - MRI:	70
Modality % - US:	0

Modality % - Nuclear Medicine:

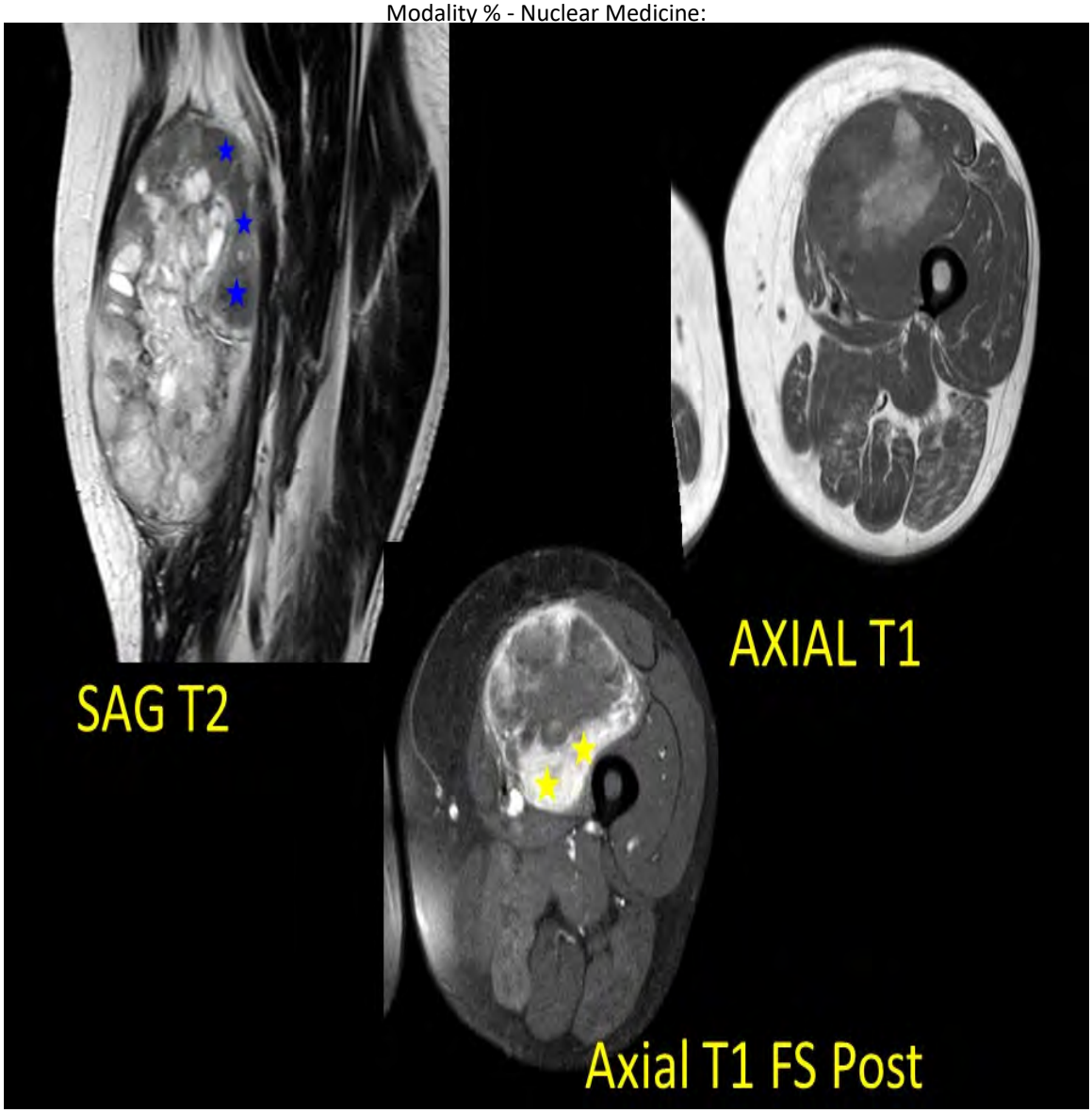

Blue stars: Focal, hypointense areas on T2
Yellow Stars: Focal enhancing area differing from the remainder of the lesion

Poster #40

IMAGING APPEARANCE OF WELL DIFFERENTIATED LIPOSARCOMAS WITH MYXOID STROMA

Yoav Morag, MD; Corrie Yablon, MD; Jon Jacobson, MD; Monica Brigido, MD; David Lucas, MD
University of Michigan Medical Center, Ann Arbor, MI, USA
(Presented by: Yoav Morag, MD, University of Michigan Medical Center)

Purpose: Describe the imaging appearance of well differentiated liposarcomas with myxoid stroma (WDLMS) and correlate with the histopathology.

Materials and Methods: A search was performed from 1/1/2000 to 3/30/2017 using a search engine that searches the entire electronic medical record for word associations. The histopathology slides of cases identified in this fashion were then reviewed. Additional cases were prospectively collected from extramural referrals and from multidisciplinary tumor boards. Diagnostic imaging studies of pathologically proven cases of WDLMS were then reviewed in consensus and correlated with pathology.

Results: Ten cases of pathologically proven WDLMS were identified (7 men, 3-women, ages 26-81). Tumor location included the retroperitoneum (n=5), thigh (n=4) and the shin (n=1). Nine cases had macroscopic fat on imaging with a variable appearance of the non-lipogenic components including septal, nodular and lacelike patterns. Only one tumor had no evidence of macroscopic fat on imaging. On CT, the non- lipogenic nodular components were hypodense or had hypodense areas. On MRI, the nodular components had intermediate/bright T2W signal. Interval non-lipogenic nodular growth was identified in 3 cases with the nodular growth disproportionate to the growth of the lipogenic component. Discordant initial histopathological diagnosis included a myxoid liposarcoma, dedifferentiated liposarcoma and intramuscular lipoma.

Conclusion: WDLMS may present on imaging as a mass with variable amounts and varied morphology of non-lipogenic components. Histopathological diagnosis of WDLMS is challenging and imaging correlation may be helpful as this tumor may have $\geq$ 50% fatty volume or may be located in the retroperitoneum, features which are unusual for myxoid liposarcoma. WDLMS with a nodular component cannot be distinguished from dedifferentiated liposarcoma based on imaging alone.

Modality % - Radiography / Fluoroscopy:	0
Modality % - CT:	45
Modality % - MRI:	45
Modality % - US:	10
Modality % - Nuclear Medicine:	0

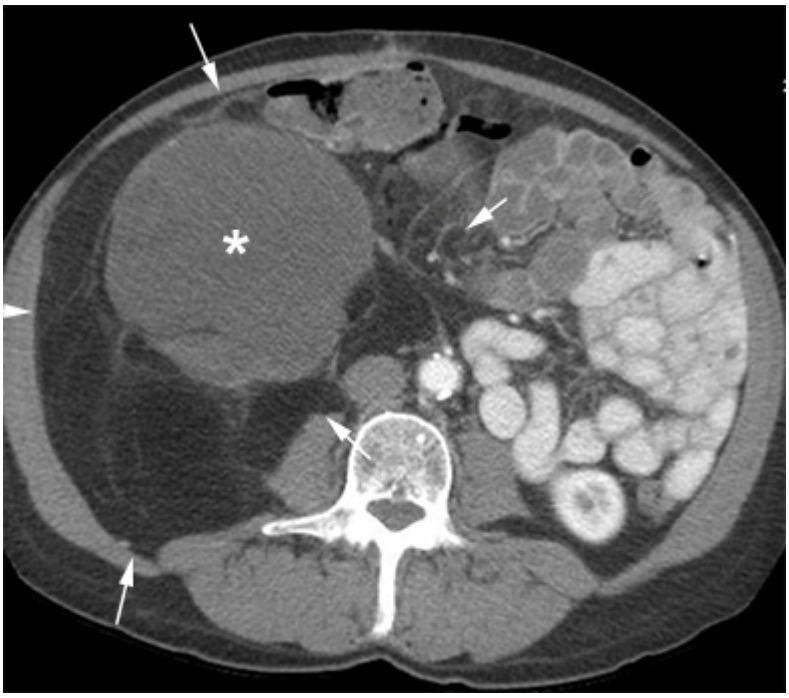

Axial post contrast CT shows a large retroperitoneal well differentiated lipogenic mass (arrows) with a myxoid nodule (asterisk).

Gross photograph of the resected specimen illustrates the cut surface of a solitary, gelatinous myxoid mass located within an otherwise typical lipomatous well-differentiated liposarcoma

Poster #41

TUMOR INDUCED OSTEOMALACIA, A REVIEW OF 5 CASES

LEE KATZ, MD; Kirsten Cooper, MD
Yale University School of Medicine, New Haven, CT, USA
(Presented by: LEE KATZ, MD, Yale University School of Medicine)

Purpose: Tumor induced osteomalacia (TIO) is a rare acquired metabolic bone disease caused by paraneoplastic production of FGF23. The disorder is infrequently characterized in the literature, with the majority of data focusing on utilization of imaging to localize the causative tumor rather than describing findings of the metabolic disease. This presentation reviews the pathogenesis of TIO and describes the skeletal manifestations of TIO on plain radiographs, with correlative findings described on CT, MRI and bone scan

Materials and Methods: Following IRB approval, the electronic medical record at our facility was retrospectively searched for patients with TIO. A unique patient cohort was present given related ongoing clinical trials at our site. The identified patient's available imaging studies were reviewed using our institution's PACS. Relevant findings were evaluated and compared to findings described in the literature

Results: Skeletal findings in TIO mimic those of genetic disorders characterized by hypophosphatemic rickets. The culprit tumor, often mesenchymal, incites a paraneoplastic syndrome with production of FGF23. High levels of FGF23 cause hypophosphatemia via renal phosphate wasting. In addition to inducing hypophosphatemic bone disease, FGF23 decreases circulating calcitriol levels and inhibits matrix mineralization and osteoblast differentiation. Unlike genetic causes of FGF23 mediated bone disease, TIO can be surgically cured with resection of the offending tumor. However, treatment can be challenging given nonspecific clinical symptoms and difficulty locating the primary tumor even when TIO is clinically suspected.

In the literature and our cohort of 5 patients, plain radiographic findings of TIO range from normal, to diffuse demineralization without or with atraumatic fractures. Multiple fractures involving the vertebra, calcaneus and femurs were noted, with some long bone fractures appearing as cortical stress fractures. These findings were correlated on CT, MRI and bone scans.

Conclusion: TIO is a rare paraneoplastic condition with skeletal manifestations mimicking those of hypophosphatemic rickets on imaging.

Modality % - Radiography / Fluoroscopy:	70
Modality % - CT:	10
Modality % - MRI:	10
Modality % - US:	-6
Modality % - Nuclear Medicine:	10

Poster #42

DISTRIBUTION OF FEMORAL SHAFT METASTATSES; IMPLICATIONS FOR PET/CT SCANNING

Michael Mulligan, MD
University of Maryland School of Medicine, Baltimore, MD, USA
(Presented by: Michael Mulligan, MD, University of Maryland School of Medicine)

Purpose: To determine the incidence of metastatic disease below the midshaft level of the femur in cancer patients.

Materials and Methods: IRB approved retrospective review of imaging studies of 137 cancer patients (mean age 62 years) with known involvement of the femur. Location of femoral shaft metastasis was noted as either proximal or distal to midshaft level on all relevant imaging studies. Patients with myeloma were excluded.

Results: Of the 137 patients, 36% had distal femoral shaft metastases. The distal site was the only femoral site in 9%. The distal site was the only area of skeletal involvement in 3%. Metastases were seen from 29 different primary carcinomas or lymphomas, most commonly from breast (25%), prostate (19%) or lung (16%).

Conclusion: More than one third of cancer patients with metastases to the femur may have involvement of the distal femoral shaft. This portion of the femur is not included on typical PET/CT staging studies. PET/CT coverage should be extended to include the distal femoral shafts to avoid missing these important lesions that could result in pathologic fracture.

Modality % - Radiography / Fluoroscopy:	40
Modality % - CT:	10
Modality % - MRI:	10
Modality % - US:	0
Modality % - Nuclear Medicine:	40

Image 1. 69 year old man with new diagnosis of esophageal cancer. Routine PET/CT showed no femoral disease. MRI shows large distal femoral shaft metastasis.

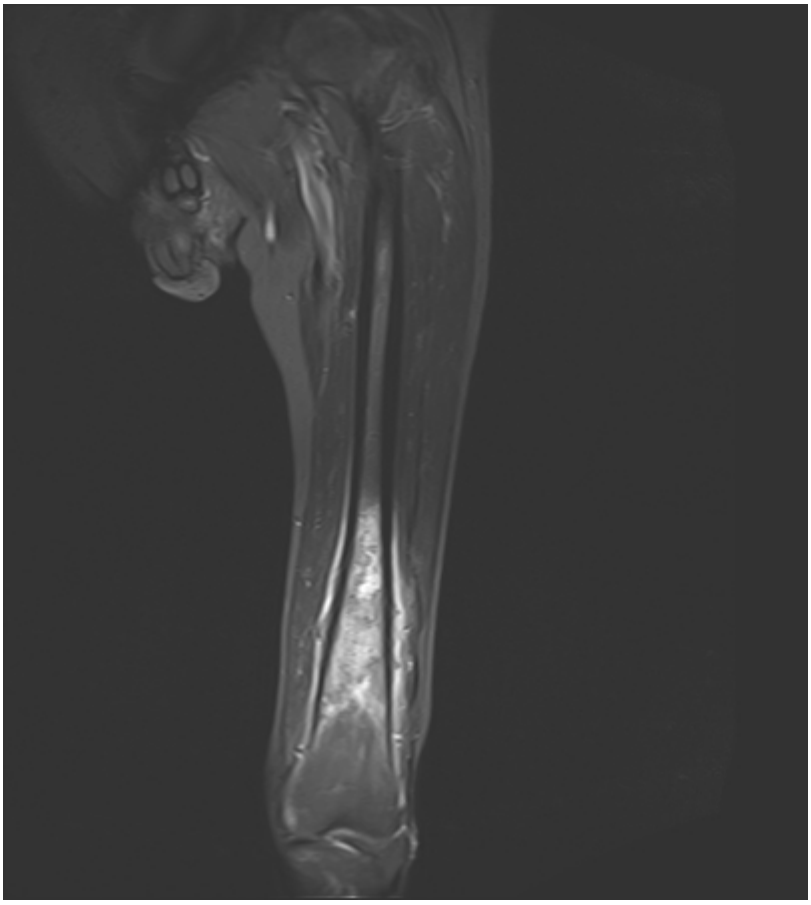

Image 2. Patient treated with extensive hardware fixation 9 days after MRI to prevent pathologic fracture.

Poster #43

COMPARISON OF DIAGNOSTIC ULTRASOUND AND MRI IN THE EVALUATION OF THE PERONEAL TENDON INJURIES IN CORRELATION WITH OPERATIVE FINDINGS

Mihra Taljanovic, MD, PhD; Lana Gimber, MD, MPH; Aamir Ahmad, MS; Tyson Chadaz, MD; L Latt, MD, PhD
University of Arizona HCS - Tucson, Tucson, AZ, USA
(Presented by: Mihra Taljanovic, MD, PhD, University of Arizona HCS - Tucson)

Purpose: To compare accuracy of diagnostic ultrasound (US) with magnetic resonance imaging (MRI) in the patients with various peroneal tendon injuries in correlation with operative findings in our patients who had both of these studies performed.

Materials and Methods: Twenty-one patients with clinically suspected peroneal tendon injuries underwent diagnostic US and MRI examinations of the affected ankle prior to surgery. US examinations were initially performed by a musculoskeletal (MSK) trained ultrasound technologist with several years of experience in conjunction with any one of our four MSK radiologists. All patients were operated by the same ankle and foot orthopaedic surgeon. MRI studies were subsequently retrospectively reviewed by two MSK radiologists in consensus for the presence of peroneus brevis (PB) and longus (PL) longitudinal split tear, rupture, tendinopathy (tendinosis and/or tenosynovitis) and subluxation. The radiologists were blinded to the initial MRI reads and surgical results. The MRI findings were then compared with initial US reads and surgical findings. The US studies were not re-interpreted.

Results: On surgery, thirteen of 21 patients had PB tendon longitudinal split tear and 3 partial-thickness tear. Two of 21 patients had PL tendon tear, one complete rupture and one longitudinal split tear. Eighteen of 21 patients had tendinopathy and three intra-sheath subluxation of the peroneal tendons. The MRI results were concordant with surgical findings (100% sensitivity and 100% specificity) for all peroneal tendon tears while US failed to diagnose 2 PB longitudinal split tears, both by the same radiologist (90% sensitivity and 100% specificity). US detected all three intrasheath subluxation while the MRI failed to detect 2 of three.

Conclusion: Compared to US, MRI showed slightly better results in diagnosis of peroneal tendon tears while US was more accurate in diagnosing intrasheath subluxations.

Modality % - Radiography / Fluoroscopy:	0	Modality % - US:	50
Modality % - CT:	0	Modality % - Nuclear Medicine:	0
Modality % - MRI:	50		

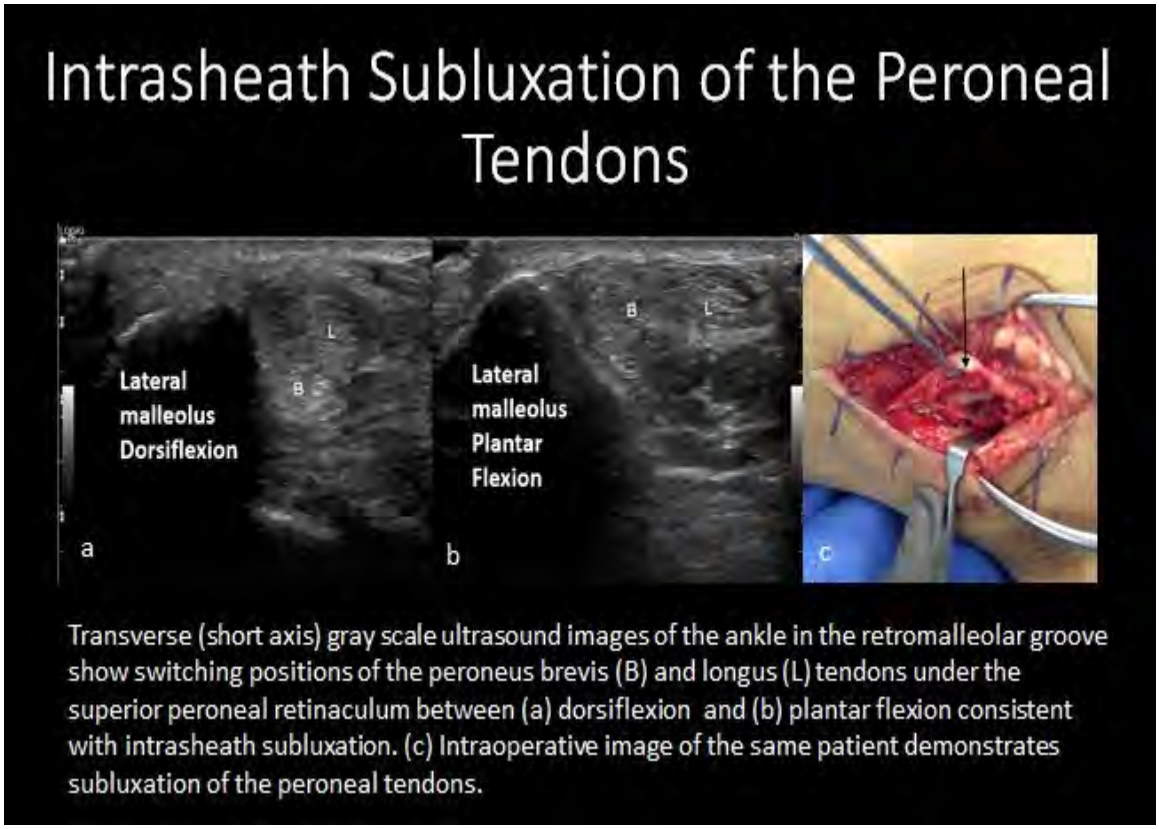

Ultrasound and intraoperative images demonstrating intrasheath subluxation of the peroneal tendons.

Poster #44

Assessing Obesity by Correlating BMI to Subcutaneous Fat Measurement on Axial Knee MRIs

Felix Gonzalez, MD[1]; Ricardo Hernandez, BS[2]; Yara Younan, MD[1]; Adam Singer, MD[1]; Gulshan Sharma, PhD, MPH[3]; Michael Mulligan, MD[4]; Monica Umpierrez, MD[1]

[1]Emory University Dept. of Radiology, MSK Division, Atlanta, GA, USA; [2]Philadelphia College of Osteopathic Medicine, Suwanee, GA, USA; [3]Cumming School of Medicine, Calgary, AB, Canada; [4]University of Maryland School of Medicine, baltimore, MD, USA

(Presented by: Felix Gonzalez, MD, Emory University Dept. of Radiology, MSK Division)

Purpose: To validate a method of correlating measurements of subcutaneous fat around the distal femur on axial MR images to body mass indices (BMI) and assessing the reliability of these measurements in predicting clinical outcomes associated with obesity.

Materials and Methods: This retrospective study include 518 consecutive subjects who presented over a two year period for a knee MRI. The most proximal axial slice of each knee MRI exam was equally divided into four quadrants. Measurements of the thickest portion of subcutaneous fat in each quadrant were independently obtained and the relationship between these measurements and the patient's BMI was determined. Additionally, chart review for each subject was performed to gather information regarding renal function status, anemia, and history of diabetes among others.

Results: Subcutaneous fat measurements in all four quadrants and BMI were significantly correlated (all four, ANOVA $p<0.0001$, $r=0.6$), with measurements of the anterior and posterior medial quadrants being significant predictors. The posterior medial quadrant subcutaneous fat measurement was shown to be the strongest predictor of all. BMI outperformed the anterior and posterior medial subcutaneous measurements for detection of sleep apnea, diabetes, hypertension and GERD within a 30.3-31.6 BMI range. However, the posterior medial index outperformed BMI in screening for asthma utilizing 24.4 mm as a subcutaneous thickness threshold, while the anterior medial index outperformed BMI in the detection of osteoporosis at a threshold of 18 mm.

Conclusion: The relative ease and cost-effectiveness of this simple measurement further enhances the value of care provided to the patient presenting with knee pain requiring MRI. Overall, our data suggests the use of anterior and posterior medial subcutaneous fat measurements as predictor of BMI regardless of gender in addition to their respective use in the screening/detection of patients with asthma and osteoporosis.

Modality % - Radiography / Fluoroscopy:	0
Modality % - CT:	0
Modality % - MRI:	1
Modality % - US:	0
Modality % - Nuclear Medicine:	0

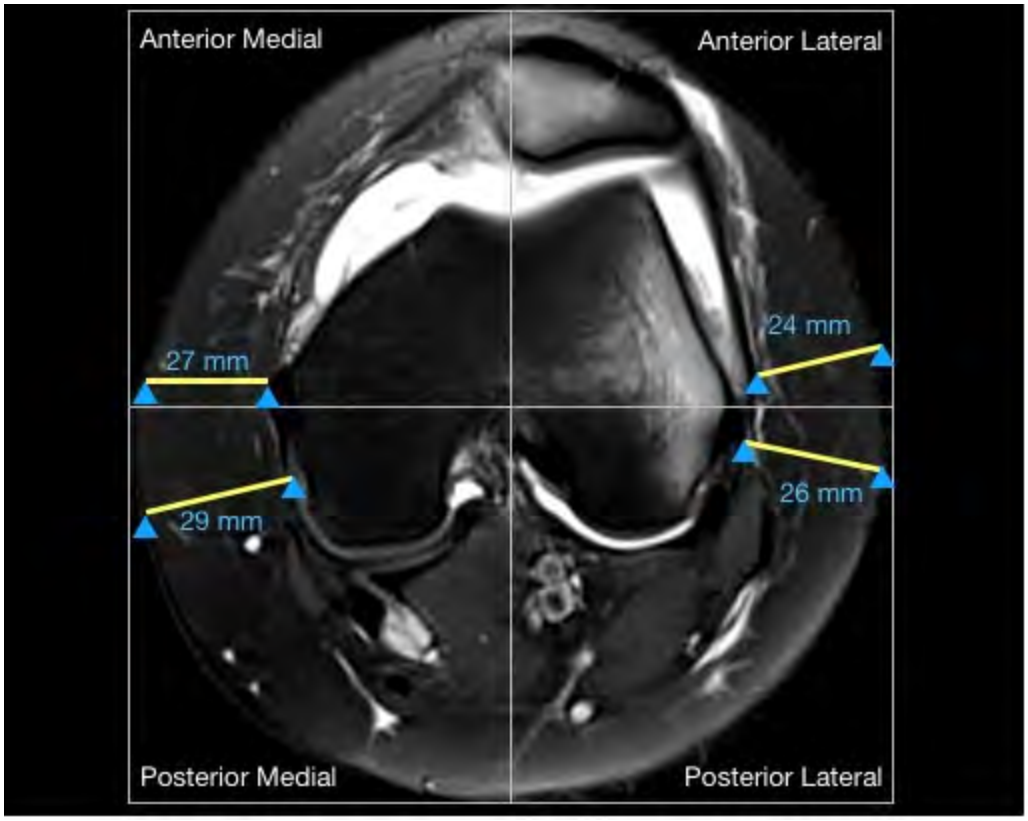

Figure 1. Axial Knee MRI showing the measurement of the thickness of subcutaneous fat in each of the four quadrants.

Poster #45

IMPROVED QUALITY OF KNEE RADIOGRAPHS IN A MULTI-CENTER PRACTICE AFTER INTRODUCTION OF A STANDARDIZED POSITIONING FRAME

Faysal Altahawi, MD; Carl Winalski, MD; Erika Schneider, PhD; Morgan Jones, MD; Spindler Kurt, MD; Schils Jean, MD
The Cleveland Clinic Foundation, Cleveland, OH, USA
(Presented by: Faysal Altahawi, MD, The Cleveland Clinic Foundation)

Purpose: Joint space width on standing knee radiographs, whether evaluated qualitatively or quantitatively, is the standard for assessing progression of osteoarthritis. Ideal tunnel-view radiographic technique minimizes the intermarginal distance (IMD) of the tibia, *i.e.* vertical distance between the anterior and posterior margins of the medial tibial plateau (MTP). Positioning frames have been used to optimize positioning in clinical trials. Our study measures the impact on quality of knee radiographs following introduction of a positioning frame into a large, multi-site clinical practice.

Materials and Methods: IRB approval was obtained. Consecutive bilateral tunnel-view knee radiographs from 3 sites were reviewed, 20 per site before and after introduction of a Synaflexer™ knee frame (120 total). Technologists received training at introduction of the frame, but not subsequently. Pre-frame images were acquired using a Schuss position of 20 degrees knee flexion with hips over/behind heels and 10-20 degrees caudal beam angulation. After frame implementation, fixed-flexion positioning was used for Synaflexer™ knee frame radiographs per the OAI X-ray manual. Standardized MTP-IMD measurements were performed with semi-automated software. In addition, Kellgren-Lawrence grading, BMI, relevant clinical history, site and technologist performing the exam were recorded.

Results: MTP-IMD was significantly improved using the positioning frame with average IMD = 2.0mm(95%CI 1.5-2.4mm) versus pre-frame IMD = 4.7mm(95%CI 3.9-5.6)($P<0.01$). All individual technologists that performed more than one radiograph before and after knee frame produced higher quality radiographs with smaller average MTP-IMD after knee frame (average IMD improvement = -3.2mm). IMD variance was also larger without the frame (11.2mm) than with (2.7mm), indicating more consistent quality radiographs.

Conclusion: Utilization of a positioning frame for knee radiography can improve quality and consistency of knee radiography for osteoarthritis evaluation in a multi-site clinical practice with minimal technologist training.

Modality % - Radiography / Fluoroscopy:	100
Modality % - CT:	0
Modality % - MRI:	0
Modality % - US:	0
Modality % - Nuclear Medicine:	0

(A)Schuss position bilateral knee radiograph. (B)Fixed-flexion bilateral knee radiograph with frame. (C)Schuss Positioning. (D)SynaflexerTM knee frame in isolation and (E)fixed-flexion knee positioning in frame.

Poster #46

WEIGHT-BEARING DIGITAL TOMOSYNTHESIS OF FOOT/ANKLE ARTHRITIS: COMPARISON TO RADIOGRAPHY AND SIMULATED WEIGHT-BEARING CT

Xue Cunningham, MD[1]; Alan Leung, MD[2]; Jennifer Favinger, MD[2]; Daniel Hippe, MS[2]; Alice Ha, MD[2]
[1]Wake Forest University School of Medicine, Winston-Salem, NC, USA; [2]University of Washington / Harborview Medical Center, seattle, WA, USA
(Presented by: Xue Cunningham, MD, Wake Forest University School of Medicine)

Purpose: Foot/ankle arthritis is common and debilitating. Weight-bearing radiography remains the gold standard in evaluating alignment, but overlapping bones or hardware limit evaluation for arthritic details. We hypothesized that digital tomosynthesis (DTS) can provide reliable quantitative alignment values like radiography with its weight-bearing capability and good qualitative arthritic details like computed tomography (CT) with its plane-by-plane images.

Materials and Methods: In this IRB-approved prospective study, adults with foot/ankle pain and arthritis referred for simulated weight-bearing CT were recruited to undergo weight-bearing radiography and DTS. Four readers independently evaluated radiography and DTS images in randomized orders for foot/ankle alignment and severity of osteoarthritis for each joint (i.e., joint space narrowing, osteophytes, subchondral cyst). Two readers performed consensus CT reading. Radiography was considered the gold standard for foot alignment (CT for osteoarthritic details). Agreement between modalities was assessed using Intraclass Correlation Coefficient (quantitative variables) and Cohen's kappa (qualitative variables).

Results: 46 patients (24 men; mean age 54 years) with total 91 ankles were included. Trauma (67%), osteoarthritis (52%), and congenital deformity (41%) were the most common prior conditions. All joints except the 1st MTP joint were significantly less obscured when seen with DTS or CT (1-30%) when compared to radiography (10-99%). For quantitative measurements of foot alignment (Table 1), DTS had moderate to good agreement with radiography, which was significantly better than CT in most cases. For qualitative osteoarthritic details of the tibiotalar joint (when not obscured), agreement was moderate to good for most features, with kappa ranging from 0.47 to 0.62 between radiography and CT and from 0.46 to 0.63 between DTS and CT.

Conclusion: DTS leads to less obscuration of joints than radiography and provides reliable weight-bearing quantitative foot/ankle alignment values when compared to radiography and osteoarthritic bony details when compared to CT.

Modality % - Radiography / Fluoroscopy:	67
Modality % - CT:	33
Modality % - MRI:	0
Modality % - US:	0
Modality % - Nuclear Medicine:	0

Table 1. Quantitative measurements of foot alignment.

Variable	Agreement b/w XR and TS ICC	(95% CI)	Agreement b/w XR and CT ICC	(95% CI)	P-value
Talonavicular coverage angle*	-		0.74	(0.63-0.82)	-
Calcaneal pitch	0.93	(0.88-0.95)	0.87	(0.80-0.91)	**0.001**
Lateral 1st metatarsal-talar angle	0.65	(0.54-0.74)	0.46	(0.29-0.61)	**<0.001**
Lateral talocalcaneal angle	0.69	(0.53-0.80)	0.53	(0.31-0.68)	**0.001**
Intermetatarsal angle*	-		0.33	(0.16-0.49)	-
Navicular overlap	0.73	(0.63-0.79)	0.39	(0.26-0.49)	**<0.001**
Cuboid height	0.66	(0.53-0.75)	0.68	(0.54-0.77)	0.54
Naviculocuboid overlap (ratio)	0.78	(0.70-0.84)	0.47	(0.33-0.59)	**<0.001**
Tibiotalar angle	0.78	(0.54-0.86)	0.82	(0.59-0.88)	0.098

XR = radiography

TS = tomosynthesis

* Talonavicular coverage angle and Intermetatarsal angle are measured on the frontal view of foot (equivalent to "axial" view on CT). This view is not available on TS and therefore not measured.

Table 1

Poster #47

LADY OR GENTLEMAN: SEX DIFFERENCES IN BONY AND CARTILAGE STRUCTURES OF THE KNEE

Laura Fayad, MD, MS; Lauren Pringle, MD
Johns Hopkins University, Baltimore, MD, USA
(Presented by: Laura Fayad, MD, MS, Johns Hopkins University)

Purpose: To identify sex differences in bone and cartilage knee anatomy based on a systematic review of world literature.

Materials and Methods: We performed a systematic review of all imaging studies of knee morphology, comparing findings between male and female subjects, in PubMed, with search terms for CT/MRI, knee anatomy, and gender. Inclusion criteria were primary imaging investigations of knee cartilage and bony anatomy with at least 15 subjects. We excluded studies of other modalities, of patients with prior surgery and comorbid conditions (example: arthritis), and review articles.

Results: Of 1550 citations reviewed, 84 studies met inclusion criteria, and fell into 5 categories (Table 1): bony axes of the knee (n=19), morphology of the distal femur (n=37), proximal tibia (n=23) and patella (n=8), and articular cartilage (n=17). Knee axes studies suggest trochlear groove-tibial tuberosity distance and posterior tibial slope are greater in women. Distal femur studies showed larger metrics in men, narrower metrics in women, and smaller intercondylar notch volumes. Regarding tibial morphology, females have smaller tibias (normalizing for height), with narrower tibial plateaus and deeper medial tibial plateaus. Female patellas were smaller and different enough in morphology to be accurate in predicting gender in forensic studies. Cartilage studies mostly agreed that articular cartilage thickness and volume is greater in men, (possibly related to height/BMI or smaller joint surface area in women).

Conclusion: Women's sports medicine is an emerging field, and most knee anatomy research has focused on sex differences in the anterior cruciate ligament. However, there is less information regarding sex differences in other anatomic structures of the knee that may be important to guide treatment. Given the importance of individualized medicine and significant differences in injury rates/outcomes in female versus male athletes, radiologists should be aware of anatomic sex differences.

Modality % - Radiography / Fluoroscopy:	0
Modality % - CT:	15
Modality % - MRI:	85
Modality % - US:	0
Modality % - Nuclear Medicine:	0

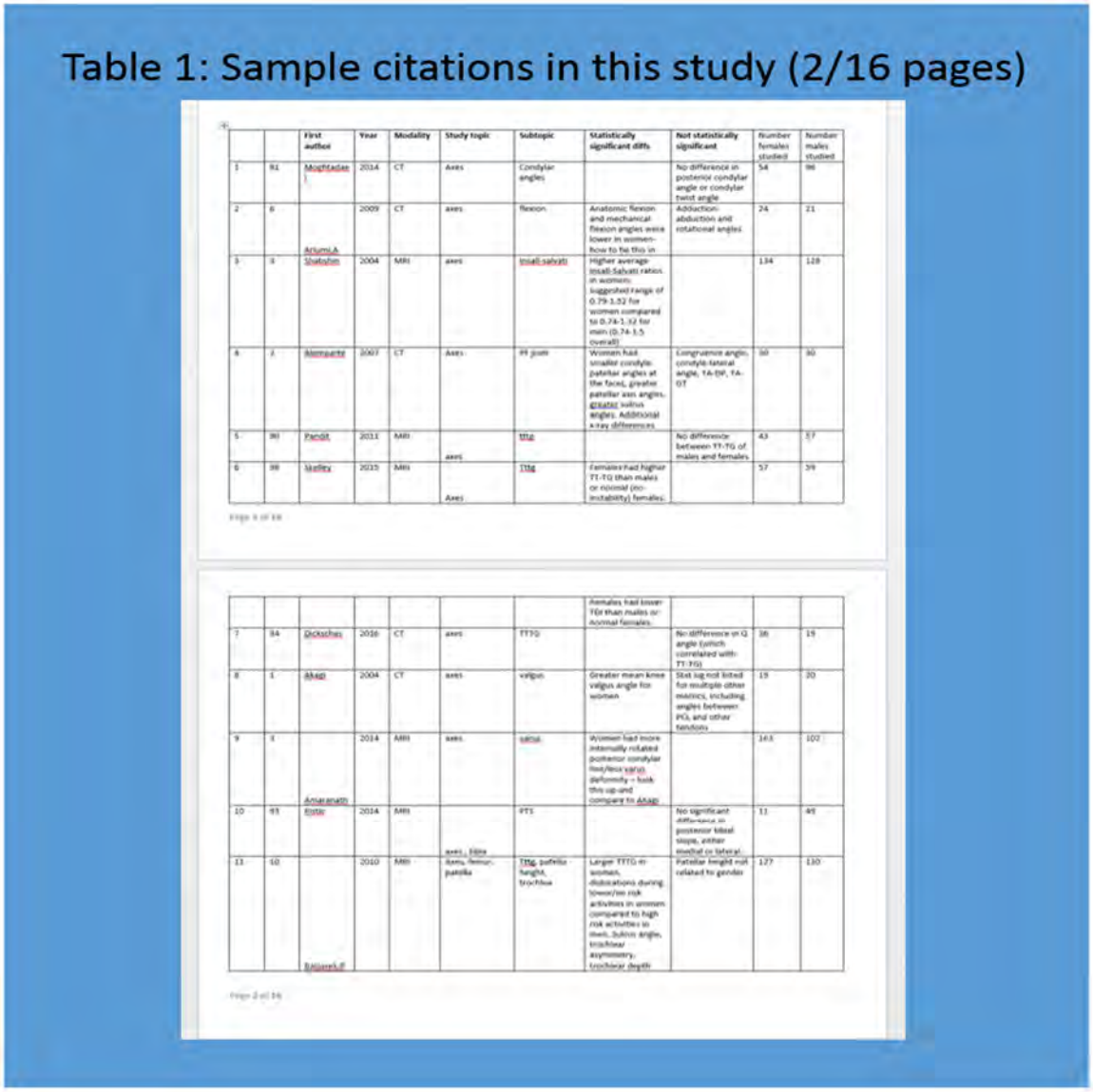

Table 1: Sample citations from systematic review of imaging literature on sex differences in bone and cartilage knee anatomy

Poster #48

IMAGING OF ANKLE IMPINGEMENT SYNDROMES

Gary LiMarzi, MD; Omar Khan, MD; Yashesh Shah, MD; Corrie Yablon, MD
University of Michigan Medical Center, Ann Arbor, MI, USA
(Presented by: Gary LiMarzi, MD, University of Michigan Medical Center)

Purpose: Ankle impingement syndromes describe a spectrum of posttraumatic bone and soft tissue abnormalities, which result in painful limitation of range of motion. Although classically described in athletes, the process of posttraumatic impingement can occur at any age. While ultimately a clinical diagnosis, characteristic features have been described on multiple imaging modalities, most commonly MRI. The role of radiology is both detecting these often subtle changes as well as differentiating them from more common causes of ankle pain. We present a comprehensive review of the different types of ankle impingement and their appearance on various imaging modalities.

Materials and Methods: Retrospective RadQuery search of the University of Michigan PACS for keywords pertaining to various ankle impingement syndromes between 1/1/2007 and the present.

Results: Ankle impingement syndromes can be classified based on location as anterior, anterolateral, anteromedial, posterior, or posteromedial. Of these, anterolateral, anterior, and posterior impingement syndromes are the most common and their typical appearances have been well documented. Anterolateral impingement is usually the result of prior ATFL injury with synovial or fibrous proliferation limiting range of motion. Anterior impingement is typically due to spur formation in the anterior recess, which may cause synovitis. Anteromedial and posteromedial impingement are much less common but can be seen in the setting of prior injury to the deep deltoid ligament fibers or masses/accessory muscles in the tarsal tunnel. Posterior impingement is most commonly associated with an os trigonum and instability at the synchondrosis, which is exacerbated by extremes of plantar flexion.

Conclusion: Ankle impingement syndromes can have sundry imaging manifestations, the presence of which require clinical correlation for the presence of active symptoms. Increasing awareness of these findings can aid the radiologist in suggesting the presence of impingement when imaging is performed to evaluate other more common causes of ankle pain.

Modality % - Radiography / Fluoroscopy:	10	Modality % - US:	20
Modality % - CT:	10	Modality % - Nuclear Medicine:	0
Modality % - MRI:	60		

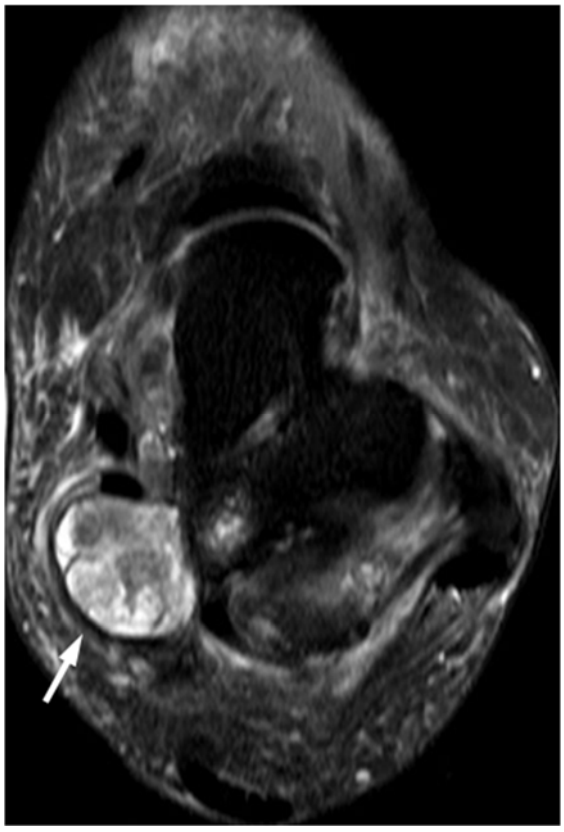

Axial T2FS ankle MRI shows a large ganglion cyst in the tarsal tunnel (arrow), situated between the FDL and FHL tendons in the posteromedial recess.

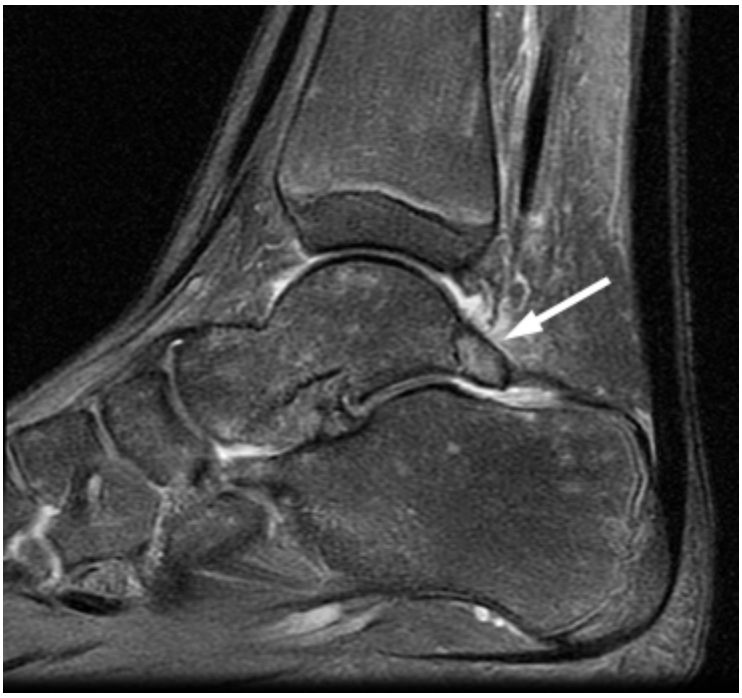

Sagittal PDFS ankle MRI shows an os trigonum (arrow) with intrinsic marrow edema and surrounding soft tissue edema and synovitis in the posterior joint recess.

Poster #49

“CYCLOPS-LIKE" LESION RELATED TO MUCOID DEGENERATION OF THE ACL

Maria Bedoya, MD[1]; Andrew Chi, MD[1]; Christian Barrera, MD[2]; Yiftah Beer, MD[3]; Nogah Shabshin, MD, MBA, BSC[1]
[1]Hospital of University of Pennsylvania, Philadelphia, PA, USA; [2]Children's Hospital of Philadelphia, Philadelphia, PA, USA; [3]Assaf Harofeh Medical Center, Zeriffin, Israel
(Presented by: Maria Bedoya, MD, Hospital of University of Pennsylvania)

Purpose: severity -Cyclops lesion has been described as a complication of ACL reconstruction, and much less commonly of an ACL tear. It represents a form of arthrofibrosis and may cause limitation of knee extension. The purpose is to describe “cyclops-like” lesions in patients with mucoid-degeneration of a native intact ACL and correlate its presence with a limited range of motion and degeneration severety.

Materials and Methods: Sixty patients with ACL mucoid-degeneration were sequentially selected. Of those, 9 were excluded (no FS sagittal, ACLor PCL reconstruction). MRIs were evaluated for: degeneration severity , ACL thickness, presence of a ganglion cyst, intraosseous cysts and "cyclops-like" lesion. Concomitant MR and physical examination (PE) findings were noted, correlation was obtained with limited range of motion and anterior stability of the joint. If available, appearance of ACL under arthroscopy was assessed.

Results: 51 patients with ACL mucoid degeneration (F:M=25:26, age 27-87, mean 51years) were included. Mean ACL width 11mm (6-20mm). 36/37 (97%) had negative Lachman test and 16/16 (100%) had intact ACL arthroscopic appearance. A cyclops-lesion was seen in 11/51(21%), mean lesion size of 11mm (6-16 mm). Only 1 case with cyclops-lesion had prior arthroscopy. No difference in limited-range-of-motion, age distribution or ACL width between patient with and without cyclops (p-values > 0.65) was found. The degeneration degree was near significantly worse in patients with cyclops: severe in 5/11(45%) with cyclops vs 7/40(18%) without ;(p-value 0.06).

Conclusion: A “cyclops-like” lesion on MRI is common in patients with ACL mucoid-degeneration. It may be related to a severe degeneration, and although protruding into the anterior joint recess, may not be associated with limited-range-of-motion.

Modality % - Radiography / Fluoroscopy:	0
Modality % - CT:	0
Modality % - MRI:	100
Modality % - US:	0

Modality % - Nuclear Medicine:

"Cyclops-like" lesions in the anterior joint recess in a patients with ACL mucoid degeneration

Poster #50

GETTING TO YOUR FEET: MR IMAGING OF FOREFOOT PAIN: WHAT THE PRACTICING RADIOLOGIST NEEDS TO KNOW

Richard Leake, MD; Sarah Stilwill, MD; Chris Hanrahan, MD, PhD
University of Utah Medical Center / SOM, Salt Lake City, UT, USA
(Presented by: Richard Leake, MD, University of Utah Medical Center / SOM)

Purpose: Forefoot pain is a common reason for primary care and emergency department visits with foot and toe injuries accounting for 3.5% of emergency department injury visits according to the 2013 National Hospital Ambulatory Medical Care Survey. While all foot injuries do not warrant MR imaging, forefoot pain is a common indication for MRI. The aim of this exhibit is to aid the practicing radiologist in interpreting conventional forefoot anatomy and common pathology seen on forefoot MR imaging.

Materials and Methods: Educational Goals/Teaching Points:

Upon completion of this exhibit, the reader should be proficient in recognizing normal and abnormal forefoot anatomy, and recognize common traumatic and non-traumatic pathology on MRI.

Results: Outline:

Following review of conventional forefoot anatomy, this exhibit will be organized into two broad categories, including traumatic and non-traumatic pathology. The distinguishing MR imaging features of each entity will be reviewed.

Case based imaging review includes the following topics:

1. Conventional forefoot anatomy
2. Forefoot MR protocol review
3. Case Based imaging review
    1. Traumatic
        1. Fractures
            1. Avulsion
            2. Stress fracture/ stress response
            3. Sesamoid fracture
        2. Plantar plate injury
        3. Freiberg infraction
        4. Ligament disruption
        5. Tendon injury
    2. Non-traumatic:
        1. Joint disorders: osteoarthritis, gout, sesamoiditis, hallux valgus
        2. Infectious: osteomyelitis, septic arthritis
        3. Soft tissue: Morton neuroma, ganglion, plantar fibroma, adventitial bursa

Conclusion: To ensure accurate diagnosis in both the traumatic and non-traumatic setting, the practicing radiologist must have adequate knowledge of forefoot anatomy and sound recognition of pathology to aid the referring clinician and improve patient care.

Modality % - Radiography / Fluoroscopy:	0
Modality % - CT:	0
Modality % - MRI:	100
Modality % - US:	0
Modality % - Nuclear Medicine:	0

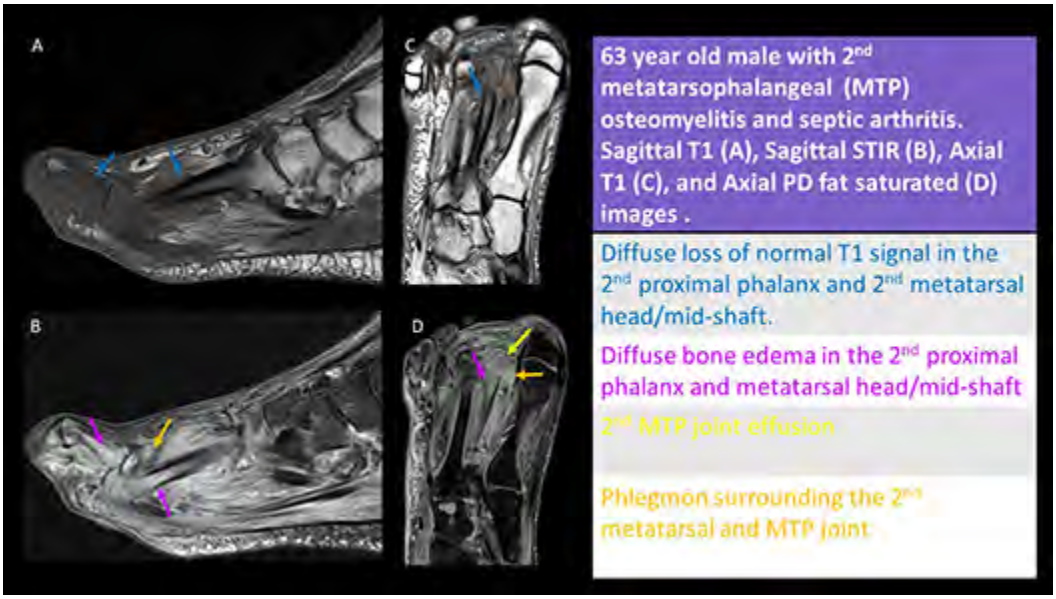

Image 1. 2nd metatarsophalangeal (MTP) osteomyelitis and septic arthritis

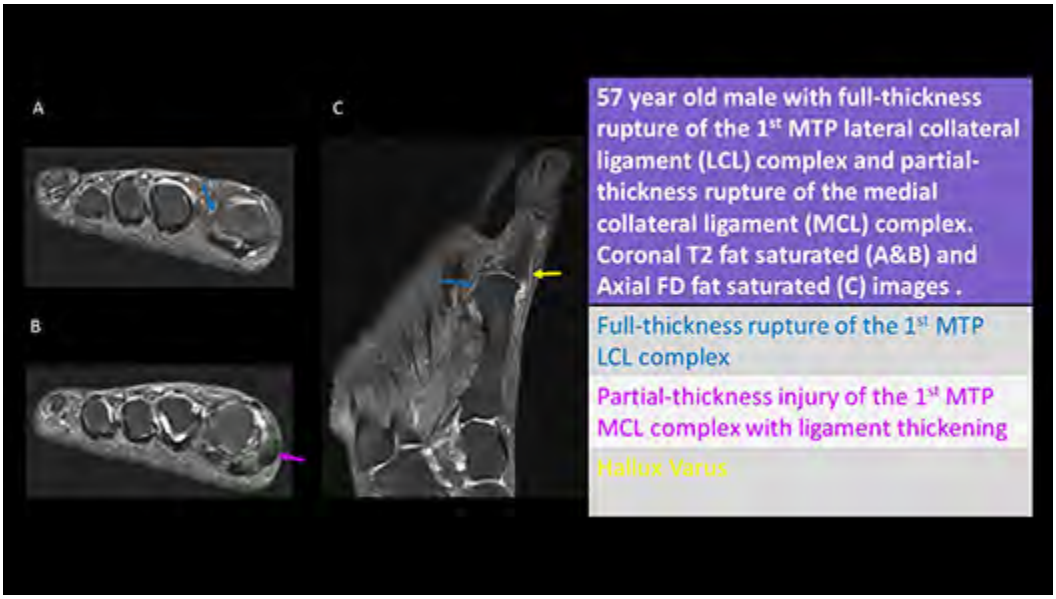

Image 2: full-thickness rupture of the 1st MTP lateral collateral ligament (LCL) complex and partial-thickness rupture of the medial collateral ligament (MCL) complex

Poster #51

OPTIMIZING BONE MARROW LESION DETECTION USING DUAL ENERGY CT: A PHANTOM STUDY

Ramya Srinivasan[1], Hsu-Cheng Huang[2], Yuxin Sun[1], Stefanie Weinstein[1], Lynne Steinbach[1], Benjamin Yeh[1]
1 University of California San Francisco, 2. Taipei City Hospital, Taipei, Taiwan
(Presented by: Ramya Srinivasan, MD, University of California San Francisco)

Purpose: Bone is the third most common site for metastases in cancer patients. Osseous metastases can cause intractable pain and may have debilitating complications. Cancer patients routinely undergo CT examinations to monitor the primary lesions and any metastatic disease. Studies have shown that conventional single-energy CT (SECT) is limited for detecting bone metastases. We hypothesize that dual-energy CT (DECT) can be used to detect bone marrow metastases that go undetected or have been diagnosed only on further evaluation with MRI or PET CT. This hypothesis is driven by several compelling clinical cases we have encountered (Fig. 1). This is a phantom study with the goal of optimizing evaluation of bone marrow lesions using DECT..

Materials and Methods: We constructed 51 semi-anthropomorphic lumbar spine phantoms embedded with 75 simulated tumors (25 mildly lytic, 25 isodense, and 25 mildly sclerotic). These phantoms were scanned in a rapid-kilovoltage-switching DECT scanner. Two radiologists independently reviewed the 70 keV virtual monochromatic reconstructions and material decomposition images (hydroxyapatite (HAP)-water, water-HAP, cortical bone-water, water-cortical bone). We recorded the reviewer's response regarding the presence of tumors, tumor conspicuity, and image quality using 3-point Likert scales. The sensitivity and specificity of the reconstruction algorithms were evaluated with the McNemar test. The Wilcoxon signed rank test was used to evaluate tumor conspicuity and image quality of the different algorithms..

Results: Outline:The HAP-water material decomposition algorithm achieved a higher sensitivity for detecting isodense lesions as compared to the 70 keV reconstructions (94% versus 82%, p=0.031) (Fig. 3). Inter-observer agreement was excellent (Kappa= 0.94). The HAP-water material decomposition algorithm also demonstrated a higher tumor conspicuity score ($p<0.0001$) compared to the 70 keV reconstructions. Case based imaging review includes the following topics:

Conclusion:

Modality % - Radiography / Fluoroscopy:	0
Modality % - CT:	100
Modality % - MRI:	0
Modality % - US:	0
Modality % - Nuclear Medicine:	0

2018 MODALITY CHARTS

Society of Skeletal Radiology

41st Annual Meeting

March 25-28, 2018

Podium/Poster Number	Modality %: Radiography / Fluoroscopy	Modality %: CT	Modality %: MRI	Modality %: US	Modality %: Nuclear Medicine
Podium 1	50	10	30	9	9
Podium 2	0	0	100	0	0
Podium 3	0	0	100	0	0
Podium 4	20	20	20	20	20
Podium 5	0	100	0	0	0
Podium 6	0	50	50	0	0
Podium 7	100	0	0	0	0
Podium 8	0	100	0	0	0
Podium 9	0	0	0	100	0
Podium 10	10	10	80	0	0
Podium 11	0	100	2	0	0
Podium 12	0	0	100	0	0
Podium 13	0	0	100	0	0
Podium 14	0	0	100	0	0
Podium 15	0	0	100	0	0
Podium 16	0	0	50	50	0
Podium 17	15	0	85	0	0
Podium 18	0	0	100	0	0
Podium 19	0	0	0	100	0
Podium 20	20	0	80	0	0
Podium 21	5	5	0	90	0
Podium 22	5	0	95	0	
Podium 23	0	100	0	0	0
Podium 24	0	60	0	40	0
Podium 25	10	0	60	30	0
Podium 26	5	95	0	0	0
Podium 27	100	0	0	0	0
Podium 28	100	0	0	0	0
Podium 29	100	7	0	0	0
Podium 30	5	95	0	0	0
Podium 31	0	0	50	50	0
Podium 32	0	0	100	0	0
Podium 33	0	0	20	80	0
Podium 34	0	0	100	0	0
Podium 35	0	0	100	0	0
Podium 36	0	100	0	0	0
Podium 37	0	0	1	0	0
Podium 38	0	0	0	1	0
Podium 39	0	0	100	0	0
Podium 40	0	10	90	0	0
Podium 41	5	90	5	0	0
Podium 42	0	0	50	0	50
Podium 43	0	100	0	0	100
Podium 44	3	19	52	6	31
Podium 45	0	20	80	0	0

Podium/Poster Number	Modality %: Radiography / Fluoroscopy	Modality %: CT	Modality %: MRI	Modality %: US	Modality %: Nuclear Medicine
Podium 46	0	50	0	0	50
Podium 47	15	30	55	0	
Podium 48	0	0	20	0	76
Podium 49	0	0	100	0	0
Podium 50	8	0	0	100	0
Podium 51	0	0	100	0	0
Podium 52	0	3	100	0	0
Podium 53	75	0	25	0	0
Podium 54	0	0	100	0	0
Podium 55	0	0	100	0	0
Podium 56	0	0	100	0	0
Podium 57	0	0	100	0	0
Poster 1	0	0	100	0	0
Poster 2	0	0	100	0	0
Poster 3	0	0	0	100	0
Poster 4	50	50	0	0	0
Poster 5	25	0	0	0	0
Poster 7	0	0	100	0	0
Poster 8	0	100	0	0	0
Poster 9	5	0	95	0	0
Poster 10	65	15	15	5	
Poster 11	20	20	60	0	0
Poster 12	10	70	10	10	0
Poster 13	25	22	50	0	6
Poster 14	0	0	100	0	0
Poster 15	85	2	0	13	0
Poster 16	40	25	25	10	
Poster 17	0	40	5	55	
Poster 18	0	0	0	100	0
Poster 19	50	0	0	50	0
Poster 20	50	0	0	50	0
Poster 21	100	0	0	0	0
Poster 22	100	0	0	0	0
Poster 23	0	0	100	0	0
Poster 25	5	95	0	0	0
Poster 26	60	20	20	0	0
Poster 27	0	0	47	50	0
Poster 28	0	0	100	0	0
Poster 29	5	5	85	5	
Poster 30	25	5	50	20	0
Poster 31	50	25	21	4	0
Poster 32	0	0	100	0	0
Poster 33	0	0	100	0	0
Poster 34	50	0	50	0	0
Poster 35	0	76	0	0	0

Podium/Poster Number	Modality %: Radiography / Fluoroscopy	Modality %: CT	Modality %: MRI	Modality %: US	Modality %: Nuclear Medicine
Poster 36	0	0	100	0	0
Poster 37	50	39	0	0	10
Poster 38	0	15	80	0	5
Poster 39	5	25	70	0	
Poster 40	0	45	45	10	0
Poster 41	70	10	10	-6	10
Poster 42	40	10	10	0	40
Poster 43	0	0	50	50	0
Poster 44	0	0	1	0	0
Poster 45	100	0	0	0	0
Poster 46	67	33	0	0	0
Poster 47	0	15	85	0	0
Poster 48	10	10	60	20	0
Poster 49	0	0	100	0	
Poster 50	0	0	100	0	0
Poster 51	0	100	0	0	0

AUTHOR INDEX

Society of Skeletal Radiology

41st Annual Meeting

March 25-28, 2018

Author Index

U

V

W

Y

Z